THE UNIVERSITY OF ALBERTA

CHARACTERISTICS OF SEMICONDUCTOR LASERS WITH OPTICAL FEEDBACK

by

JANN OLUF BINDER

(C)

A THESIS

SUBMITTED TO THE FACULTY OF GRADUATE STUDIES AND RESEARCH

IN PARTIAL FULFILMENT OF THE REQUIREMENTS FOR THE DEGREE

OF DOCTOR OF PHILOSOPHY

DEPARTMENT OF ELECTRICAL ENGINEERING

EDMONTON, ALBERTA

FALL 1989

THE UNIVERSITY OF ALBERTA

RELEASE FORM

NAME OF AUTHOR: JANN OLUF BINDER

TITLE OF THESIS: CHARACTERISTICS OF SEMICONDUCTOR LASERS WITH OPTICAL FEEDBACK

DEGREE: DOCTOR OF PHILOSOPHY

YEAR THIS DEGREE GRANTED: FALL 1989

Permission is hereby granted to THE UNIVERSITY OF ALBERTA LIBRARY to reproduce single copies of this thesis and to lend or sell such copies for private, scholarly or scientific purposes only.

The author reserves other publication rights, and neither the thesis nor extensive extracts from it may be printed or otherwise reproduced without the author's written permission.

(SIGNED) Jann Binder

PERMANENT ADDRESS:

Eschelbachstr. 29

D-7038 Holzgerlingen

West Germany

DATE: 29th June 1989

THE UNIVERSITY OF ALBERTA

FACULTY OF GRADUATE STUDIES AND RESEARCH

The undersigned certify that they have read, and recommend to the Faculty of Graduate Studies and Research for acceptance, a thesis entitled CHARACTERISTICS OF SEMICONDUCTOR LASERS WITH OPTICAL FEEDBACK submitted by JANN OLUF BINDER in partial fulfilment of the requirements for the degree of DOCTOR OF PHILOSOPHY

G. D. Cormack

Supervisor

Brian Gaiside

W. Degen

R. Charlton

C. G. Englefield

Date: 29th June 1989

ABSTRACT

This thesis is concerned with the improvement of the spectral characteristics of semiconductor laser diodes as a result of optical feedback. Discrete optical and fiber optic components were used together with the semiconductor diode to create both Fabry-Perot and ring type external cavity lasers.

In the domain of weak optical feedback, with feedback power ratios of less than -40 dB in a fiber-ring feedback assembly, the number of external cavity modes and the distribution of power in these modes is studied. Oscillation in the external cavity mode with minimum linewidth is experimentally observed and shown to agree with a frequency fluctuation model. The upper limit for stable operation in the weak feedback domain and the trade-off between minimum linewidth and minimum number of external cavity modes is discussed. A fiber-ring feedback assembly with optimized feedback-parameter values, was observed to reduce the linewidth from ~ 100 MHz to ~ 2 MHz, to provide a greater than 20 dB suppression of side modes of the external cavity, and a tuning range of ~ 1 GHz.

In the domain of strong optical feedback, with one or two anti-reflection (AR) coated facets on the semiconductor cavity, large changes of the carrier-density and in turn changes of gain and resonance frequency of the semiconductor cavity occur due to the injection of light. Those changes are analyzed and a model is presented for (1) the experimentally observed bistability and tuning range of an external grating laser, i.e. a one-side AR-coated laser exposed to strong frequency selective optical feedback from an optical grating, (2) the effect of the residual reflectivity of the laser on the tuning characteristics of the external grating laser, and (3) the change of the threshold current with resonator loss for a laser. Estimating parameter values by comparing experimentally observed light versus current (LI)-characteristics with the calculated LI-characteristic for different values of resonator loss is shown to allow prediction of the gain versus current characteristic of individual laser amplifiers. Finally, the LI-characteristic and spectral properties of a unidirectional semiconductor optical-fiber ring laser are investigated.

ACKNOWLEDGEMENT

I would like to thank my supervisor, Dr. G.D. Cormack, for his encouragement, advice and support throughout this project. Also I would like to thank the members of the examining committee for reviewing this work. Fruitful discussions with Dr. R. Fedosejevs have been very helpful. My special thanks go to Azmina Somani for many stimulating discussions and the use of some of her work. I am grateful to Drs. C.G. Englefield and P.A. Goud, for supporting this cooperation.

It is my pleasure to thank Drs. W. Krzymien and J. McMullin for technical discussions, Rod Anderson, Dominique Jodoin, Fred Chan and Sunit Lothia for their friendly support and cooperation, Joanne Whalen for her help in typing reports and finishing this thesis, and David Johnson and Keith Wilcox for their technical assistance and for drawing some of the figures. Thanks are also due to the staff of the Alberta Telecommunications Research Centre, who have provided a pleasant working environment. My special thanks are extended to Herward Gans, Conrad Doerrbecker, Craig Korth and Roman Lipiecki for carefully fabricating the mechanical components and Barry Arnold for applying AR-coatings.

Stimulating discussions with Drs. B. Tromborg and H. Olesen of the Telecom Research Lab., Copenhagen, DK, and Dr. N. Schunk and Prof. K. Petermann of the TU Berlin are gratefully acknowledged. I sincerely thank Drs. H.G. Weber, G. Grosskopf, and R. Ludwig of the HHI, Berlin, FRG, for supplying AR-coatings on two laser diodes and for the thorough characterization of these devices, also Mr. E. Bambach of ANT, Backnang, FRG, for providing samples of fiber tapers.

For providing financial assistance, I express my gratitude to the Alberta Telecommunications Research Centre, the University of Alberta, the Government of Canada Awards program, NSERC and the German Academic Exchange Service (DAAD).

Finally, I thank my family, who has always been caring and supportive, and my dear friends, who have made Edmonton "home" to me for many years. They gave me the opportunity to pursue this work in confidence and good spirit.

TABLE OF CONTENTS

CHAPTER	PAGE
1. INTRODUCTION	1
2. THEORY FOR THE SOLITARY LASER	6
2.1. INTRODUCTION	6
2.2. BASIC PRINCIPLES OF LASER OPERATION	6
2.3. LANGEVIN RATE EQUATIONS	9
2.3.1. *Introduction*	9
2.3.2. *Numerical Simulations*	13
2.3.3. *Output Power*	14
2.3.4. *Laser Dynamics*	15
2.3.5. *Linearization of the Rate Equations*	17
2.4. NOISE CHARACTERISTICS	18
2.4.1. *Definitions*	18
2.4.2. *AM-Noise*	19
2.4.3. *Power Spectrum*	20
2.4.3.1. *Below Lasing Threshold*	21
2.4.3.2. *Above Lasing Threshold*	23
2.4.3.3. *Comparison of Linewidths*	25
2.4.3.4. *Resonant Noise Enhancement*	26
2.4.4. *FM-noise*	27
2.4.5. *Frequency Fluctuation Model*	30
3. THEORY FOR THE EXTERNAL CAVITY LASER	34
3.1. INTRODUCTION	34
3.2. RATE EQUATIONS	35
3.3. OSCILLATION CONDITION GRAPH	37
3.3.1. *Governing Equations*	37
3.3.2. *Graphical Representation*	40
3.3.3. *Wavelength Dependent Feedback*	45
3.4. CHIRP-REDUCTION	46
3.5. CHARACTERISTICS FOR WEAK FEEDBACK	49
3.6. FEEDBACK REGIMES	53
3.7. GENERAL DISCUSSION, STRONG VERSUS WEAK FEEDBACK	56
4. WEAK FEEDBACK	57
4.1. INTRODUCTION	57
4.2. MODELLING OF EXTERNAL CAVITY MODES	58
4.3. RING FEEDBACK VERSUS REFLECTIVE FEEDBACK	59
4.4. EXTERNAL CAVITY MODES - EXPERIMENT	62
4.5. FREQUENCY FLUCTUATION MODEL	69
4.6. CRITICAL FEEDBACK LEVEL	73
4.7. SHORT RING CAVITY	75
4.8. CONCLUSION	81

5. STRONG FEEDBACK....84
5.1. INTRODUCTION....84
5.2. EXPERIMENTAL RESULTS....87
5.2.1. *High Reflectivity Laser*....91
5.2.2. *Low Reflectivity Laser*....91
5.3. KEY EQUATIONS....96
5.4. TUNING CHARACTERISTICS....97
5.4.1. *In-Phase and Out-of Phase Feedback*....99
5.4.2. *Oscillation away from the Gain Maximum*....102
5.4.3. *Intermode Tuning Characteristics*....107
5.5. STABILITY OF OSCILLATION....110
5.5.1. *Single Mode Stability*....110
5.5.2. *Linewidth*....115
5.5.3. *Lens-Alignment*....120
5.5.4. *Fine Tuning*....122
5.6. CONCLUSION....123

6. GAIN VERSUS CURRENT CHARACTERISTIC....124
6.1. INTRODUCTION....124
6.2. THEORETICAL ANALYSIS....127
6.3. GENERAL MODELLING....133
6.3.1. Computation of LI-Characteristics....134
6.3.2. Gain vs. Current Characteristics....137
6.3.3. Nominal Threshold Current....139
6.3.4. Leakage Current....141
6.3.5. Width of the active region....143
6.4. SPECIFIC DEVICE MODELLING....144
6.4.1. Comparison of Calculated and Measured LI-Characteristics....144
6.4.2. Deduced Gain vs. Current Characteristic....148
6.4.3. Differences Between Individual Devices....148
6.4.4. Change of the Nominal Threshold Current....150
6.5. CONCLUSION....154

7. RING LASER....156
7.1. INTRODUCTION....156
7.2. LI-CHARACTERISTICS....158
7.3. SPECTRAL CHARACTERISTIC....161
7.4. CONCLUSION....168

8. CONCLUSIONS....170

REFERENCES....175

APPENDIX A: EXPERIMENTAL SETUP....186

APPENDIX B: SELF-HETERODYNE TECHNIQUE....191

APPENDIX C: LI-CHARACTERISTIC OF THE EXTERNAL GRATING LASER....197

LIST OF TABLES

TABLE PAGE

6.1: Values for general semiconductor laser parameters.....136

6.2: Values for specific device parameters.....136

LIST OF FIGURES

FIGURE PAGE

2.1. Sketch of the gain profile and optical power spectrum of a semiconductor laser.....7

2.2 Sketch of (a) the AM-noise spectrum, (b) the optical power spectrum and (c) the FM-noise spectrum.....19

2.3 Setup for the measurement of the FM-noise spectrum. To convert FM-noise into amplitude noise with the FP-interferometer, its resolution has to be low, in our case $\Delta\omega_{FP} \geq 2 \cdot \omega_R$.....28

2.4 (a) Setup for the conversion of frequency fluctuations in the optical output of a test laser into amplitude changes of the signal $a_{FD}(t)$ in the electrical domain. Sketch of (b) random fluctuations of $a_{FD}(t)$ and ω^{IF}, and (c) the probability distribution function of these fluctuations.....31

2.5 Sketch of the transfer function of the IF-filter used in Fig. 2.4 and definition of the filter bandwidth B.....31

3.1 Sketch of a semiconductor laser with optical feedback from an external reflector.....34

3.2 Dependence of gain, g, and refractive index, n_ϵ, on the carrier density, n, in the semiconductor. Also, definition of the linewidth enhancement factor, α, as the ratio between the change in refractive index and change in gain.....39

3.3 Plot of loss and constant phase curves for (a) no optical feedback, (b) to (d) weak optical feedback, (e) strong feedback and (f) feedback from an optical grating. The following parameters were used: $\alpha = 6$, $L_{ex} = 7.5$ cm, $L_{in}' = 300\ \mu m$. The reflectivities R_1 and R_{ex} were respectively: (a) 0.31 and 0, (b) 0.31 and $25 \cdot 10^{-6}$, (c) 0.31 and 10^{-4}, (d) 0.31 and $16 \cdot 10^{-4}$, (e) 10^{-4} and 0.31, and (f) $R_1 = 10^{-4}$ and wavelength dependent feedback from a grating ($r_G^2 = 0.31$ and $f_G = 15$ GHz).....41

3.4 Enlargement of (a) a section of Fig. 3.3(a) and (b) a section of Fig. 3.3 (e). Also indicated are the parameters A and B introduced by [83]. For clarity of $\Delta f'$, the slope of the constant phase curve in the lower graph is less steep by a factor of 4.6 than it should be using the parameter values of Fig. 3.3(e).....44

3.5 Effect of a change of the external cavity length, expressed in terms of a change in the roundtrip phase shift ψ_e, on a plot of the loss and constant phase curves. Graphs (a) and (c) are for $\psi_e = 0°$ and (b) and (d) are for $\psi_e = 180°$. All other parameters are: in the case of weak feedback, (a) and (b), the same as in Fig. 3.3(a), and in the case of strong feedback, (c) and (d), the same as in Fig. 3.5(f).....52

4.1 (a) Sketch of the experimental setup used to provide optical feedback to a laser by means of an optical fiber ring. (b) Sketch of a comparable setup utilizing reflective feedback. 60

4.2 Sketch of the measurement setup showing the test laser with optical feedback from a fiber ring and the reference laser with strong frequency selective feedback from a diffraction grating.....63

4.3 Optical spectra of the test laser recorded for different feedback levels using a reference laser with negligible (<10 kHz) linewidth. Displayed is the power spectrum of the APD-current (a) on a logarithmic scale and (b) on a linear scale. The IF-filter bandwidth of the spectrum analyzer was 300 kHz. In the IF-spectrum $\omega_0/2\pi$ is 1.457 GHz. The traces for (a) R_{ex} = -47, -55, -60 dB and $R_{ex} = 0$, and (b) R_{ex} = -60 dB and -55 dB are offset vertically for clarity. In Fig. 4.3(b) the area under each external cavity mode is given in percent of the area under the spectrum for $R_{ex} = 0$. The limits of integration are indicated by markers on each side of the external cavity modes.....64

4.4 Gain versus frequency charts showing constant phase curves (positive slope) and loss curves (sinusoidal) for 3 different feedback levels and phase-shifts ψ_e: (a) R_{ex}=-60 dB and ψ_e=0°, (b) -60 dB and -140°, (c) -55 dB and -30° and (d) -47 dB and 0°. Other parameters used in the calculations were $\Delta\nu_{in}$= 150 GHz, $1/\tau_{ex}$= 175 MHz, $\alpha = 6$ and $R_1 = .35$. The lower curves are the measured spectra.....66

4.5 Mode hopping frequency μ versus feedback level R_{ex} calculated from (4.5).....71

4.6 Optical power spectra recorded with a Fabry-Perot interferometer (FSR = 30 GHz) for R_e = -55 dB to -30 dB (top to bottom). One sweep of the interferometer encompasses two spectral orders. The time of reset of the sweep is marked in the diagram.....74

4.7 Heterodyne beat spectra for no optical feedback (bottom trace) and -37 dB of optical feedback (top trace). Notice the set of external cavity modes that is separated from line-center by 2.8 GHz (= relaxation resonance frequency). 74

4.8 Self-heterodyne beat spectra for (a) 29 cm and (b) 17 cm long fiber rings and R_{ex} = -43 dB, showing laser linewidths of 1.5 MHz and 2.5 MHz, respectively, and more than 25 dB suppression of neighboring external cavity modes.....77

4.9 Dependence of (a) the linewidth and (b) to (d) the side-mode suppression on changes of the external cavity length by fractions of a wavelength. The data is obtained for L_{ex} = 17 cm and R_{ex} ~ -43 dB. A linear increase of L_{ex} is achieved be applying a voltage ramp to the piezo-electric micrometer controlling the axial position of the tapered fiber end closest to the optical isolator in Fig. 4.1. (b) and (c) show the external cavity mode amplitude in the self-heterodyne beat spectrum, measured at (A) and (B) of Fig. 4.9(a), respectively. (d) shows the amplitude of the semiconductor cavity modes, recorded with a monochromator at point (A) and (B) of Fig. 4.9(a) and for the laser without feedback, respectively.....78

4.10 Beat spectra between the laser with fiber-ring feedback, L_{ex} = 17 cm and R_{ex} ~ -43 dB, and an external grating laser with negligible linewidth. The ten traces are recorded as the fiber-ring length is swept from (C) to (D) in Fig. 4.9(a). The experimental setup shown in Fig. A.1 is used for this experiment, however the acousto-optic frequency shifter is turned off.....80

4.11 Linewidth reduction as a function of the feedback level. The measured values are indicated by dots.....80

4.12 Sketch of the laser with feedback from a fiber ring with double tapered fiber. The circumference of the fiber-ring is 8.05 cm. 82

4.13 Self-heterodye beat spectrum recorded for the laser in the feedback arrangement of Fig. 4.12 and showing a linewidth of the laser with feedback of 1.7 MHz.....82

5.1 Sketch of (a) a laser with optical feedback from an external reflector, (b) the optical power spectrum of the laser without optical feedback, (c) the spectral characteristic of the external cavity, the optical power spectrum of the laser (d) coupled to the external reflector, and (e) coupled to an external grating.....85

5.2 Sketch of the laser with feedback from a diffraction grating.....88

5.3 Output power of the external grating laser (TH 557), normalized to zero-feedback output, vs. tuning of the center frequency of optical feedback. Also, definitions of Regimes I to IV.....88

5.4 Longitudinal mode-spectrum (TH 557 laser) measured with a monochromator in (a) and (b), Regime I and (c), Regime II to IV.....89

5.5 Fabry-Perot spectrum (TH 557 laser) for increasing detuning from (a) to (h). (a) Regime I, (b) and (c) Regime II, (d) Regime III, (e) to (h) Regime IV.....89

5.6 Beat spectrum (TH 557 laser) measured with the self-heterodyne technique in (a) Regime III and (b) Regime IV. The frequency-shift between the two beams was 80 MHz. The '-1' indicates a negative frequency domain component (Appendix B).....90

5.7 Output power of the external grating laser (TY 224) versus tuning of the center wavelength of optical feedback for the two laser currents I_L = 30 and 40 mA, respectively. The trace for I_L = 30 mA is vertically offset by -.5 mW for clarity.....92

5.8 Fabry-Perot spectrum (TY 224 laser) for decreasing detuning.....92

5.9 Measured LI-characteristics of the low-reflectivity laser for different wavelengths of optical feedback.....94

5.10 Dependence of the threshold current of the external grating laser on the wavelength of optical feedback.....95

5.11 Sketch of a standing wave pattern in a laser with strong optical feedback.....95

5.12 Computed loss versus frequency graphs for a laser with strong optical feedback..... 98

5.13 (a) Graph of the composite reflectivity versus feedback power ratio for a residual reflectivity of R_2 = 2%. (b): Graph of the composite reflectivity versus roundtrip-phase shift in the external cavity for R_2 = 2%.....101

5.14 (a): Graph of the composite reflectivity versus feedback power ratio for a residual reflectivity of R_2 = .05%. (b): Graph of the composite reflectivity versus roundtrip-phase shift in the external cavity for R_2 = .05%.....101

5.15 Computed loss versus frequency graph $\alpha_0(\lambda)$ and $\alpha_G(\lambda)$ for, respectively, a laser with optical feedback from a mirror (dotted line, R_1 = .35, R_{ex} = .06, R_2 = .02 and $\Delta\nu_{in}$ = 20 x 135 GHz) and a laser with optical feedback at λ_G from an external grating. Also, spectral gain profile, $g_N^0(\lambda)$, $g_N^1(\lambda)$ and $g_N^4(\lambda)$, of the semiconductor laser for three different operating points of the external grating laser.....103

5.16 (a): Computed loss and gain versus frequency graphs for a laser with strong optical feedback (R_1 = 0.35, R_{ex} = 0.06, R_2 = 0.02 and $\Delta\nu_{in}$ = 135 GHz). (b): Sketch of the output power vs. tuning characteristic showing hysteresis.....108

5.17 (a): Computed loss and gain versus frequency graphs for the high reflectivity laser TH 557, $\alpha_0(\omega)$ and $\alpha_H(\omega)$, and for the low reflectivity laser TY 224, $\alpha_L(\omega)$. (b): Sketch of the output power vs. tuning characteristic showing hysteresis for the high reflectivity laser, $P_H(\omega)$, and continuous tunability for the low reflectivity laser, $P_L(\omega)$.....111

5.18 (a): Computed loss and constant phase curve for an external grating laser with fixed detuning of Δf_G = -80 GHz. (b): Loci of all external cavity modes for various amounts of detuning, $\forall f_G$. Also, loss versus frequency curve, $\alpha_H(f)$ with $f = \omega/2\pi$, based on the assumption $f = f_G$. For each value of detuning, the threshold gain of the external cavity mode with minimum threshold gain is marked by an open circle.....112

5.19 Loci of the chirp reduction of all external cavity modes for various amounts of detuning Δf_G. For each value of detuning, the open circle indicates the chirp reduction of the external cavity mode with minimum threshold gain (see Fig 5.18(a)) and the rectangle the chirp reduction of the external cavity mode at Δf_G.....118

5.20 Change of the power versus tuning characteristic due to partial blocking of the collimated beam between lens and diffraction grating in Fig. 5.2. The beam was blocked as follows: (1) a 1 mm horizontal slice from the center of the beam, (2) ~ 30% of the upper portion of the collimated beam in Fig. 5.2 and (3) ~ 30% of the lower portion of the collimated beam. (4) is recorded without aperture.....121

6.1 Sketch of the forward and backward travelling waves within the active region of a one-side AR-coated laser diode.....129

6.2 Block diagram of the curve-fitting procedure.....134

6.3 Light versus active region current-characteristic for various facet reflectivities. Graphs a to h: one side AR-coated laser with respectively R_2 = 35%, 11%, 3.5%, 1.1%, .35%, .11%, .035%, 0.011% and R_1 = 35%. Graph i: both side AR-coated laser with R_1 = .1% and R_2 = .05%.....138

6.4 Gain versus active region current-characteristic for various facet reflectivities. R_1 and R_2 have the same values as in Fig. 6.3.....138

6.5 Sketch of the tangent to the LI-curve that defines the *nominal* threshold current, I_{th}, for a laser with given facet reflectivities.....140

6.6 Plot of the residual reflectivity vs. nominal threshold current for the active region of a one-side AR-coated laser.....140

6.7 Sketch of the relationship between active region current, I_a, and diode terminal current, I.....141

6.8 Comparison of the calculated LI-characteristics (solid and dashed lines) with measured values (crosses) for individual lasers. The graphs show the characteristics of (i) the uncoated laser, (ii) the power emitted from the coated facet of the one-side coated device and (iii) the power from the uncoated facet.....145

6.9 Calculated peak single-pass gain vs. current characteristic for the two lasers of Fig. 6.8. The graphs show the characteristics of (i) the uncoated device, (ii) the one-side AR-coated device and (iii) the both side AR-coated device. Measured values [106] for a device of the same type (HLP5400) as the one used in Fig. 6.9(b) are indicated by dots.....149

6.10 Plot of the reflectivity R_x vs. increase in the nominal threshold current I_{tx}-I_{t0} for the one-side AR-coated devices (a) TY 224 and (b) 6M3772. Also, plot of the single pass gain G_{ps} vs. current increase with respect to the threshold current of the uncoated laser, I-I_{t0}, for the same two devices ((c) TY 224 and (d) 6M3772)). The rectangles indicate the measured values of (R_2, I_{t2}) for the lasers of table II, the circles indicate the measured values of (G_{ps}, I) obtained in [106] for the device 5F3432.....151

6.11 Plot of the reflectivity R_x vs. increase in the nominal threshold current I_{tx}-I_{t0} for one-side AR-coated devices. The dotted line is identical to curve (a) in Fig. 6.10. (1) to (3) are calculated from (6.38), using I_{t0} = 15 mA and (1) α_{mat} = 60 cm^{-1}, (2) α_{mat} = 30 cm^{-1} and (3) α_{mat} = 15 cm^{-1}. Other pairs of parameter values can be found that lead to the same graphs. For instance, the values I_{t0} = 11.7 mA and α_{mat} = 15 cm^{-1} or I_{t0} = 21 mA and α_{mat} = 60 cm^{-1} produce a graph that is identical to the solid line.....153

7.1 Sketch of (a) the semiconductor-fiber ring laser and (b) its spectral characteristics.....157

7.2 Light versus current (LI-) curve of the ring laser with an optical amplifier (# 6M3772) in the fiber ring. (a) with an optical isolator as part of the ring and (b) without isolator. The length of the ring is 17 cm. The 4 traces in each graph are: (1): output of port 1, (2) output of port 2. The traces (3) and (4) correspond to the output of port 1 and 2, respectively, when the ring feedback is interrupted by misalignment of the right (3) or left (4) tapered fiber (see Fig. 7.1).....160

7.3 Optical power spectrum of the fiber-ring laser, (a) with and (b) without optical isolator as part of the fiber ring, as recorded with a monochromator. The travelling wave amplifier # 6M3772 is operated at 66 mA injection current and is part of the 17 cm long ring-laser arrangement 162

7.4 Self-heterodyne beat spectra of the fiber-ring laser, (a) with and (b) without optical isolator as part of the fiber ring. The same operating conditions apply as in Fig. 7.3.....163

7.5 Self-heterodyne beat spectra of the fiber-ring laser, (a) with and (b) without optical isolator as part of the fiber ring. The same operating conditions apply as in Fig. 7.3 and 7.4, except that the fiber-ring length is adjusted to yield narrowest linewidth for the mode displayed at 80 MHz and low power for the components at ±1.2 GHz separation from this mode.....164

7.6 Self-heterodyne beat spectra of the fiber-ring laser, (a) with and (b) without optical isolator as part of the fiber ring. The same operating conditions apply as in Fig. 7.3, except that the recordings cover a different frequency range than in Fig. 7.3.....166

7.7 Optical power spectra of the fiber-ring laser recorded with a Fabry-Perot interferometer, (a) with and (b) without the optical isolator as part of the fiber ring. The free spectral range of the FP-interferometer is 143 GHz and the Finesse ~ 30. The lower trace of Fig. 7.7(a) shows a recording of the same optical power spectrum as Fig. 7.3, except using a different instrument and plotted versus frequency instead of wavelength.....167

A.1 Sketch of the laser with fiber-ring feedback, coupled to the measurement setup, consisting of the self-heterodyne setup, a Fabry-Perot interferometer and a monochromator.....187

B.1 Plot of the measured delayed self-heterodyne beat spectrum of the external grating laser in (a) Regime III and (b) Regime IV of Section 5.2.1. Also, calculated functions using (B.2) for (a) $\Delta\nu$ = 50 kHz and (b) $\Delta\nu$ = 5 kHz.....192

B.2 Delayed self-heterodyne beat spectra for a laser with fiber ring feedback (ω_{ex} = 129 cm) for three different levels of optical feedback (a) R_{ex} ~ -65 dB, (b) -55 dB and (c) -40 dB.....194

B.3 Original recording of the heterodyne beat spectrum shown in Fig. 4.7. 196

C.1 Original recordings of the LI-characteristics of the laser with frequency selective feedback provided by the diffraction grating at different wavelengths.....198

LIST OF SYMBOLS

A	gain coefficient (= dg/dn).
B	equivalent low-pass filter bandwidth.
c	velocity of light.
d	height of the active region of the laser.
D_{ij}	diffusion coefficient (2.9).
$\hat{e}(t)$	deviation of the instanteneous amplitude of the laser field from steady state.
$E(t)$	electric field of the laser.
$E_0(t)$	amplitude of the electric field.
f	frequency in Hz (= $\omega/2\pi$).
f_R	relaxation oscillation frequency of the laser.
F	chirp-reduction factor.
$F_E(t)$	Langevin force driving E(t).
$F_E(\omega)$	Fourier transform of the Langevin force $F_E(t)$.
$F_i(t)$	Langevin noise force driving the variable a_i (2.8).
$F_m(z)$	z-dependent light intensity in photons per unit area per second per mode (6.10).
g	gain per unit length.
g_m	gain per unit length at ω_m.
$g_N(\omega)$	gain profile (per unit length).
g_p	peak gain (per unit length).
G	rate of gain per unit time (= $v_{gr} \cdot g$).
G_{ms}	single pass gain at λ_m (6.19).
G_n	gain coefficient (= $\partial G/\partial \bar{n}$).
G_{ps}	single pass gain at λ_p.
$\hbar$	Planck's constant.
I	injection current of the laser.
I_0	constant part of the leakage current.
I_a	current in the active region.
I_a/q	pumping term in carriers per second.
I_{th}	threshold current.
I_{t0}	threshold current of the uncoated semiconductor laser.
I_{t2}	threshold current of a one-side AR-coated device without optical feedback (facet R_2 coated).

I_{tx}	threshold current of a laser with facet reflectivities R_1 and R_x.
k	feedback power ratio ($= \kappa \cdot \tau_{in}$).
k_{pol}	polarization mismatch between the laser field and the feedback field coupled back into the laser.
L_{ex}	length of the external cavity (Fig. 3.1).
L_{in}	length of the semiconductor cavity.
n	carrier density ($= N/V$).
n_ϵ	refractive index.
n_{gr}	group index.
n_{sp}	spontaneous emission factor (2.25).
n_{th}	carrier density at lasing threshold.
n_{tr}	transparency carrier density.
N	total number of carriers in the active region.
P_1, P_2	total power emitted from facet 1 and 2, respectively, in mW.
$P_H(\omega), P_L(\omega)$	power versus wavelength (tuning)-characteristic of the laser with high and low values of R_2, respectively.
P_{m1}, P_{m2}	power emitted in the m^{th} mode from facet 1 and 2, respectively, in photon per second.
q	electron charge.
r	reflection coefficient.
$r_e(\omega)$	composite reflection coefficient (3.5).
r_G	reflection coefficient of the grating at ω_G.
R	reflectivity ($= r^2$).
R_0	modal reflectivity of the uncoated semiconductor laser facets.
R_1, R_2	modal reflectivities of the semiconductor laser facets.
R_x	unknown facet reflectivity.
$R_{ex}(\omega)$	feedback power ratio (in %) or feedback level (in dB).
R_{sp}	spontaneous emission rate (2.24).
S	number of photons in the active region.
S_0	average number of photons.
S_m	number of photons in the m^{th} semiconductor cavity mode.
V	volume of the active region ($= d \cdot w \cdot L_{in}$).

v_{gr}	group velocity in the active region.
v_{Ph}	phase velocity.
w	width of the active region.
W	width of the gain profile.
$W_E(\omega)$	optical power spectrum.
$W_S(\omega)$	amplitude-noise spectrum.
$W_{\Delta\omega}(\omega)$	frequency-noise spectrum.

Subscripts

ex	refers to the external cavity.
G	refers to the diffraction grating.
i	refers to the i^{th} external cavity mode.
in	refers to the semiconductor cavity.
m	refers to the m^{th} semiconductor cavity mode.
p	refers to the peak gain of the gain profile.

Superscripts

0	refers to the laser without optical feedback.

Greek Letters

α	linewidth enhancement factor (Fig. 3.2).
$\alpha(\omega)$	frequency dependent loss of the compound cavity per unit length.
$\alpha(\omega_i)$	loss of the i^{th} compound cavity mode per unit length.
α_L	total loss per unit length ($= \alpha_s + \alpha_R$).
α_{mat}	wavelength independent material loss per unit length.
α_R	facet loss per unit length.
α_s	scattering loss per unit length.
α_{sol}	loss of the solitary laser per unit length.
γ	rate of loss in photons per unit time ($= \tau_p^{-1}$).
Γ	confinement factor for the electric field in the active region; also damping rate of the relaxation resonance.

Δf	frequency deviation.
Δf_G	detuning ($= (\omega_G - \omega_m^0)/2\pi$).
ΔG	net gain per unit time ($= \gamma - G$).
$\Delta\lambda$	spacing of the semiconductor cavity modes.
$\Delta\nu$	linewidth.
$\Delta\nu_0$	linewidth of the lasing mode without optical feedback.
$\Delta\nu_i$	linewidth of the i-th external cavity mode.
$\Delta\nu_{ex}$	separation of external cavity modes.
$\Delta\nu_{in}$	separation of internal (semiconductor) cavity modes.
$\Delta\omega$	frequency deviation with respect to ω_0.
$\Delta\omega_G$	full width at half maximum of $r_G(\omega)$.
κ	feedback rate.
λ	optical wavelength.
λ_0	wavelength of oscillation of the solitary laser.
λ_G	wavelength of maximum reflection from the grating.
$\sigma_{\Delta\omega}$	standard deviation (2.83).
τ_e	carrier lifetime.
τ_p	photon lifetime.
τ_{ex}	roundtrip time in the external cavity.
τ_{in}	roundtrip time in the semiconductor laser cavity.
$\phi(t)$	phase fluctuations of E(t) compared to steady state.
ϕ_{RT}	roundtrip phase shift.
ψ_e	phase shift defined in (3.45)
ω	frequency in radians per second ($= 2\pi \cdot f$).
$\omega(t)$	instantaneous frequency of oscillation.
ω_0	oscillation frequency of the laser without optical feedback and without spontaneous emission noise.
ω_0^{IF}	center frequency of oscillation of the test laser in the IF-spectrum.
ω_c	frequency of the mode with lowest value of ΔG.
ω_G	frequency of maximum reflection from the grating.
ω_m^0	frequency of the m^{th} semiconductor cavity mode at threshold of the solitary laser.

Abbreviations

APD	Avalanche photo diode.
AR	anti-reflection (coating).
ASE	amplified spontaneous emission (spectrum).
EMBH	etched mesa buried heterostructure (laser)
FP	Fabry-Perot (interferometer).
FWHM	full width at half maximum.
LEC	long external cavity (laser).
LI	light versus current (characteristic).

1. INTRODUCTION

The analysis of optical feedback effects in semiconductor lasers can be considered to have two objectives. The first is to obtain an understanding of the adverse effects of optical feedback in a system where optical feedback is not desired and the second is to develop methods to improve the spectral characteristics of lasers by using a controlled amount of optical feedback. In this work a general description of optical feedback effects is given that provides guidelines to understand the severity of the problems associated with optical feedback as well as possible benefits. Our focus will be to identify the domains of optical feedback that can be most effectively utilized to improve the spectral characteristics of laser diodes and to study the effects of changing the parameters that characterize the optical feedback arrangement so that we are better able to optimize the performance of a laser with optical feedback.

A multitude of effects have been observed, studied and reported on in the literature concerning semiconductor lasers with optical feedback. Initially, increased intensity noise was observed in lasers under the influence of relatively high feedback levels of -30 to -10 dB [1],[2]. In intensity modulation/direct detection communication systems, delayed optical feedback from optical connectors leads to pattern dependent mode-hopping and frequency-chirp of the laser diode and as a consequence to errors in high speed transmission systems [3]. The higher the spectral purity of the laser, characterized by the number of longitudinal modes and the linewidth of each mode, the more severe are the effects of optical feedback. One way to prevent these errors from occurring is to protect the laser diode from reflections by adding an optical isolator between the laser and the fiber [4]. The growing emphasis on coherent optical communication systems, with their requirement for frequency-tunable, stable narrow-linewidth sources, has renewed interest in optical feedback effects. A thorough understanding of these effects for long and short external cavities having both wavelength dependent and wavelength independent optical feedback has

assisted in the design of compact frequency-tunable, narrow-linewidth sources, the latest development being integrated two-section DFB lasers [5] and three-section DBR lasers [6].

Feedback effects are normally studied in a controlled fashion by exposing a semiconductor laser diode to optical feedback from an external reflector. The reflector is placed at a fixed distance, L_{ex}, from the laser facet. A large number of researchers (e.g. [7]-[21]) have investigated different aspects of the behavior of the laser in this arrangement. A first attempt to classify a large number of the observed feedback effects was by Tkach et. al. [17] who described 5 regimes of feedback effects. Tkach et. al. obtained their experimental data with a single device, a 1.5 μm DFB-laser, over a range of feedback levels from R_{ex} = -80 dB to -8 dB and found well-defined boundaries between the regimes as a function of feedback level. These values of R_{ex} are lower than the modal reflectivity ($R_1 = R_2 \approx 35\%$ [22]) of the cleaved facet of a semiconductor laser. With an anti-reflection (AR) coating on a laser facet, the reflectivity of this facet can be reduced to a fraction of one percent and therefore made lower than the reflectivity provided by the external reflector.

Regime I to III of [17] are the domains of weak optical feedback with $R_{ex} \ll R_2$. We enter Regime IV of [17] as R_{ex} is increased above ~ -40dB. A large increase of frequency noise, a phenomenon which Lenstra et. al. [13] describe with the term "coherence collapse", marks the transition from Regime III into Regime IV. In the domain of weak feedback the semiconductor cavity is dominant, i.e. the resonance frequencies of the coupled cavity arrangement, and therefore the power in the optical power spectrum, are centered around the resonance frequency of the solitary laser. It is normally necessary to AR-coat the facet closest to the external reflector to be able to enter the domain of strong optical feedback Regime V of [17], where $R_{ex} > R_2$. In this domain, stable laser operation is observed with the external cavity being dominant.

Feedback effects in both weak and strong optical feedback regimes are investigated in this thesis. The focus is on the improvement of the spectral characteristics and frequency-tunability of semiconductor laser diodes. The domain of "coherence collapse" has been of interest to us

with respect to only the feedback level that leads to the transition into this domain of unstable operation.

Chapter 2 provides a review of the basic principles of laser operation as well as the dynamic and spectral characteristics of semiconductor lasers. The representation of the semiconductor laser by the noise driven Langevin-rate equations and the derivation of the dynamic and spectral characteristics from these equations will be discussed. This derivation allows us to link macroscopically observed characteristics of the laser to the physical mechanisms that are responsible for these characteristics. The physical mechanisms involved are in particular the interaction between photons and carriers in the population inversion of the laser, the dependance of the refractive index on the carrier density and the spontaneous emission. We become familiar with the approximations made in the derivation and the simplifications in the theoretical description of the laser characteristics that result from those approximations.

In Chapter 3 the theory for a laser with optical feedback from an external cavity will be reviewed. We stress the assumptions required in order to obtain a basic set of equations that is adequate for the majority of our investigations. These equations can be graphically displayed such that the solutions to the oscillation condition of the compound cavity laser and tuning characteristics are evident. The tuning characteristics provide the change of oscillation frequency and stability of oscillation as parameters of the compound cavity arrangement are changed. From the same graph the effect of optical feedback on the linewidth of the laser, i.e. the spectral spread of the power spectrum around the resonance frequency of the compound cavity, can be seen. Finally, in Chapter 3, we give an overview of the spectral and stability effects observed in the different regimes of optical feedback defined by [17]. We then compare these effects with the predictions of the oscillation condition graph. The latter sections, 3.6 and 3.7, are extensions of the present introductory chapter, as they review optical feedback effects based on the background knowledge provided in Chapters 2 and 3. Also, in these sections, the author's contributions are placed in the framework of previously published work.

In Chapter 4 the case of weak optical feedback is discussed. We provide experimental proof for the prediction made by [21], based on their numerical simulations, that in the presence of multiple solutions to the oscillation condition, the external cavity mode with minimum linewidth carries most of the power. A frequency fluctuation model is introduced that is verified by predicting mode hopping frequencies experimentally observed by [17]. This same model is suitable to explain why the oscillation of the laser in the mode with narrowest linewidth is favored [23]. Finally, a domain of operation within the regime of weak optical feedback is identified that leads to optimized spectral performance of the laser [24].

Narrow linewidth operation of ~ 10 kHz and tunability over tens of nanometers of a semiconductor laser that was AR-coated and exposed to optical feedback from a diffraction grating, has been reported by Fleming et.al. [25] and Wyatt et.al. [26]. Since those first reports, the external grating laser has proven to be a versatile optical source for laboratory use, employable as an externally modulated transmitter [27] or a local oscillator [28] for coherent communications systems as well as a tool to characterize passive integrated-optics components [29], semiconductor lasers [30] and semiconductor laser amplifiers [31]. Despite its frequent use, only a few additional reports [18],[32],[33] have appeared on the characterization of the external grating laser. Although the external grating laser shows many interesting features and dependencies, not all of them are desirable in practical applications of the device. A detailed characterization of the external grating laser is therefore of practical use.

The dependence of the tuning characteristic on the residual reflectivity of the AR-coated laser facet was pointed out by [18]. Also, [18] observed bistability in the tuning characteristic for high values of residual reflectivity. Experimentally, [34] and [35] noted improved stability of oscillation of the external grating laser, if a desired frequency of oscillation is reached by tuning towards lower frequencies. A theoretical explanation for these observations is provided in Chapter 5 of this thesis. The tuning characteristic of lasers with different values of residual reflectivity, R_2, of the

AR-coated facet, and optical feedback from an external grating are investigated, both experimentally and theoretically [36].

We were fortunate to be able to obtain experimental data for a laser with strong frequency selective optical feedback using a setup that had been developed in an independent study [37]. This independent study solved the problems of AR-coating semiconductor lasers [38], choosing suitable optical elements and a suitable geometry for the optical setup and provided the initial characterization of the working external grating laser.

A comparison of the experimental and theoretical results in Chapter 5 relies on an accurate estimate of the level of optical feedback applied to the laser. Estimating the optical feedback from the change in the threshold current of the laser requires accurate modelling of the gain versus current characteristic of the particular laser used in the experiment. We introduce in Chapter 6 a model that allows us to calculate gain and light versus current characteristics for lasers with uncoated and AR-coated facets. Parameter values necessary for this model and specific to the laser used in the experiment are determined from data obtained before and after AR-coating of this laser. We consider the proposed method not only to be useful to determine the optical feedback provided to a laser but also to determine the gain versus current characteristic of individual laser amplifiers [39].

In Chapter 7 we ask what are the spectral properties of an extended cavity semiconductor laser when spatial hole-burning is prevented by not allowing the presence of standing waves in the semiconductor gain medium. For this purpose, a semiconductor laser with two AR-coated facets, i.e. a travelling wave amplifier, was placed together with an optical isolator in a 17-cm long fiber ring. The spectral properties of this unidirectional semiconductor fiber ring laser are compared in Chapter 7 to the properties of the semiconductor fiber ring laser without optical isolator.

2. THEORY FOR THE SOLITARY LASER

2.1. INTRODUCTION

In this chapter the basic mechanisms that are responsible for the characteristics of a semiconductor laser are reviewed. We then consider the rate equation model and outline the procedure used to obtain laser characteristics from the rate equations, in particular the output power, frequency noise and linewidth of a laser.

2.2. BASIC PRINCIPLES OF LASER OPERATION

Gain and feedback are necessary attributes of an oscillator. An optical oscillator, or laser, shows absorption, spontaneous emission and stimulated emission of radiation. Gain or amplification of light is possible through the stimulated emission process, and the in-phase feedback required is achieved by embedding the gain medium in an optical resonator configuration. The conditions for resonance are then [40,41]

1. the roundtrip phase shift, ϕ_{RT}, within the cavity is a multiple of 2π

$$\phi_{RT} = m \cdot 2\pi \qquad m = 1,2,3, \ldots \tag{2.1}$$

$$= \frac{2\omega_m L_{in}}{v_{Ph}} \tag{2.2}$$

where L_{in} is the length of the semiconductor laser cavity, v_{Ph} is the phase velocity in the active region of the semiconductor laser and ω_m is the frequency in radians/second of the m^{th} longitudinal mode of the solitary laser.

2. the accumulated gain for one roundtrip is equal to unity

$$G_{RT} = R_1 R_2 \, e^{2 \cdot (g(\omega,n) - \alpha_s) \cdot L_{in}} = 1 \tag{2.3}$$

where R_1 and R_2 are the reflectivities of the cavity end faces. α_s is the material loss per unit length in the active region. The gain per unit length, $g(\omega,n)$, when plotted for a given carrier density, n, versus the frequency is called the gain profile. Temperature and carrier density influence the shape and the center frequency of the gain profile of a semiconductor laser.

Assuming that the loss due to the laser facets can be distributed over the active region, (2.3) can be written in the form

$$\alpha_s + \alpha_R - g(\omega,n) = 0 \qquad (2.4)$$

where $$\alpha_R = -(1/2L_{in})\cdot\ln(R_1R_2) \qquad (2.5)$$

is the facet loss per unit length.

The maximum of the gain profile and the periodic resonances of the Fabry-Perot resonator determine the frequency of laser oscillation (Fig. 2.1). Index guided 1.3 μm and 1.55 μm lasers oscillate in 4 to 6 strong longitudinal modes, where individual modes are competing for the available gain (homogeneous broadening [42],[43]) and hence do not oscillate simultaneously. The experimental work reported on in this

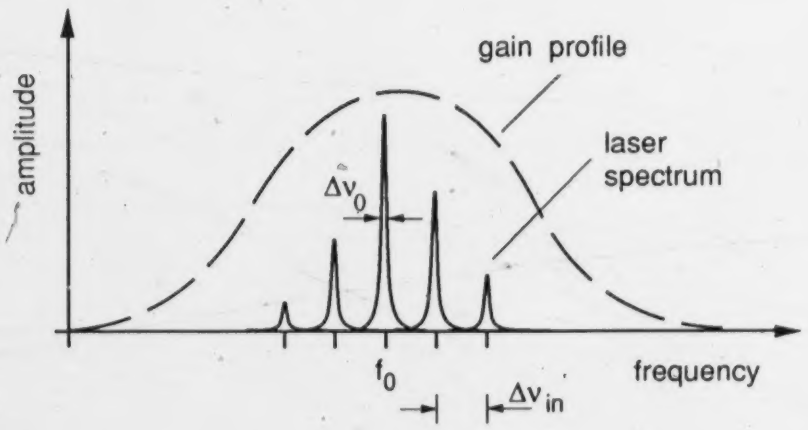

Fig. 2.1: Sketch of the gain profile and optical power spectrum of a semiconductor laser.

thesis has been carried out using semiconductor lasers emitting at 1.3 μm wavelength. The conversion from a change in optical frequency df to a change in wavelength $d\lambda$ is described by the equivalence $d\lambda/df = -\lambda/f$, which means that 17.8 GHz is equal to .1nm @ 1.3 μm. Defining the linewidth and longitudinal mode spacing in the optical frequency domain with the symbol $\Delta\nu$, approximate values for the parameters indicated in Fig. 2.1 are $\Delta\nu_0 \approx 500$ MHz for the linewidth of the individual modes in the case of multi-mode operation and $\Delta\nu_0 \approx 100$ MHz in the case of single mode operation [44]. Also, $\Delta\nu_{in} \approx 150$ GHz or .84 nm for the separation of longitudinal modes. The FWHM (full width at half maximum) of the gain profile is ~ 10.7 THz or 60 nm.

The spontaneous emission of light is responsible for the noise properties of the laser. Five quantum noise properties can be specified [45]: the probability density function for the total number of photons, prob(S), and for the instantaneous frequency, prob(ω), also the three frequency-domain representations for these probabilities, the AM-noise spectrum, $W_S(\omega)$, FM-noise spectrum, $W_{\Delta\omega}(\omega)$, and optical power spectrum, $W_E(\omega)$.

The cavity of a semiconductor laser is short ($\approx$.3mm) and the reflectivity of the endfaces relatively low (R=.35). This accounts for the short photon lifetime within the cavity and hence for the low quality of the resonator of a semiconductor laser compared to that of a gas laser [40],[41]. Due to the low quality of the semiconductor cavity, frequency fluctuations caused by spontaneously emitted photons of random phase are not suppressed effectively. This is in contrast to fluctuations in the amplitude of the oscillation, which are reduced significantly by the gain saturation process. With the instantaneous gain of the laser reacting to photon-number fluctuations due to spontaneous emission, the phase-fluctuations of a semiconductor laser are enhanced due to the coupling between gain and index of refraction [45],[46],[47].

The characteristics of lasers will be treated in the following section using the rate equations for the two independent variables carrier number, N, and photon number, S, in the active region of the laser. The noise properties that are observed macroscopically are the response of the laser to stimuli provided by the spontaneous emission

process resulting in photon number and carrier number fluctuations. These stimuli are represented in a semiclassical treatment of the laser by adding Langevin noise terms [48] to the rate equations. These noise terms represent the effect of quantum fluctuations of the independent variables of carrier number and photon number and thus allow us to describe the laser adequately without using a more complicated quantum mechanical treatment.

2.3. LANGEVIN RATE EQUATIONS

2.3.1. *Introduction*

Following the normalization chosen by Lax [49], we describe the electric field of the laser as

$$E(t) = E_0(t)\, e^{j\omega_0 t}\, e^{j\phi(t)} \tag{2.6}$$

with

$$E_0(t) = S_0^{1/2} + \hat{e}(t) \tag{2.7}$$

where $E_0(t)$ is the amplitude of the electric field, normalized in such a way that S_0 is the average number of photons in the lasing mode in the active region, ω_0 is the frequency of the semiconductor cavity resonance and $\hat{e}(t)$ and $\phi(t)$ represent amplitude and phase fluctuations. In equation (2.6) we neglect spatial variations of the electric field in the active medium of the laser. Also, we consider in this chapter only the rate equations for a single longitudinal mode of the laser.

The laser behavior is described by either the real and complex part of the electric field, $E(t)$, and the carrier density, $N(t)$, or by the three variables S, ϕ and N. In both cases, a set of three real-valued differential equations governs the dependence of these variables on time. To account for the fluctuations of the variables in time Langevin forces are included in these equations. This semiclassical treatment of the laser is a result of the work by Lax and Louisell [50]. They started from a full quantum mechanical model of a laser. They then transformed this quantum problem into a classical problem of calculating statistical properties of a fluctuating wave field by adding Langevin forces to the set of equations that describe the classical averages of the wave field.

In general, for a system with variables $\underline{a} = (a_1, a_2, a_3)$, the Langevin rate equations are

$$da_i/dt = A_i(\underline{a},t) + F_i(t) , \quad i = (1,2,3) \tag{2.8}$$

The A_i are chosen so that the time-average of $F_i(t)$ satisfies $\langle F_i(t) \rangle = 0$, a quite important condition. Without the Langevin-forces, (2.8) is the set of rate equations that governs the time averaged values of the variables a_i.

It was pointed out earlier that the Langevin forces represent the statistical properties of the variables $a_i(t)$. Without the restoring force caused by the drift term A_i, which tries to maintain the steady state value, the variables $a_i(t)$ would move away from the steady state value in a random walk driven by the random force $F_i(t)$ [51]. A process of this type is called diffusion. In a semiconductor laser the major source of fluctuations is spontaneous emission [46]. In most cases we can assume that the random forces have no memory, since spontaneous emission is correlated only for the carrier scattering time of approximately 10^{-13}s. The autocorrelation function of the random forces is then given by

$$\langle F_i(t)\ F_j(t-\tau) \rangle = 2D_{ij}\ \delta(\tau) \tag{2.9}$$

where D_{ij} is called the diffusion coefficient [48]. To calculate the frequency fluctuations and the lineshape of the laser it is necessary to make an assumption on the amplitude distribution of the Langevin forces. It is generally assumed that this distribution is Gaussian [47].

The equation for the complex variable E(t) is given by [47]

$$\frac{dE}{dt} = \left\{ -j\omega_0(n) + \frac{1}{2}\left[G(n) - \tau_p^{-1}\right] \right\} E(t) + F_E(t) \tag{2.10}$$

where τ_p is the photon lifetime and n is the carrier density defined by N/V where V is the volume of the active region. $F_E(t)$ is the Langevin force term for E(t), $\omega_0(n)$ is the angular frequency of the solitary laser

$$\omega_0(n) = \omega_0(n_{th}) + \frac{1}{2}\alpha\,[G(n) - \tau_p^{-1}] \tag{2.11}$$

and G(n) is the carrier dependent gain per unit time

$$G(n) = G_n\cdot(n-n_{tr}) \tag{2.12}$$

$$= \tau_p^{-1} + G_n\cdot(n-n_{th}) \tag{2.13}$$

where n_{tr} is the transparency carrier density, n_{th} the carrier density at lasing threshold, $G_n = \partial G/\partial n$ the gain coefficient, and α is the linewidth enhancement factor [46]. Gain and loss are equal at threshold, therefore

$$G(n_{th}) = \tau_p^{-1} = (\alpha_s + \alpha_R)\cdot v_{gr}. \tag{2.14}$$

where v_{gr} is the group velocity in the active medium.

The diffusion coefficients for the complex noise force $F_E(t)$ [47],[49],[52],[53],[54] are defined by

$$2D_{EE} = 2D_{E^*E^*} = 0 \tag{2.15}$$

and

$$2D_{EE^*} = R_{sp} \tag{2.16}$$

where R_{sp} is the spontaneous emission rate coupled into the lasing mode.

It is often convenient to express the complex equation (2.10) in terms of two real equations for the photon number, $S(t) = E(t)\cdot E^*(t) = |E_0(t)|^2$, and the phase, $\phi(t)$, [47]:

$$\frac{dS}{dt} = [G(n) - \tau_p^{-1}]\,S(t) + R_{sp} + F_S(t) \tag{2.17}$$

and

$$\frac{d\phi}{dt} = \frac{\alpha}{2}\,[G(n) - \tau_p^{-1}] + F_\phi(t) \tag{2.18}$$

where $F_S(t)$ and $F_\phi(t)$ are the Langevin forces for S and ϕ. The rate equation for the carrier number is

$$\frac{dN}{dt} = \frac{I_a}{q} - \frac{N}{\tau_e} - G(n)\cdot S(t) + F_N(t) \qquad (2.19)$$

where (I_a/q) represents the pumping term in carriers per second, I_a is the current in the active region, q the electron charge, τ_e the electron lifetime and $F_N(t)$ is the Langevin force for N. The diffusion coefficients of $F_S(t)$ and $F_\phi(t)$ are [55],[47]

$$2D_{SS} = 2\,R_{sp}\cdot S, \quad 2D_{\phi\phi} = R_{sp}/2S \qquad (2.20)$$

$$2D_{S\phi} = 0, \quad \text{and} \quad 2D_{NS} = -R_{sp}\cdot S$$

We notice that the zero mean noise-force $F_E(t)$ for the amplitude of the electric field in (2.10) is replaced by the contribution $R_{sp}+F_S(t)$ to the intensity of the optical field in equation (2.17). The transformation of the noise force for the field amplitude to a noise force for the intensity leads to a noise force that has the finite value of R_{sp} when averaged over time. It can be shown that R_{sp} is equal to the spontaneous emission that is coupled into the lasing mode. R_{sp} is therefore one of the previously mentioned small corrections to the steady state value in the rate equations that is caused by the fluctuations.

For completeness, we will also give the differential equation for $E_0(t)$ [56]:

$$\frac{dE_0(t)}{dt} = \frac{1}{2}\left[G(N) - \tau_p^{-1}\right] E_0(t) + R_{sp}/2E_0(t) + F_{E_0}(t) \qquad (2.21)$$

where the diffusion coefficient of $F_{E_0}(t)$ is

$$2D_{E_0E_0}(t) = \frac{1}{2} R_{sp} \qquad (2.22)$$

The rate equations have proven to be a powerful tool for researchers to analyze and predict various aspects of the behavior of a laser. These include the dynamics of laser operation, noise characteristics and the response of the laser to injected light, either a time-delayed

portion of its own light (optical feedback) or injection of light from a second laser.

The number of terms in the rate equation is rather small. Nevertheless, the variety of phenomena it can explain is quite large and it is often not obvious which elements or interaction between elements explains a certain behavior of the laser. In the following sections 2.3.2 to 2.3.6 different approaches will be described that can be used to derive the steady state characteristics and dynamics of the laser from the rate equations. In section 2.4 we will focus on the noise characteristics of the laser and describe how the typical measures of the noise-characteristics (AM-noise, FM-noise, optical power spectrum and linewidth) are derived from the rate equations and which assumptions are generally made to arrive at closed form solutions for these noise characteristics.

2.3.2. *Numerical Simulations*

The set of three real-valued rate equations (2.18), (2.19) and (2.21) for E_0, ϕ and N, can be integrated numerically starting from a set of initial values E(0), $\phi(0)$ and N(0) at time t = 0. In these calculations, the noise forces $F_{E0}(t)$, $F_{\phi}(t)$ are represented by random number generators with autocorrelation function $2D_{E_0E_0}\cdot\delta(\tau)$ and $2D_{\phi\phi}\cdot\delta(\tau)$, respectively. The Langevin noise term $F_N(t)$ is of minor importance for the principle noise-characteristic of the laser, FM-noise and linewidth [57], and can be neglected. Possible ways to represent the noise terms in calculations and considerations regarding the stepsize for the integration are specified in [56] and [58]. As a result of the numerical integration one obtains a sample of the time evolution of E, ϕ and N. The FM-noise spectrum $W_{\Delta\omega}(\omega)$ and the field power spectrum $W_E(\omega)$ for the sample can then be calculated [56]; they are equal to the square of the magnitude of the Fourier transform of $[d\phi(t)/dt]$ and E(t), respectively. The linewidth of the laser is then equal to $W_{\Delta\omega}(0)/2\pi$ (see Chapter 2.4.4).

2.3.3. *Output Power*

The output power of a laser under steady-state conditions can be calculated from the number of photons in the active cavity, S, and the rate of loss of photons due to output coupling. We obtain the steady-state value of S from (2.17) by setting dS/dt = 0 and neglecting the noise forces:

$$S = -\frac{R_{sp}}{G-\gamma} = -\frac{R_{sp}}{v_{gr}\cdot(g-\alpha_L)} \tag{2.23}$$

where $\gamma = \tau_p^{-1}$ is the rate of loss of photons, $\alpha_L = \alpha_s + \alpha_R$ is the loss per unit length in the active region and G is the rate of gain for a given carrier density n and equals $g\cdot v_{gr}$. According to (2.23) the laser can be viewed as a regenerative noise amplifier ([59], p. 228). R_{sp} is amplified by $(G-\gamma)^{-1}$. The rate of spontaneously emitted photons, R_{sp}, coupled into the lasing mode per unit time is

$$R_{sp} = n_{sp}\cdot K_R\cdot v_{gr}\cdot g \tag{2.24}$$

where

$$n_{sp} = \left(1 + \exp\left[\frac{\hbar\omega_0 - qV}{kT}\right]\right)^{-1}. \tag{2.25}$$

n_{sp} is the spontaneous emission factor, accounting for the increase in spontaneous transitions in a semiconductor laser due to the incomplete inversion [47], and

$$K_R = \frac{(r_1 + r_2)\,(1 - r_1 r_2)}{2 r_1 r_2 \ln(r_1 r_2)} \tag{2.26}$$

accounts for the increase of the spontaneous emission that is coupled into the lasing mode due to the loss of power at the facets [60]. The same factor K_R appears, if the z-dependence of the photon density within the active cavity is taken into account [61],[22]. For high-reflecting

facets ($r_1 = r_2 = 1$), i.e. lack of z-dependence of the photon density, we obtain from (2.26), $K_R = 1$; for a typical semiconductor laser $r_1^2 = r_2^2 = .35$), $K_R = 1.13$. From (2.23) and (2.24) we obtain

$$S = K_R \cdot n_{sp} \cdot \frac{g}{\alpha_L - g} \tag{2.27}$$

The output power P_1^{out} and P_2^{out} emitted from the two laser facets when the two reflectivities R_1 and R_2 are equal is ([59], p.227)

$$P = P_1 = P_2 = (1/2) \cdot \hbar\omega \cdot v_{gr} \cdot \alpha_R \cdot S \; . \tag{2.28}$$

$\hbar\omega = 0.152 \times 10^{-18}$ Ws at 1.3 μm is the energy per photon and $v_{gr} \cdot \alpha_R$ the rate of loss of photons through a laser facet.

For a laser with $P_1 = 2$ mW in a single mode and $L_{in} = 250$ μm, $R_1 = R_2 = 35\%$ and $v_{gr} = 0.75 \cdot 10^{10}$ cm/s we obtain from (2.28) $S = 0.94 \cdot 10^5$ photons for the number of photons in the lasing mode. Using $\alpha_L = \alpha_S + \alpha_R = 62$ cm^{-1} and $n_{sp} = 1.7$ we calculate the gain at $P_1 = 2$ mW from (2.27) and (2.28) to be $g = 61.99874$ cm^{-1}, at $P_1 = 0.2$mW, $g = 61.985$ cm^{-1} and at $P_1 = 0.02$mW, $g = 61.851$ cm^{-1}. With increasing output power the gain g approaches the value of the loss α_L asymptotically, a process called "gain saturation". In many cases it is sufficient to assume gain and loss to be equal above lasing threshold. However, to calculate LI-curves in multimode operation the difference between α_L and g is of importance (Chapter 6).

2.3.4. *Laser Dynamics*

The two time constants found in the rate equations are the photon lifetime $\tau_p \sim 2$ ps and the carrier lifetime $\tau_e \sim 2$ ns. The time constant that governs a change of the output power of a laser depends on the mechanism used to create this change in output power: we can (1) change the injection current to the laser or (2) inject a short pulse of light into the laser.

In steady state operation an equilibrium exists between the loss of carriers due to spontaneous and stimulated emission and the gain of carriers due to the injection current. The carrier density increases or decreases until this equilibrium is reached in response to any disturbance. A steplike increase of the injection current leads to an initial increase of the carrier density which in turn increases the gain, increases stimulated emission and decreases the carrier density due to the increased stimulated emission. The response to the steplike increase of the injection current is therefore an increase of the output power governed by a damped relaxation oscillation with frequency f_R where [59]

$$f_R = \left[\frac{1 + G_n \cdot N_{tr} \cdot \tau_e}{\tau_p \tau_e} \left(\frac{I}{I_{th}} - 1 \right) \right]^{1/2} \tag{2.29}$$

Here N_{tr} is the number of carriers in the active region at transparency, where stimulated emission and absorbtion are in balance. Typically $G_n \cdot N_{tr} \cdot \tau_p \sim 1$ ([59], p. 247) and $f_R \sim 2 \ldots 10$ GHz.

Considerably faster changes in the output power of a laser can be achieved by light injection, if the laser is operated just below threshold [62], [63]. In this situation the carrier density is not high enough to obtain a roundtrip gain that compensates the resonator loss and the laser does not oscillate on its own. However, light that is injected into the cavity can take advantage of the high gain and is amplified. The large amount of stimulated emission necessary to amplify the injected light leads to an abrupt decrease of the carrier density and a loss of amplification until the carrier density recovers. The time constants governing the increase in output power due to light injection and the subsequent loss in amplification due to the abrupt decrease of the carrier density are on the order of the photon lifetime τ_p. The above principle can be utilized by placing a laser in an external cavity and modulating the injection current immediately below threshold with the peak current exceeding threshold and a frequency that corresponds to the round-trip time in the external cavity [64],[63]. In this configuration the laser is modelocked and has been reported to produce pulse trains with individual pulse widths of the order of a few ps [63].

2.3.5. *Linearization of the Rate Equations*

To derive the small signal response of the laser and to arrive at a closed form solution for some of the noise characteristics it is necessary to linearize the rate equations in the vicinity of the steady state operating point. The steady state values of S and N are obtained [57] from (2.17) and (2.19) by setting $\partial S/\partial t = \partial N/\partial t = 0$ and neglecting the Langevin forces. We obtain,

$$S = -\frac{R_{sp}}{G\cdot\gamma} \tag{2.30}$$

and

$$\frac{I_a}{q} = \frac{N}{\tau_e} - G(N)\cdot S. \tag{2.31}$$

We introduce the deviations $\Delta s(t)$ and $\Delta n(t)$ from the steady state values of S and N

$$N(t) = N + \Delta n(t) \tag{2.32}$$

$$S(t) = S + \Delta s(t) \tag{2.33}$$

The dependence of the gain, G, and the carrier lifetime, τ_e, on N and S are expressed in linearized form as

$$G = G_0 + G_N\cdot\Delta n - G_S\cdot\Delta s \tag{2.34}$$

$$\tau_e = \tau_{e0} + T_N\cdot\Delta n \tag{2.35}$$

where $G_N = \partial G/\partial N$ and $T_N = \partial\tau_e/\partial N$. Δn and Δs are considered as time dependent variables. The spectral hole burning ([59], p. 238) is taken into account with the coefficient $G_S = \partial S/\partial N$.

Following Henry [57], we neglect quadratic terms in Δn and Δs and obtain from (2.17) to (2.19) and (2.32) to (2.35)

$$\dot{\Delta n} = \Gamma_N\cdot\Delta n - G_0\cdot\Delta s + F_N(t) \tag{2.36}$$

$$\dot{\Delta s} = G_N\cdot S\cdot\Delta n - \Gamma_S\cdot\Delta s + F_S(t) \tag{2.37}$$

$$\dot{\phi} = \frac{\alpha}{2} G_N \cdot \Delta n + F_\phi(t) \tag{2.38}$$

where

$$\Gamma_N = (N/T_N) + G_N \cdot S \tag{2.39}$$

and

$$\Gamma_S = G_S \cdot S + (R/S). \tag{2.40}$$

Following the steps taken by Henry [57] to linearize the rate equations provides us with the definition of the parameters that will appear in the expression for the noise-characteristics. The Fourier analysis of (2.36) to (2.38) leads to a complex pair of poles, representing the relaxation resonance. The damping rate, Γ, and radian frequency, $\Omega = 2\pi f_R$, of the relaxation resonance are [57]

$$\Gamma = \frac{1}{2} (\Gamma_N + \Gamma_S) \tag{2.41}$$

and

$$\Omega = (G \cdot G_N \cdot S + \Gamma_N \Gamma_S - \Gamma^2)^{1/2}. \tag{2.42}$$

2.4. NOISE CHARACTERISTICS

2.4.1. *Definitions*

The AM noise, FM noise and optical power spectrum (Fig. 2.2) are noise characteristics defined in the frequency domain. The rate equations describe the behavior of the laser in the time domain. They include the Langevin noise terms, which allow us to calculate sample functions for the change of S, ϕ and N with time, but no closed form solutions of S(t), ϕ(t), and N(t). However, if we know the statistical properties of $F_S(t)$, $F_\phi(t)$, and $F_N(t)$, a closed form solution of the autocorrelation functions of S, ϕ and N can be obtained. According to the Wiener-Kintchine theorem, the power spectra can then be obtained from the autocorrelation functions through a Fourier transform, if we are dealing, as we are, with a stationary process.

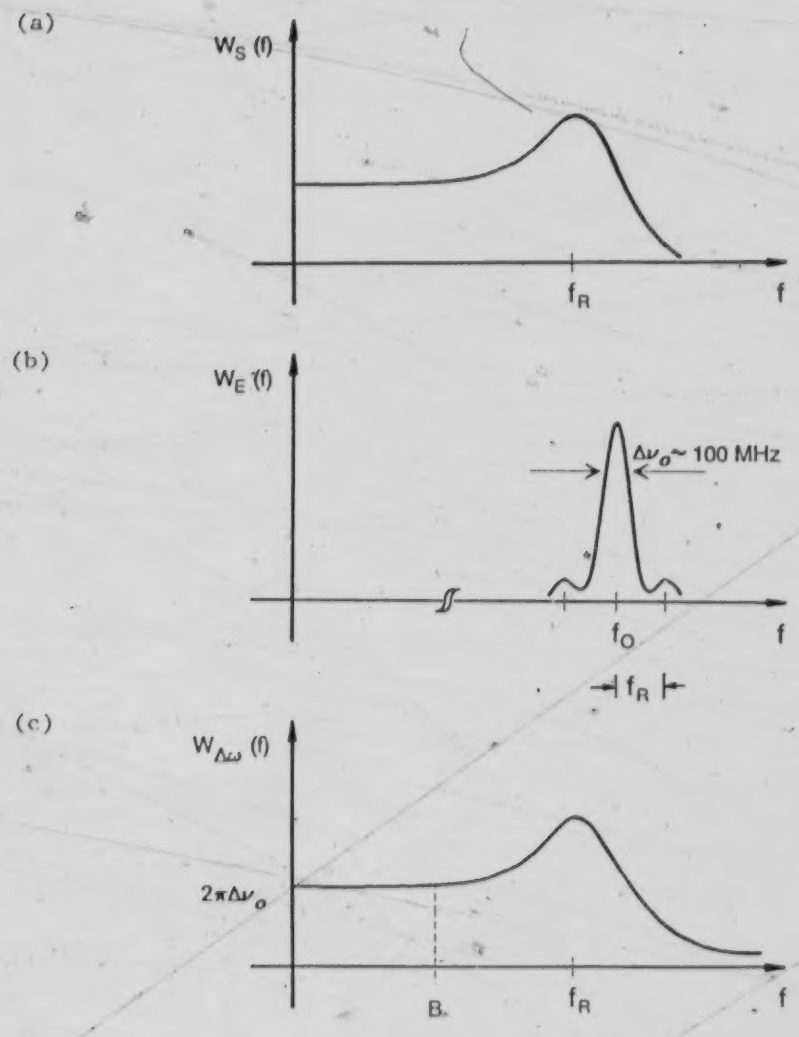

Fig. 2.2: Sketch of (a) the AM-noise spectrum, (b) the optical power spectrum and (c) the FM-noise spectrum.

2.4.2. *AM-Noise*

AM-noise in semiconductor lasers [65],[66] is essentially due to shot noise attributable to the quantized nature of light. The amplitude of the laser output is effectively clamped due to the nonlinear process

of gain saturation, leading to a good suppression of AM noise. After each stimulus caused by spontaneous emission the amplitude returns to its steady state value with a damped relaxation oscillation of frequency f_R. This relaxation leads to an enhancement of the AM noise at f_R (Fig. 2.2(a)).

2.4.3. *Power Spectrum*

Phase fluctuations caused by spontaneously emitted photons are not suppressed effectively, due to the low quality of the semiconductor cavity. Frequency noise is therefore the dominant feature of semiconductor lasers and we will be principally concerned with this characteristic. The optical power spectrum is a function of amplitude and phase fluctuations. Since the FM-noise is the dominant feature, the optical power spectrum will be derived in the following from only the phase noise characteristic of the laser.

Vahala [65] has shown that the only feature lost in the optical power spectrum if the AM noise is neglected is a small asymmetry in the side peaks of the power spectrum due to the coupling in the amplitude and phase fluctuations. For the calculation of the linewidth of the laser, it will be shown later that even the simplistic model that neglects the time constant involved in the gain saturation process (f_R) leads to very accurate results (in the adiabatic analysis: it is assumed that N follows S immediately which leads to a description of the laser with a Van der Pol equation).

The optical power spectrum $W_E(\omega)$ of the laser is mathematically defined as the square of the Fourier transform of the electric field,

$$W_E(\omega) = \frac{1}{2\pi} \left| \int_{-\infty}^{+\infty} E(t)\, e^{j\omega t}\, dt \right|^2 . \qquad (2.43)$$

Using the Wiener-Khintchine theorem, valid for stationary processes, $W_e(\omega)$ is also given by the Fourier transform of the autocorrelation function $R_E(\tau)$ of E(t)

$$W_E(\omega) = \frac{1}{2\pi} \int_{-\infty}^{+\infty} R_E(\tau)\, e^{j\omega\tau}\, d\tau \qquad (2.44)$$

where

$$R_E(\tau) = \langle E(t+\tau)^* E(t) \rangle .$$

Finally, $W_e(\omega)$ can be express in terms of the statistical average of $E(\omega)$ ([67], sect. 118)

$$\delta(\omega-\omega') \cdot W_E(\omega) = \langle E(\omega')^* \cdot E(\omega) \rangle \qquad (2.45)$$

where

$$E(\omega) = \frac{1}{2\pi} \int_{-\infty}^{+\infty} E(t)\, e^{j\omega t}\, dt \qquad (2.46)$$

is the Fourier transform of $E(t)$. All three definitions of $W_e(\omega)$ are used in the following derivation of the power spectrum and the linewidth of the laser from the rate equations.

2.4.3.1. *Below Lasing Threshold*

Following Henry [47], we make different assumptions for the two regimes of laser operation below threshold and above threshold, to be able to perform the analysis. Below threshold a large proportion of the radiation is due to spontaneous emission. The pool of carriers is depleted by a constant rate of spontaneous emission and replenished at the same rate through carrier injection. Changes in the carrier density due to stimulated emission can be neglected. The gain G due to stimulated emission, being a linear function of the carrier density, can be assumed to be constant. Since the rate of loss, γ, is much larger than G the difference $\Delta G = G-\gamma$ can also be assumed constant.

The above argument becomes very clear when we consider the situation above threshold, where the gain is almost equal to the loss, and even small relative changes in G translate into large relative changes of ΔG. In addition, above threshold the rate of stimulated emission is much larger than the rate of spontaneous emission into the lasing mode and

the influence of changes in the rate of stimulated emission on the carrier density cannot be neglected.

Below threshold, with ΔG assumed to be constant, in particular independent of $|E(t)|^2$, (2.10) is a linear equation and can be written in terms of its Fourier components

$$E(\omega) = \frac{F_E(\omega)}{j(\omega_0 + \alpha \frac{\Delta G}{2} - \omega) - \frac{\Delta G}{2}} \tag{2.47}$$

where $F_E(\omega)$ is the Fourier transform of $F_E(t)$. It can be shown [57] that the autocorrelation function computed from the Fourier components has the same diffusion coefficient as that computed from the time components, thus (2.9) and (2.16) lead to

$$< F_E(\omega')^* \cdot F_E(\omega) > = R_{sp}\, \delta(\omega-\omega') \tag{2.48}$$

Using (2.45), (2.47) and (2.48), we obtain for the optical power spectrum below threshold [57]

$$W_E(\omega) = \frac{R_{sp}}{[\omega_0 + \alpha \frac{\Delta G}{2} - \omega]^2 + (\frac{\Delta G}{2})^2} \tag{2.49}$$

which describes a Lorentzian lineshape with linewidth (FWHM) of

$$\Delta\nu_{ST} = \frac{\Delta G}{2\pi} = \frac{R_{sp}}{2\pi S} \tag{2.50}$$

(2.50) is the Schawlow-Townes formula for the linewidth of a laser and $\Delta G = R_{sp}/S$ is the steady state value derived from (2.17) by setting $\partial S/\partial t = 0$ and noting that $<F_E(t)> = 0$.

2.4.3.2. *Above Lasing Threshold*

Above threshold the laser radiation is predominantly stimulated emission. If S is large the difference between gain and loss, $\Delta G = G - \gamma = R_{sp}/S$, is small. Differentiation of S with respect to G yields

$$\frac{dS}{S} = -\frac{d\Delta G}{\Delta G} . \tag{2.51}$$

From (2.51) we observe that for small ΔG an increase in gain, $d\Delta G$, results in a large value of dS. However, this large increase in S reduces the carrier density, n, and therefore reduces the gain. Therefore, above threshold the absolute value of G is almost constant and only slightly less than γ, a process that has been termed earlier gain saturation (Section 2.3.3). However, ΔG, the difference of two large quantities, does change and we can no longer assume $\Delta G = 0$.

If S is deviating from its steady-state value, N will change and with it ΔG, which in turn counteracts the initial change in the number of photons S in the mode very effectively. This feedback mechanism effectively clamps the number of photons in the mode. Since the line broadening is primarily due to low frequency fluctuations, and the feedback mechanism process is fast, limited only by the relaxation oscillation frequency, we can neglect $\partial S/\partial t = 0$ and obtain from (2.17)

$$\Delta G = -\frac{R_{sp}}{S} - \frac{F_S(t)}{S} \tag{2.52}$$

and, from (2.18), neglecting the constant term R/S

$$\frac{d\phi}{dS} = -\frac{\alpha}{2S} F_S(t) + F_\phi(t). \tag{2.53}$$

We use (2.44) to calculate the optical power spectrum above threshold from the autocorrelation function of the complex electric field

$$R_E(t) = \langle E(t'+t)^* E(t') \rangle. \tag{2.54}$$

Stationarity makes $R_E(t)$ independent of a timeshift and therefore

$$R_E(t) = \langle E(t)^* E(0) \rangle. \tag{2.55}$$

We assume that amplitude fluctuations can be neglected and obtain using (2.6) in (2.55)

$$\langle E(t)^* \cdot E(0) \rangle = S\, e^{j\omega_0 t} \langle \exp(j \cdot \Delta\phi(t)) \rangle \tag{2.56}$$

where $$\Delta\phi(t) = \phi(t) - \phi(0). \tag{2.57}$$

In the case where $\Delta\phi(t)$ is a variable with Gaussian distribution [48],[55] it can be shown by integration that ([68], eq. (1.1.96))

$$\langle \exp(j\Delta\phi(t)) \rangle = \exp[-\frac{1}{2} \langle \Delta\phi(t)^2 \rangle]. \tag{2.58}$$

$\Delta\phi(t)$ can be obtained from (2.53) by integration

$$\Delta\phi(t) = \int_0^t F_\phi(t)\, dt - \frac{\alpha}{2S} \int_0^t F_S(t)\, dt. \tag{2.59}$$

From the definition of the diffusion coefficients (2.9) and relation (2.59) we obtain

$$\langle \Delta\phi(t) \cdot \Delta\phi(t) \rangle = 2D_{\phi\phi} \cdot |t| + (-\frac{\alpha}{2S})^2 \cdot 2D_{SS} \cdot |t| - \frac{\alpha}{2S} \cdot 2D_{\phi S} \cdot |t|$$

and with the values of the diffusion coefficients in (2.20)

$$\langle \Delta\phi(t)^2 \rangle = \frac{R_{sp}}{2S} (1 + \alpha^2) \cdot |t|. \tag{2.60}$$

With the aid of (2.54), (2.56), (2.58) and (2.60) we obtain

$$R_E(t) = S\, e^{j\omega_0 t} \exp[-\frac{R_{sp}}{4S} (1 + \alpha^2) \cdot |t|] \tag{2.61}$$

The Fourier transform of this autocorrelation function is given in Tables and we find that the optical power spectrum of the laser above threshold has again a Lorentzian lineshape

$$W_E(\omega) = \frac{2\pi\Delta\nu_0}{(\pi\Delta\nu_0)^2 + (\omega - \omega_0)^2} \tag{2.62}$$

with the linewidth

$$\Delta\nu_0 = \frac{R_{sp}}{4\pi S}(1 + \alpha^2) \ . \tag{2.63}$$

2.4.3.3. *Comparison of Linewidths*

We summarize the preceding linewidth results (eqs. (2.50) and (2.63)):

$$\Delta\nu_{ST} = \frac{R_{sp}}{2\pi S} \qquad \text{below threshold} \tag{2.64}$$

and

$$\Delta\nu_0 = \frac{1}{2}\Delta\nu_{ST}(1 + \alpha^2) \qquad \text{above threshold.} \tag{2.65}$$

The linewidth is essentially a measure of the low-frequency component of the FM-noise of a laser. Spontaneous emission events produce fluctuations of the phase and intensity of the lasing field. Henry has depicted this mechanism graphically in a vector diagram ([46], Fig. 1). The magnitude of the phase fluctuations increases with the rate of spontaneously emitted photons, R_{sp}, and decreases if an increased number of photons, S, is stored in the active cavity; this intuitively confirms the relation (2.64) between linewidth, R_{sp} and S.

Compared to the linewidth below threshold, the linewidth above threshold is increased by a factor of $(1 + \alpha^2)/2$. The reduction of the linewidth by the factor 2 is due to the suppression of intensity

fluctuations above threshold [47]. The suppression of intensity fluctuations ($\partial S/\partial t = 0$) however is achieved at the expense of increased gain fluctuations (2.52) which in turn enhance the phase fluctuations (2.53), through the coupling between gain and refractive index expressed by α, thus accounting for the increase in linewidth by $(1 + \alpha^2)$ [47].

For a 1.3 μm laser, $\alpha \sim 6$, which results in an increase of the linewidth due to the coupling between gain and oscillation frequency by a factor of $(1 + \alpha^2) \sim 40$.

2.4.3.4. *Resonant Noise Enhancement*

In this section we expand on the discussion of $\langle\Delta\phi(t)^2\rangle$, (2.60), and will include the effect of carrier noise and relaxation oscillation. This discussion will enable us to justify the validity of the approximate analysis in the preceding three sections. From the Fourier analysis of the linear rate equations (2.36) - (2.38) of small deviations, Δn, Δs and ϕ, Henry [57] and Vahala et. al. [65] have derived that

$$\langle\Delta\phi(t)^2\rangle = \frac{R_{sp}}{2S}\{(1 + \alpha^2 A)\cdot t + \frac{\alpha^2}{2\Gamma\cos\delta}[A(\cos 3\delta - \exp(-\Gamma t)\cdot\cos(\Omega t - 3\delta)) + B(\cos\delta - \exp(-\Gamma t)\cdot\cos(\Omega t - \delta))]\} \quad (2.66)$$

where

$$A = [(1 + \frac{\Gamma_S}{G})^2 + \frac{\Gamma_S{}^2 S}{G^2 R_{sp} S}]\cdot[1 + \frac{\Gamma_N\cdot\Gamma_S}{G\cdot G_N\cdot S}]^{-2} \quad (2.67)$$

$$B = [\frac{G_N(N/\tau_{eo} + R_{sp}\cdot S}{G\cdot R_{sp}}]\cdot[1 + \frac{\Gamma_N\cdot\Gamma_S}{G\cdot G_N\cdot S}] \quad (2.68)$$

and

$$\cos(\delta) = \frac{\Omega}{(\Omega^2 + \Gamma^2)^{1/2}}\,. \quad (2.69)$$

The definitions of Γ, Γ_S, Γ_N, G_N, τ_{eo} and Ω are the same as in Section 2.3.5.

From (2.67) we find that A = 1 if $\Gamma_S = 0$, i.e. if spectral holeburning is neglected. For A = 1, the first term of (2.66) is identical to the expression derived for $\langle\Delta\phi(t)^2\rangle$ assuming that $\partial S/\partial t = 0$ (2.60). Only for time t short compared to the inverse of the damping rate of the relaxation oscillation $1/\Gamma$ (~.5 nsec) are the additional terms in (2.66) significant and (2.60) is no longer an accurate representation for $\langle\Delta\phi(t)^2\rangle$. From (2.68), it is found that B = 0 if $G_N = 0$, i.e. if the influence of carrier number fluctuations on the gain are neglected. Using the laser-parameters quoted by Henry [57], A = .97 and $B = 1.05 \times 10^{-3}$. Hence, a good approximation to the optical power spectrum is obtained if holeburning and carrier number fluctuations are neglected (A = 1 and B = 0).

Using (2.44) and (2.54) to (2.58) the optical power spectrum can be expressed in terms of the phase fluctuation by

$$W_S(\omega-\omega_0) = \frac{S}{2\pi}\int_{-\infty}^{+\infty} e^{-(1/2)\cdot\langle\Delta\phi(t)^2\rangle} \cdot e^{j\omega t}\, dt. \qquad (2.70)$$

Using (2.66) to express $\langle\Delta\phi(t)^2\rangle$, a closed form solution for $W_S(\omega)$ would be difficult if not impossible to obtain.

For the case of weakly damped relaxation oscillations, [65] has obtained an approximation for $W_S(\omega)$ using modified Bessel functions to re-express $\langle\Delta\phi(t)^2\rangle$. A numerical solution of (2.70) can be obtained using a fast Fourier transform algorithm [57]. Depending on the output power and damping rate of the relaxation oscillations, the power density of the side modes at $\pm f_R$ in the optical power spectrum is 10 to 25 dB less than the power density at the center frequency of oscillation. For examples, refer to [57], [65]. Fig. 2.2(b) provides a sketch of a power spectrum.

2.4.4. *FM-noise*

The definition of the FM-noise spectrum and relevant equations thereof will be given in this section. The FM-noise spectrum can be measured by passing the output of the laser through an optical frequency

discriminator, e.g. a Fabry-Perot interferometer that is operated at the rising or falling edge of its passband (Fig 2.3) or a Michelson interferometer set in quadrature [69],[70], thus converting frequency noise into amplitude noise. We then measure the amplitude noise of the optical power at the output of the frequency discriminator using a fast photodetector and an electrical spectrum analyzer (Fig. 2.3). Ideally, an optical limiter would have to be used to remove the amplitude noise of the laser before the signal is passed through the frequency discriminator. However, it is generally assumed that the amplitude noise of lasers can be neglected. To measure the amplitude noise the same arrangement as in Fig. 2.3 can be used, except that the frequency discriminator (the Fabry-Perot interferometer) has to be removed.

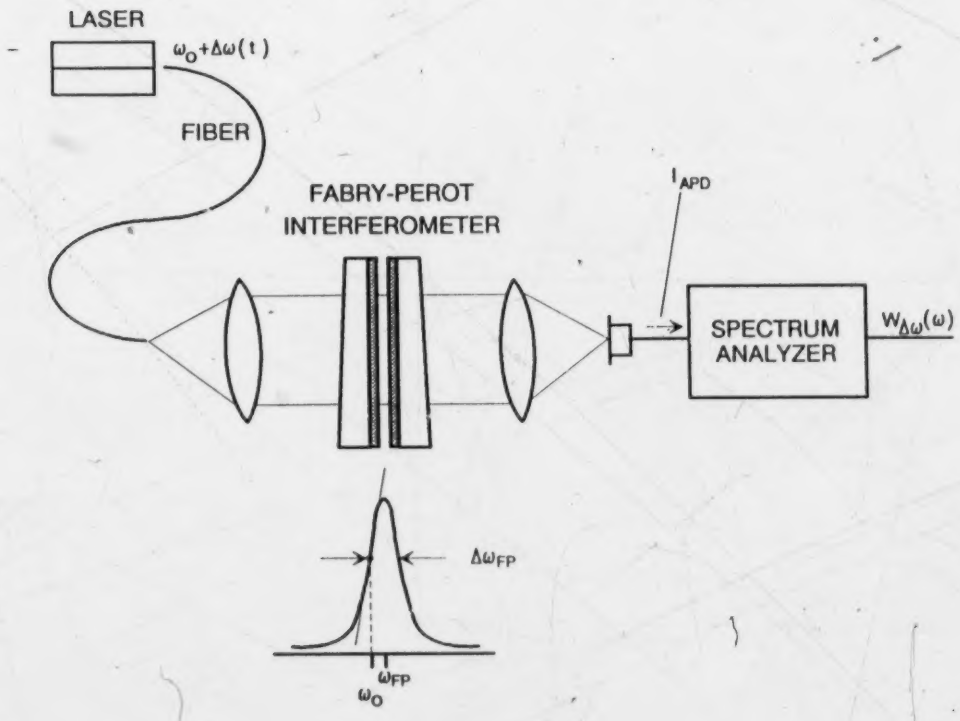

Fig. 2.3: Setup for the measurement of the FM-noise spectrum. To convert FM-noise in amplitude noise with the FP-interferometer, its resolution has to be low, in our case $\Delta\omega_{FP} \geq 2\cdot\omega_R$.

The frequency-noise spectrum $W_{\Delta\omega}(\omega)$ as measured with the arrangement of Fig. 2.3 can be mathematically expressed by

$$W_{\Delta\omega}(\omega) = \int_{-\infty}^{+\infty} R_{\Delta\omega}(\tau)\, e^{j\omega\tau}\, d\tau \tag{2.71}$$

where $$R_{\Delta\omega}(\tau) = \langle \Delta\omega(t+\tau)\, \Delta\omega(t) \rangle \tag{2.72}$$

is the autocorrelation function of the frequency fluctuations. Following Vahala we re-express (2.72) in terms of $\phi(t)$:

$$R_{\Delta\omega}(\tau) = \langle \dot{\phi}(t+\tau)\, \dot{\phi}(\tau) \rangle . \tag{2.73}$$

Using equation (2.53) for $\phi(t)$, that was derived for the laser above threshold assuming $\partial S/\partial t = 0$, and using the properties of the Langevin noise forces (2.9) and (2.20) we obtain

$$\begin{aligned} R_{\Delta\omega}(\tau) &= \langle \left[-\frac{\alpha}{2} \frac{F_S(t+\tau)}{S} + F_\phi(t+\tau) \right] \\ &\quad \cdot \left[-\frac{\alpha}{2} \frac{F_S(\tau)}{S} + F_\phi(\tau) \right] \rangle \qquad (2.74) \\ &= \left(\frac{\alpha}{2} \frac{2D_{SS}}{S} + 2D_{\phi\phi} \right) \cdot \delta(\tau) \quad , \end{aligned}$$

or $$R_{\Delta\omega}(\tau) = \frac{R_{sp}}{2S} (1 + \alpha^2)\, \delta(\tau) = 2\pi\Delta\nu_0\, \delta(\tau). \tag{2.75}$$

The autocorrelation function of the frequency noise, assuming infinitely fast suppression of intensity fluctuations, is a delta function with area $2\pi\Delta\nu$, leading to a white frequency-noise spectrum

$$W_{\Delta\omega}(\omega) = 2\pi\Delta\nu_0 . \tag{2.76}$$

If the time delay in the suppression of intensity noise is taken into account, the FM-noise spectrum is obtained as [66]

$$W_{\Delta\omega}(\omega) = 2\pi\Delta\nu_0 \left[1 + \frac{\alpha^2 f_R^4}{(f_R^2 - f^2)^2 + 4(\Gamma/2\pi)^2 f^2}\right]. \qquad (2.77)$$

A sketch of a typical FM-noise spectrum is shown in Fig. 2.2(c). The FM-noise is enhanced at the relaxation oscillation frequency and falls above f_R below the level predicted by (2.76). This is because the suppression of intensity fluctuations, which in turn enhances the FM-noise by $(1 + \alpha^2)$, does not occur for frequencies above f_R.

We find from (2.77) that the linewidth $\Delta\nu_0$ of a laser is equal to the spectral density of the FM noise spectrum for low frequencies $f \ll f_R$:

$$\Delta\nu_0 = W_{\Delta\omega}(\omega \to 0)/2\pi \; . \qquad (2.78)$$

2.4.5. *Frequency Fluctuation Model*

The preceding sections have shown that the electric field of the laser can be expressed in the form

$$E(t) = S^{1/2} e^{j\omega_0 t} e^{j\phi(t)} . \qquad (2.79)$$

This relation suggests that at any time t we can define the instantaneous frequency of the laser by

$$\omega = \omega_0 + \frac{d\phi}{dt} \qquad (2.80)$$

where

$$\Delta\omega(t) = \frac{d\phi}{dt} \qquad (2.81)$$

is the deviation of ω from the center frequency of oscillation, ω_0, of the laser.

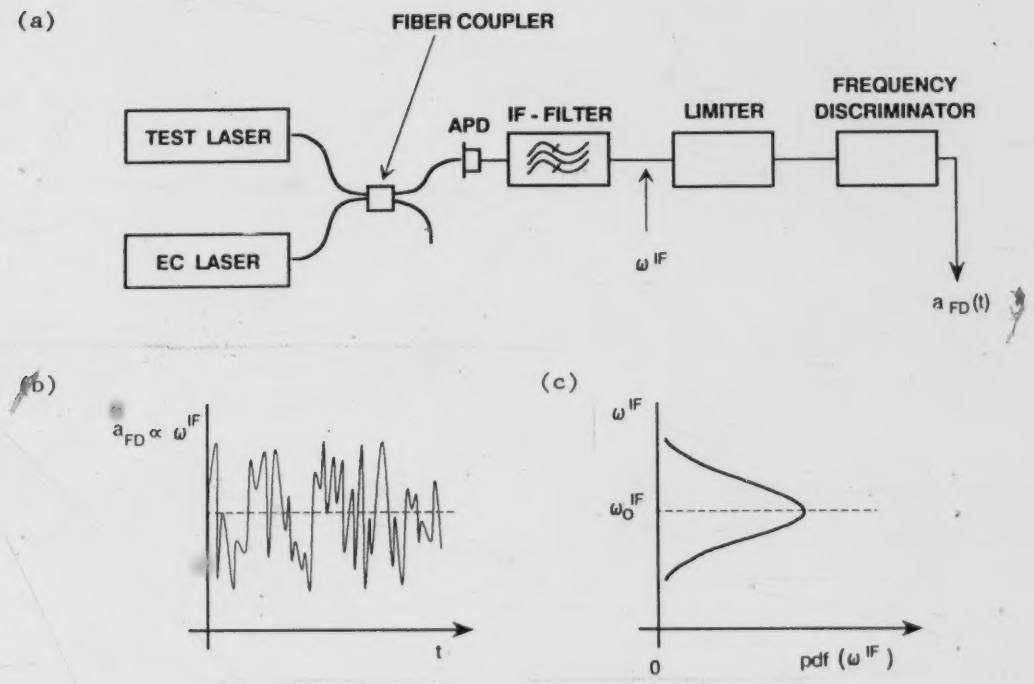

Fig. 2.4: (a) Setup for the conversion of frequency fluctuations in the optical output of a test laser into amplitude changes of the signal $a_{FD}(t)$ in the electrical domain. Sketch of (b) random fluctuations of $a_{FD}(t)$ and ω^{IF}, and (c) the probability distribution function of these fluctuations.

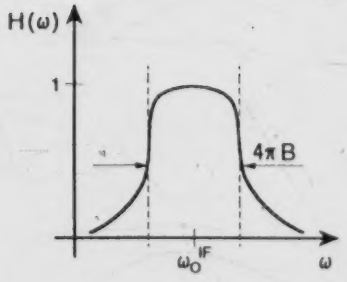

Fig. 2.5: Sketch of the transfer function of the IF-filter used in Fig. 2.4 and definition of the filter bandwidth B.

The frequency fluctuations of a test laser can be observed in the electrical domain using the arrangement of Fig. 2.4, where the optical signal of an external grating laser (having negligible linewidth compared to the test laser) is mixed with the test laser spectrum. The IF-spectrum is passed through an IF-filter of equivalent lowpass bandwidth B (Fig. 2.5). The pass band of the IF-filter is centered around ω_0^{IF}, where ω_0^{IF} is the offset center-frequency of oscillation of the test laser in the IF-spectrum. The integral of the bandlimited FM-noise spectrum at the output of the IF-filter is (Fig. 2.2(c))

$$\int_{-B}^{+B} W_{\Delta\omega}(f) \cdot df = 2\pi\Delta\nu_0 \cdot 2B \tag{2.82}$$

if the resonance peak is not within the IF passband. According to the Wiener-Kintchine theorem, the area under the spectral density of a random process is equal to the autocorrelation function of this process at $t = 0$, $R_{\Delta\omega}(0)$. $R_{\Delta\omega}(0)$ in turn is equal to the variance of the probability distribution function (pdf) for a wide-sense stationary process [71]. The variance is equal to the square of the standard deviation, $\sigma_{\Delta\omega}^2$, if the process has a Gaussian pdf [71], hence

$$\sigma_{\Delta\omega}^2 = 2\pi\Delta\nu_0 \cdot 2B. \tag{2.83}$$

Lax [48] has shown that the Lorentzian noise forces have Gaussian statistics, since they are representing a large number of uncorrelated events, namely spontaneous emission events. These events, in accord with the central limit theorem, result in a Gaussian random process. The transformation of the noise forces in the rate equations is linear, which ensures that all parameters affected by the noise forces show a Gaussian probability distribution. In particular, $\Delta\omega(t)$ can also be assumed to have a Gaussian probability distribution. Garrett and Jacobsen [72] have analyzed the effect of the finite bandwith B of the IF filter on the statistics of the frequency fluctuations at the output of the filter. They found in [72] that, provided $B > 2 \cdot \Delta\nu_0$ and assuming a Gaussian pdf for the frequency fluctuations at the input of the

filter, the frequency fluctuations at the filter output are also described by a Gaussian pdf, hence we obtain using (2.83)

$$P_{\Delta f}(\Delta f) = \frac{1}{\sqrt{2\Delta\nu_0 B}} \exp\left(- \frac{\Delta f^2 \pi}{2\Delta\nu_0 B} \right) \tag{2.84}$$

where $\Delta f(t) = 2\pi\Delta\omega(t)$. The cumulative probability function (cdf) of the frequency fluctuation is

$$C_{\Delta f}(\Delta f) = \frac{1}{2} - \frac{1}{2} \operatorname{erf}\left(\frac{\Delta f^2 \sqrt{\pi}}{\sqrt{2\Delta\nu_0 B}} \right) . \tag{2.85}$$

For a DFB laser it has been verified experimentally by Pedersen et. al. [30] that the cdf of the filtered laser beat-frequency fluctuations obey the characteristic (2.85) and hence the assumption of a Gaussian distribution for the frequency fluctuations of a laser seems to be justified. Good agreement between theoretical and experimental results, however, was found to require a value of B in (2.83) to (2.85) that deviates by up to a factor of 1/2 from the value of the equivalent low pass filter bandwidth of the IF filter. The dependence of this correction factor on the IF filter characteristic and the position of the mean beat frequency within the IF filter has been derived by the same authors [73] in a recent study.

The frequency fluctuation model has been used [74] to calculate error probabilities in optical heterodyne transmission systems. We will use this model in Section 4.3 to calculate mode-hopping frequencies and explain the power distribution between modes of different linewidth.

3. THEORY FOR THE EXTERNAL CAVITY LASER

3.1. INTRODUCTION

Typically, optical feedback is provided to the laser by an external reflecting surface a fixed optical pathlength, L_{ex}, away from the laser (Fig. 3.1). In general, $R_{ex}(\omega)$, the reflectivity of this surface can be frequency dependent, as in the case of feedback from an external grating. We will be concerned with the situation where L_{ex} is large compared to L_{in}, i.e. with long external cavity lasers (LEC-lasers). In this case, the laser can be viewed as a lumped element, where time delays due to the finite transition time of light through the active region can be neglected. We therefore express the electric field of the laser by (2.6)

$$E(t) = (S_0^{1/2} + \hat{e}(t))\, e^{j\omega_0 t}\, e^{j\phi(t)} \qquad (3.1)$$

where the z-dependence of the electric field within the laser is neglected.

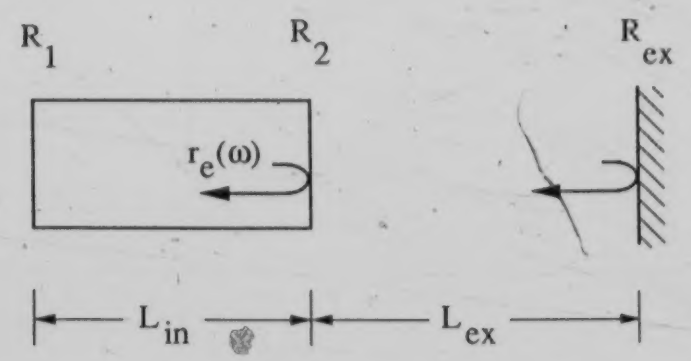

Fig. 3.1: Sketch of a semiconductor laser with optical feedback from an external reflector.

3.2. RATE EQUATIONS

The equation commonly used to describe the laser field in the presence of an external reflecting surface [7],[15],[75],[76], can be obtained from (2.10) by adding a delayed and attenuated component of the laser field to the rate equation for the electric field

$$\frac{dE}{dt} = [-j\omega_0(n_{th}) + \frac{\Delta G}{2}(1-j\alpha)]\, E(t) + \kappa\, E(t-\tau_{ex}) + F_E(t). \qquad (3.2)$$

τ_{ex} is the round-trip time in the external cavity, $\Delta G = G(n)-\tau_p^{-1}$ and

$$\kappa = \frac{(1 - r_2^2) \cdot r_{ex}}{r_2 \cdot \tau_{in}} \qquad (3.3)$$

is the feedback rate, where τ_{in} is the round trip time in the semiconductor laser cavity and $k = \kappa \cdot \tau_{in}$ is the feedback power ratio as seen from a point immediately to the left of the laser facet R_2 in Fig. 3.1, i.e.. the ratio between the power travelling towards the facet R_2 and the reflected power that is coupled back into the laser. R_{ex} includes coupling losses between the external reflector and the laser. The rate equation (2.19) for the carrier density of the solitary laser remains valid for the laser with optical feedback, with $S = |E(t)|^2$.

In general, a closed form solution for the characteristics of the laser with optical feedback cannot be derived from the nonlinear delay-differential equations (3.2) and (2.19). By adding an expression for the time delayed field, the degrees of freedom in the rate equations for the laser has increased from two to infinity [19]. Depending on the values for the characteristic parameters of the differential equations, the feedback rate κ and the decay constants τ_p and τ_e, a variety of behaviors can be observed: stable operation in longitudinal modes of the semiconductor cavity for weak feedback [10], dynamic instabilities or "chaos" [77]-[82] for intermediate levels of feedback [13], and finally stable operation in external cavity modes for very strong optical feedback from a diffraction grating [26]. In the regimes of weak and strong feedback the random noise caused by spontaneous emission events is the dominant source of phase noise. In the intermediate

feedback regime of "coherence collapse" [13], having typically -35 dB < R_{ex} < -10 dB, the random-noise sources $F_N(t)$, $F_\phi(t)$ and $F_S(t)$ can be switched off in numerical simulations without significantly affecting the phase noise [15], indicating that dynamic instabilities are the dominant source of noise.

Rate equations of the form of (3.2) and (2.19) have been numerically integrated by several authors (e.g. [7],[15],[21]) and their results show, as far as experimental results are available, good agreement with the experimentally observed behavior of a laser having optical feedback.

A common approach to reducing the complexity of (3.2) is to assume that the roundtrip-time in the external cavity is short compared to fluctuations in E and ω over time. In this case optical feedback can be represented by assuming that the facet R_2 in Fig. 3.1 has a frequency dependent reflection coefficient

$$r_e(\omega) = |r_e(\omega)| \exp [j\phi_r(\omega)] \tag{3.4}$$

where $\omega(t)$ is the instantaneous frequency of oscillation. In the simplest case of a mirror separated from R_2 by L_{ex} we obtain

$$r_e(\omega) = \frac{r_2 + r_{ex} \exp(j\Phi(\omega))}{1 + r_2 r_{ex} \exp(j\Phi(\omega))} . \tag{3.5}$$

In representing optical feedback by a complex facet reflectivity the delayed feedback term $\kappa\, E(t-\tau_{ex})$ in (3.2) is replaced by a frequency dependent loss rate $\gamma(\omega) = -(v_{gr}/L_{in}) \cdot \ln (r_1 r_e(\omega))$. Since $r_e(\omega)$ is defined as a function of the instantaneous frequency, ω, it is advantageous to study the effect of the frequency dependent loss rate on the mathematical representation of the laser not in the time domain but in the frequency domain. The laser can be viewed as a noise amplifier (Section 2.3.3), where each frequency component $F_E(\omega)$ of the Langevin noise force is amplified in proportion to $[1 - r_1 r_e(\omega) \exp(2jkL_{in})]^{-1}$. The frequency components of E(t) are then given by [83]

$$E(\omega) = \frac{F_E(\omega)}{1 - r_1 r_e(\omega) \exp(2jkL_{in})} \tag{3.6}$$

where $F_E(\omega)$ is a small quantity. Large values of $E(\omega)$ are obtained when the denominator approaches zero, i.e. when the roundtrip gain approaches one and the roundtrip phase shift is equal to 2π. These two conditions, previously introduced as the oscillation conditions and discussed for the solitary laser (Sect. 2.2), are analyzed in the following section for lasers with optical feedback.

3.3. OSCILLATION CONDITION GRAPH

In this section we describe a graphical representation of the steady state equations that provides the conditions for oscillation of the laser. This graphical representation will allow us to distinguish between different solutions of the oscillation condition for a laser with optical feedback based on threshold gain, stability and linewidth. Also, this model provides insight into the tuning characteristics of lasers when the external feedback parameters are changed.

3.3.1. *Governing Equations*

Following (3.6), with the external feedback expressed by the frequency dependent facet reflectivity of (3.4), the oscillation condition for the laser with feedback can be written in the form

$$r_1 \cdot |r_e(\omega)| \cdot \exp\{2jkL_{in} + j \cdot \phi_r(\omega)\} = 1 \qquad (3.7)$$

where the complex propagation constant for the amplitude of the electric field is

$$jk = j \cdot \frac{\omega}{c} \cdot n_\epsilon(\omega, g) + \frac{g}{2} \, . \qquad (3.8)$$

Here g is the net gain per unit length for the intensity after subtraction of the scattering losses, α_s, and the refractive index $n_\epsilon(\omega, g)$ is a function of frequency and gain. If the mirror loss is distributed over the length of the active region, (3.7) can be rewritten in the form

$$\exp\left(2jkL_{in} + j\cdot\phi_r(\omega) - \ln\frac{1}{r_1 r_2}\right) = 1 \qquad (3.9)$$

and, by inserting (3.8), in the form

$$\exp\left\{2L_{in}\left(j\cdot\frac{\omega}{c}\cdot n_\epsilon(\omega,g) + \frac{g}{2} - \frac{1}{2L_{in}}\ln\frac{1}{r_1 r_2}\right) + j\cdot\phi_r(\omega)\right\} = 1. \qquad (3.10)$$

From the real part of the exponent we obtain an expression for the gain

$$g(\omega) = \frac{1}{L_{in}}\cdot\ln\frac{1}{r_1\cdot|r_e(\omega)|} \qquad (3.11)$$

and from the imaginary part an expression for the roundtrip phase shift

$$\phi_{RT} = 2\pi\cdot m = \frac{2\omega\cdot L_{in}}{c}\cdot n_\epsilon(\omega,g) + \phi_r(\omega). \qquad (3.12)$$

Linearizing equation (3.12) close to the resonance frequency ω_0 of the solitary laser, then using both the group index $n_{gr} = (\partial n_\epsilon/\partial\omega)$ to account for the frequency dependence of n_ϵ and the linewidth enhancement factor [46]

$$\alpha = \frac{2\omega_0}{c}\cdot\frac{\partial n_\epsilon/\partial n}{\partial g/\partial n} \qquad (3.13)$$

to account for the change of the refractive index with gain we obtain

$$\phi_{RT} = 2\pi\cdot m = \frac{2\omega_0 L_{in} n_\epsilon}{c} + \frac{2L_{in} n_{gr}}{c}\cdot\Delta\omega - \alpha\cdot L_{in}\Delta g + \phi_r(\omega) \qquad (3.14)$$

where $\Delta\omega = \omega-\omega_0$. Noting that the roundtrip phase shift of the solitary laser $2\omega_0 L_{in} n_\epsilon/c = 2\pi m_0$ (a multiple of 2π) and introducing $\Delta m = m-m_0$ and $g = g_0 + \Delta g$, where

$$g_0 = (1/L_{in})\cdot\ln(1/r_1 r_2) \qquad (3.15)$$

is the threshold gain per unit length of the solitary laser, we obtain

from (3.14)

$$g(\omega) = \frac{1}{\alpha L_{in}} \left\{ \frac{2L_{in}}{v_{gr}} \cdot \Delta\omega + \phi_r(\omega) - 2\pi\Delta m \right\} + g_0. \qquad (3.16)$$

Also, from (3.11), $g = g_0 + \Delta g$ and (3.15), it follows that

$$g(\omega) = \frac{1}{L_{in}} \ln \frac{r_2}{|r_e(\omega)|} + g_0. \qquad (3.17)$$

In conclusion, the phase and gain conditions lead us to two equations that express the gain as a function of frequency, (3.16) and (3.17), respectively. Why are there two equations that specify the gain as a function of frequency? In (3.17) the gain is a function of frequency because we required "gain = loss" at lasing threshold, where optical feedback was represented as a frequency dependent facet reflectivity and hence frequency dependent loss. (3.17) is therefore an expression for the threshold gain in terms of the frequency dependent loss. In order to change the gain in the semiconductor the carrier density has to change. A change in carrier density (Fig. 3.2) leads to a change in gain and also to a change of the refractive index in the

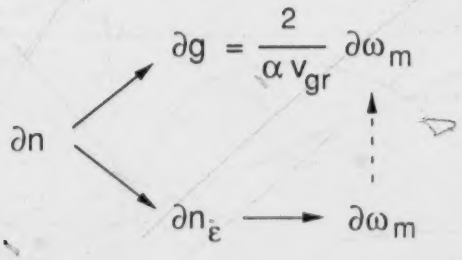

Definition:

$$\alpha = \frac{2\,\omega_0}{c} \; \frac{\partial n_\varepsilon / \partial n}{\partial g / \partial n}$$

Fig. 3.2: Dependence of gain, g, and refractive index, n_ε, on the carrier density, n, in the semiconductor. Also, definition of the linewidth enhancement factor, α, as the ratio between the change in refractive index and change in gain.

semiconductor cavity and hence to a change in the oscillation frequency. We can express the frequency that satisfies the phase condition, i.e. the resonance frequency of the semiconductor cavity, as a function of gain instead of a function of N. The inverse of this relation, the gain expressed as a function of oscillation frequency, leads to (3.16).

3.3.2. *Graphical Representation*

Equations (3.16) and (3.17) are graphically represented in Fig. 3.3 for (a) a solitary laser and (b) to (e) five nonzero values of external reflectivity $R_{ex} = r_{ex}^2$. The intersections between a constant phase curve (3.16) [83] and loss curve (3.17) define all frequencies that satisfy the oscillation condition as the gain is varied. For the solitary laser only one intersection between constant phase and loss curve is shown in Fig. 3.3(a), corresponding to the longitudinal mode at frequency $\Delta f = \Delta\omega/2\pi = 0$ with $\Delta m = 0$. The spacing between longitudinal modes is $\Delta\nu_{in} = v_{gr}/2L_{in} = 125$ GHz for $L_{in} = 300$ μm. The constant phase curve for the neighboring modes ($\Delta m = \pm 1$ in (3.16)) is outside the plotting range of Fig. 3.3. With $R_{ex} = 2 \cdot 10^{-4}$ in Fig. 3.3(c) several intersections between the constant phase curve and the loss curve appear for one value of m. Each intersection is characterized by a different oscillation frequency and threshold gain. As the gain is increased in a semiconductor laser, the laser will start to oscillate with the frequency of the mode that requires the lowest gain. With the onset of oscillation, the gain does not increase further (gain saturation or gain clamping) and modes that require a higher gain to oscillate will not be occupied, if the difference in threshold gain between neighboring modes is high enough.

The gain is a function of the carrier density in the active medium. The carrier density, representing a stored energy, cannot change rapidly. Transitions to modes with higher gain can occur only if the gain fluctuations caused by quantum noise are larger than the threshold-gain difference between modes. Fluctuations between modes of equal threshold gain are not restricted, and the presence of a series of modes with the same minimum gain will therefore lead to fluctuations of the oscillation frequency of the laser between longitudinal modes.

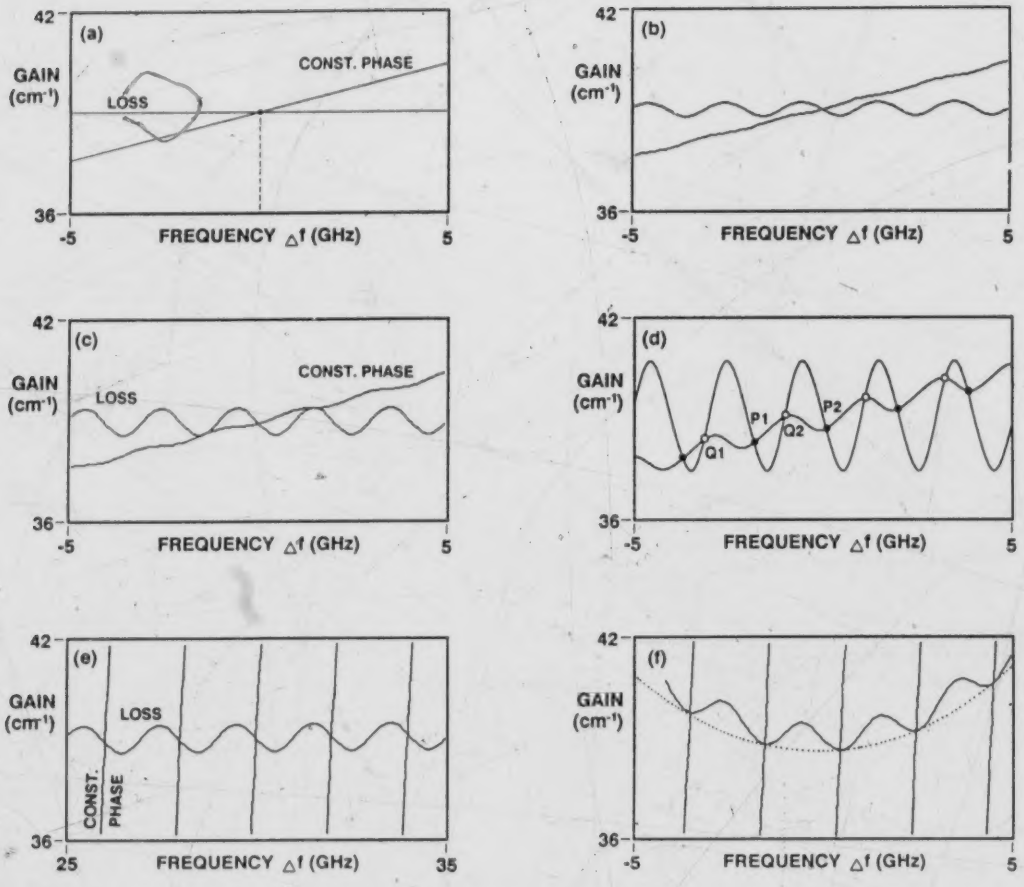

Fig. 3.3: Plot of loss and constant phase curves for (a) no optical feedback, (b) to (d) weak optical feedback, (e) strong feedback and (f) feedback from an optical grating. The following parameters were used: $\alpha = 6$, $L_{ex} = 7.5$ cm, $L_{in} = 300$ μm. The reflectivities R_1 and R_{ex} were respectively: (a) 0.31 and 0, (b) 0.31 and $25 \cdot 10^{-6}$, (c) 0.31 and 10^{-4}, (d) 0.31 and $16 \cdot 10^{-4}$, (e) 10^{-4} and 0.31, and (f) $R_1 = 10^{-4}$ and wavelength dependent feedback from a grating ($r_G^2 = 0.31$ and $f_G = 15$ GHz).

The slope of the phase curves in Figs. 3.3(a)-(c) is proportional to $2/\alpha v_{gr}$ (3.16). If there were no coupling between gain and refractive index (eq. (3.16): $\alpha = 0$) the slope of the phase curve would be infinite and we would obtain only one intersection, leading to single mode oscillation for weak feedback. However, with $\alpha = 6$ and $L_{ex} = 5$cm we observe multiple intersections with little threshold-gain difference for coupling efficiencies as low as 10^{-4} (Fig. 3.3(c)). A small threshold-gain difference means that the laser oscillation can fluctuate between several external cavity modes (Section 4.2).

In the case of strong feedback (Fig. 3.3(e)and (f)) one facet of the laser is AR-coated and the optical feedback through this facet is larger than that directly attributable to this facet ($R_2 < R_{ex}$). We can think of the laser as having an extended cavity that is only partially filled with a gain medium. We expect intersections of constant phase and loss-curves to occur with frequency separation almost equal to the free spectral range of the extended cavity. This is confirmed in Fig. 3.3(e) and (f), where $\Delta\nu_{ex} = c/2L_{ex} = 0.45$ GHz.

Again there is only a small threshold-gain difference between adjacent modes, which suggests that the oscillation frequency can fluctuate between external cavity modes. However, the threshold-gain difference necessary for single mode oscillation is dependent on the amplitude of the gain fluctuations. Due to the large number of photons stored in the external cavity of a laser with strong feedback, each spontaneous emission event will contribute less phase and amplitude noise to the laser field than for a laser without optical feedback [83]. Since the amplitude of gain fluctuations is not only governed by the rate of spontaneous emission events but also by the reaction of the laser to fluctuations in the intensity of the electric field (see derivation of (2.52)), gain fluctuations are reduced in a laser having strong optical feedback. We expect therefore, that in a strong optical feedback arrangement, the threshold-gain difference between modes necessary to ensure single mode oscillation is less than in the weak feedback case.

Kazarinow and Henry [83] found that the increase or reduction of laser phase noise due to optical feedback can be calculated from the slopes of the constant phase and loss curves in the oscillation

condition graph. In steady state, loss and gain are equal. A spontaneous emission event causes a change of the gain, Δg, depicted in Fig. 3.4(a) for a solitary laser by a reduction of the gain (dashed line) with respect to the loss (solid horizontal line). The associated change in oscillation frequency $\Delta\omega$ (Fig. 3.4(a)) can be calculated from the slope of the constant phase curve (3.16): $\Delta\omega = (\alpha v_{gr}/2)\cdot\Delta g$. Following [83], we plot now the same diagram as before, but for a laser with optical feedback, Fig. 3.4(b). In Fig. 3.4(b), the change in frequency $\Delta\omega'$ for the same initial change in gain Δg as in Fig. 3.4(a) appears reduced by a factor of $F = \Delta\omega/\Delta\omega' = 1 + A + B$, where $(1+A)\cdot(2/v_{gr}\alpha)$ is the slope of the constant phase curve and $-B\cdot(2/v_{gr}\alpha)$ is the slope of the loss curve. F is the chirp reduction factor that has been derived by Olesen et.al. [15], using a small signal analysis based on the rate equation of the laser with optical feedback. In the same paper [15] the linewidth reduction factor, defined as the ratio of the solitary laser linewidth $\Delta\nu_0$ to the linewidth of the laser with optical feedback $\Delta\nu$, was shown to be equal to the square of the chirp-reduction factor $F^2 = \Delta\nu_0/\Delta\nu$.

It is not surprising that linewidth reduction is equal to the square of the chirp-reduction if we consider equations (2.71) to (2.73), used to derive the FM-noise spectrum, $W_{\Delta\omega}$, and the relation (2.78): $\Delta\nu_0 = W_{\Delta\omega}(\omega\to 0)/2\pi$. If frequency changes $\Delta\omega$ are scaled due to optical feedback by the chirp-reduction factor F, the magnitude of the autocorrelation function $R_{\Delta\omega}(\tau)$ (2.72) and $W_{\Delta\omega}(\omega)$ (2.71) are reduced by F^2. With the same relationship between $W_{\Delta\omega}$ and $\Delta\nu$ as (2.78) being valid for the laser with optical feedback, the linewidth is reduced by F^2.

The open circles in Fig. 3.3(d) mark intersections between constant phase and loss curves where the slope of the constant phase curve is less than the slope of the loss curve and therefore, in analogy to Fig. 3.4(b), $F = 1 + A + B < 0$. The small signal analysis of the rate equations shows that $F < 0$ indicates unstable solutions to the oscillation condition [15]. Stable solutions to the oscillation condition are marked by the solid circles in Fig. 3.3(d), which correspond to $F > 0$. For $0 < F < 1$, the frequency change $\Delta\omega'$ with optical feedback is larger than without optical feedback and the linewidth of the laser with optical feedback is broadened. For $F > 1$,

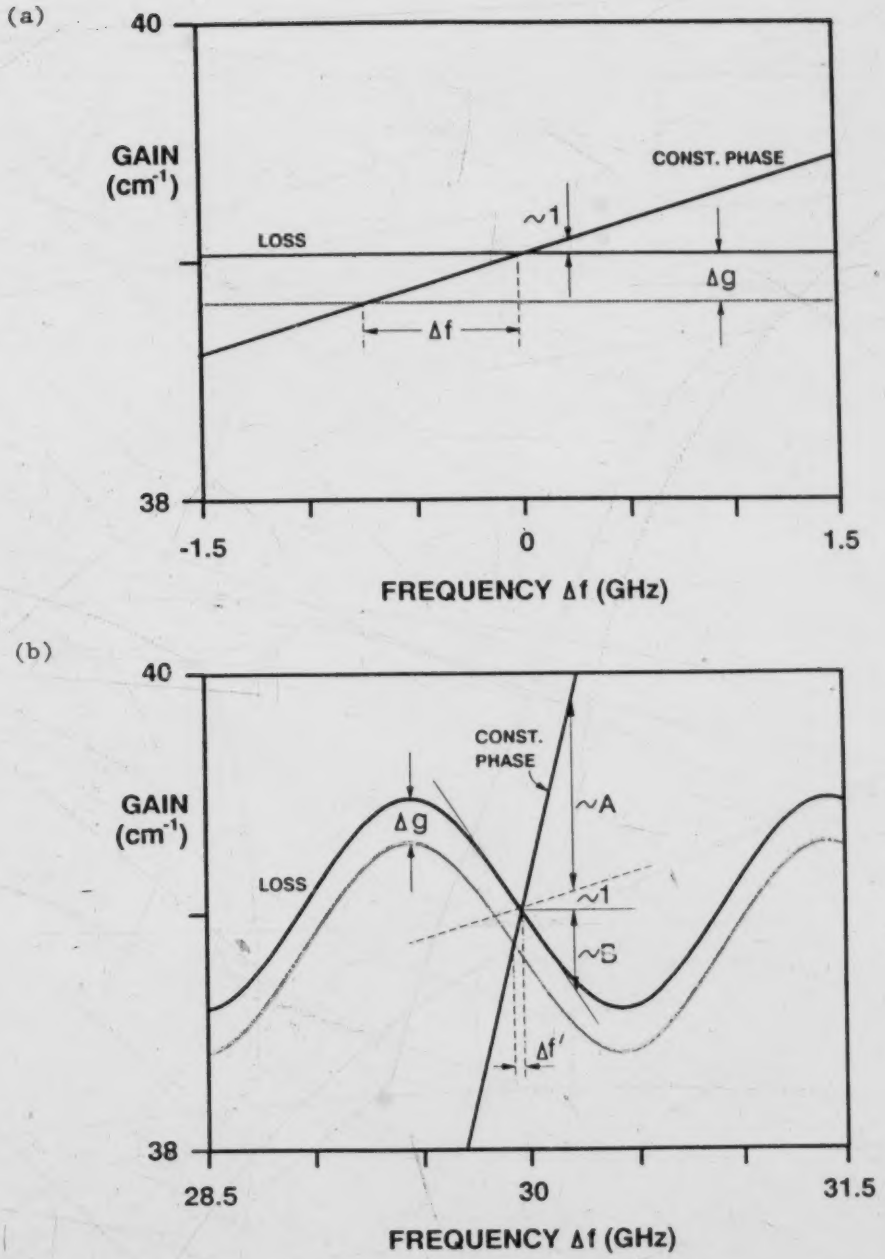

Fig. 3.4: Enlargement of (a) a section of Fig. 3.3(a) and (b) a section of Fig. 3.3(e). Also indicated are the parameters A and B introduced by [83]. For clarity of $\Delta f'$, the slope of the constant phase curve in the lower graph is less steep by a factor of 4.6 than it should be using the parameter values of Fig. 3.3(e).

the linewidth is narrowed due to optical feedback. The linewidth reduction is particularly pronounced for strong optical feedback from a long external cavity, Fig. 3.3(e). In this situation the slope of the constant phase curves is increased approximately by the ratio of the external cavity length to the semiconductor cavity length, and therefore [83]:

$$F^2 = (1 + A)^2 = (L_{ex}/L_{in})^2 \tag{3.18}$$

In conclusion, we have presented an intuitive derivation of the phase noise reduction of a laser due to optical feedback.

3.3.3. *Wavelength Dependent Feedback*

The threshold-gain difference between adjacent modes is increased in Fig. 3.3(e), which applies to the situation where the external reflection coefficient is wavelength dependent and in particular for the case of optical feedback from an external grating reflector. Assuming that the grating is illuminated by a Gaussian beam, the frequency dependent reflectivity is given by [84]

$$r_{ex}(\omega) = r_G \exp\left\{ -(\ln 2) \frac{(\omega - \omega_G(\theta_G))^2}{\Delta\omega_G^2} \right\} \tag{3.19}$$

where $\Delta\omega_G$ is the full width at half maximum of $r_{ex}(\omega)$, and ω_G is the frequency and r_G the reflection coefficient at maximum reflection of the grating. ω_G depends on the incident angle θ_G of the light with respect to the grating

$$\omega_G(\theta_G) = \frac{2a}{c} \sin \theta_G \tag{3.20}$$

where "a" is the spacing between rulings of the grating and "c" is the velocity of light. $\Delta\omega_G$ depends on the spot size, b, of the illuminating beam [84]

$$\Delta\omega_G = \frac{2b}{a \cos \theta_G}. \qquad (3.21)$$

For Fig. 3.3(e) the values $\omega_G = \omega_0$, $\Delta\omega_G = 2\pi \cdot 15$ GHz and $r_0^2 = .31$ apply.

In conclusion, in Section 3.3, we have shown that the oscillation condition graph is a useful tool to study the tuning characteristics of coupled cavity arrangements because it provides a plot of all lasing frequencies. For example, it allows us to examine the change in oscillation frequency when the external cavity length is varied by a fraction of a wavelength, when the feedback ratio is altered, or when the wavelength of maximum reflectivity, $\lambda_G = 2\pi c/\omega_G(\theta_G)$, is altered by, for example, rotating the external grating.

3.4. CHIRP-REDUCTION

The representation of optical feedback by a frequency dependent facet reflectivity leads to a modification of the rate equations of a solitary laser. Following [83], we outline in this section the derivation of this modification of the rate equations. We start by representing a solitary laser as a noise amplifier in the frequency domain (3.6) and change the denominator in (3.6) to

$$1 - \exp\left(2jkL_{in} - \ln \frac{1}{r_1 r_2}\right) = 1 - \exp\left(2jk' L_{in}\right). \qquad (3.21)$$

From (3.8) we obtain an expression for k', the complex propagation constant including facet loss for a solitary laser,

$$jk' = j\left[\frac{\omega}{c} - n_\epsilon(\omega, g)\right] + \frac{g}{2} - \frac{1}{2L_{in}} \ln \frac{1}{r_1 r_2}. \qquad (3.22)$$

Using a similar procedure to that for the derivation of (3.14), we define the propagation constant k_0' for the laser oscillating at ω_0:

$$jk_0' = j\left(\frac{2L_{in}\omega_{in} n_{Ph}}{c}\right) + \frac{g}{2} - \frac{1}{2L_{in}} \ln \frac{1}{r_1 r_2} = 0 \qquad (3.23)$$

and the change $\Delta k'$ of the propagation constant $k' = k_0' + \Delta k'$ due to changes in frequency and gain:

$$j\Delta k' = j\left(\frac{\Delta\omega}{v_{gr}} - \alpha\frac{\Delta g}{2}\right) + \frac{\Delta g}{2} . \qquad (3.24)$$

We now repeat the procedure that led to (3.22); however, this time we consider a laser with optical feedback expressed by $r_e(\omega)$ as in equations (3.4) and (3.5). In this case we obtain for the complex propagation constant instead of (3.22) the following expression

$$jk' = j\left[\frac{\omega}{c} n_\epsilon(\omega,g)\right] + \frac{g}{2} - \frac{1}{2L_{in}} \ln\frac{1}{r_1|r_e(\omega)|} + j\cdot\frac{1}{2L_{in}}\cdot\phi_r(\omega) \qquad (3.25)$$

We again linearize k' around its steady state value k_0' and obtain the equation for $\Delta k'$,

$$j\Delta k' = j\cdot\left(\left[1 + \frac{1}{\tau_{in}}\left(\frac{d\phi_r}{d\omega} - \frac{j\cdot\ln(|r_e|)}{d\omega}\right)\right]\cdot\frac{\Delta\omega}{v_{gr}} - \alpha\frac{\Delta g}{2}\right) + \frac{\Delta g}{2}. \qquad (3.26)$$

We notice, by comparing (3.23) and (3.26), that the factor for the term $\Delta\omega/v_{gr}$ is increased due to optical feedback by

$$A - j\frac{B}{\alpha} = \frac{1}{\tau_{in}}\cdot\frac{d\phi_r}{d\omega} - \frac{j}{\tau_{in}}\cdot\frac{d\,\ln(|r_e|)}{d\omega} . \qquad (3.27)$$

Kazarinov and Henry [83] have introduced the variables A and B and have noted that 1 + A corresponds to an increase in slope of the constant phase curve and B to a decrease in slope of the loss curve due to optical feedback, as discussed previously for Fig. 3.4.

In Section 3.3.1 we noted that the condition $jk_0' = 0$, (3.23), leads to the gain and phase condition of the solitary laser. Using (3.27) and the relation $(1 + \exp(x)) \sim x$ for $x \ll 1$, we can expand the denominator of (3.6) around $jk_0' = 0$ and obtain

$$E(\omega) \sim \frac{F_E(\omega)}{j\Delta k'} . \qquad (3.28)$$

For the laser without optical feedback, $j\Delta k'$ is given by (3.24), for the laser with optical feedback by (3.26). From the inverse Fourier transform of (3.28) for the laser with feedback and without feedback, Kazarinov and Henry [83] have found that the rate equation for the electric field of the laser with optical feedback can be written in the form

$$(1 + A - jB/\alpha)(\dot{E} + j\omega_0 E) = \frac{\Delta G}{2}(1 - j\alpha)\, E + F_E(t) \qquad (3.29)$$

where $\Delta G = \Delta g / v_{gr}$.

We observe that this equation is identical to the rate equation for the laser without optical feedback ((3.2) with $\kappa = 0$) except for the factor of $(1+A-jB/\alpha)$, modifying the magnitude of the term $\dot{E} + j\omega_0 E$. The transformation of (3.29) into two real Langevin rate equations for $S(t)$ and $\phi(t)$ yields [83]:

$$(1 + A)\,\dot{S} - \frac{2B}{\alpha} S \cdot \phi = \Delta G \cdot S + R + F_s(t) \qquad (3.30)$$

and

$$(1 + A)\,\dot{\phi} + \frac{B}{2\alpha}\frac{\dot{S}}{S} = \frac{\alpha \Delta G}{2} + F_\phi(t). \qquad (3.31)$$

The same procedure is now used to derive the FM-noise and linewidth of the laser with optical feedback as for the solitary laser (Section 2.4.3.2). We restrict ourselves to low frequency fluctuations, which were shown previously to be responsible for the linewidth of the laser, and can therefore set $\partial S/\partial t = 0$ in (3.30). Eliminating ΔG in (3.30) and (3.31) we obtain, apart from constant terms which produce a small offset of the oscillation frequency of the laser [83],

$$\dot{\phi} = \frac{F_\phi(t) - (\alpha/2S)F_S(t)}{1 + A + B}. \qquad (3.32)$$

This is a key result, which shows, when compared to (2.53), that frequency fluctuations are reduced due to optical feedback by $F = 1 + A + B$, where F is the chirp-reduction factor. In an analogous way to the derivation of equations (2.60) and (2.63) we can conclude that the linewidth of the laser above threshold and with optical feedback is

$$\Delta\nu = \frac{\Delta\nu_0}{F^2} \tag{3.33}$$

where $\Delta\nu_0 = (R_{sp}(1+\alpha^2)/(4\pi S))$ is the linewidth of the solitary laser.

3.5. CHARACTERISTICS FOR WEAK FEEDBACK

For the case of weak reflection from an external mirror we can neglect multiple reflections in the external cavity and (3.5) can be replaced by

$$r_e(\omega) = r_2 \cdot (1 + k \cdot e^{j\Phi}) \tag{3.34}$$

$$\text{where} \quad k = \frac{(1-r_2^2)}{r_2} \cdot r_{ex} \quad \text{and} \quad \Phi = \omega\tau_{ex}. \tag{3.35}$$

We assume weak reflections ($k \ll 1$) and use the approximation $\arctan x \approx x$ for $x \ll 1$ to obtain from (3.34)

$$|r_e(\omega)| = r_2 \cdot (1 + k \cdot \cos\Phi) \tag{3.36}$$

$$\text{and} \quad \phi_r(\omega) = k \cdot \sin\Phi \,. \tag{3.37}$$

Inserting (3.36) into (3.17) yields for $k \ll 1$

$$g(\omega) = g_0 \cdot \frac{1}{L_{in}} \cdot k \cdot \cos(\omega\tau_{ex}) \tag{3.38}$$

$$\text{where} \quad g_0 = \frac{1}{L_{in}} \ln \frac{1}{r_1 r_2} \,. \tag{3.39}$$

Inserting the gain condition (3.38) into the phase condition (3.16) we obtain a relation for the external cavity mode frequencies, ω, in implicit form:

$$\omega - \omega_0 = -\kappa \sqrt{1 + \alpha^2} \cdot \sin(\omega\tau_{ex} + \psi) \tag{3.40}$$

where $$\psi = \tan^{-1}\alpha \tag{3.41}$$

and $$\kappa = \Delta\nu_{in} \cdot k. \tag{3.42}$$

ω_0 is the oscillation frequency of the solitary laser.

In the discussion of Fig. 3.4 and equation (3.32), we pointed out that optical feedback reduces the frequency change of a laser due to injection current changes or phase noise by the factor $F = d\omega_0/d\omega$, where F is called the chirp reduction factor and $d\omega_0/d\omega$ is the ratio of the change in oscillation frequency ω_0 of the solitary laser to the change in oscillation frequency ω of the laser with optical feedback. Also, it was noted that the linewidth reduction $\Delta\nu_0/\Delta\nu$, being the ratio of the linewidth $\Delta\nu_0$ of the solitary laser to the linewidth $\Delta\nu$ of the laser with optical feedback, is equal to F^2. Using the relation $F = d\omega_0/d\omega$, F can be obtained for the case of weak feedback from the derivative of (3.40) with respect to ω:

$$F = 1 + \kappa \cdot \tau_{ex} \sqrt{1 + \alpha^2} \cdot \cos(\omega\tau_{ex} + \psi). \tag{3.43}$$

Using (3.40) again to replace $\omega\tau_e$ in (3.43) we obtain:

$$F = 1 \pm \sqrt{(\kappa\tau_{ex})^2 \cdot (1+\alpha^2) - (\Delta\omega\tau_{ex})^2} \tag{3.44}$$

where $\Delta\omega = \omega - \omega_0$ is the separation of the external cavity mode frequencies from the solitary laser frequency.

Equations (3.38), (3.40) and (3.43) are key equations that have been used by a number of authors [7]-[10],[12],[17],[85] to discuss the behavior of lasers with weak optical feedback. The multiple values of frequency ω that satisfy the oscillation conditions are given by (3.40). The gain and linewidth reduction associated with each of those frequencies can then be found from (3.38) and (3.43). The number of

solutions of the oscillation condition (3.40) depends on the value of $\kappa \cdot \sqrt{1+\alpha^2}$. Solutions of (3.40) that lead to $F < 0$ are dynamically not stable [15], a value of $0 < F < 1$ leads to line broadening and and a value of $F \geq 1$ causes line narrowing (Section 3.3.2).

Figs. 3.3(a) to (d) show that the threshold gain for weak feedback for the external cavity decreases as the frequency of the modes decreases. Considering only modes with $F > 1$, we notice from (3.44) that the linewidth reduction F^2 is largest for modes closest to ω_0.

For a given value of $\kappa \cdot \sqrt{1+\alpha^2}$ the values of ω that satisfy (3.40) depend on the roundtrip phase shift in the external cavity, $\omega\tau_e$. We use the solitary laser frequency as a reference and define the parameter

$$\psi_e = \omega_0 \tau_{ex} + \tan^{-1}\alpha. \tag{3.45}$$

(3.40) can then be rewritten in the form

$$\Delta\omega = -\kappa \sqrt{1 + \alpha^2} \sin (\psi_e + \Delta\omega\tau_{ex}). \tag{3.46}$$

Fig. 3.5(a) and (b) show the solutions of (3.46) for the situation where the external cavity length is adjusted to provide $\psi_e = 0°$ and $\psi_e = 180°$, respectively. In both cases the external cavity modes are located symmetrically with respect to ω_0. This symmetry is evident from (3.46). Also, we observe from (3.44) that modes located symmetrically with respect to ω_0 have equal values of F. For $\psi_e = 0°$ an external cavity mode exists at $\omega = \omega_0$. The linewidth reduction factor of this mode has a value of $F = F_{max}$

$$F_{max} = 1 + \kappa\tau_{ex} \cdot \sqrt{1 + \alpha^2} \tag{3.47}$$

which is the largest value F can assume for any external cavity mode at a given feedback rate κ and roundtrip time, τ_{ex}, in the external cavity. For $\psi_e = 180°$ two stable solutions with lowest linewidth exist. The solution of (3.46) at $\Delta\omega = 0$ leads to $F < 1$ (3.43) and is therefore not stable.

The frequency of the external cavity mode with minimum threshold gain, given by the leftmost intersection between loss and constant phase

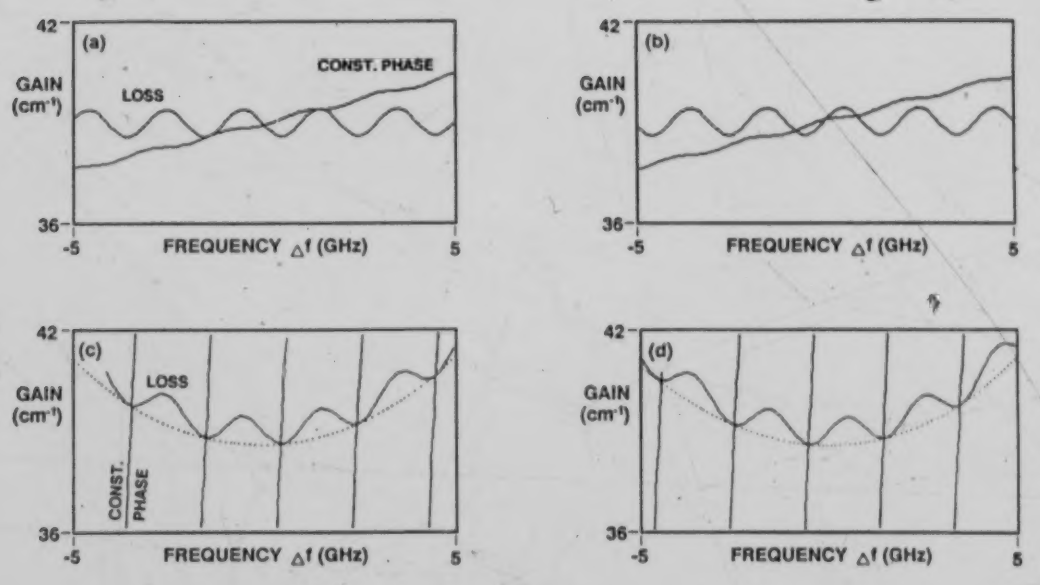

Fig. 3.5: Effect of a change of the external cavity length, expressed in terms of a change in the roundtrip phase shift ψ_e, on a plot of the loss and constant phase curves. Graphs (a) and (c) are for $\psi_e = 0°$ and (b) and (d) are for $\psi_e = 180°$. All other parameters are: in the case of weak feedback, (a) and (b), the same as in Fig. 3.3(a), and in the case of strong feedback, (c) and (d), the same as in Fig. 3.5(f).

curve in Fig. 3.3(c), is obtained from (3.38) by setting

$$\cos(\omega\tau_{ex}) = 1. \tag{3.48}$$

The equivalence $\sqrt{1+\alpha^2}\cdot\cos(\phi + \arctan(\alpha)) = \cos(\phi) - \sin(\phi)$ allows us to rewrite (3.43) and insert (3.48) in (3.43) to obtain for the chirp reduction, $F = F_{min}$, of the external cavity mode with minimum gain

$$F_{min} = 1 + \kappa\tau_{ex}. \tag{3.49}$$

The chirp reduction of all stable external cavity modes, if more than one external cavity mode exists, has a value between F_{min} and F_{max}. The expressions (3.47) and (3.49) for the linewidth reduction of the mode with maximum F and the mode with minimum threshold gain, respectively, have been derived previously in [10].

The change of the constant phase and gain curves associated with a change of the external cavity length by a quarter of the optical wavelength is shown in Fig. 3.5(c) and (d) for the case of strong feedback. In contrast to the case of weak feedback, Fig. 3.5(a) and (b), we notice no significant change in the slopes of the constant phase and gain curves at the intersections of these curves for strong feedback, although the external cavity mode frequencies change. The linewidth reduction F^2 stays essentially constant, therefore, for the case of strong optical feedback if the external cavity length is changed.

3.6. FEEDBACK REGIMES

In the preceding section the basic theory for lasers with optical feedback was presented. In this section we outline the feedback properties that have been observed and classified by other researchers and place the focus of our work and our contribution within this framework.

A first attempt to classify the multitude of feedback effects that have been observed was by Tkach et. al. [17] who described 5 regimes of feedback effects. [17] obtained experimental data with a single device, a 1.5 μm DFB-laser, over a range of feedback levels from R_{ex} = -80 dB to -8 dB and found well-defined boundaries between the regimes as a function of feedback level. In this section we follow the classification system of [17] and describe the features observed for a laser operating in the various regimes of feedback effects. At the same time we will compare features of the constant phase and loss curve in the oscillation condition graph with the observed feedback effects and find that there is good correlation between them.

The first three feedback regimes apply to weak and moderate feedback levels of up to roughly -40 dB. Multiple reflections in the external cavity can be neglected and the oscillation condition can be written in the form of and (3.40), whereas the chirp-reduction is given by (3.43).

Regime I: Experimentally this regime is defined by line broadening and line narrowing dependent on the phase of the reflected light. There is never more than one solution to the oscillation condition in this regime. Two external cavity modes are always separated by an unstable solution ($F < 0$) to the oscillation condition (Fig. 3.3(d)). Therefore, the feedback rate κ^{II} at the transition from Regime I to Regime II is, from (3.43)

$$\kappa^{II} \cdot \tau_{ex} \sqrt{1 + \alpha^2} = 1 \tag{3.50}$$

and the feedback power ratio R_{ex}^{II} at this boundary, from (3.3) and (3.50), is

$$R_{ex}^{II} = \frac{r_2^2}{(1 - r_2^2)^2 (1 + \alpha^2)} \frac{\tau_{in}^2}{\tau_{ex}^2}. \tag{3.51}$$

Since $\tau_{in} \ll \tau_{ex}$, very low levels of optical feedback do affect the laser. Tkach [17] observed changes of the linewidth by 30 percent at -80 dB feedback power ratio with an external reflector at a distance of 40 cm. The feedback level for the transition from Regime I to II is found from (3.51) to be inversely proportional to the square of the external cavity length.

Regime II: The line broadening observed in Regime I for out of phase feedback changes into line splitting as the feedback is increased to enter Regime II. Within Regime II the number of external cavity modes that are observed is increasing as the feedback level is increased (Sect. 4.2). In the case of multiple solutions of the oscillation condition, it is generally assumed [12],[86] that the laser is predominantly oscillating in the external cavity mode with minimum threshold gain. However Schunk et. al. [21] have observed in numerical simulations that the mode with minimum linewidth has higher power. We add experimental proof to this finding in Sect. 4.4. For the case of two modes, [17] shows that the mode-hopping frequency between the modes decreases as the feedback level is increased.

Regime III: At the feedback level $R_{ex}^{III} = -45$ dB that is independent of the external cavity length, Tkach et. al. observed that the mode-

hopping stopped for the DFB-laser used in their experiment. Also, the laser operated independently of the feedback phase in a single external cavity mode. We will discuss this phenomenon in Sect. 4.5.

Regime IV: Above R_{ex}^{IV} - -40 dB, satellite modes appear that are separated from the main mode by the relaxation oscillation frequency [17],[82]. [87] has provided an estimate of R_{ex}^{IV} based on an analysis of the stability of the solutions of the oscillation condition:

$$R_{ex}^{IV} = \frac{2\,\omega_R^2\,\tau_{in}^2\,r_2^2}{(1 - r_2^2)^2\,(1 + \alpha^2)} \tag{3.52}$$

If the factor 2 is omitted, R_{ex}^{IV} corresponds to the situation where the range of external cavity modes that are provided as solutions to the oscillation condition exceed $2\omega_R$. The significance of this finding is discussed in Sect. 4.6.

As the feedback level is increased further, satellite modes appear at $\pm 2\omega_R$, $\pm 3\omega_R$, etc. [82], with the laser line eventually broadening to up to 50 GHz. This behavior has been characterized by the term "coherence collapse" [13]. There is evidence that the behavior of the laser in this regime is chaotic, [15] and [78]-[82], i.e.. governed by dynamic instabilities due to the delayed feedback, rather than by effects related to the amplification of stochastic noise.

Regime V: It is necessary to anti-reflection coat the laser facet R_2 in Fig. 3.1 to achieve optical feedback that is stronger than the reflection from the laser facet. In this regime of strong optical feedback the laser operates with an extended optical cavity. Very narrow linewidths are observed. This can be expected from the oscillation condition graph, Fig. 3.3(e) and (f) based on the strongly increased slope of the constant phase curve which provides for a large linewidth-reduction factor F^2. However, the gain diffference between neighboring modes is very small (Fig. 3.3(e)) which allows fluctuations between external cavity modes to occur. This gain difference can be increased (Fig. 3.3(f)) if a diffraction grating is used to provide wavelength dependent optical feedback.

3.7. GENERAL DISCUSSION, STRONG VERSUS WEAK FEEDBACK

The five feedback regimes of [17] define unique characteristics of laser operation. Of practical interest for the improvement of the spectral characteristics of a laser are Regime III, with moderate optical feedback, and Regime V with very strong optical feedback. These two Regimes are separated by a Regime of dynamic instabilities, where the frequency noise and linewidth of the laser are dramatically increased due to optical feedback. Regime II is characterized by the presence of multiple external cavity modes. Although the linewidth of each individual mode might be low, the purity of the laser spectrum is degraded by the presence of strong sidemodes in the optical spectrum. Regime I is characterized by a limited reduction of the laser linewidth which is in addition sensitive to the phase of the returned light, thus making the arrangement very sensitive to mechanical disturbances.

We find in Chapter 4 that the optimal solution to obtain fairly stable narrow linewidth and single mode operation in the weak feedback domain, Regimes I to III, is to choose the external cavity length short enough such that Regime II disappears. In this case external cavity modes are not present and the linewidth of the laser is more or less reduced over a large range of the feedback phase. It will be shown in Chapter 4 that, starting from a solitary laser oscillating in several longitudinal chip modes, we obtained single mode operation with a sidemode suppression of ~1:20 and a linewidth reduction of ~50, i.e. from 100 MHz to 2 MHz [24].

A substantial improvement in the spectral characteristics of a laser is only possible by providing very strong optical feedback, i.e. by operating in Regime V, and *at the same time* using a frequency selective reflector, such as an optical grating. Not only are linewidths below 10 kHz and sidemode suppression ratios greater than 30 dB obtained [37], but the arrangement also allows tuning of the optical frequency to anywhere within a band of 50 nm (2000 THz), if the AR-coating of the laser is of sufficient quality. For the case of strong frequency selective optical feedback, the present study focuses in Chapter 5, on the spectral characteristics and the single-mode stability of the external grating laser during tuning of its oscillation frequency [36].

4. WEAK FEEDBACK

4.1. INTRODUCTION

In this chapter, we are concerned with the behavior of a laser in the three regimes of weakest optical feedback, i.e. with less than approximately -35 dB feedback power ratio. Weak optical feedback was recognized to provide a convenient means to reducing the linewidth of semiconductor lasers by several research groups [8]-[10],[12],[88]. The semiconductor laser does not have to be anti-reflection coated and the alignment tolerances required to achieve the required feedback levels from an external reflector are not very stringent. However, the phase of the returned light has a pronounced effect on the linewidth reduction factor (3.43) [10], which makes the arrangement sensitive to changes in the external cavity length by fractions of a wavelength and to changes in the oscillation frequency of the laser due to injection current and temperature drift. A control mechanism has been proposed [89] that adjusts the external cavity length automatically to achieve minimum linewidth operation.

Depending on the length of the external cavity and the strength of the optical feedback, the oscillation condition can be satisfied for more than one frequency in the vicinity of the solitary laser modes (Section 3.3.2. and Fig. 3.3). These frequencies are the frequencies of the external cavity modes. In Section 4.2 we review theoretical models that have been used by other authors to describe the nature of external cavity modes. Section 4.3 introduces the experimental arrangement used for our investigations. In Section 4.4 we present measurements that show the time-averaged distribution of optical power of the laser in the different external cavity modes. We will show that the mode with lowest linewidth carries most of the power. A frequency fluctuation model is proposed (Section 4.5) that explains this behavior and allows us to correctly predict mode-hopping frequencies. In Section 4.6 we show that the frequency span of the external cavity modes determines the critical

feedback level that causes coherence collapse (a version of Section 4.2 to 4.4 has been submitted for publication [23]).

Our attempts to narrow the linewidth of a semiconductor laser by weak external feedback were meant to provide sources suitable for coherent optical communication schemes. However the presence of several external cavity modes in the optical power spectrum degrades the purity of the optical oscillator. Schunk et. al. [90] calculated the bit error rates achieved in a FSK-heterodyne transmission scheme having lasers frequency stabilized with weak feedback from long external cavities. He noted that the presence of the external cavity modes to some extent cancels the advantages of the narrow linewidth. The amplitude of the external cavity mode oscillation can be reduced by choosing a short external cavity. This approach was experimentally verified and will be discussed in Section 4.7 (a version of this section has been published in [24])

4.2. MODELLING OF EXTERNAL CAVITY MODES

Due to the coupling between gain and oscillation frequency in a semiconductor laser the solution of the oscillation condition in a coupled cavity arrangement becomes multi-valued, leading to a set of external cavity modes centered around each solitary laser mode. This phenomenon has been discussed in Section 3.3.2 using Fig. 3.3(a) to (d). Each solution to the oscillation condition is associated with a different threshold gain and therefore with a different carrier-density.

In early work the characteristics of the laser with weak optical feedback were analyzed using small signal analysis [12]. This approach requires knowledge of the steady state operating point conditions. Generally it was assumed [12],[86] that the laser would oscillate in the mode with minimum threshold gain. On first examination this seems reasonable, considering that the gain saturates and does not increase further as the injection current is increased as soon as the laser starts oscillating (gain saturation). The small signal analysis does provide optical power spectra and frequency noise spectra that agree with the experimentally observed characteristics. The analysis is done in the frequency domain, the laser being viewed as a resonant noise

amplifier (3.28). External cavity modes appear as poles in the left half of the complex plane [12], i.e. represent additional damped resonances of the external cavity laser. Since the analysis is done in the frequency domain, the time evolution of the oscillation frequency of the laser is not considered.

Tkach et. al. [17] observed distinct frequency-hopping of the output of a laser when the external cavity was aligned to obtain two external cavity modes of equal linewidth. Schunk [21] observed in numerical simulations, using the rate equations of the laser with external feedback (3.2) and (2.19), that the laser tends to oscillate in the external cavity mode with minimum linewidth rather than the mode with minimum threshold gain. He proposed an intuitive explanation for this phenomenon by suggesting that the output frequency of the laser actually fluctuates between external cavity modes and that the average time the laser spends oscillating at the frequency of a narrow-linewidth mode is larger than for a large-linewidth mode.

Since each external cavity mode is associated with a different carrier-density, we require at the same time that the fluctuations of the carrier-density are large enough to allow transitions of laser oscillation from one external cavity mode to the neighboring mode. For weak feedback the threshold-gain difference between solutions of the oscillation condition is small and fluctuations of the carrier-density allow transitions between neighboring modes. This is in contrast to strong feedback, where the difference in carrier-density for neighboring solutions of the oscillation condition can become large enough that transitions between compound cavity modes are not possible any more merely due to spontaneous emission, leading to bistability in the laser operation (Chapter 5).

4.3. RING FEEDBACK VERSUS REFLECTIVE FEEDBACK

Experimental results were obtained with a 1.3-μm buried heterostructure laser (HLP 5400) configured as shown in Fig. 4.1(a) with optical feedback from a fiber ring. The optical isolator (Appendix A) prevented unwanted optical reflections, which might enter the fiber ring through port A4 in Fig. 4.1, from affecting the laser. Compared to an

(a)

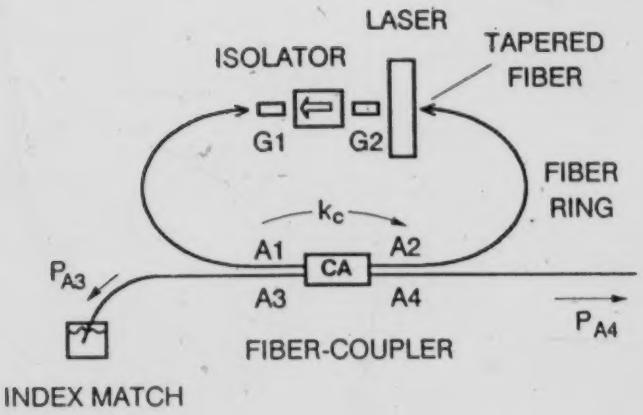

(b)

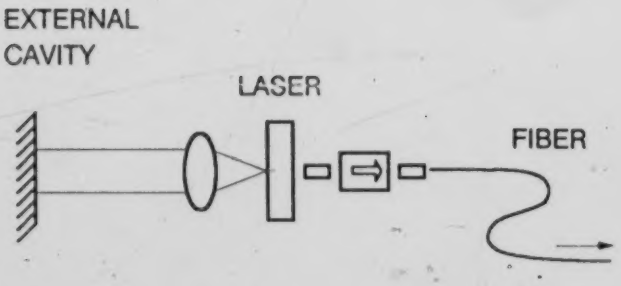

Fig. 4.1: (a) Sketch of the experimental setup used to provide optical feedback to a laser by means of an optical fiber ring. (b) Sketch of a comparable setup utilizing reflective feedback.

arrangement utilizing feedback from an external mirror, Fig. 4.1(b), the fiber-ring configuration is easier to align (only laser to fiber coupling has to be performed), has greater stability since only compact fiber-optic elements are used, and allows the feedback power ratio R_{ex} to be measured directly.

We assume that the external cavity mode behavior is independent of travelling wave or standing wave effects in the semiconductor laser cavity. This assumption is reasonable, since the external cavity is long compared to the laser cavity and the external cavity mode behavior is well described by a model of the semiconductor laser that considers this laser as a lumped element, namely the rate-equation model (3.2). Therefore, for the following observation of the external cavity mode behavior it is of no significance whether optical feedback is provided in a ring configuration or from an external mirror.

In the feedback arrangement of Fig. 4.1(b) a direct measurement of the optical feedback power ratio R_{ex}, i.e. the ratio between the power emitted from the laser, P_0, and the power coupled back into the fundamental mode of the laser, is not possible. [17] used a variable optical attenuator in the path of the collimated light between laser and external reflector. Like [91] and [14], [17] obtained a value for R_{ex} by increasing the optical feedback until two external cavity modes appeared in the optical spectrum. This transition between feedback regimes I and II defines the value for R_{ex}^{II}, (3.51). From this point on one has to rely on the calibration of the optical attenuator, when R_{ex} is changed. Changes in the distortion of the phase front by the optical attenuator, as the attenuator-setting is changed, lead to errors in the estimated value of R_{ex}.

In the fiber-ring arrangement R_{ex} can be determined from P_0 and the output P_{A3} and P_{A4} from port A3 and A4 of the fiber coupler in the fiber ring (Fig. 4.1(a)):

$$R_{ex} = \frac{P_{A3} \cdot P_{A4}}{P_0^2} \frac{k_c}{(1-k_c)^2} \frac{1}{\eta_c} k_{pol} \qquad (4.1)$$

where k_{pol} accounts for the polarization mismatch between the laser field and the feedback field coupled back into the laser, k_c is the ratio of the power coupled from port A1 to port A2 of the fiber coupler

and $\eta_c = 10^{-(x/10)}$, where x is the excess power loss of the coupler in dB. The value of $k_{pol} \sim .6$ was determined experimentally by observing the output from the tapered fiber on the right side of the laser in Fig. 4.1(a) through a polarizer. Since we want to compare the number and location of the external cavity modes in the optical power spectrum with the prediction from the oscillation condition graph, R_{ex} has to be determined independent of the oscillation condition graph, which is achieved by using (4.1).

4.4. EXTERNAL CAVITY MODES - EXPERIMENT

The experiment described in this section was designed to answer the question, "which of the external cavity modes in the optical power spectrum carries most of the power?". The spectra given in Fig. 4.3 were obtained with the experimental setup shown in Fig. 4.2, by heterodyning the output of the test-laser with that of an external grating laser [37] (Chapter 5). The IF-spectrum of the test-laser without optical feedback from the fiber ring was recorded initially (Fig. 4.3, $R_{ex} = 0$) to allow determination of ω_0 in the IF-spectrum. Oscillation in a single longitudinal mode of the laser-cavity was ensured by utilizing the weak optical feedback from the .23 mm external cavity between the front facet of the laser and the GRIN-rod lens facet closest to the laser (Fig. 4.2) [92],[93]. Both facets of the GRIN-rod lens were AR-coated. The optical isolator prevented optical reflections from the measurement system from affecting the test-laser. The length of the fiber section of the ring cavity, including the 3-dB fiber coupler, was measured to be 115.1 cm, and the overall length of the optical isolator assembly to be 4.24 cm (equivalent optical path length in air), leading to an estimated roundtrip-time in the ring-cavity of $\tau_{ex} = (1/175)\ \text{MHz}^{-1}$. The spectrum of the laser with fiber-ring feedback was recorded for different feedback levels by adjusting the coupling efficiency between the laser and the tapered fiber at the rear facet of the laser using a piezo-driven micrometer to move the fiber perpendicular to the plane of the active region of the laser. The total time taken for all measurements was short enough (~ 1 min) to prevent frequency-drifts of the oscillation

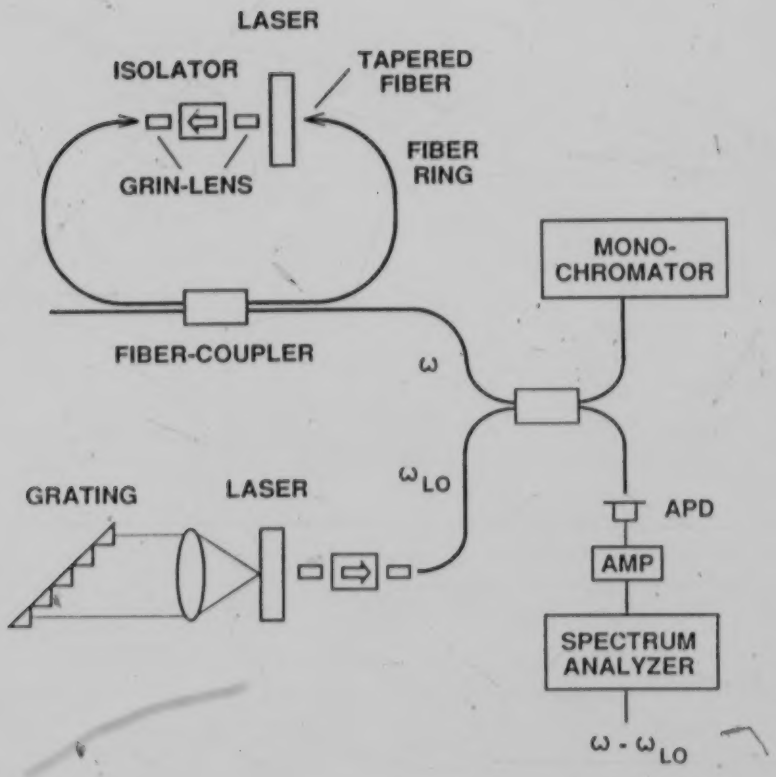

Fig. 4.2: Sketch of the measurement setup showing the test laser with optical feedback from a fiber ring and the reference laser with strong frequency selective feedback from a diffraction grating.

frequency of the reference laser and the solitary test laser from affecting the results.

The power in each external cavity mode is proportional to the area under the lineshape of the mode, if the optical power spectrum is plotted on a linear scale as in Fig. 4.3(b). It can be seen from Fig. 4.3(b) that the power in the mode closest to the solitary laser frequency is approximately 6 times larger than the power in the neighboring external cavity modes for R_{ex} = -60 dB and -55 dB. Therefore, the mode closest to the solitary laser frequency carries not only most of the power, but is also, as shown in the argument associated with equation (3.44), the mode with lowest linewidth.

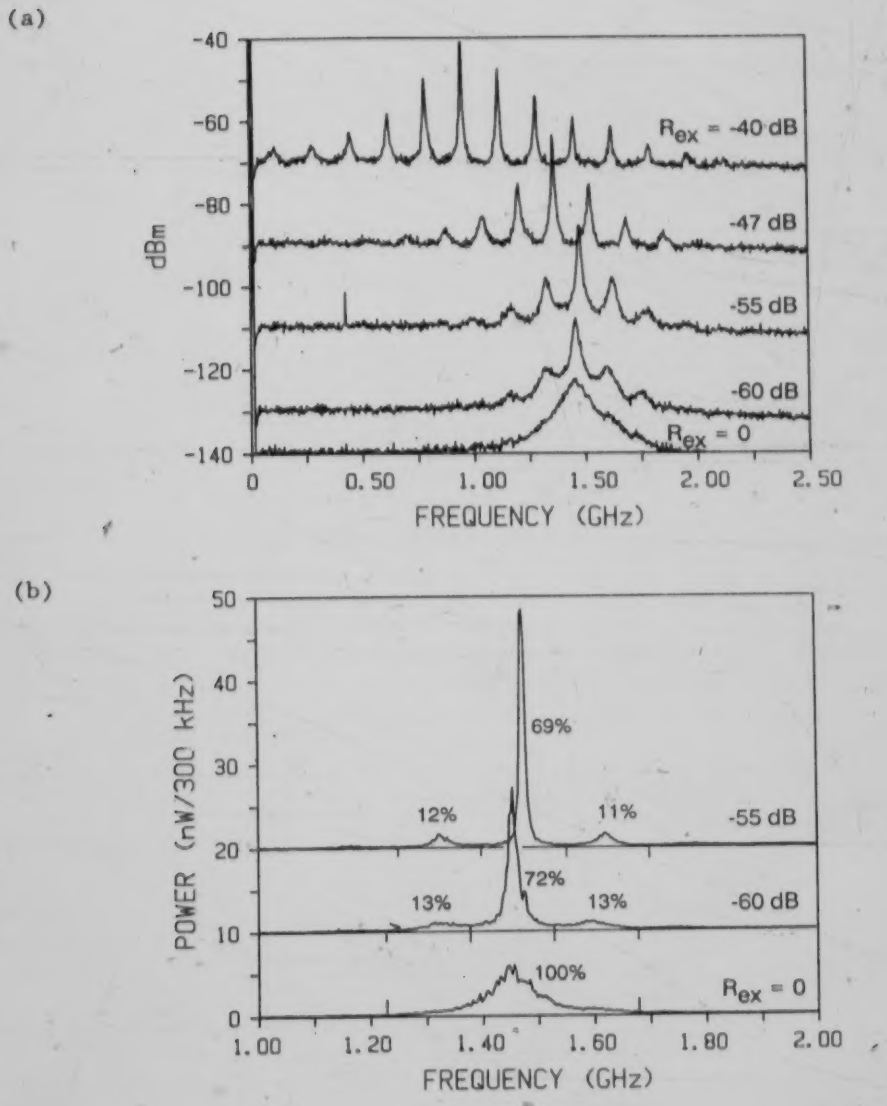

Fig. 4.3: Optical spectra of the test laser recorded for different feedback levels using a reference laser with negligible (<10 kHz) linewidth. Displayed is the power spectrum of the APD-current (a) on a logarithmic scale and (b) on a linear scale. The IF-filter bandwidth of the spectrum analyzer was 300 kHz. In the IF-spectrum $\omega_0/2\pi$ is 1.457 GHz. The traces for (a) R_{ex} = -47, -55, -60 dB and R_{ex} = 0, and (b) R_{ex} = -60 dB and -55 dB are offset vertically for clarity. In Fig. 4.3(b) the area under each external cavity mode is given in percent of the area under the spectrum for R_{ex} = 0. The limits of integration are indicated by markers on each side of the external cavity modes.

For R_{ex} = -55 dB, the ratio of power in the external cavity modes has also been determined by curve fitting a Lorentzian lineshape to each external cavity mode. The linewidths of the five lineshapes fitted to the external cavity modes of the spectrum shown in Fig. 4.4(c) were 45, 25, 7.5, 25 and 45 MHz, respectively, and their separation was 149 MHz. The scaling factor in the Lorentzian-lineshape equation had values of .04, .2, 1.5, .2 and .03 μW, respectively. These scaling factors are equal to the power in each lineshape. The dash-dotted curve in Fig. 4.4(c) is obtained from the superposition of a constant noise floor of -69 dBm and these five Lorentzian lineshapes. This curve provides a good approximation to the measured spectrum. The above linewidth and power values indicate for this spectrum that most of the power is in the mode with minimum linewidth.

The power in the center mode of the spectrum remains highest for the traces R_{ex} = -47 dB and -40 dB of Fig. 4.3(a). For those two traces the area under the lineshape of the center mode was found to be respectively 5.5 and 3.7 times larger than the area under the strongest neighboring mode. However, the center mode does not remain close to the solitary laser frequency for higher feedback levels. The envelope of the external cavity modes is shifted at R_{ex} = -47 dB by approximately 100 MHz towards negative frequencies and at R_{ex} = -40 dB this shift is approximately 500 MHz.

The number of external cavity modes, their frequency and optical power are compared in Fig. 4.4 to the intersections between constant phase and loss curves in the gain versus frequency chart. The mode with minimum gain in Fig. 4.4(d) is 670 MHz lower in frequency than the solitary laser mode. This offset is much larger than the measured shift by ~100 MHz of the envelope of the optical power spectrum for the same feedback level of R_{ex} = -47 dB. For R_{ex} = -40 dB the corresponding frequency shifts are 1.7 GHz for the mode with minimum gain and ~500 MHz for the spectral envelope (Fig. 4.3). We can therefore conclude that the laser does not oscillate in the external cavity mode that has minimum threshold gain.

Olesen et al. [15] attributed the parallel shift of all external cavity modes towards negative frequencies, distinctly visible in Fig. 4.3(a) at feedback levels of -47 dB and higher, to incoherent feedback.

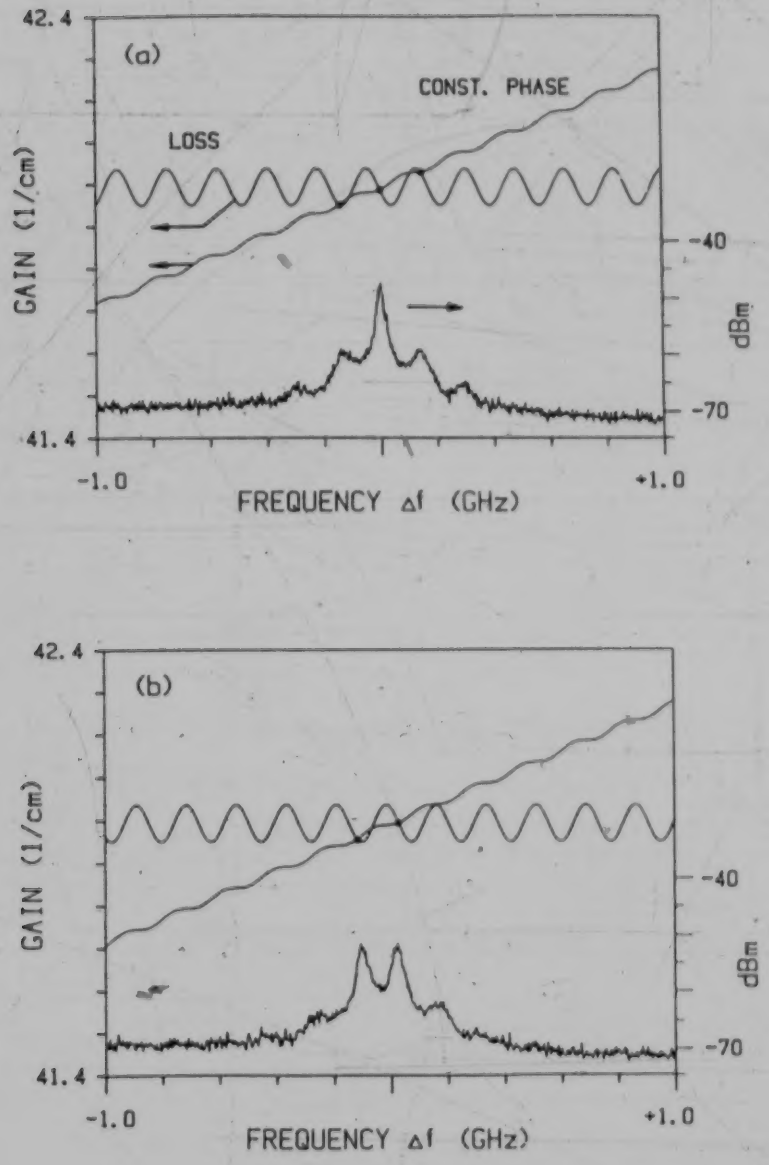

Fig. 4.4: Gain versus frequency charts showing constant phase curves (positive slope) and loss curves (sinusoidal) for 3 different feedback levels and phase-shifts ψ_e: (a) R_{ex}=-60 dB and ψ_e=0°, (b) -60 dB and -140°, (c) -55 dB and -30° and (d) -47 dB and 0°. Other parameters used in the calculations were $\Delta\nu_{in}$= 150 GHz, $1/\tau_{ex}$= 175 MHz, α = 6 and R_1 = .35. The lower curves are the measured spectra.

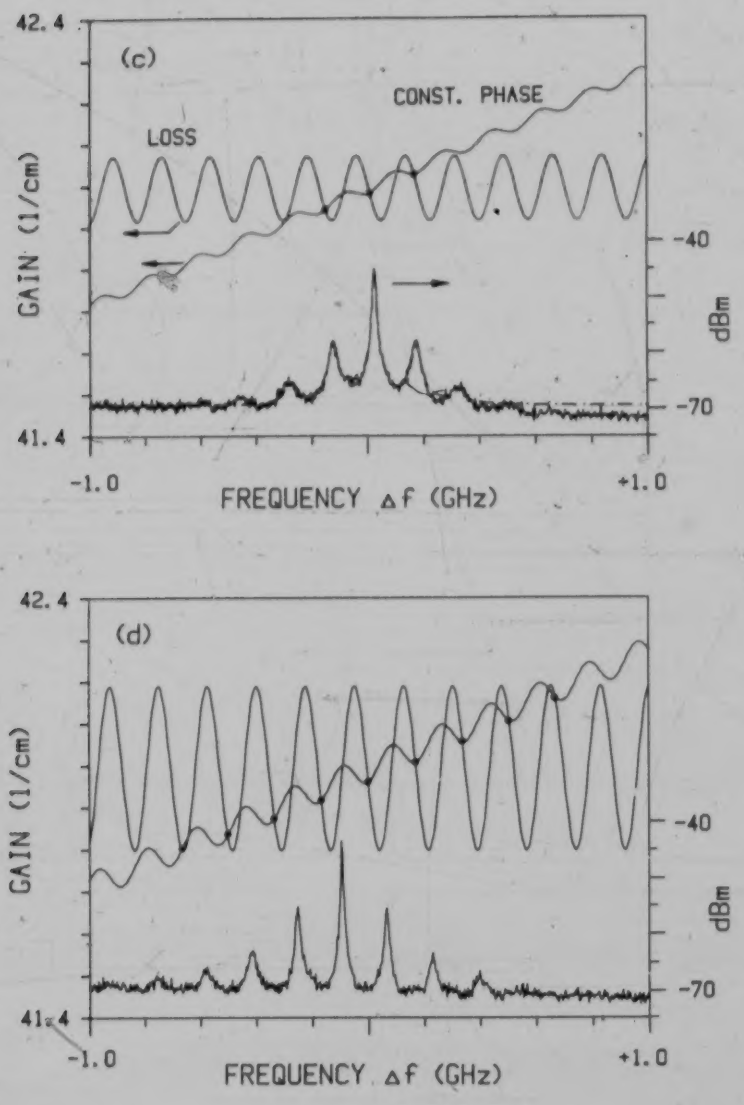
42.4
(c)
CONST. PHASE
LOSS
GAIN (1/cm)
-40
dBm
-70
41.4
-1.0
FREQUENCY Δf (GHz)
+1.0
42.4
(d)
GAIN (1/cm)
-40
dBm
-70
41.4
-1.0
FREQUENCY Δf (GHz)
+1.0

Fig. 4.4 (cont.)

His argument is that if the random fluctuations of the oscillation frequency of the laser are large during a time-interval equal to the roundtrip time in the external cavity, the light fed back into the laser is no longer phase-coherent with the electric field in the laser. For a short period of time the injected light does not interfere with the light in the cavity any more but still reduces the carrier-density in the laser, hence reducing the gain and providing a frequency shift of the oscillation frequency of the laser towards negative frequencies. In the steady state picture of the oscillation condition chart, fluctuations of the oscillation frequency are not taken into account, thus explaining the lack of shift towards negative frequencies of the calculated external cavity modes in Fig. 4.4(d).

The lower traces in Fig. 4.4(a) and (b) have been recorded for the same feedback level but for different values of the parameter ψ_e (3.45), i.e. different lengths of the external cavity resulting in different roundtrip-phase shifts in the feedback path. In Fig. 4.4(b) the two external cavity modes have equal power. The oscillation condition graph, that has a shift of external cavity mode frequencies with respect to ω_0 that is equal to the observed shift in Fig. 4.4(b), has a value of $\psi_e = -140°$.

Tkach et. al. [17] claimed that two modes of equal power exist when there are two modes of minimum linewidth, which occurs for $\psi_e = -180°$ (Fig. 3.5(b)). However, no mention is made in [17] as to the technique used to verify this claim. The direct measurement of ψ_e is not possible because the external cavity length and the optical frequency can not be measured to the required accuracy. The numerical simulations of [21] show a higher power in the mode with lower threshold gain mode when the linewidth of the two modes is equal ($\psi_e = -180°$). [21] also shows that an imbalance of the linewidth reduction factor between modes leads to an increase in power of the lower linewidth mode; to the extent that a mode with higher threshold gain but lower linewidth can have higher power, a situation that we observe in our experimental data for instance in Fig. 4.4(a). There has to be a cross-over point where the advantage of lower threshold gain and disadvantage of higher linewidth for the lower frequency mode lead to a balance in power between two external cavity modes. A feedback condition of this type is observed in the

experimental data of Fig. 4.4(b). The value of ψ_e = -140° is located between ψ_e = -180° where the lower frequency mode has more power, and ψ_e = 0° where the higher frequency mode has more power according to our discussion.

In conclusion our experimental results confirm the postulate for weak feedback, namely that the linewidth of the external cavity modes is the dominant factor in determining the power of the individual modes.

4.5. FREQUENCY FLUCTUATION MODEL

This model allows us to calculate the duration of oscillation in each external cavity mode depending on the linewidth of this mode. The model is based on a calculation of the probability that the fluctuation of the instantaneous frequency of the laser, oscillating in one specific external cavity mode, is larger than half of the external cavity mode separation, $\Delta\nu_{ex}/2$. We assume that a frequency deviation of this magnitude causes the laser to switch from oscillation centered on one external cavity mode to an oscillation within the potential well of the adjacent mode.

The treatment of laser frequency fluctuations by [72], outlined in Section 2.4.5, refers to the frequency fluctuations of a solitary laser observed in the electrical domain after optical heterodyning and bandpass filtering (Fig. 2.4). To be able to use the same approach to estimate the frequency fluctuations of a laser within one external cavity mode, we make the following simplifying assumptions:

(1) the noise process governing the frequency fluctuations of the laser, while the laser is oscillating in the i-th external cavity mode, can be described by the same noise process that is valid for a solitary laser with linewidth $\Delta\nu_i$ (Fig. 2.2(b)), where $\Delta\nu_i$ is the linewidth of the i-th external cavity mode.

(2) the frequency noise power spectrum $W_{\Delta\omega}(f)$ has a constant amplitude of $W_{\Delta\omega}(f) = 2\pi\Delta\nu_i$ up to a frequency of $B = f_R$, where f_R is the relaxation oscillation frequency of the laser. For frequencies larger than f_R, the frequency noise is assumed to be zero.

Using the same argument that led to (2.83) and (2.84) we can now determine the square of the standard deviation, $\sigma_{\Delta\omega}^2$, of the frequency fluctuations

$$\sigma_{\Delta\omega}^2 = 2\pi\Delta\nu_i \cdot 2f_R \quad . \tag{4.2}$$

and the probability distribution function of the instantaneous frequency, $\Delta f = \Delta\omega/2\pi$,

$$P_{\Delta f}(\Delta f) = \frac{1}{\sqrt{2\Delta\nu_i f_R}} \exp\left(- \frac{\Delta f^2 \pi}{2\Delta\nu_i f_R} \right) \tag{4.3}$$

where $\Delta\nu_i$ is the linewidth of tne external cavity mode the laser actually oscillates in. The probability for a frequency deviation greater than $\Delta\nu_{ex}/2$ is given by the cumulative probability distribution function

$$C_{\Delta f}(\Delta\nu_{ex}/2) = 0.5 - 0.5 \text{ erf} \left(\frac{\Delta\nu_{ex}\sqrt{\pi}}{\sqrt{8\Delta\nu_i f_R}} \right) . \tag{4.4}$$

When the system is bandlimited to bandwidth f_R, samples of the instantaneous frequency of oscillation become uncorrelated if we sample with a rate of $1/2f_R$ (first zero of the autocorrelation function if an ideal bandpass is assumed for the bandlimiting system [94]). We assume therefore that the probability of no frequency deviation larger than $\Delta\nu_{ex}/2$ within the time $1/2f_R$ is $1 - C_{\Delta f}(\Delta\nu_{ex}/2)$. The assumption that the probability of a frequency deviation larger than $\Delta\nu_{ex}/2$ is proportional to the length of the time interval, leads us to a Poisson distribution ([94], p. 495). For a Poisson distribution the average number of frequency deviations greater than $\Delta\nu_{ex}/2$ per second is then given by [94]

$$\mu = - 2f_R \ln[1 - C_{\Delta f}(\Delta\nu_{ex}/2)]$$

or

$$\mu \approx f_R \left(1 - \text{erf} \left(\frac{\Delta\nu_{ex}\sqrt{\pi}}{\sqrt{8\Delta\nu_i f_R}} \right) \right) \tag{4.5}$$

where we use the relation $\ln(1+x) \approx x$ for $x \ll 1$. From $\Delta\nu_i = \Delta\nu_0/F^2$, (3.43)

and the assumption of $\kappa\tau_{ex}\sqrt{1+\alpha^2} \gg 1$, we obtain for the modes close to ω_0,

$$\mu \approx f_R \left(1 - \mathrm{erf}\left(\frac{\Delta\nu_{in}(1-R_1)\sqrt{\pi(1+\alpha^2)R_{ex}}}{\sqrt{8R_1\Delta\nu_0 f_R}}\right)\right). \qquad (4.6)$$

Equation (4.5) shows that the frequency of mode-hops decreases as the linewidth $\Delta\nu$ of the external cavity mode decreases, supporting the model that postulates that a longer mean-duration of stay ($1/\mu$) in the mode results in a lower linewidth [21].

We will now compare the predictions of (4.5) and (4.6) with the experimental results obtained by Tkach et. al. [17] for a DFB-laser with optical feedback. In the special case where two modes of equal power exist in the center of the optical spectrum (Fig. 4.4(b)), Tkach et. al. have observed a decreasing frequency of mode-hops between these two modes as the feedback level, R_{ex}, is increased. This is in agreement with (4.5), plotted in Fig. 4.5 as a solid line for $\Delta\nu_{ex}$= 375 MHz,

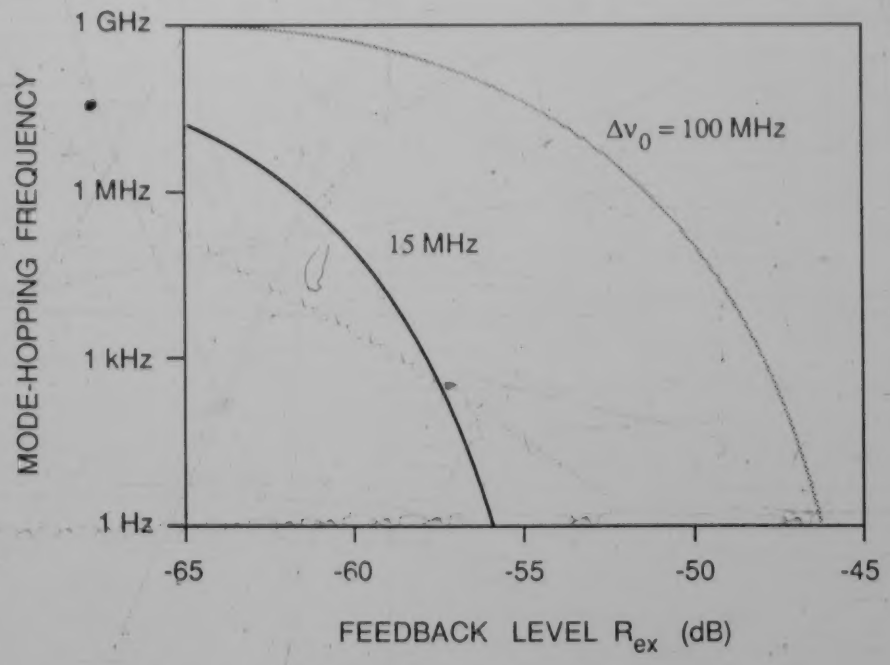

Fig. 4.5: Mode hopping frequency μ versus feedback level R_{ex} calculated from (4.5).

$\alpha = 6$, $f_R = 5$ GHz, $\Delta\nu_0 = 15$ MHz and $\Delta\nu_{in} = 150$ GHz. The first three parameters are data provided in [17], the last two parameters were chosen to obtain agreement between the calculated (4.5) and the measured [17] value of the mode-hopping frequency $\mu = 1$ MHz at $R_{ex} = -62$ dB. We note that this agreement is obtained using reasonable values for $\Delta\nu_0$ and $\Delta\nu_{in}$.

At higher feedback levels the calculated mode-hopping frequency reduces to very low values (1 Hz at $R_{ex} = -56$ dB), suggesting that transitions between external cavity modes become very unlikely and stable oscillation in one external cavity mode becomes possible. In the experiment [17], the oscillation frequency of the laser stabilizes in one external cavity mode at a feedback level of $R_{ex}^{III} = -45$ dB (Section 3.6, Regime III). The important experimental observation is that this feedback level is independent of the external cavity length. The gain difference between external cavity modes at these feedback levels is approximately $(2/\alpha v_g) \cdot 2\pi\Delta\nu_{ex}$ and is therefore inversely proportional to the external cavity length. The independence of R_{ex}^{III} on the external cavity length can therefore not be related to the gain difference of these modes, as suggested in [17]. However if we use the frequency fluctuation model and the approximation (4.6), which is valid if a large number of external cavity modes satisfy the oscillation condition and therefore valid at the transition to Regime III if $L_{ex} > 10$ cm, the mode-hopping frequency is indeed independent of $\Delta\nu_{ex}$ and therefore independent of the external cavity length L_{ex}. We conclude that the model of frequency fluctuations describes the behavior of the laser with optical feedback correctly, and can be used to explain the increased power in the mode of narrowest linewidth, rather than the mode with minimum threshold gain.

The modehopping frequency μ in the approximation (4.6) increases if the linewidth of the solitary laser $\Delta\nu_0$ increases. If we relate the feedback level at the transition into Regime III, R_{ex}^{III}, to a certain, very low value of μ, then R_{ex}^{III} must increase as $\Delta\nu_0$ increases. For example, the level of feedback, R_{ex}, that leads to a mode-hopping frequency of $\mu = 1$ Hz, is increased by 10 dB in Fig. 4.5, when $\Delta\nu_0$ is increased from 15 MHz to 100 MHz. Regime III, as determined by [17] using one single DFB-laser, spans the range $R_{ex} = -45$ dB to -39 dB. In

contrast to [17], we used a Fabry-Perot laser in our experiment, which has, in single-mode operation, a linewidth of $\Delta\nu_0 \sim 100$ MHz. Based on the previous comparison of feedback levels for the same values of μ for the DFB and the Fabry-Perot laser, we expect an increase of R_{ex}^{III} by 10 dB for our laser. This leads, however, to $R_{ex}^{III} > R_{ex}^{IV}$ and therefore to the absence of Regime III for our laser. In agreement with this prediction, a regime of stable oscillation in a single external cavity mode was not observed in our experiments, Fig. 4.3. The sidemode-suppression in Fig. 4.3 between the mode of highest power and the neighboring modes was -10 dB for $R_{ex} \sim$ -60 dB to -40 dB.

4.6. CRITICAL FEEDBACK LEVEL

In the above model we have not considered the presence of a resonance peak in the frequency fluctuation spectrum at $f_R = \omega_R/2\pi$ [65] and the resulting components in the optical power spectrum at $\omega_0 \pm \omega_R$. A strong increase in the power of the components at $\omega_0 \pm \omega_R$ marks experimentally the feedback level that defines the transition [17] to Regime IV (Section 3.6), the regime of coherence collapse.

The optical power spectrum of the laser with external feedback, as R_{ex} is increased from -55 dB to -30 dB and observed with a Fabry-Perot interferometer, is shown in Fig. 4.6. The peaks in the optical power spectrum separated from the center frequency of oscillation by the relaxation oscillation frequency of the laser, ~ 3 GHz in Fig. 4.6, are clearly visible. The increased resolution obtained in the heterodyne beat spectrum, Fig. 4.7, allows us to verify that the oscillation of the laser remains centered at the frequencies of the external cavity modes even in Regime IV. The set of external cavity modes centered around ~ -2 GHz in Fig. 4.7 belongs to the relaxation oscillation peak of the laser. The technique used to record Fig. 4.7 is explained in Appendix B (Fig. B.3).

The good correlation between calculation and measurement for the frequencies and the total range of frequencies, $2\Delta\omega_{max}$, of external cavity modes in Fig. 4.4 and the fact that even the peak in the optical power spectrum at the relaxation oscillation frequency of the laser

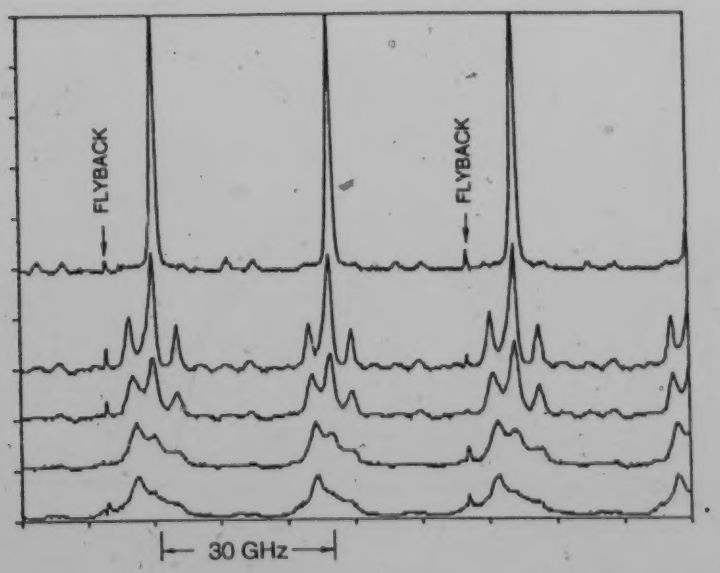

Fig. 4.6: Optical power spectra recorded with a Fabry-Perot interferometer (FSR = 30 GHz) for R_e = -55 dB to -30 dB (top to bottom). One sweep of the interferometer encompasses two spectral orders. The time of reset of the sweep is marked in the diagram.

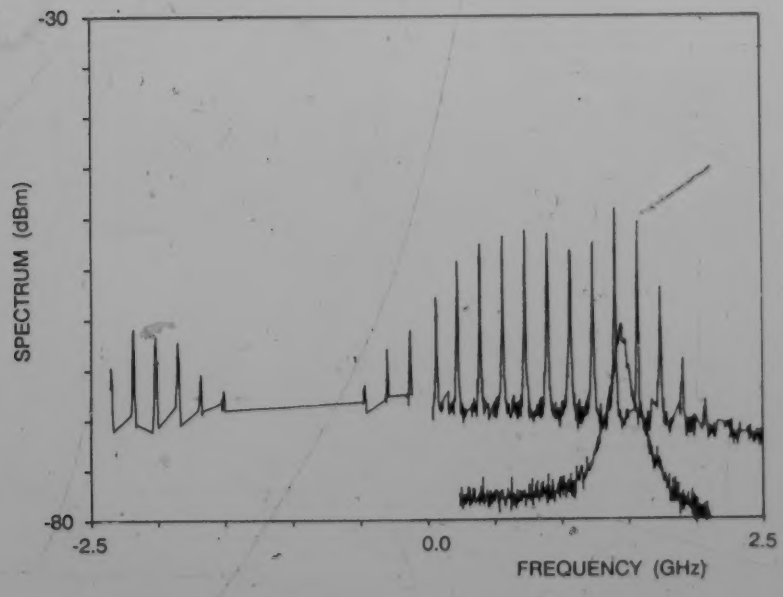

Fig. 4.7: Heterodyne beat spectra for no optical feedback (bottom trace) and -37 dB of optical feedback (top trace). Notice the set of external cavity modes that is separated from line-center by 2.8 GHz (= relaxation resonance frequency).

shows a structure linked to external cavity mode frequencies, suggests that external cavity modes at $\omega_0 \pm \omega_R$ will appear when $\Delta\omega_{max} \geq \omega_R$. Using (3.46) this condition can be written as $\kappa\sqrt{1+\alpha^2} \geq \omega_R$, or in terms of the feedback level R_{ex}^{IV} that leads to coherence collapse

$$R_{ex}^{IV} \geq \frac{\omega_R^2 R_2}{(1-R_2)^2 (1+\alpha^2) \Delta\nu_{in}^2} . \qquad (4.7)$$

Although (4.7) is derived from a model that considers only the steady state solutions of the oscillation condition of a laser with optical feedback, it nevertheless agrees with predictions made by others. Henry and Kazarinov [86] have stated that the onset of coherence collapse occurs when κ is comparable to ω_R. Mørk and Tromborg [90] have derived an expression for R_{ex}^{IV} that is equal to (4.7) except for a factor of 2 in the numerator by analyzing the stability of the solutions of the oscillation condition for a laser with optical feedback. Finally, the dependence of R_{ex}^{IV} on $\Delta\nu_{in}$, α and the output power P of the laser ($\omega_R \propto \sqrt{P}$) as described by equation (4.7) agrees with the results obtained by [21] from computer simulations based on the rate equations of a laser with optical feedback.

4.7. SHORT RING CAVITY

Weak optical feedback was shown in Section 4.4 and Fig. 4.3 to not only provide the desired narrow-linewidth mode in the center of the optical spectrum but also external cavity modes that degrade the spectral purity of the optical oscillator.

The amplitude of the oscillations of the loss curve in Fig. 4.4 is proportional to r_{ex}, (3.35) and (3.38), and the period is proportional to the round-trip time in the external cavity, τ_{ex}^{-1}. By decreasing the external cavity length at a given feedback level the number of external cavity modes at a given feedback level are reduced. At the same time the chirp reduction, F, of the center mode is reduced, (3.47), which is not desirable but has to be tolerated in the tradeoff between presence of multiple external cavity modes and maximum achievable linewidth reduction.

Ultimately it is desirable to have the external cavity short enough to obtain $\Delta\nu_{ex} > f_R$. In this situation external cavity modes would be located at frequencies separated from the center frequency of oscillation by more than the relaxation oscillation frequency and external cavity modes next to the center mode would only appear as we increase the feedback level to enter Regime IV. Theoretical frequency noise spectra presented in [75] indicate that external cavity modes in the optical spectrum can be avoided if tex-1 > fR, in agreement with our considerations based on the presence of multiple solutions in the oscillation condition graph.

Our experimental results for short fiber ring cavities are presented in Fig. 4.8 to 4.13. The power spectra were obtained using a self-heterodyne setup (Appendix B). Instead of mixing the output of the test laser with the output of an independent reference laser, Fig. 4.2, the output of the test laser is divided into two components with a 3 dB optical splitter. One component is shifted by 80 MHz in the optical frequency domain with an acousto-optic frequency shifter and the other component delayed in time by τ_d using a fiber of length L_d (Fig. A.1). A heterodyne output signal is obtained by squaring the sum of both components via the square law characteristic (current proportional to square of an electrical field) of the APD. The center frequency of the self-heterodyne beat spectrum is at 80 MHz. Features of this spectrum that are translated by the mixing process into the negative frequency domain are displayed by the spectrum analyzer in the positive frequency domain. In Fig. 4.8 the external cavity mode marked "-1" is such a negative-frequency component of the self-heterodyne beat spectrum.

A suppression of external-cavity side modes by more than 25 dB and a linewidth of 1.5 and 2.5 MHz, respectively, compared to a solitary laser linewidth of ~ 120 MHz is obtained in Fig. 4.9(a) and (b) for a laser configured as shown in Fig. 4.1(a). The length of the fiber-ring including the optical coupler and the optical isolator assembly was 29 and 17 cm, respectively, and the feedback level was Rex ~ -43 dB. The separation of the external cavity modes was 680 MHz and 1 GHz, respectively.

Fig. 4.9(a) is a trace of the amplitude of the self-heterodyne beat spectrum at 80 MHz as the external cavity length is changed. This

(a)

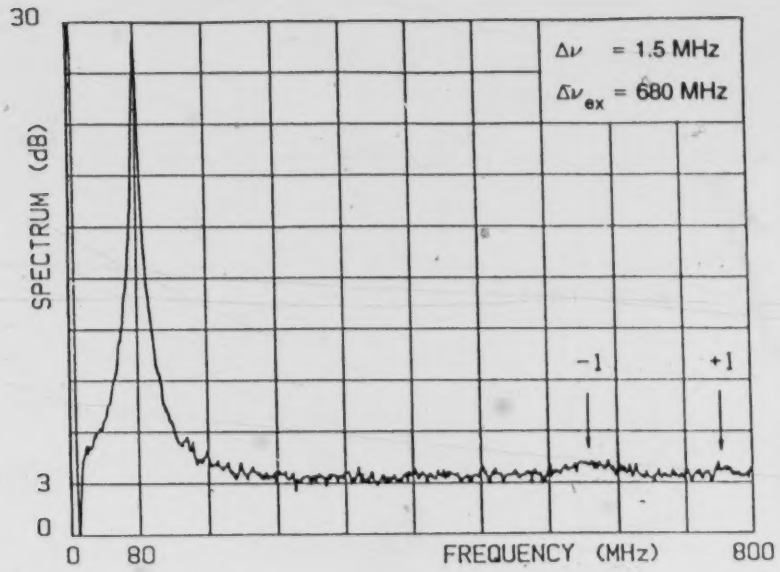

(b)

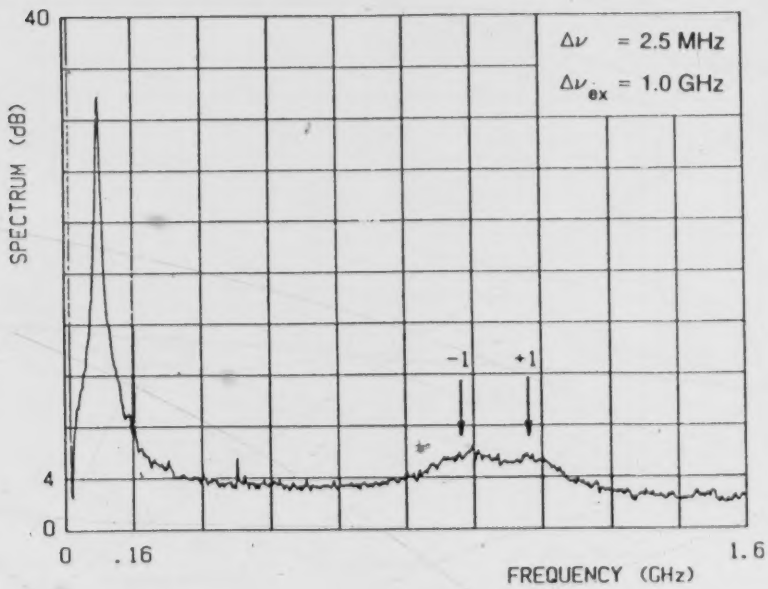

Fig. 4.8: Self-heterodyne beat spectra for (a) 29 cm and (b) 17 cm long fiber rings and R_{ex} = -43 dB, showing laser linewidths of 1.5 MHz and 2.5 MHz, respectively, and more than 25 dB suppression of neighboring external cavity modes.

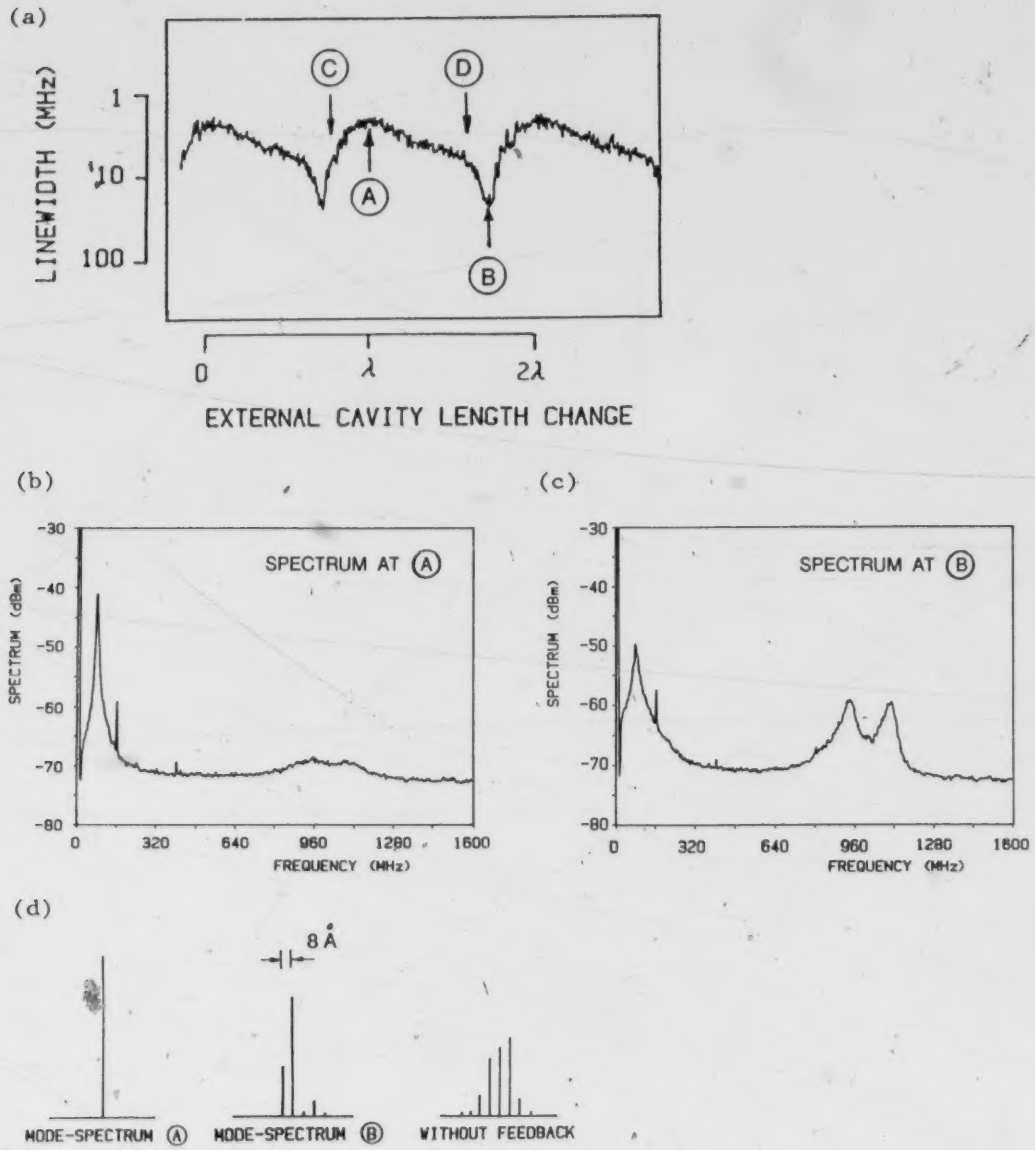

Fig. 4.9 Dependence of (a) the linewidth and (b) to (d) the side-mode suppression on changes of the external cavity length by fractions of a wavelength. The data is obtained for L_{ex} = 17 cm and R_{ex} ~ -43 dB. A linear increase of L_{ex} is achieved be applying a voltage ramp to the piezo-electric micrometer controlling the axial position of the tapered fiber end closest to the optical isolator in Fig. 4.1. (b) and (c) show the external cavity mode amplitude in the self-heterodyne beat spectrum, measured at (A) and (B) of Fig. 4.9(a), respectively. (d) shows the amplitude of the semiconductor cavity modes, recorded with a monochromator at point (A) and (B) of Fig. 4.9(a) and for the laser without feedback, respectively.

amplitude is inversely proportional to the linewidth, as can be seen from eq. (B.1) in Appendix B. Fig. 4.9(a) provides us therefore with the dependence of the linewidth of the laser at a fixed feedback level of R_{ex} ~ -43 dB on the external cavity length. The linewidth versus fiber ring length-characteristic is periodic with period g, where g = 1293 nm is the wavelength of the light emitted by the laser. Within 80% of each period, the linewidth is below 7 MHz, the minimum linewidth being ~2.5 MHz, at point (A) in Fig. 4.9 with a beat spectrum as shown in Fig. 4.9(b), the maximum linewidth being ~13 MHz at point (b) with a beat spectrum as shown in Fig. 4.9(c). Not only does the laser oscillate at point (B) in several external cavity modes, as indicated in the beat spectrum 4.9(c), but also in several longitudinal modes of the semiconductor laser cavity, Fig 4.9(d). At point (A) the laser oscillates in one longitudinal mode of the semiconductor laser cavity. The longitudinal mode spectrum of the laser without optical feedback from the fiber-ring is shown also in Fig. 4.9(d).

As the length of the external cavity is changed, the roundtrip phase shift $\omega_0\tau_{ex}$ changes and therefore ψ_e, as defined in (3.45), and the frequency that satisfies the oscillation condition (3.46) changes. Altering the external cavity length therefore changes the frequency of oscillation of the laser with fiber-ring feedback. The recording of the beat spectrum between the laser with fiber-ring feedback and a reference laser (Fig. 4.2) is shown in Fig. 4.10. As the fiber-ring length is decreased continuously over one wavelength, the laser oscillates in a single mode, where the frequency of oscillation increases continuously over a range of ~700 MHz. Further decrease in the fiber-ring length causes the oscillation frequency of the laser to repeat its scan through the same band of 700 MHz.

The linewidth reduction $(1/F^2) = (\Delta\nu/\Delta\nu_0)$ in Fig. 4.11 is determined from the ratio of the measured linewidth $\Delta\nu$ to the linewidth of $\Delta\nu_0$ ~ 120 MHz of the solitary laser oscillating in a single longitudinal mode with sidemode suppression ratio of ~10 dB. Oscillating in multiple longitudinal modes, a laser of the type used in our experiment (HLP 5400) has a linewidth of the individual modes of ~ 500 MHz [44]. The experimentally observed dependence of the linewidth reduction, $(1/F^2)$, on the feedback level, R_{ex}, shows for low feedback levels a decrease of

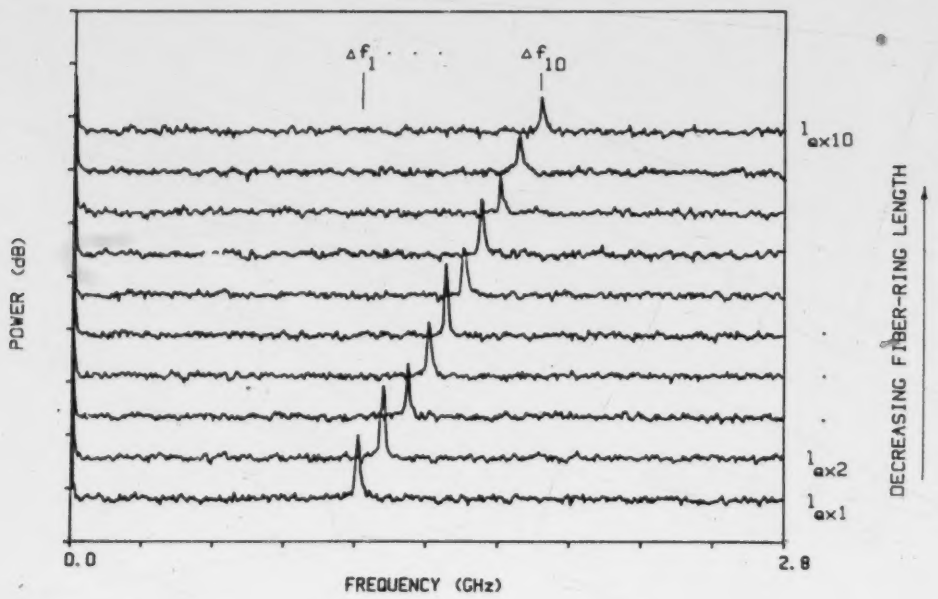

Fig. 4.10: Beat spectra between the laser with fiber-ring feedback, L_{ex} = 17 cm and R_{ex} ~ -43 dB, and an external grating laser with negligible linewidth. The ten traces are recorded as the fiber-ring length is swept from (C) to (D) in Fig. 4.9(a). The experimental setup shown in Fig. A.1 is used for this experiment, however the accousto-optic frequency shifter is turned off.

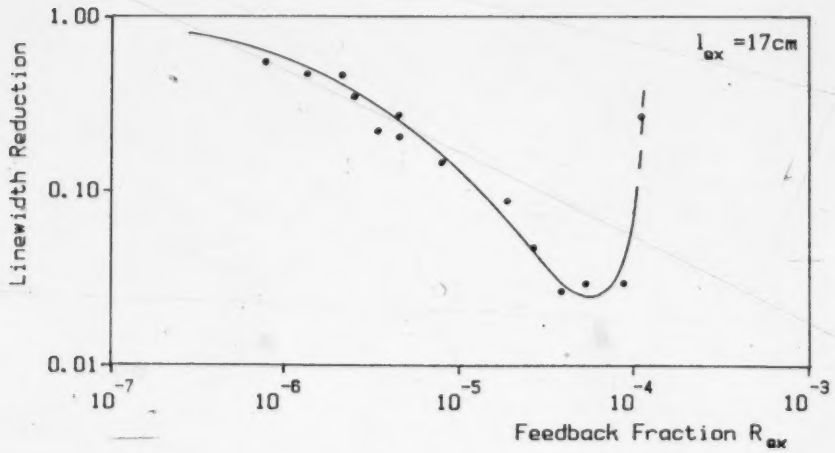

Fig. 4.11: Linewidth reduction as a function of the feedback level. The measured values are indicated by dots.

$(1/F^2)$ with increase in R_{ex} in accordance with (3.3) and (3.47). At $R_{ex} \sim 10^{-4}$ the sudden increase of linewidth that is characteristic for the transition to the regime of coherence collapse (Section 3.6) is observed.

In our experimental setup, it was not possible to reduce the length of the ring cavity significantly below $L_{ex} = 17$ cm, considering the length of the fiber-coupler housing of ~4 cm, the physical length of the isolator assembly of ~3 cm, and the restricted bending radius of the fiber. The size of the fiber ring as it appears in Fig. 4.1 is in fact 75% of the actual size of the fiber ring. The inverse of the roundtrip time in the external cavity for $L_{ex} = 17$ cm is $\tau_{ex}^{-1} = 1.2$ GHz and therefore still significantly lower than the relaxation oscillation frequency of the laser of $f_R \sim 2.8$ GHz. An attempt to increase τ_{ex}^{-1} was made by employing the arrangement shown in Fig. 4.12, where a double-tapered fiber [95] was used to couple light out of the fiber ring. The fiber-ring length was 8.05 cm leading to $\tau_{ex}^{-1} = 2.5$ GHz. Fig. 4.12 shows the fiber ring ~ 1.5 times enlarged compared to its actual size. The tapered fiber ends and the double-tapered fiber were produced with a manual fiber splicing machine. The loss of power in the double-tapered fiber was substantial and the maximum of the recorded beat spectrum is therefore only about 10 dB above the noise level (Fig. 4.13). A minimum linewidth of 1.7 MHz was observed. External cavity modes were not detected.

4.8. CONCLUSION

Measurements of sufficiently high resolution have been presented to show the external cavity modes of a laser with optical feedback and the frequency of these modes relative to the oscillation frequency of the solitary laser. It was verified that the mode with maximum output power is also the mode with minimum linewidth. A frequency fluctuation model that explains the minimum linewidth operation provides an estimate of the mode-hopping frequencies between external cavity modes that agrees with measurements. We find agreement between the functional dependence of the feedback level that leads to coherence collapse and the feedback

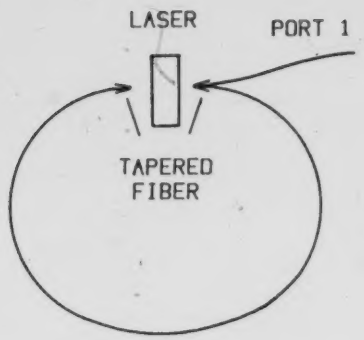

Fig. 4.12: Sketch of the laser with feedback from a fiber ring with double tapered fiber. The circumference of the fiber-ring is 8.05 cm.

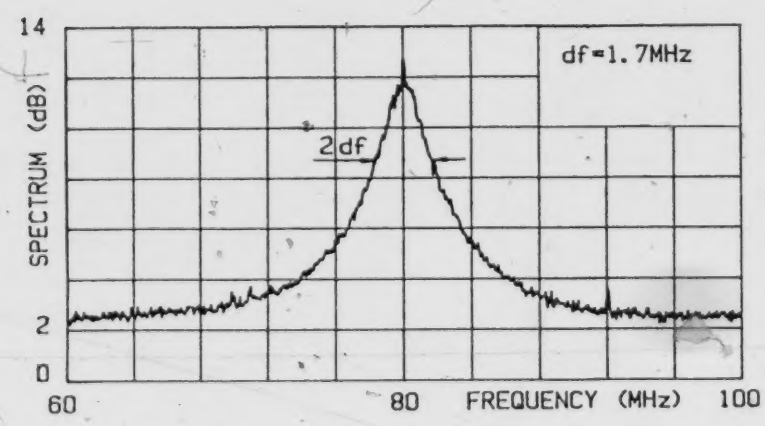

Fig. 4.13: Self-heterodye beat spectrum recorded for the laser in the feedback arrangement of Fig. 4.12 and showing a linewidth of the laser with feedback of 1.7 MHz.

level that leads to a frequency span of external cavity modes equal to the relaxation oscillation frequency.

The best performance of a laser with weak optical feedback in terms of the purity of the optical spectrum was found to be for relatively short external cavity lengths. We have shown that feedback of R_{ex} ~ -43 dB from fiber-ring assemblies of 17 and 29-cm length lead to a reduction of the linewidth of a laser by a factor of 1/50 and 1/80, respectively, with low external cavity mode amplitudes. Linewidths of ~2 MHz at 1.3 μm were achieved. The frequency of oscillation can be continuously tuned over several 100 MHz by changing the ring length by fractions of the optical wavelength. The assembly is relatively easy to align since only laser to fiber coupling procedures are necessary. An optical isolator makes the assembly insensitive to optical reflections from its main output port A4 (Fig. 4.1(a)). Since R_{ex} is low, little power has to be coupled back into the laser through port A2 and most of the power can be coupled out of the fiber ring using a fiber coupler with unsymmetrical coupling ratio.

Considering that the separation of longitudinal modes of a laser is ~130 GHz or 0.8 nm, a tuning range of several 100 MHz is not sufficient to ensure that the oscillation frequency of two lasers with the described ring feedback can be brought close enough to allow the observation of a beat spectrum in the electrical domain. The fiber-ring laser can therefore only be used as one out of the two lasers that would be required in an optical heterodyne experiment. The tuning range of the second laser needs to be considerably larger, so that its frequency can be adjusted over a range of many hundreds of GHz (Chapter 5).

5. STRONG FEEDBACK

5.1. INTRODUCTION

To enter the regime of strong optical feedback, Regime V described in Section 3.6, requires that the feedback provided by the external cavity is larger than the power reflected from the laser facet that faces the external cavity. To reach this condition it is typically necessary to AR-coat the respective laser facet. For a given output power the number of photons stored in the resulting extended cavity laser is increased substantially, which leads, according to (2.63), to a large reduction of the linewidth compared to the solitary laser diode. In this situation, the extended cavity determines the resonance frequencies, and the separation of longitudinal modes is reduced by the ratio of the optical pathlength in the semiconductor cavity to the sum of the optical pathlengths in the semiconductor and the external cavity, that is, from 130 GHz to 2 GHz for the example shown in Fig. 3.3(e).

The number of modes that can be observed depends on the discrimination between modes in terms of each mode's threshold gain, linewidth and separation in frequency from the maximum of the gain profile of the active medium of the laser. The selectivity based on the separation from the maximum of the gain profile results in, for a solitary laser, 4 to 6 strong longitudinal modes. The residual reflectivity of the AR-coated laser facet, R_2, determines how much influence the resonance of the semiconductor cavity has on the compound cavity loss seen by the individual external cavity modes. For low values of R_2, the decrease in loss for external cavity modes close to the resonance frequencies $\omega_m(n)$ of the semiconductor cavity can be quite small. Therefore we generally observe a number of external cavity modes centered on each $\omega_m(n)$ (Fig. 5.1(d)). The above is true for wavelength independent optical feedback, as in the case of an external mirror (Fig. 5.1(a)) or an optical amplifier in a fiber loop (Chapter 7).

A single set of low loss modes can be created by using strong wavelength selective optical feedback (Fig. 3.3(f)). When optical

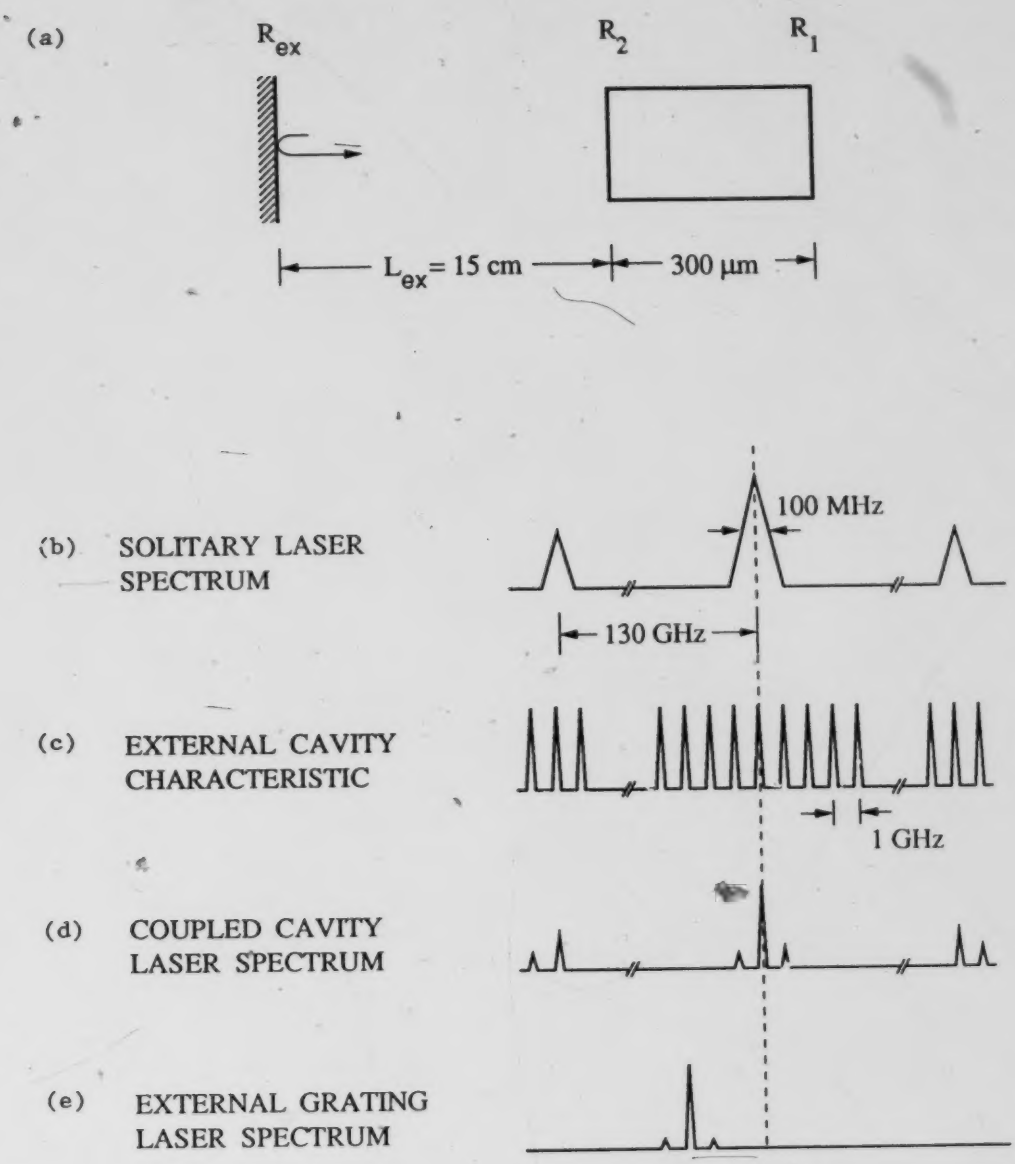

Fig. 5.1: Sketch of (a) a laser with optical feedback from an external reflector, (b) the optical power spectrum of the laser without optical feedback, (c) the spectral characteristic of the external cavity, the optical power spectrum of the laser (d) coupled to the external reflector, and (e) coupled to an external grating.

feedback is provided by a diffraction grating, the wavelength of maximum feedback, $\lambda_g = 2\pi c/\omega_g$, can be changed by rotating the grating which, in turn, alters the oscillation frequency of the laser. However, the residual reflectivity of the AR-coated laser facet still provides loss minima at the resonance frequencies of the semiconductor cavity. The value of R_2 and the level of optical feedback, R_{ex}, determine the range of continuous tuning between semiconductor cavity modes, $\Delta\omega_{im}$, that can be obtained by rotating the grating [18].

In this chapter we deal with the contribution of the frequency selective mechanisms of the external grating, the semiconductor cavity, the external cavity and the gain profile to the tuning characteristics of the external grating laser. We start in Section 5.2 with an account of the experimental results that were obtained for two lasers with 2% and .05% residual reflectivity and optical feedback from an external grating. These results allow us to examine the effect of the value of R_2 on the tuning characteristics. For ease of reference, we repeat the key equations in Section 5.3 and present them in a form most suited for the analysis in the following sections. In Section 5.4 we assume that the oscillation occurs in a single external cavity mode at λ_G and explain the power versus tuning characteristic and the presence of bi-stability in this characteristic using a graphical representation of the laser operation at different carrier density levels.

Ideally we want the external grating laser to oscillate in a single external cavity mode of narrow linewidth. The experimental results show that the single-mode stability of the external grating laser is a function of R_2 and the oscillation frequency of the laser. In Section 5.5 a plot of the constant phase and loss curves is used to examine the difference in threshold gain and linewidth of neighboring external cavity modes, allowing us to explain the observed dependence of single-mode stability on R_2 and the oscillation frequency (a version of Section 5.3 to 5.5 has been published in [36]).

5.2. EXPERIMENTAL RESULTS

Experimental results were obtained with two laser diodes emitting at 1.3 μm wavelength (Fujitsu FLD130D4SJ-A, V-groove laser), the first diode (TH 557) having ~2% reflectivity for the facet closest to the grating (Fig. 5.2) and the second (TY 224) ~0.05%. The residual reflectivities were obtained from the amplified emission spectrum of the one-side coated laser using the method of [96],[97]. The threshold currents (a) before AR-coating, (b) after coating and (c) after coating with optical feedback from the grating applied were: (a) 11.7 and 15.0 mA, (b) 22 and 39 mA and (c) 16.5 and 17.7 mA for the TH 557 and TY 224 lasers, respectively, at 20°C. From these threshold currents a feedback power ratio, R_{ex}, of 3% for laser TH 557 and 13% for laser TY 224 were determined using the method discussed in Section 6.4.4.

The optical quality of lens and grating has to be high and these two elements must be aligned carefully relative to the laser in order to maximize the coupling of optical power diffracted from the grating back into the fundamental mode of the semiconductor laser cavity. The higher feedback power ratio for the laser TY 224 is attributed to the fact that only in the experiment with this low residual reflectivity laser, the lens was positioned using piezo-micrometers. Therefore better alignment could be achieved in this experiment. Also it is much more difficult to find an optimal alignment of the lens and grating for a laser with high residual reflectivity of the AR-coated facet, since this laser shows higher output power fluctuations during intermode tuning, as will be described in the following section.

The length of the external cavity was 19 cm, leading to a separation between external cavity modes of 790 MHz. The longitudinal-mode spectrum of the external cavity laser was observed with a monochromator (resolution 0.3 nm) and a Fabry-Perot interferometer (FSR = 143 GHz, Finesse ~ 30). The linewidth and fluctuations between external cavity modes were observed using the self-heterodyne technique (Appendix B) and using the laser with feedback from a 17-cm long fiber ring, described in Section 4.7, as a reference laser.

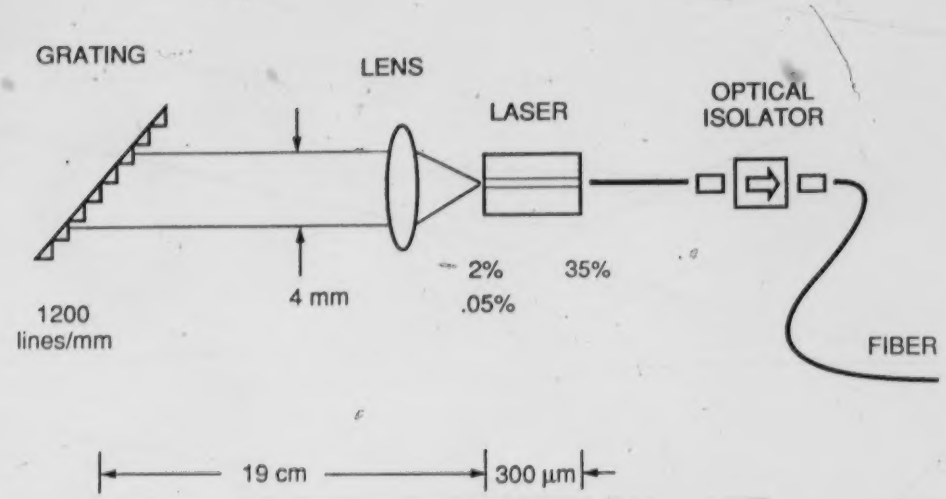

Fig. 5.2: Sketch of the laser with feedback from a diffraction grating.

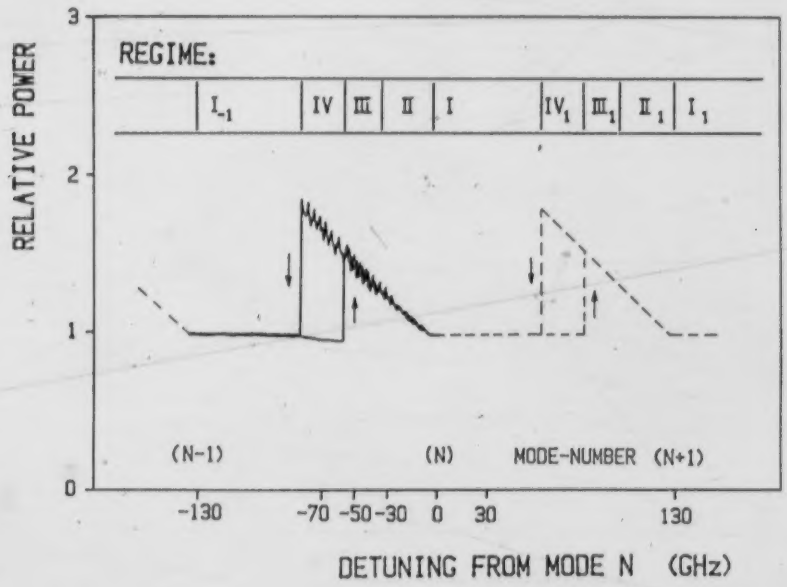

Fig. 5.3: Output power of the external grating laser (TH 557), normalized to zero-feedback output, vs. tuning of the center frequency of optical feedback. Also, definitions of Regimes I to IV.

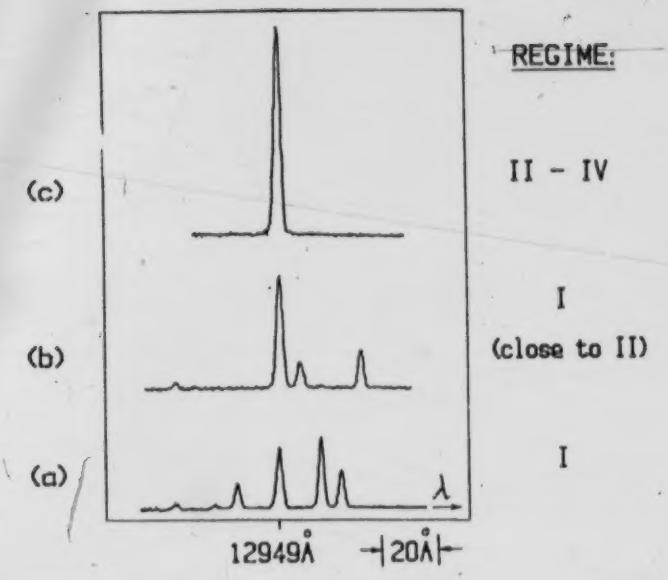

Fig. 5.4: Longitudinal mode-spectrum (TH 557 laser) measured with a monochromator in (a) and (b), Regime I and (c), Regime II to IV.

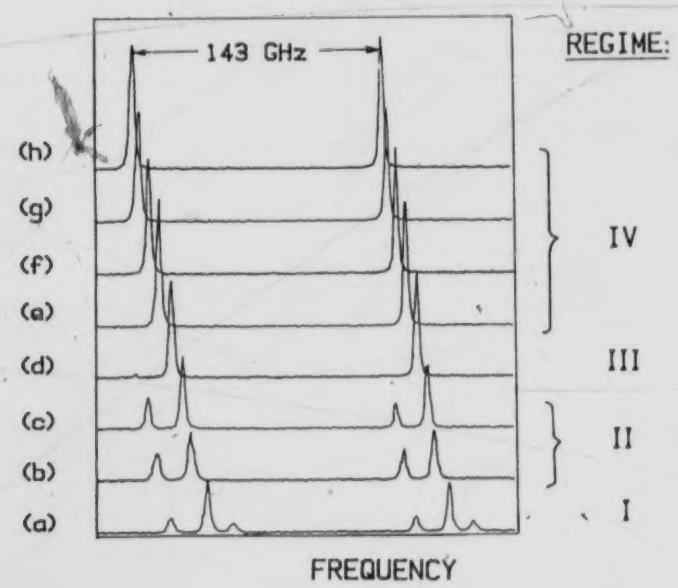

Fig. 5.5: Fabry-Perot spectrum (TH 557 laser) for increasing detuning from (a) to (h). (a) Regime I, (b) and (c) Regime II, (d) Regime III, (e) to (h) Regime IV.

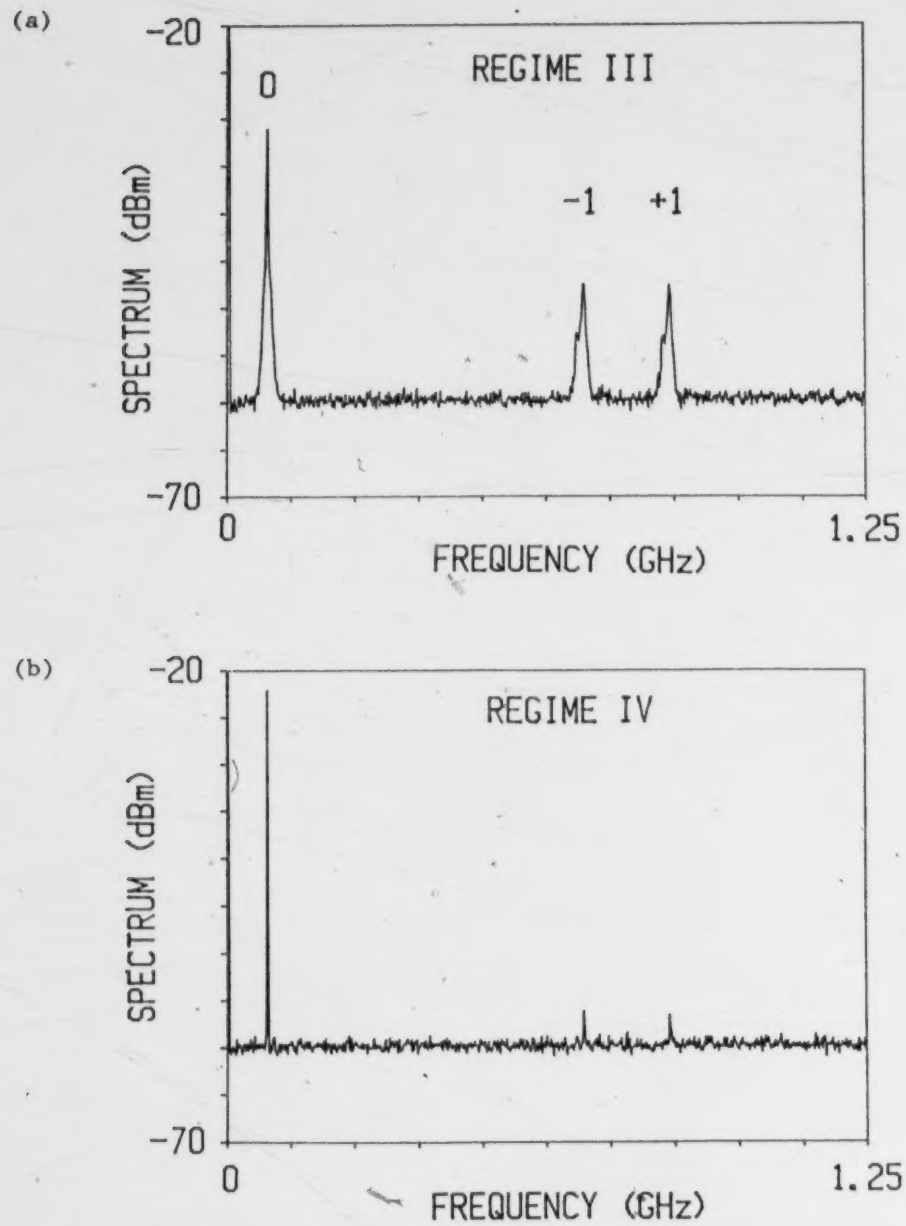

Fig. 5.6: Beat spectrum (TH 557 laser) measured with the self-heterodyne technique in (a) Regime III and (b) Regime IV. The frequency-shift between the two beams was 80 MHz. The '-1' indicates a negative frequency domain component (App. B).

5.2.1. *High Reflectivity Laser*

For the laser with 2% residual reflectivity and 3% optical feedback, we observe a large change in output power depending on the detuning shown in Fig. 5.3. We define four regimes of operation based on the observed spectral properties:

Regime I (no detuning, maximum grating reflectivity close to one of the solitary laser mode frequencies): the laser is oscillating in several solitary laser diode modes (Fig. 5.4(a),(b)).

Regime II (approx. -30 GHz detuning): the grating starts to control the frequency of oseillation of the laser, however, the oscillation takes place in two sets of longitudinal modes spaced apart by approximately 20 GHz (Figs. 5.5(b), 5.5(c), 5.4(c)). Each set consists of several external cavity modes.

Regime III (approx. -50 GHz detuning): the lower frequency set of modes reduces in intensity for detuning towards negative frequencies (Fig. 5.5(d)). The laser oscillation still fluctuates between several external cavity modes (Fig. 5.6(a)). The linewidth of each mode is on the order of 50 kHz (Fig. B.1(a)).

Regime IV (approx. -70 GHz detuning) - Regime of bistability [18]: the laser oscillates in one single longitudinal mode (Figs. 5.5(e) to (h), 5.6(b)) with a linewidth of approximately 5 kHz (Fig. B.1(b)). Tuning to lower frequencies produces an abrupt transition from Regime IV into Regime I_{-1} (Fig. 5.3). The same transition occurs when the feedback is momentarily interrupted. As shown in Fig. 5.3, the optical power remains low in region IV as we increase the frequency of optical feedback moving from Regime I_{-1} to III.

5.2.2. *Low Reflectivity Laser*

Only small fluctuations of the output power are observed (inset of Fig. 5.7) for the laser with .05% residual reflectivity and 13% of optical feedback from the grating. Over a tuning range of 60 nm the output power of the laser does not drop to the level of output power without optical feedback (Fig. 5.7), which indicates that the grating does not lose control over the frequency of oscillation of the laser.

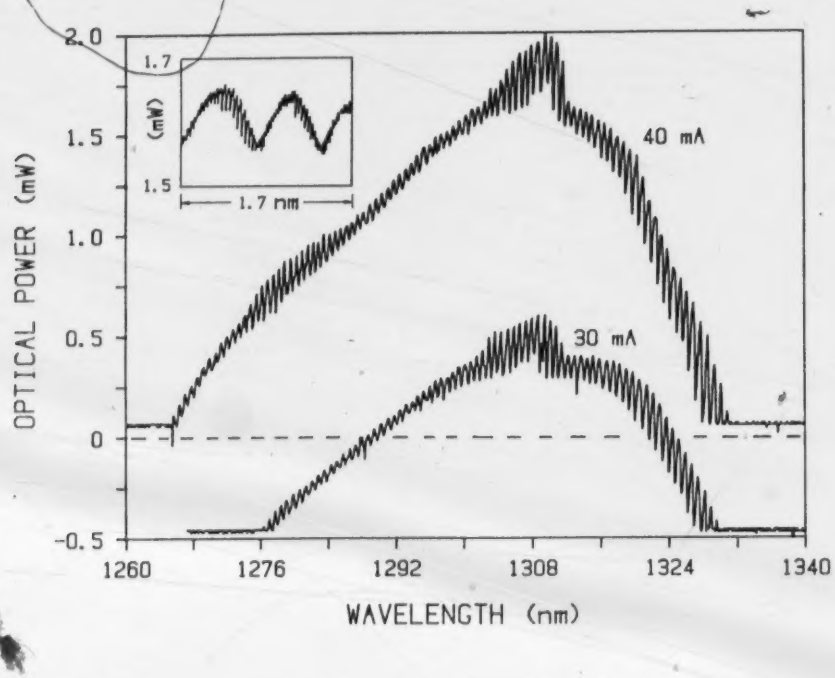

Fig. 5.7: Output power of the external grating laser (TY 224) versus tuning of the center wavelength of optical feedback for the two laser currents I_L = 30 and 40 mA, respectively. The trace for I_L = 30 mA is vertically offset by -.5 mW for clarity.

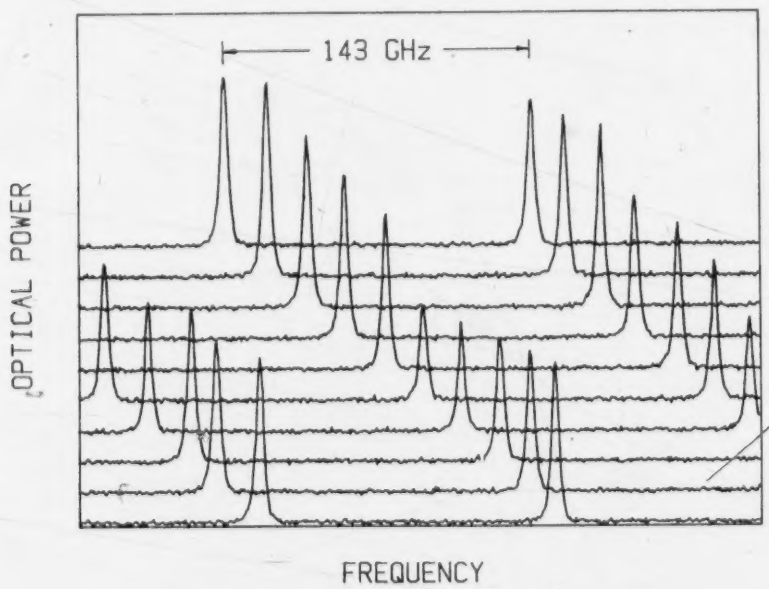

Fig. 5.8: Fabry-Perot spectrum (TY 224 laser) for decreasing detuning.

Fig. 5.8 compared to Fig. 5.5 indicates that low facet reflectivity results in continuous tuning (within the resolution of the Fabry-Perot interferometer) over more than 150 GHz, i.e. a range greater than the separation of longitudinal modes of the semiconductor cavity. The beat spectrum between the external grating laser and a second stabilized reference laser (single mode, 2.5 MHz linewidth, Fig. 4.8(b)) shows that changing the grating angle alters the oscillation frequency of the external grating laser in steps corresponding to the external cavity mode separation. Changing the external cavity length by one-half wavelength was observed to provide continuous frequency tuning within one of these steps, in agreement with the experimental results of [32].

Contrary to the results obtained with the high reflectivity laser, a clear dependence of the stability of single mode oscillation on the amount of detuning could not be observed for the low reflectivity laser. However it was found that the single-mode stability at a given frequency of oscillation was improved by careful adjustments to the position of the lens between laser and grating.

The light versus current (LI-) characteristic for laser TY 224 at ~15°C (1) before AR-coating, (2) after coating and (3) after coating and with optical feedback from the grating applied at different wavelengths λ_G are shown in Fig. 5.9(a) and (b). At a given current and wavelength λ_G, the output power of the laser fluctuates as small adjustments with magnitude $< \pm .5$ nm are made to λ_G. These small fluctuations are shown in Fig. 5.7. The solid LI-curves in Fig. 5.9 represent the LI-curves that are obtained when λ_G is continuously adjusted to keep the output power at a maximum. The dashed lines in Fig. 5.9(a) show the LI-curves obtained for the three wavelengths of 1309, 1291 and 1253 nm if λ_G is adjusted to keep the output power at a minimum. The original experimental data that was used to obtain Fig. 5.9(a) and (b) is reproduced in Appendix C.

Fig. 5.10 shows the measured dependence of the threshold current of the external grating laser on the wavelength of maximum reflection from the grating, λ_G. Fig. 5.10 data was obtained by making fine adjustment to λ_G mentioned above, to obtain maximum power from the external grating laser. The adjustment for minimum power leads to slightly higher threshold currents (dashed curve in Fig. C.1).

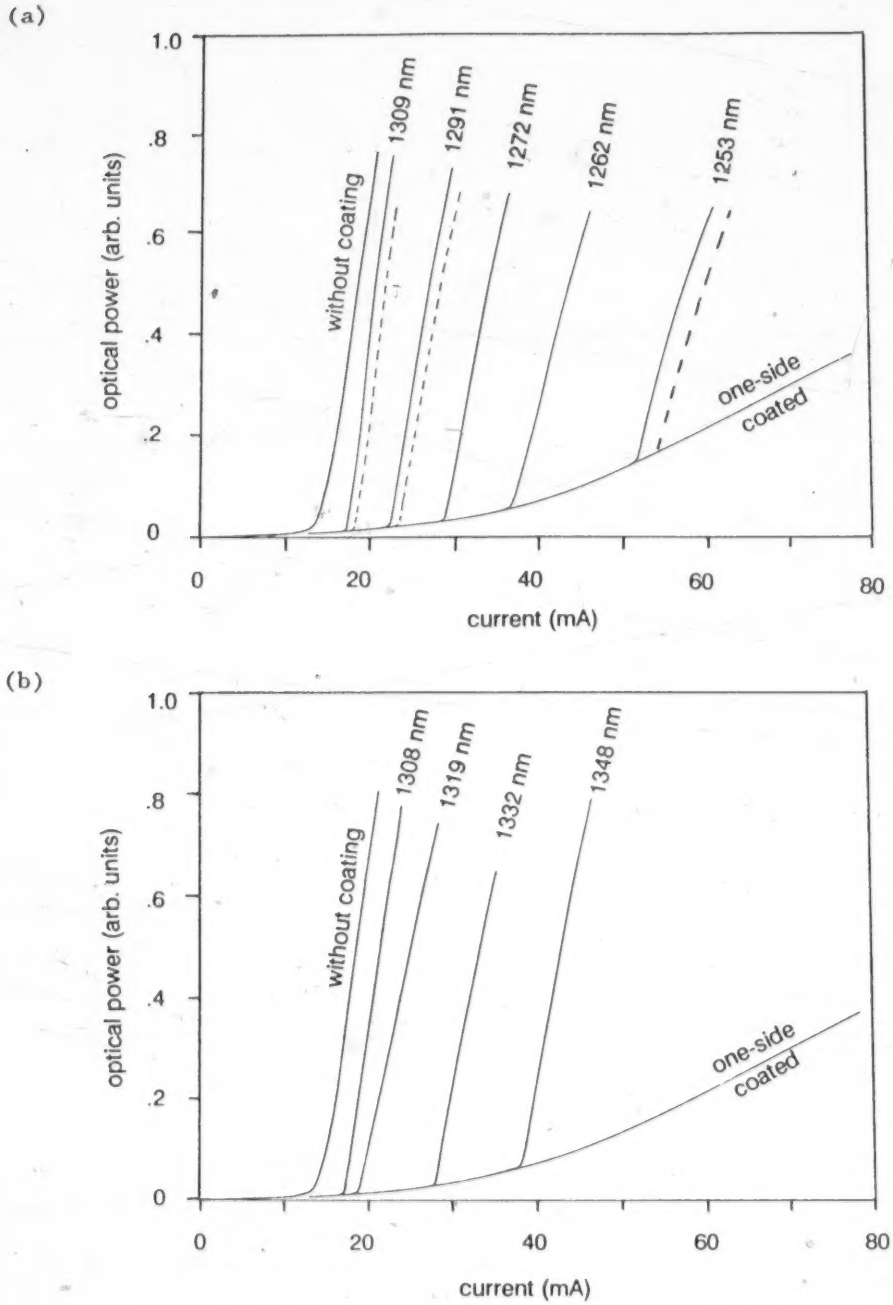

Fig. 5.9: Measured LI-characteristics of the low-reflectivity laser for different wavelengths of optical feedback.

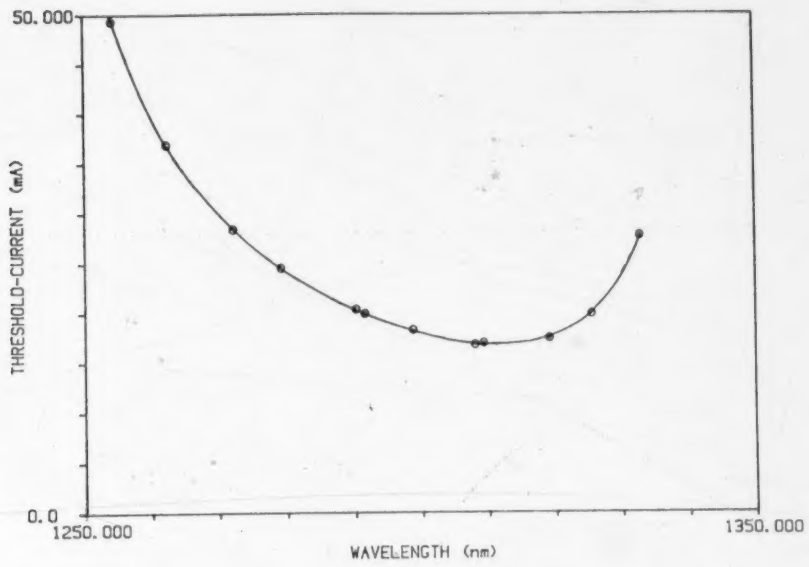

Fig. 5.10: Dependence of the threshold current of the external grating laser on the wavelength of optical feedback.

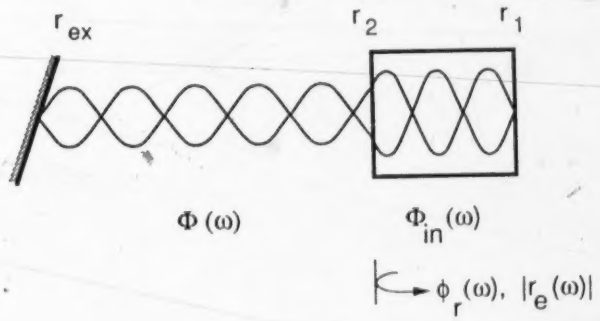

Fig. 5.11: Sketch of a standing wave pattern in a laser with strong optical feedback.

5.3. KEY EQUATIONS

The composite reflection coefficient, $r_e(\omega)$, for the combination of the AR-coated facet and the grating is, (3.4) and (3.5),

$$r_e(\omega) = \frac{r_2 + r_{ex}(\omega)\ \exp(j\Phi(\omega))}{1 + r_2 r_{ex}(\omega)\ \exp(j\Phi(\omega))} \tag{5.1}$$

$$\text{or} \quad r_e(\omega) = |r_e(\omega)|\ \exp\ [i\phi_r(\omega)] \tag{5.2}$$

where $\Phi(\omega) = (\omega/c)L_{ex}$ is the roundtrip phase-shift in the external cavity of length L_{ex}. As in [84], we assume $r_{ex}(\omega)$ to be a Gaussian function, (3.19),

$$r_{ex}(\omega) = r_G \exp\left\{ -(\ln 2)\ \frac{(\omega - \omega_G)^2}{\Delta\omega_G^{\,2}} \right\} \tag{5.3}$$

where ω_G is the frequency of maximum reflection (amplitude r_G) from the grating. The loss, $\alpha(\omega)$, of the compound cavity that has to equal the gain g at the frequency ω to ensure oscillation is

$$\alpha(\omega) = -(1/L_{in})\ \ln\ (\ r_1|r_e(\omega)|) \tag{5.4}$$

where r_1 is the reflection coefficient of the uncoated laser facet. The frequency of the longitudinal modes of the compound cavity laser are the solutions to the phase condition for the semiconductor cavity with the two facet reflection coefficients r_1 and $r_e(\omega)$, (3.12) and Fig. 5.11,

$$\phi_{in}(\omega,g) + \phi_r(\omega) = 2\pi \cdot m \tag{5.5}$$

where m is an integer. The phase shift $\phi_{in}(\omega,g)$ within the laser cavity can be expressed in terms of the "detuning" of ω with respect to the chip mode $\omega_m(g)$, i.e. with respect to the M-th longitudinal mode of the semiconductor cavity which depends on the gain g

$$\phi_{in}(\omega,g) = \frac{\omega-\omega_m(g)}{\Delta\nu_{in}} \tag{5.6}$$

where $\Delta\nu_{in} = v_{gr}/2L_{in}$ is the frequency separation between longitudinal modes of the semiconductor laser cavity. The discussion associated with Fig. 3.2 showed that the ratio of the incremental changes in ω_m and g due to a change in n is $\Delta\omega_m/\Delta g = \alpha v_{gr}/2$ where α is the linewidth enhancement factor [46]. If ω_m^0 is the chip mode of the solitary laser with gain g_0, $\omega_m(g)$ is given by

$$\omega_m(g) = \omega_m^0 + \frac{\alpha v_{gr}}{2}\ \Delta g \tag{5.7}$$

where $\Delta g = g - g_0$. Loss and gain are equal for the solitary laser if $g_0 = \alpha_{sol}$, where α_{sol} is the loss of the solitary laser. α_{sol} can be calculated from (5.4) by replacing $|r_e(\omega)|$ with r_2.

Inserting (5.6) and (5.7) into the phase condition (5.5) we obtain

$$\omega-\omega_m^0 = \Delta\nu_{in}\ \{\ -\alpha\cdot L_{in}\cdot\Delta g - \phi_r(\omega)\}. \tag{5.8}$$

In this section we purposefully distinguish between the gain in the laser, which is determined by the carrier density, and the resonator loss as a function of frequency. For the following discussion we must be aware that gain and loss are equal only at the frequency that the laser actually oscillates in. Equations (5.1), (5.3) (5.4) and (5.8) are the key equations describing the relations between ω, $\alpha(\omega)$ and ω_G.

5.4. TUNING CHARACTERISTICS

The loss curve $\alpha(\omega)$ is plotted in Fig. 3.3(e) for $R_1 = 31\%$, $R_2 = .01\%$ and $R_{ex} = 31\%$. The minimum introduced in the oscillations of the loss curve by a frequency dependent external reflector, (5.3), is shown in Fig. 3.3(f). To analyze the tuning characteristic, i.e. the behavior of the laser as the frequency of maximum reflection from the grating is changed, we plot $\alpha(\omega = \omega_G)$, an approach taken by [18]. In this approach

the length of the external cavity is assumed to be adjusted to a value where the phase condition (5.8) is satisfied for $\omega = \omega_G$. Also, it is assumed that the mode at $\omega = \omega_G$ has the lowest loss and the laser is therefore oscillating in this mode. This second assumption is not strictly true for all values of R_1, R_2, R_{ex} and ω_G (Section 5.5), however it leads to a very useful graph that allows us to explain the tuning characteristic of the external grating laser and the bistability observed.

In Fig. 3.3(e), $\alpha(\omega)$ is plotted versus the generalized frequency ω, which leads to a period in $\alpha(\omega)$ of $\tau_{ex}^{-1} = 2$ GHz. The plot of values of $\alpha(\omega)$ at the frequencies that satisfy (5.8), i.e. the values of $\alpha(\omega)$ at the intersections of constant phase curves and loss curve in Fig. 3.3(e), is shown as a dashed line in Fig. 5.12, labeled $\alpha_L(\omega)$, and has a period of $\tau_{in}^{-1} = 130$ GHz.

$\alpha_L(\omega)$ specifies the loss of a compound resonator mode at ω if we assume that the carrier density in the laser is adjusted to provide a gain at ω that is equal to $\alpha_L(\omega)$. Also plotted in Fig. 5.12 is $\alpha_0(\omega)$,

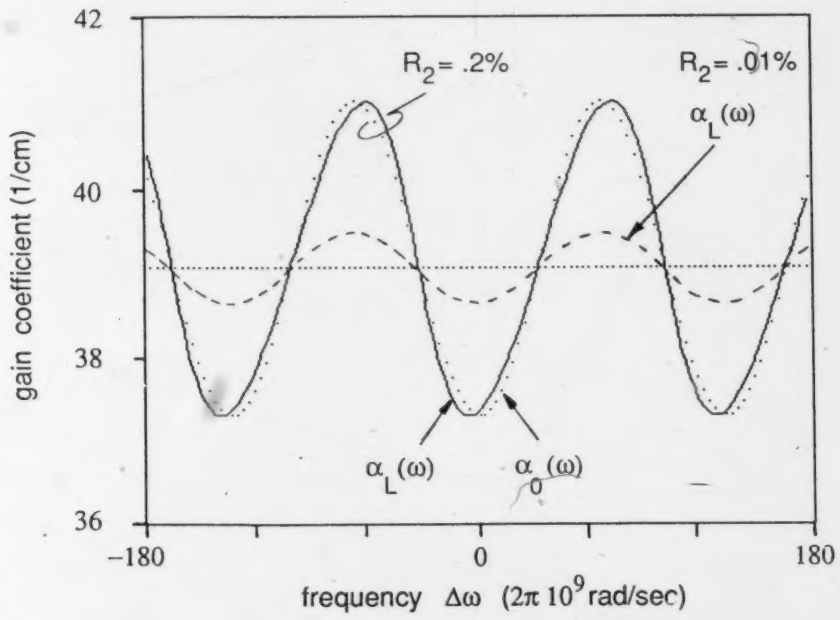

Fig. 5.12: Computed loss versus frequency graphs for a laser with strong optical feedback

which describes the loss of a compound resonator mode at ω if we assume that the carrier density is clamped to the value that provides a gain of $g = \alpha_{sol}$. The plots of $\alpha_L(\omega)$ and $\alpha_0(\omega)$ in Fig. 5.12 are visibly different only for $R_2 = 2\%$. $\alpha_0(\omega)$ and $\alpha_L(\omega)$ are obtained from (5.1), (5.4) and (5.8). In both cases we let Φ in (5.1) assume values between -5π and $+5\pi$, calculate $|r_e(\Phi)|$ and $\phi_r(\Phi)$ for each value of Φ and use these values first to calculate $\alpha(\Phi)$ from (5.4) and then to calculate $\omega_0(\Phi)$ from (5.8) by assuming $\Delta g = 0$ and finally to calculate $\omega_L(\Phi)$ from (5.8) by assuming $\Delta g = \alpha(\Phi) - \alpha_{sol}$. $\alpha_0(\omega)$ and $\alpha_L(\omega)$ are then obtained by plotting $\alpha(\Phi)$ as a function of $\omega_0(\Phi)$ and $\alpha(\Phi)$ as a function of $\omega_L(\Phi)$, respectively. In Fig. 5.12 $\alpha_0(\omega)$ and $\alpha_L(\omega)$ are plotted versus $\Delta\omega = \omega - \omega_m^0$, where ω_m^0 is the frequency of oscillation of the solitary laser.

5.4.1. *In-Phase and Out-of Phase Feedback*

The loss of the compound cavity has a minimum for $\phi_{in}(\omega,g) = 0°$, in Fig. 5.12 for $\Delta\omega \sim 0$. In this case ω coincides with a resonance frequency of the semiconductor cavity and the composite reflectivity therefore has the maximum value of

$$R_e(\omega)_{max} = \left[\frac{r_{ex} + r_2}{1 + r_2 r_{ex}}\right]^2 . \qquad (5.9)$$

We can also refer to this case as "in-phase-feedback", because the light that is returned from R_{ex} and from R_2 add constructively within the semiconductor cavity. It is important to note that a change in the external cavity length does not affect, to first order, the roundtrip-phase shift, $\Phi(\omega)$, in the external cavity. This seems at first surprising, since $\Phi(\omega) = (\omega/c)\cdot L_{ex}$. However we note from Fig. 5.11 that for oscillation to occur, nodes of the standing wave have to exist at the facets r_{ex} and r_1. As L_{ex} is increased the standing wave pattern in Fig. 5.11 is stretched. Increasing L_{ex} by $\lambda/2$ decreases ω by $-2\pi\cdot\Delta\nu_{ex}$ ($L_{ex} >> L_{in}$). To increase the number of nodes within the semiconductor cavity by one, however, i.e. to increase the roundtrip phase shift $\phi_{in}(\omega,g)$ from 0° to 360°, the frequency has to be increased by $\Delta\nu_{in}$, where $\Delta\nu_{in} >> \Delta\nu_{ex}$. Thus the change of $\phi_{in}(\omega,g)$ and, using (5.1), (5.2)

and (5.3), the change of $\Phi(\omega)$ that occurs for a frequency change within $\Delta\nu_{ex}$ is small and an increase of L_{ex} leads to a decrease of the resonance frequency ω, such that the product $\omega \cdot L_{ex}$ stays almost constant.

The compound-cavity loss has a maximum when $\phi_{in}(\omega,g) = 180°$. The composite reflectivity for out-of-phase feedback is

$$R_e(\omega)_{min} = [\frac{r_{ex} - r_2}{1 - r_2 r_{ex}}]^2. \qquad (5.10)$$

Fig. 5.13(a) shows the values of $R_e(\omega)_{max}$ and $R_e(\omega)_{min}$ for $R_2 = 2\%$ and variable R_{ex}. We notice a surprisingly large increase and decrease of the composite reflectivity $R_e(\omega)$ with respect to R_{ex} due to, respectively, in-phase and out-of-phase feedback from R_2. In-phase-feedback, i.e. optical feedback at the frequency of the semiconductor cavity resonance, $\omega_m(g)$, increases the combined reflectivity from 2% for $R_{ex} = 0$ to $R_e(\omega)_{max} = 15.3\%$ for $R_{ex} = 7\%$, and therefore decreases the resonator loss $\alpha(\omega)$. Detuning of ω_G from $\omega_m(g)$ leads to a gradual increase of ϕ_{in} from 0° to 180° and a decrease of the composite reflectivity $R_e(\omega)$. For $R_{ex} = 7\%$, we obtain $R_e(\omega)_{min} = 1.5\%$, which is lower than the residual reflectivity of the coated facet ($R_2 = 2\%$). The compound cavity loss at ω_G is in this case higher than the loss of the laser at $\omega_m(g)$, and the laser will not oscillate at ω_G but at $\omega_m(g)$.

In order for the laser to oscillate at ω_G, the resonator loss at ω_G has to stay lower than the loss at $\omega_g(g)$. To satisfy this requirement for all values of detuning, we require $R_e(\omega)_{min} > R_2$, from which we obtain, for the feedback level that leads to continuous tuning of the oscillation frequency of the laser:

$$R_{ex}^{cont} \geq 4R_2/(1+R_2)^2. \qquad (5.11)$$

We note from (5.11) that R_{ex} has to be substantially higher than the residual reflectivity of the laser to ensure continuous tuning.

Fig. 5.14 shows the equivalent of Fig. 5.13 for $R_2 = .05\%$. We note that the modulation of $R_e(\omega)$ depending the phase shift, Φ, shown in Fig. 5.14(b), is reduced substantially compared to Fig. 5.13(b).

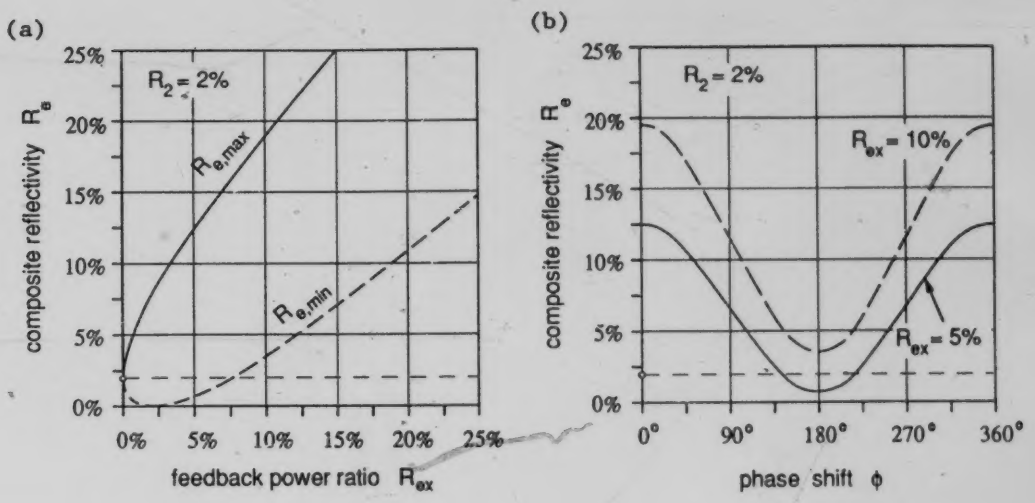

Fig. 5.13(a) Graph of the composite reflectivity versus feedback power ratio for a residual reflectivity of R_2 = 2%.
(b): Graph of the composite reflectivity versus roundtrip-phase shift in the external cavity for R_2 = 2%.

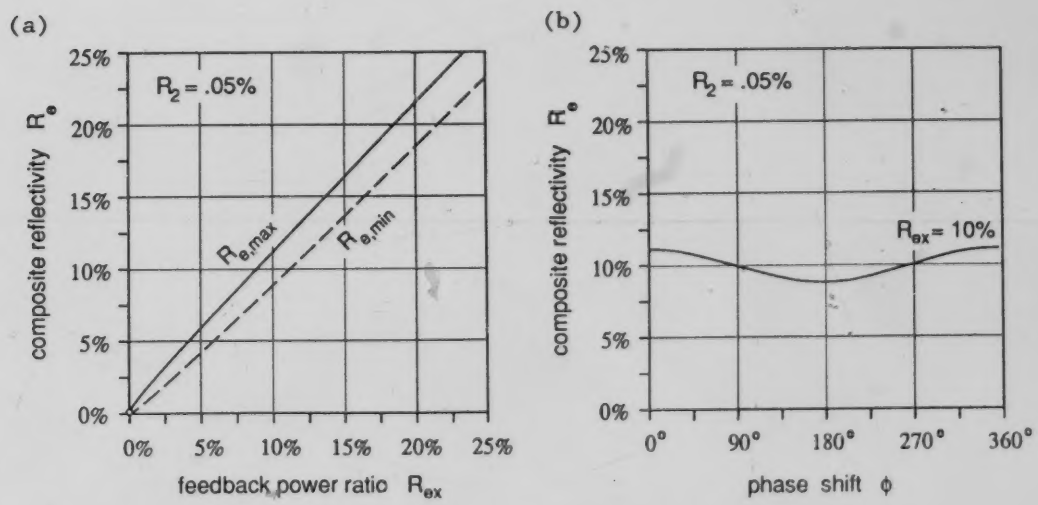

Fig. 5.14(a) Graph of the composite reflectivity versus feedback power ratio for a residual reflectivity of R_2 = .05%.
(b): Graph of the composite reflectivity versus roundtrip-phase shift in the external cavity for R_2 = .05%.

5.4.2. *Oscillation away from the Gain Maximum*

We now consider the effect of the spectral gain profile on the conditions under which optical feedback from the external grating controls the oscillation of the laser. These conditions determine the range of wavelength tuning, $\Delta\omega_{wt}$, and its dependence on R_{ex} and R_2.

The spectral gain profile, i.e. the gain versus wavelength characteristic for a given carrier density is given by [99]

$$g_N(\lambda) = g_p - \left[\frac{\lambda - \lambda_p}{W}\right]^2 \tag{5.12}$$

where $$g_p = A\,(n-n_{tr})\,\Gamma \tag{5.13}$$

In (5.12) and (5.13) g_p is the peak gain, occurring at wavelength λ_p, and W the width of the gain profile. $A = dg/dN$ is the gain coefficient, n_{tr} the transparency carrier-density, and Γ the confinement factor for the electric field in the active region. $g_N(\lambda)$ is plotted for three carrier densities in Fig. 5.15. n_0 is the carrier density that leads to the gain profile g_N^0 with peak gain $g_p^0 = \alpha_{sol}$, i.e. n_0 is the carrier density that exists in the solitary laser above lasing threshold.

From the gain profile and the loss versus wavelength characteristic we can determine the distribution of power in the longitudinal modes of the laser. Introducing wavelength dependence into (2.23) and (2.24), we obtain

$$S(\lambda) = \frac{R_{sp}(\lambda)}{v_{gr}\,\{\alpha(\lambda) - g_N(\lambda)\}} \tag{5.14}$$

and $$R_{sp}(\lambda) = n_{sp}\,K_R\,v_{gr}\,g_N(\lambda) \tag{5.15}$$

We define the ratio between the output power, P in mW, and the number of photons in the active cavity, S, to be

$$K_p = P/S \tag{5.16}$$

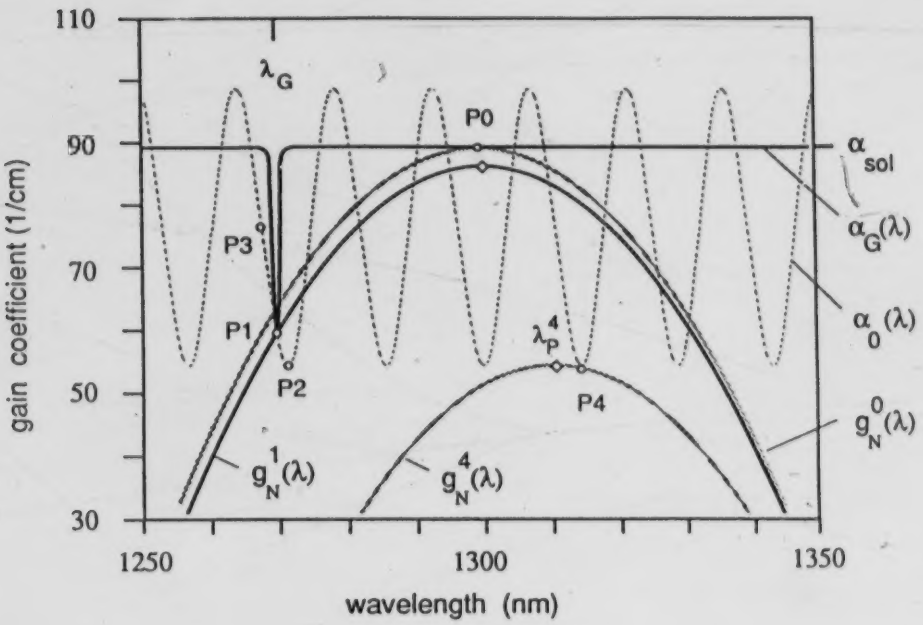

Fig. 5.15: Computed loss versus frequency graph $\alpha_0(\lambda)$ and $\alpha_G(\lambda)$ for, respectively, a laser with optical feedback from a mirror (dotted line, $R_1 = .35$, $R_{ex} = .06$, $R_2 = .02$ and $\Delta\nu_{in} = 20 \times 135$ GHz) and a laser with optical feedback at λ_G from an external grating. Also, spectral gain profile, $g_N^0(\lambda)$, $g_N^1(\lambda)$ and $g_N^4(\lambda)$, of the semiconductor laser for three different operating points of the external grating laser.

where $K_P = \hbar\omega \cdot v_{gr} \cdot \alpha_R/2$ for a solitary laser, according to (2.28). K_P is independent of the wavelength. From (5.15) we find that the spontaneous emission rate and the gain have the same spectral distribution. However, the output power being the sum of spontaneous and stimulated emission of radiation, is given by the spontaneous emission amplified by the laser cavity, i.e. in (5.14) the spontaneous emission rate is weighted by the inverse of the difference between gain and loss

$$\Delta g_N(\lambda) = \alpha(\lambda) - g_N(\lambda). \qquad (5.17)$$

As $\Delta g_N(\lambda)$ decreases, the output power increases rapidly, as shown in the discussion associated with (2.27). For the solitary laser, the loss at the resonance frequencies of the semiconductor cavity is independent of

the wavelength. The laser will therefore emit largest power in the mode closest to the wavelength of peak gain, λ_p^0. λ_p^0 is equal to the wavelength of oscillation of the solitary laser, λ_0, and is assumed in Fig. 5.15 to have the value of 1300 nm. In the numerical example of Section 2.3.3 the value of $\Delta g_N(\lambda)$ for the mode with highest power was 0.0013 cm^{-1} at P = 2 mW, which is small compared to the gain and loss changes we are currently examining. Unless we are concerned with the ratio of the output power in different longitudinal cavity modes, we can therefore assume that gain and loss are equal for the mode with highest output power.

The loss of the laser can be reduced in a narrow spectral range by using an external grating reflector and the situation can be created where $\Delta g_N(\lambda)$ has a minimum and the output power a maximum at a wavelength that does not coincide with λ_p. The numerical example of Section 2.3.3 indicates that a laser emitting 2 mW of power in one longitudinal mode will show a sidemode suppression ratio of 1:100 if the gain difference $\Delta g_N(\lambda)$ for the sidemode is increased compared to the gain difference of the main mode by only 0.15 cm^{-1}. Therefore, if there is sufficient difference in $\Delta g_N(\lambda)$ for the different longitudinal modes of the laser, we can therefore assume that oscillation takes place only at the wavelength where $\Delta g_N(\lambda)$ has a minimum.

Also plotted in Fig. 5.15 is $\alpha_0(\omega)$, the loss of the compound cavity modes of a laser with optical feedback. The conversion from a change in optical frequency df to a change in wavelength $d\lambda$ is described by the equivalence $d\lambda/df = -\lambda/f$, which means that 17.8 GHz is equivalent to 0.1nm @ 1.3 μm. The calculation of $\alpha_0(\omega)$ is done as described before for $\alpha_0(\omega)$ in Fig. 5.12. The values $R_1 = 0.35$, $R_{ex} = 0.06$, $R_2 = 0.02$ and $\Delta\nu_{in} = 20 \times 135$ GHz were assumed in Fig. 5.15. This value of $\Delta\nu_{in}$ is ~20 times larger than in a typical semiconductor laser and this value has been chosen to provide clarity to Fig. 5.15.

When the external reflector is a grating, the loss of the laser is only affected at λ_G, the wavelength for which the grating reflects light back into the laser. At all other wavelengths, $r_e(\omega)$ is equal to r_2 and therefore the loss equals α_{sol}. The resulting loss versus wavelength characteristic of the external grating laser is $\alpha_G(\lambda)$, shown in Fig. 5.15. As the grating angle is changed, λ_G changes and the minimum of

$\alpha_G(\lambda)$ travels along $\alpha_0(\lambda)$. In Fig. 5.15 the minimum of $\alpha_G(\lambda)$ coincides with $\alpha_0(\lambda)$ at λ_1, where λ_1 is the wavelength at P1. As λ_G is increased to move the loss minimum at λ_G from P1 to P2 the bell shaped gain profile is lowered, such that the gain $g_N(\lambda_G)$, stays always slightly lower than the loss $\alpha_G(\lambda_G)$. $\Delta g_N(\lambda_G)$ is very small and $\Delta g_N(\lambda_0) >> \Delta g_N(\lambda_G)$ in Fig. 5.15. The laser therefore oscillates only at λ_G. Thus, the grating controls the oscillation frequency of the laser if we move from P1 to P2. If λ_G is decreased from P1 towards P3, the bell-shaped curve of the frequency dependent gain moves upwards in Fig. 5.15 until it coincides with $g_N^0(\lambda)$. In this situation $\Delta g_N(\lambda)$ becomes smallest at λ_0, the laser starts to oscillate at the frequency of the solitary laser and the grating has lost control over the oscillation frequency of the laser.

The range of wavelength tuning $\Delta\omega_{wt}$, i.e. the range of wavelengths over which the grating can have control over the laser oscillation frequency, is given in Fig. 5.15 by the range of wavelengths over which the minima of $\alpha_0(\lambda)$ are below $g_N^0(\lambda)$. The value of $\alpha_0(\lambda)$ at these minima is, from (5.3) and (5.9), $\alpha_{min} = -(1/L_{in}) \ln(R_1 \cdot R_e(\omega)_{max})$. Using (5.12) we obtain for $\Delta\lambda_{wt}$

$$\Delta\lambda_{wt} = 2 \cdot [(g_p - \alpha_{min}) \cdot W]^{1/2} \qquad (5.18)$$

Fig. 5.15 shows that the peak gain of $g_0(\lambda)$ is $g_p = \alpha_{sol}$. For $R_{ex} = 3\%$, $R_2 = 2\%$ and $W = .47\ \mu m^{3/2}$ (Table 6.1) we obtain $\Delta\lambda_{wt} = 75$ nm. Experimentally values of $\Delta\lambda_{wt} = 43$ nm [37] ($R_{ex} = 3\%$, $R_2 = 2\%$), $\Delta\lambda_{wt} = 55$ nm ($R_{ex} = 6.5\%$, $R_2 = .7\%$) and $\Delta\lambda_{wt} = 55$ nm ($R_{ex} = 13\%$, $R_2 = .05\%$) have been observed. The calculated value is almost twice as large as the measured value. We attribute this to an uncertainty in our value of W, and also to the finite spectral width of the grating response, which does prevent the loss from reaching α_{sol} even if λ_G is outside the range of wavelength tuning. The limited increase of $\Delta\lambda_{wt}$ with decreasing R_2, observed in the experimental data, can be explained when we consider that g_p does not reach α_{sol} any more if $R_2 < 1\%$, which will be considered in Section 6.

In general there can be sections within the range of wavelength tuning, where the grating loses control over the laser oscillation.

These sections are centered on the wavelengths where the grating provides out-of-phase feedback and appear in Fig. 5.15 as the sections where $\alpha_0(\lambda) > g_N^0(\lambda)$. They are visible in the tuning characteristic of the high-reflectivity laser, Fig. 5.3, as sections where the power of the laser drops to the level of power the laser emits without optical feedback.

The condition for continuous tuning (5.11) specifies the value of R_{ex} that is necessary to maintain $\alpha_0(\lambda) < \alpha_{sol}$. We notice from Fig. 5.7 that this condition is only sufficient close to λ_p^0. In general we require $\alpha_0(\lambda) < g_N^0(\lambda)$. The value for R_{ex} which is required to ensure continuous tuning therefore increases as λ_G is moved away from λ_0.

The threshold current, I_{th}, of a laser is roughly proportional (Section 6) to the threshold carrier density, n_{th},

$$I_{th} \propto n_{th}. \tag{5.19}$$

This proportionality relation can be derived from (2.31) and (5.13), assuming $S = 0$ at threshold, $n_{th} \gg n_{tr}$ and using the relation $g_p = G(n)/v_{gr}$. Furthermore it is assumed that the injection currents measured at the laser diode terminals, I and I_{th}, are proportional to the active region currents, I_a and $I_{a,th}$, respectively.

The height of the gain profile for in-phase-feedback, i.e. at the minima of $\alpha_0(\lambda)$, depends on the detuning of λ_G. The gain profile with lowest peak gain, i.e. with lowest carrier density for the onset of lasing, is observed in Fig. 5.15 if the grating provides feedback at λ_4, where λ_4 is the wavelength at P4. The threshold current of the external grating laser for in-phase-feedback is therefore expected to be lowest close to λ_0 and to increase as λ_G is moved away from λ_0. The measured dependence of the threshold current of the external grating laser on the wavelength of optical feedback, Fig. 5.10, is therefore in agreement with the theoretical prediction.

The lack of symmetry in Fig. 5.10 with respect to the wavelength of minimum threshold current is due to the dependence of λ_p on the carrier density [100]. As indicated in Fig. 5.15, the wavelength of the maximum of the gain profile decreases as the gain profile is shifted upward and the carrier density increases. This shift of λ_p favors tuning of the

external grating laser towards wavelengths lower than the wavelength of minimum threshold current.

5.4.3. *Intermode Tuning Characteristics*

The intermode tuning characteristics describe the behavior of a laser with feedback from an external grating, when the center frequency of reflection of the grating is tuned continuously from one solitary laser longitudinal mode to the adjacent lower frequency mode. We analyze this characteristic using Fig. 5.16. Fig. 5.16(a) shows a narrow vertical section taken from the center of Fig. 5.15, except that we plot this time the gain coefficient versus frequency and use a realistic value of $\Delta\lambda_{in}$ = 0.76 nm ($\Delta\nu_{in}$ = 135 GHz). Drawn on this scale, the amplitude of the gain profile $g_N(\omega)$ has a shallow maximum and, since we use a realistic value of $\Delta\nu_{in}$, the difference between $\alpha_L(\omega)$ and $\alpha_0(\omega)$ now becomes evident.

The change of carrier density, associated with a change in peak gain, and the resulting change in the resonance frequency of the semiconductor cavity, $\omega_m(g)$, have been expressed in (5.7) through the use of the linewidth enhancement factor α (Fig. 3.2 and eq. (3.13)). Since the gain profile shifts towards lower frequencies as the peak gain increases, the same change in gain lowers the gain profile less for $\lambda < \lambda_p$ than for $\lambda > \lambda_p$. The coupling between gain and oscillation frequency is therefore less for $\lambda < \lambda_p$. This phenomenon expresses itself in the dependence of the linewidth enhancement factor α on the wavelength. K.-Y.Liou et al. [100] found values for α between α = 2 at 1.28 μm and α = 9 at 1.34 μm. For operation close to the gain maximum of the laser α values of 5 or 6 are frequently used for 1.3 μm lasers.

Fig. 5.16, like Fig. 5.12, shows the loss of the compound resonator modes taking carrier density changes into account, $\alpha_L(\omega)$, and assuming constant carrier density, $\alpha_0(\omega)$. The parameter values that apply for Figs. 5.15 and 5.16 are R_1 = 35%, R_2 = 2%, R_{ex} = 6%, L_{in} = 0.028 cm, $v_{gr} = 0.75 \cdot 10^{10}$ cm/sec and α = 5. $\alpha_G(\omega)$ in Fig. 5.16(a) is the loss versus frequency characteristic of the external grating laser where optical feedback is provided at ω_G.

(a)

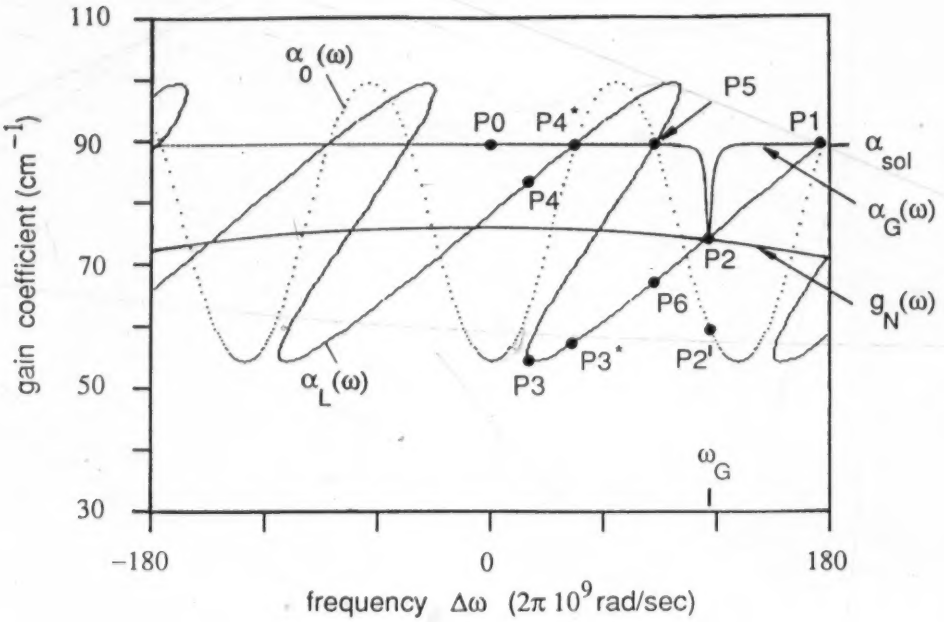

(b)

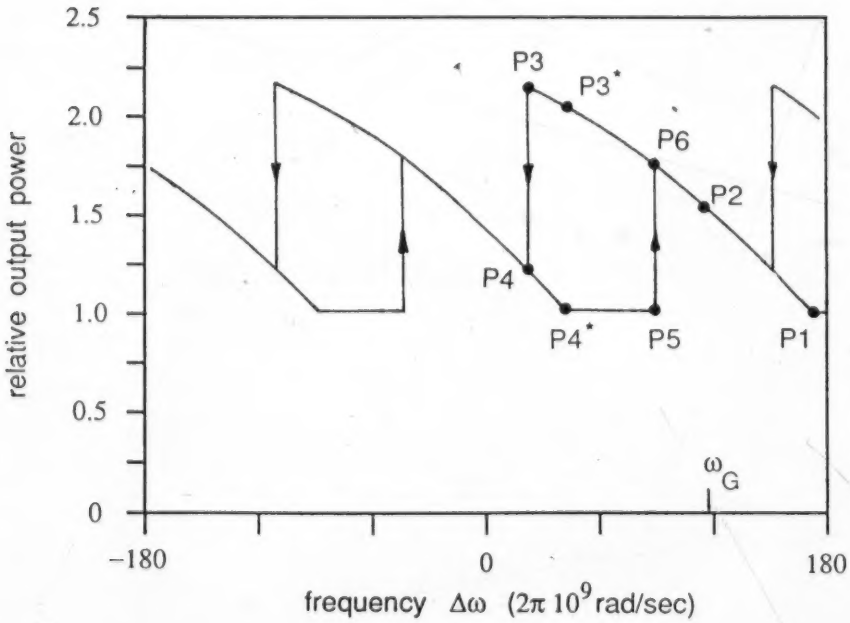

Fig. 5.16(a): Computed loss and gain versus frequency graphs for a laser with strong optical feedback (R_1 = .35, R_{ex} = .06, R_2 = .02 and $\Delta\nu_{in}$ = 135 GHz). (b): Sketch of the output power vs. tuning characteristic showing hysteresis.

Without optical feedback the loss in the laser cavity is α_{sol}, carrier density and gain profile are high and oscillation takes place at the frequency for which $g_N(\omega)$ has a maximum, i.e. $\omega = \omega_m^0$ at P0. With optical feedback from the grating suddenly restored, light is reflected back into the laser at $\omega = \omega_G$ and the loss of the compound cavity at this frequency decreases to below α_{sol}. The threshold gain at ω_G drops from α_{sol} to $\alpha_0(\omega_G)$, i.e. point P2'. However, as the carrier-density decreases because of this decreased threshold gain, the resonant frequency of the semiconductor laser $\omega_m(g)$ decreases as well, which in turn increases the threshold gain. This effect was taken into account in the calculation of $\alpha_L(\omega)$. Therefore, with feedback from the grating at $\omega = \omega_G$, oscillation takes place at P2. If ω_G is now decreased by rotating the grating, the compound cavity laser operating characteristic follows $a_L(\omega)$ and the threshold gain decreases to P3.

If the laser is operated anywhere between P6 and P3* (the minimum of $\alpha_G(\omega)$ moves to the left in Fig. 5.16(a) and coincides with $\alpha_H(\omega)$ between P6 and P3*), and the optical feedback between the laser and the grating is interrupted by blocking the light, the laser returns to the high gain and low output power state of the solitary laser, P0. Upon re-establishing the optical feedback, the carrier density still equals the carrier density of the solitary laser. $\alpha_G(\omega)$ coincides in this situation with a point between P4* and P5 on $\alpha_0(\omega)$, which represents a threshold gain that is higher than α_{sol}, and oscillation therefore remains at the frequency determined by P0. The laser does not return to the same operating conditions it was in before the feedback was interrupted. To return to operation between P6 and P3* on $\alpha_L(\omega)$ either the injection current must be decreased to reduce the carrier density such that $\alpha_L(\omega)$ applies again or the grating must be rotated to approach P6 from P1. In conclusion, Fig. 5.16 provides an explanation for the bistability of an external grating laser.

The output power vs. tuning characteristic can be derived from Fig. 5.16(a) using the relationship between optical output power P and injection current I [22]

$$P \propto (I - I_{th}) \tag{5.20}$$

with [101]
$$I_{th} \propto \alpha_{mat} + \alpha(\omega) \tag{5.21}$$

where I_{th} is the threshold current and α_{mat} the wavelength independent material loss. (5.21) is based on the same assumptions as (5.19) and the assumption of $g_N(\lambda_G) = \alpha_L(\lambda_G)$ at the threshold current (Section 6). (5.20) can be derived from (2.31), noting that $P \propto S$, $I_a \propto I$ and $N = N_{th}$ = const. above lasing threshold.

Fig. 5.16(b) provides a sketch of the output power vs. tuning characteristic derived from Fig. 5.16(a) using (5.20) and (5.21). This sketch shows the bistability. Fig. 5.17 is equivalent to Fig. 5.16, except (1) $R_2 = 2\%$ and $R_{ex} = 3\%$ for the graphs α_{sol}, $\alpha_0(\omega)$, $\alpha_H(\omega)$, and $P_H(\omega)$, and (2) $R_2 = 0.05\%$ and $R_{ex} = 13\%$ for the graphs $\alpha_L(\omega)$, and $P_L(\omega)$, respectively. The subscript L or H refers to a low or high residual reflectivity of the coated facet of the laser, respectively. $\alpha_H(\omega)$ and $\alpha_L(\omega)$ in Fig. 5.17(b) are calculated in the same way that $\alpha_L(\omega)$ was in Fig. 5.16(a). $P_H(\omega)$ and $P_L(\omega)$ in Fig. 5.17(b) are the power versus tuning characteristic obtained in the same way as $P_L(\omega)$ in Fig. 5.16(b). The values of R_2 and R_{ex} in Fig. 5.17 are the same as for the experimental data shown in Figs. 5.3 to 5.9. The experimentally observed output power versus tuning characteristic, Fig. 5.3 and insert of Fig. 5.7, are in good agreement with the theoretical curves shown in Fig. 5.17(b). Bistability and non-continuous tunability for the high reflectivity laser, $P_H(\omega)$ in Fig. 5.17(b), and continuous tunability for the low reflectivity laser, $P_L(\omega)$ in Fig. 5.17(b), are therefore predicted correctly with the model described in this thesis.

5.5. STABILITY OF OSCILLATION

5.5.1. *Single Mode Stability*

To analyze the stability of single mode oscillation we plot, for a fixed value of ω_G, the constant phase curve and the loss curve (Fig. 5.18(a)), the intersections of which provide ω_i, the frequencies of the compound cavity modes and $\alpha(\omega_i)$, the compound cavity loss for these modes. This technique [83] allows us to determine the external cavity modes that exist for a given detuning, and therefore, both to locate the

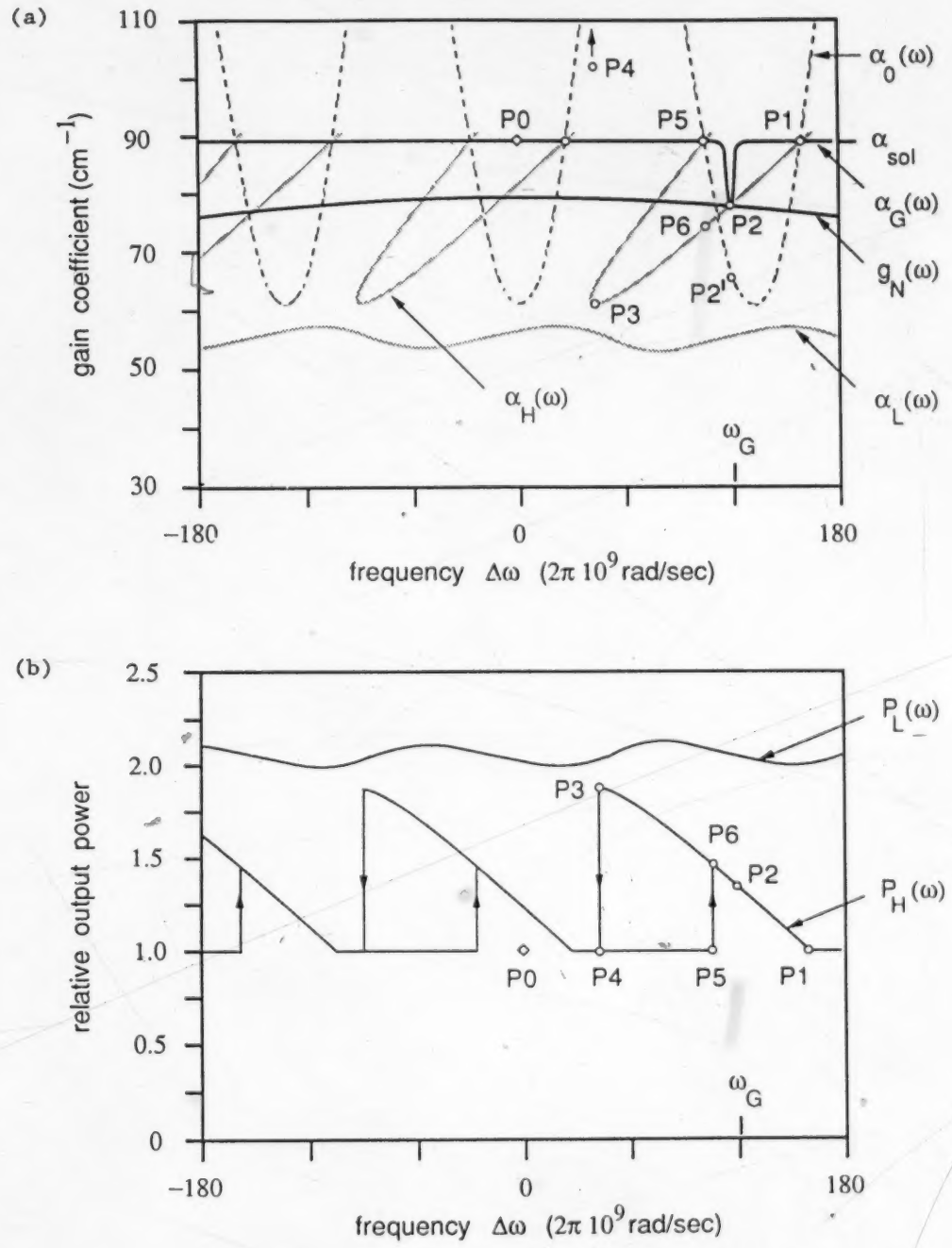

Fig. 5.17(a): Computed loss and gain versus frequency graphs for the high reflectivity laser TH 557, $\alpha_0(\omega)$ and $\alpha_H(\omega)$, and for the low reflectivity laser TY 224, $\alpha_L(\omega)$.
(b): Sketch of the output power vs. tuning characteristic showing hysteresis for the high reflectivity laser, $P_H(\omega)$, and continuous tunability for the low reflectivity laser, $P_L(\omega)$.

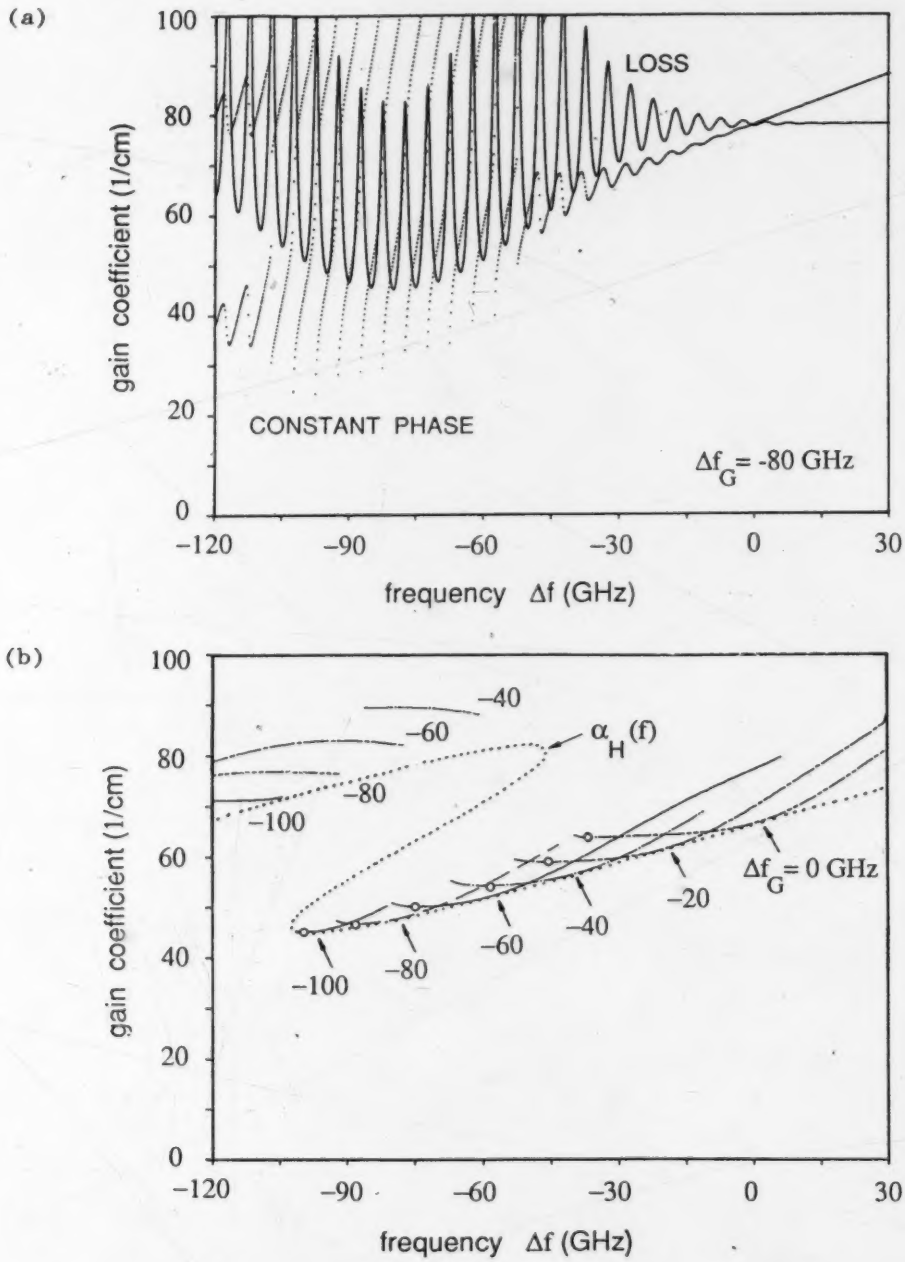

Fig. 5.18(a): Computed loss and constant phase curve for an external grating laser with fixed detuning of Δf_G = -80 GHz.
(b): Loci of all external cavity modes for various amounts of detuning, Δf_G. Also, loss versus frequency curve, $\alpha_H(f)$ with $f = 1/2\pi$, based on the assumption $f = f_G$. For each value of detuning, the threshold gain of the external cavity mode with minimum threshold gain is marked by an open circle.

mode with minimum threshold gain and to analyze its stability compared to neighboring modes for a given detuning.

We assume the FWHM of the spectral response of our grating to be $\Delta\omega_G = 2\pi \cdot 30$ GHz [37], based on a Gaussian beam of spot size 4 mm illuminating a 1200 lines/mm grating in Littrow configuration with incident angle of 50°. Assuming a fixed value of detuning, $\Delta f_G = (\omega_G - \omega_m^0)/2\pi$, and letting $\Delta f = (\omega - \omega_m^0)/2\pi$ run from -120 GHz to +30 GHz, we calculate, for each Δf, the values for the constant phase curve $g_{ph}(\omega) = \alpha_{sol} + \Delta g$ with Δg obtained from (5.1) and (5.8) and the loss curve $\alpha(\omega)$ from (5.4). Fig. 5.18(a) is calculated for $r_1^2 = 31\%$, $r_2^2 = 3\%$ and $r_{ex}^2 = 10\%$, $L_{in} = .03$ cm, $L_{ex} = 3$ cm, $v_{gr} = .75 \cdot 10^{10}$ cm/sec and $\alpha = 5$. The intersections of $g_{ph}(\omega)$ and $\alpha(\omega)$ define the values of ω_i. They are slightly closer spaced than the external cavity mode spacing calculated from $\Delta\nu_{ex} = c/L_{ex}$. Fig. 5.18(b) shows the loci of all values of ω_i for different amounts of detuning.

Also plotted in Fig. 5.18(b) is $\alpha_H(f)$, the same function shown as $\alpha_L(\omega)$ in Fig. 5.16(a) but for the parameter values used in Fig. 5.18(a). We recall that $\alpha_H(f)$ was calculated in Section 5.4 using the assumption that the oscillation frequency of the external grating laser coincides with the peak of the grating response, $f_G = \omega_G/2\pi$. Accordingly, $\alpha_H(f)$ coincides at $f = f_G$ in Fig. 5.18(b) with the locus of external cavity modes calculated for a given detuning Δf_G. Fig. 5.18(b) shows, however, that the mode with minimum loss, marked for each value of Δf_G by an open circle, coincides with f_G only for large detuning. For small detuning the frequency of the mode with minimum loss, which is equal to the oscillation frequency of the external grating laser, is up to ~30 GHz lower than f_G. The oscillation frequency of the laser is pulled away from ω_G towards the resonant frequency of the semiconductor cavity immediately below ω_G, $\omega_m(g)$.

The power in each compound cavity mode, ω_i, is given by (5.14) to (5.16) [59]

$$P(\omega_i) = K_p \frac{R_{sp}(\omega_i)}{v_{gr} \cdot (\alpha(\omega_i) - g_N(\omega_i))} \tag{5.22}$$

We introduce ω_c, the frequency of the mode with lowest difference between gain and loss, $\Delta g_N(\omega_i) = \alpha(\omega_i) - g_N(\omega_i)$, and therefore largest output power. The change of gain due to the curvature of the gain profile is small between external cavity modes. We can therefore assume $g_N(\omega_i) = g_N(\omega_c)$ and obtain from (5.22), (5.15) and (5.17)

$$\frac{P(\omega_c)}{P(\omega_i)} = 1 + \frac{\alpha(\omega_i) - \alpha(\omega_c)}{\Delta g_N(\omega_i)} \tag{5.23}$$

and

$$P(\omega_i) \propto \frac{g_N(\omega_i)}{\Delta g_N(\omega_i)} . \tag{5.24}$$

$P(\omega_c)/P(\omega_i)$ is the side-mode suppression between the center mode, ω_c, and the neighboring mode, ω_i. The side-mode suppression in (5.23) increases (1) if the difference between the loss of neighboring modes is increased and (2) if $\Delta g_N(\omega_i)$ decreases, which takes place for a given value of output power if the threshold gain $g_N(\omega_c)$ decreases, (5.24). We can see from Fig. 5.18(b), that both low threshold gain and increased loss difference between adjacent modes is achieved for large detuning from the solitary laser mode. Close to the loss minima in Fig. 5.18(b), the loss-difference between adjacent modes is $\sim .025$ cm^{-1} and .12 cm^{-1} for a detuning of 0 GHz and -80 GHz, respectively, and for an external cavity length of $L_{ex} = 15$ cm. We therefore expect higher single-mode stability for large detuning. This is in agreement with the experimental result, where we find better single-mode stability in Regime IV for the high reflectivity laser. For the low reflectivity laser, little modulation of the threshold gain is achieved during tuning (Fig. 5.17(a)) and therefore no significant dependence of the detuning on the side-mode stability is to be expected, which again conforms with the experimental results.

The sidemode suppression for an external grating laser can become very high, on the order of 10^3 to 10^4 [32]. Due to the close spacing of external cavity modes the loss-difference between adjacent modes is low. Kazaninov and Henry [83] concluded that the loss-difference between adjacent modes is not sufficient to explain the observed side-mode

suppression ratios. They refer to one of their earlier papers [102] where they describe two optical nonlinear effects that cause gain suppression similar to holeburning, however gain suppression not for the oscillating mode but on both sides of this mode. The gain for the immediately neighboring modes decreases and the difference in $\Delta g_N(\omega_1)$ between these modes and the center modes increases, thereby stabilizing the oscillating mode. For a solitary laser this "self-stabilization" of the oscillating mode is not observed, because the two nonlinear mechanisms cancel each other if a center mode has neighboring modes that are spaced equally and have equal power [102].

For a laser with feedback from a short integrated frequency selective Bragg reflector, the calculations of [83] show unequal spacing of longitudinal modes. This unequal spacing was held responsible for the excellent sidemode suppression of this device. Asymmetry in the number and the loss of the modes on each side of the mode with the lowest loss (the lasing mode) is also observed for the external grating laser in Fig. 5.18(b), to an increasing extent for large detuning.

Both the increased loss difference for neighboring modes and the lack of symmetry facilitate "self-stabilization" of the center mode. These effects, shown to be present for large detunings in Fig. 5.18(b), thus provide theoretical substantiation for the increased single-mode stability experimentally observed and noted in Section 5.2.1.

5.5.2. *Linewidth*

The linewidth of the solitary laser above threshold is (Section 2.4.3.2, eq. (2.63))

$$\Delta\nu_0 = \frac{R_{sp}}{4\pi S}(1 + \alpha^2) \tag{5.25}$$

where R_{sp} is the spontaneous emission factor of the solitary laser and S the number of photons stored in the semiconductor cavity. Assuming a residual reflectivity of $R_2 = 0$ for the one-side coated laser, the linewidth of a laser with passive external cavity is [61]

$$\Delta\nu = \frac{R_{sp}\cdot(1+\alpha^2)}{4\pi S}\cdot\left(\frac{\tau_{in}}{\tau_{ex}+\tau_{in}}\right)^2 \qquad (5.26)$$

where τ_{in} and τ_{ex} are the roundtrip times in the semiconductor cavity and in the passive external cavity, respectively. The linewidth reduction term in (5.26), $F_0^2 = (\tau_{ex}+\tau_{in})^2/\tau_{in}^2$, can be intuitively understood [47] as follows. Instead of using (5.26), we can express the linewidth in terms of the spontaneous emission rate, R_{sp}^{ext}, of the extended cavity laser and the number of photons, S^{ext}, in the extended cavity, including the passive section. We obtain $\Delta\nu = R_{sp}^{ext}\cdot(1+\alpha^2)/(4\pi S^{ext})$, where R_{sp}^{ext} is smaller than R_{sp} by the factor F_0 due to the closer spacing of external cavity modes, which leads for a fixed overall rate of spontaneous emission, N/τ_e, to a reduced rate of spontaneously emitted photons coupled into the individual modes. Also S^{ext} is larger than S by the factor F_0 due the increased size of the cavity.

As an example, if $L_{in} = .025$ cm, $L_{ex} = 15$ cm and the group-velocities in the semiconductor cavity and the external cavity are $v_{gr}^{in} = 0.75\cdot10^{10}$cm/sec and $v_{gr}^{ex} = 3\cdot10^{10}$cm/sec, respectively, a linewidth reduction of $F_0^2 = (150)^2 = 22{,}500$ is predicted from $F_0 = (\tau_{ex}+\tau_{in})/\tau_{in}$, which leads for a laser with $\Delta\nu_0 \sim 100$ MHz to a linewidth of $\Delta\nu \sim 4$ kHz. Although we assumed $R_2 = 0$ instead of $R_2 = 2\%$ and $.05\%$, respectively, the calculated value of linewidth agrees well with the experimentally observed linewidths of the external grating laser, when this laser oscillates in a single external cavity mode (Sect. 5.2).

A more involved calculation method is required to determine the linewidth reduction if $R_2 \neq 0$. We use the relation for the chirp reduction $F = 1 + A + B$, as defined in the paragraph following (3.32). If $R_2 = 0$, we note from (3.5) and (3.27) that $B = 0$ and therefore $F_0 = 1 + A$. The linewidth reduction, $F_0^2 = (\tau_{ex}+\tau_{in})^2/\tau_{in}^2$, is the increase in the slope of the constant phase curve of the laser with feedback compared to that without feedback, Fig. 3.4. Only if $R_2 \neq 0$, is there an amplitude modulation of the compound cavity loss and therefore (3.27)

$$B = \alpha\cdot\Delta\nu_{in}\frac{d\ \ln|r_e|}{d\omega} \neq 0 \qquad (5.27)$$

The slope B of the loss-curve can be either positive and negative. However, we see from Fig. 5.18 that low-loss intersections of the loss and constant phase curves occur only for $B > 0$. Since the amplitude of the oscillations of $\alpha(\omega)$ increase with R_2 (Fig. 5.13(b), 5.14(b) and eq. (5.4)) higher values of B and in turn an increase of F compared to F_0 is possible for large values of R_2. We will therefore investigate whether external grating lasers with high residual reflectivity R_2 show larger linewidth reduction than lasers with low R_2, as has been suggested by Wyatt [103] who calculated F for different detunings and different values of R_2.

We recall that stable single-mode oscillation was obtained for the high reflectivity laser in our experiment for large detunings (Section 5.2.1). We therefore ask, what are the values of F for large detunings. Fig. 5.18(a) shows that the intersections of loss and constant-phase curves are close to the minimum of the loss ripple for large detunings and therefore B is close to zero and F close to F_0. In fact for maximum detuning the intersection with lowest loss is at the minimum of the loss-ripple and therefore $B = 0$. In other words, for maximum detuning the linewidth reduction is independent of the amplitude of the loss-ripple (and therefore independent of R_2) and equal to F_0^2.

Fig. 5.19 shows the loci of $F(\omega_i)$ for all external cavity modes plotted for various detunings. For the calculation the same parameter values as for Fig. 5.18(a) have been assumed except for L_{ex}, which has been increased to $L_{ex} = 15$ cm for Fig. 5.19. $F(\omega_i)$ can be calculated [83] using

$$A - j\frac{B}{\alpha} = \frac{v_{gr}^{in} L_{ex}(1 - r_2^2)\, r_G(\omega)\, \exp(j\phi(\omega))}{v_{gr}^{ex} L_{in}(r_2 + r_G(\omega)\exp(j\phi(\omega)))(1 + r_2 r_G(\omega)\exp(j\phi(\omega)))} \quad (5.28)$$

and $F = 1 + A + B$. (5.28) can be derived from (3.27) and (5.1) to (5.3). To obtain $F(\omega_i)$ we first have to find ω_i, i.e. the frequency of the intersections between loss and constant phase curve in a plot similar to Fig. 5.18. The values for ω_i are obtained from (5.4), (5.8) and $\Delta g = \alpha_{sol} - \alpha(\omega)$ with the help of a zero-finding algorithm. We then replace ω in (5.28) with the values for ω_i and calculate A, B and finally $F(\omega_i)$.

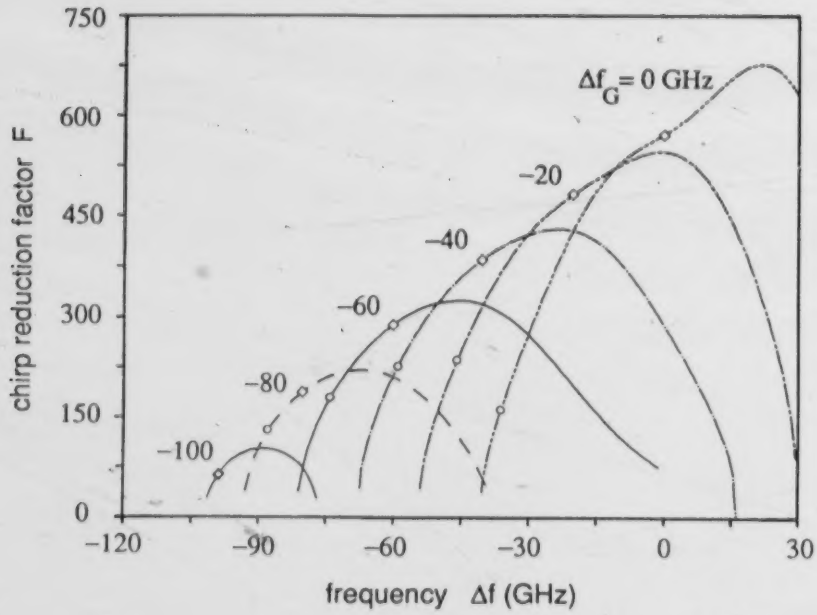

Fig. 5.19: Loci of the chirp reduction of all external cavity modes for various amounts of detuning Δf_G. For each value of detuning, the open circle indicates the chirp reduction of the external cavity mode with minimum threshold gain (see Fig 5.18(a)) and the rectangle the chirp reduction of the external cavity mode at Δf_G.

The squares in Fig. 5.19 mark the value of linewidth reduction of the external cavity mode closest to the frequency of the maximum grating response, f_G. In the derivation of the tuning characteristic we assumed for simplicity and following [18] and [103] that f_G is the frequency of oscillation of the external grating laser. In Section 5.5.1 we noted however, that for a given value of f_G, the frequency of the mode with lowest threshold gain, marked in Fig. 5.18(a) and 5.19 by open circles, is only identical to f_G, marked by squares in Fig. 5.19, at maximum detuning, Δf_G = -100 GHz in Fig. 5.19. We note from Fig. 5.19, that the chirp reduction of the mode with minimum threshold gain (open circles) depends far less on the detuning as the chirp reduction of the mode at

f_G (squares). In fact the values of F obtained for the mode with minimum threshold gain are centered around the value of F = 150. We obtained the same value at the beginning of this section, using the expression $F_0^2 = (r_{ex} + r_{in})^2/r_{in}^2$, which applies to the case of $R_2 = 0$.

The preceding paragraph shows that the assumption of oscillation of the external grating laser at f_G leads to an overestimation of the dependence of the linewidth reduction on the detuning. It is this assumption, that Wyatt's [103] calculations are based on. For the comparison of Wyatt's results with our results we note that "in-phase" or resonant [103] feedback occurs in our definition of detuning for maximum detuning, in Wyatt's definition for zero detuning. Therefore, we have to assume that Wyatt defines detuning with respect to $\omega_m(g)$, where we recall that $\omega_m(g)$ depends on the threshold gain and therefore on the amount of detuning. Our definition of detuning is with respect to the fixed frequency ω_m^0.

To determine the dependence of the linewidth on the detuning we have to consider not only the change in F but also the changes of R_{sp} and S with detuning. $\Delta\nu$ decreases as R_{sp} decreases, where R_{sp} is proportional to g_N, (5.25) and (5.15), and decreases with an increase in S, (5.25). For large detunings $g_N = \alpha(\omega)$ is lower and using (5.21) and (5.20), the output power is larger for a given injection current, therefore S is larger. Both effects lower the linewidth according to (5.25) for large detunings. The change in $\alpha(\omega)$ with detuning, responsible for both effects, can be seen from (5.4) and Figs. 5.16(b) and 5.17(b) to be more pronounced for lasers with larger values of R_2. In conclusion an increase of F with respect to R_0 can only be obtained with large values of R_2 and when operating at low detunings. However low detunings are not desirable if R_2 is large, because they lead to high rates of spontaneous emission, where spontaneous emission is the principle source of the frequency noise we want to suppress, and low detunings lead to low output powers at a given injection current.

The experiments with our highest reflectivity laser show that the dependence of the linewidth on detuning is connected with the presence or absence of multiple external cavity modes (Section 5.2.1). This is not surprising since a substantial increase of the linewidth is predicted theoretically [44],[104], if the oscillation frequency of the

laser fluctuates between several longitudinal cavity modes. In the domain of stable oscillation in a single external cavity mode no significant dependence of the linewidth on detuning was observed. The linewidths achieved with the high-reflectivity laser and the low reflectivity laser, when feedback from the grating was applied, where distributed, depending on the quality of the alignment, within the same range of a few kHz.

In conclusion, linewidth reduction ratios of $F_0 = 2 \cdot 10^5$ were calculated for the external grating laser, with the assumption of $R_2 = 0$. The low linewidth observed in the experiment is thus in accord with theory. No significant difference in the linewidths for lasers with different values of R_2 was observed experimentally, provided that oscillation in a single external cavity mode occurred. Theoretically a finite value of R_2 allows for an increase of F above the value of F_0. However we observe that stable single-mode oscillation is not achieved for large values of R_2 and low detunings, where this increase of F would be significant. Even the experimental data provided in [103] does not support the claim made in the latter paper that high values of R_2 lead to lower linewidths. Our observations and Wyatt's data [103] support our finding that increased spontaneous emission and decreased single-mode stability prevent one from being able to take advantage of the increased values of F that exists for low values of detuning and high values of R_2.

5.5.3. *Lens-Alignment*

The lens between the laser and the diffraction grating in Fig. 5.2 has to be aligned very carefully. Poor alignment and lens imperfections affect the phase front of the collimated beam and therefore degrade the spectral amplitude response of the grating and reduce the optical power that is coupled back into the active region of the laser. We have to expect both an increase in the FWHM of the spectral response of the grating under conditions of poor alignment and possibly sidelobes in the spectral response. Experimentally, intentional partial blocking of the collimated beam between lens and grating leads to the same kinks in the sawtooth-like power vs. tuning characteristic (Fig. 5.20, trace (1))

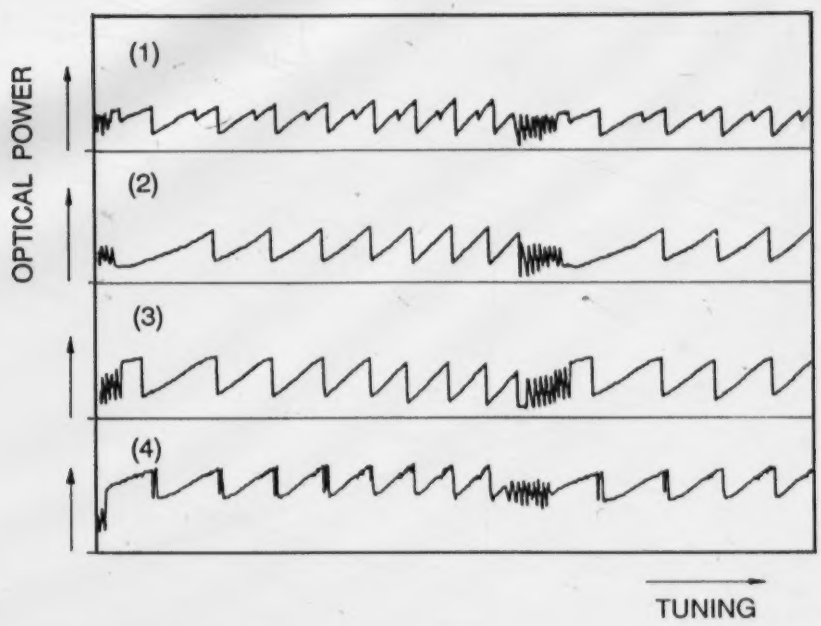

Fig. 5.20: Change of the power versus tuning characteristic due to partial blocking of the collimated beam between lens and diffraction grating in Fig. 5.2. The beam was blocked as follows: (1) a 1 mm horizontal slice from the center of the beam, (2) ~ 30% of the upper portion of the collimated beam in Fig. 5.2 and (3) ~ 30% of the lower portion of the collimated beam. (4) is recorded without aperture.

that can be observed for poor lens alignment. We therefore attribute deviations of the tuning characteristic from its ideal sawtooth-like shape to a multi-lobed spectral response of the grating due to a poor phase front of the collimated beam.

The lower envelope of the loss-ripple in Fig. 5.18(a) is caused by the spectral response of the grating. In Fig. 5.18(a) a smooth-Gaussian spectral response of the grating is not necessarily better in providing good side-mode suppression than a multi-lobed uneven response. The only requirement for stable single-mode oscillation is that the FWHM of the main lobe of the response remains reasonably narrow and that the spectral response of the grating does not lead to two sets of external cavity modes that have similar threshold gain. This explains why, in the experiment, the alignment that leads to the most ideal tuning

characteristic does not necessarily lead to the most stable oscillation of the external grating laser at one frequency. Generally changes of the lens position within a few μm help to establish single-mode oscillation at a given oscillation frequency.

5.5.4. *Fine Tuning*

The frequency of the maximum of the spectral grating response decreases as the grating is rotated to decrease the incident angle of light. Therefore, decreasing the incident angle of the incoming light moves the minimum of the lower envelope of the loss ripple in Fig. 5.18(a) to lower frequencies. The loss of the external cavity mode that previously had minimum threshold gain increases, and the loss of its low-frequency neighbor decreases until finally the frequency of oscillation jumps to the low-frequency neighbor. Therefore, if the grating angle is changed, the frequency of oscillation decreases or increases in steps of $\Delta\nu_{ex}$ (= 1 GHz for L_{ex} = 15 cm). To access frequencies within this 1 GHz range, the length of the external cavity has to be changed by up to $\lambda/2$. In Fig. 5.18(a) a change of the external cavity length causes a horizontal shift of the periodic pattern of the constant phase curve and an equal shift of the ripple of the loss curve. The slopes of the constant phase curve and loss curve at the intersections of both curves stay essentially constant. The linewidth of the oscillating mode is therefore not affected by the change of the external cavity length.

The tuning characteristics described above agree with the experimental results of [32]. They have also been experimentally verified during the course of the present project, by observing the change of the beat frequency between the external cavity laser and a second single-mode laser, stabilized with optical feedback from a fiber ring (Section 4), while the grating angle and the external cavity length were changed independently.

5.6. CONCLUSION

The dependence of the operating characteristics of an external grating laser on the frequency of optical feedback has been examined. Experimental results have been presented for lasers with different residual reflectivity of the AR-coated facet. They show that detuning of a high residual-reflectivity laser affects the output power, linewidth and stability of oscillation in a single external cavity mode.

It has been shown that the range of frequencies accessible to the external grating laser and the power versus tuning characteristics can be determined from the width of the gain profile of the semiconductor laser, the residual reflectivity of the AR-coated facet and the level of optical feedback. Bistability in the tuning characteristic of the high reflectivity laser was observed and explained using the loss versus frequency graph plotted for different carrier density levels.

A periodically repeating domain of stable single mode oscillation was identified for the high reflectivity laser, which coincides with the condition of large detuning from the solitary laser mode and with the regime of high output power due to large detuning. The stability of oscillation in this domain was explained with the increased loss difference between neighboring modes in this domain and the lack of symmetry in the distribution of external cavity modes with respect to the mode with lowest loss.

For the low reflectivity laser, stable single mode operation was observed to be independent of the detuning from the solitary laser mode provided that the grating and lens are carefully aligned. Laser, lens and grating have to be aligned as carefully as in an interferometric setup; the laser emits light in a single spatial mode and only light that is coupled back into the same mode can control the laser operation. Also, the spectral response of the grating is distorted if the grating is illuminated by imperfectly collimated light. Consequently, a poor alignment was found not only to reduce the effective level of optical feedback, but also to distort the tuning characteristic of the laser.

6. GAIN VERSUS CURRENT CHARACTERISTIC

6.1. INTRODUCTION

To compare the experimental results for strong optical feedback with the theoretical predictions it is necessary to know the level of optical feedback applied to the laser. The loss in the resonator and therefore the level of optical feedback can be determined from the light versus current (LI) characteristic of the laser. The threshold current, which is defined by the LI-characteristic as long as the loss in the resonator is not too high, can serve as a reference value to characterize the change of the LI-characteristic with resonator loss. The simple relation (5.21) [101] between threshold current and loss in the resonator is valid only if we assume that there is no stimulated emission of radiation below lasing threshold, that the leakage current is proportional to the injection current, the carrier lifetime independent of the carrier density, the gain proportional to the carrier density, and gain and loss are equal at the lasing threshold. If we deal with large changes of the resonator loss, those assumptions are no longer valid.

To determine the threshold current versus resonator-loss characteristic without making the preceding assumptions, we have to calculate first the gain versus current characteristic and then the light versus current characteristic for different values of resonator loss. It will be shown that each LI-characteristic can be interpreted to provide one value of the threshold current for a particular resonator loss.

The theoretical model used in this paper to calculate power and gain vs. current characteristics accounts for the leakage current (that part of the diode current that does not flow through the active region), the nonlinear change of the spontaneous emission rate with carrier density, the dependence of the photon-density on the axial position in the laser and the spectral dependence of the gain which determines the distribution of the output-power in multiple longitudinal modes. The values for a large number of parameters are required to calculate the gain and

output power of a laser as a function of the current using this model. Some of these parameters stay constant for all lasers of the same wavelength. Other parameters change with laser structure and others vary between individual lasers of the same structure. For the two types of lasers in this work, V-groove and etched mesa buried heterostructure (EMBH) lasers emitting at 1.3-μm wavelength, we define a set of general parameters that stay constant for these lasers and we determine numerical values for a set of 4 device dependent parameters. Suitable values for the general parameters were selected from values quoted in the literature [59],[105].

To obtain strong optical feedback, it is necessary to AR-coat one facet of the laser (Chapter 5). The LI-characteristics of the laser can be recorded before and after AR-coating. Also we can determine the loss of the resonator before coating from the modal reflectivity of the cleaved facets [22] and after coating from a measurement of amplified spontaneous emission spectrum of the coated device [96],[97]. We use a curve-fitting method on the measured LI-curves before and after AR-coating to determine the four device dependent parameters for the particular laser. Good agreement was obtained between calculated and measured LI-curves for different facet reflectivities for both the V-groove and EMBH-lasers. We conclude we have chosen the correct parameters to represent the differences in characteristics both between structurally different devices and individual devices of identical structure.

As a result we obtain a model that describes the change of the LI-characteristics of a particular laser with the resonator loss, and which provides LI-curves that agree with the measured LI characteristics for the two extremes of low and high resonator loss. From a set of LI-curves calculated for different values of resonator loss we determine the threshold current versus resonator loss characteristic for the particular laser being analyzed. If we apply optical feedback to the AR-coated facet of the laser, the compound resonator loss will reach a value that is between the values of the loss for the uncoated and the coated laser. We can measure the threshold current of the laser with optical feedback and, from the threshold current versus resonator loss characteristic of this particular laser, determine the resonator loss of

the compound cavity laser. From the resonator loss and knowledge of the facet reflectivities, we can then calculate the level of optical feedback.

During the calculation of the LI-curves, we also obtain the data necessary to plot the gain versus current characteristics for different values of resonator loss. Also, in particular, we obtain the gain versus current characteristic for the device with two AR-coated facets, i.e. for an optical amplifier [98] built from the particular device. We conclude that we have found a method to determine the gain versus current characteristics of individual semiconductor laser amplifiers from data obtained during the AR-coating procedure. This data is the LI-curve of the uncoated laser, the LI-curve of the one-side coated laser, measured at the AR-coated facet, and a measured value for the residual reflectivity of the laser. These measurements are normally made during the coating process to determine the quality of the AR-coating and to verify that the device is in good working condition after AR-coating. They are therefore readily available and do not require addition experimental effort. We calculate the gain vs. current characteristic based on this method and find good agreement with the measured data provided by Enning et.al. [106] for a specific laser amplifier.

We believe that this method for determining the gain versus current characteristic of individual semiconductor laser amplifiers is a particularly useful aspect of the work presented in this chapter. The focus of the presentation is chosen accordingly. Only in the last Section, 6.4.4, do we return to the problem of determining the amount of optical feedback from the change of the threshold current. In this latter section we plot the dependence of the threshold current on the reflectivity of one facet of the laser, when the other facet reflectivity is assumed to be constant. We use this characteristic to determine the strength of optical feedback from the change of the threshold current due to optical feedback and compare our results to the results of the approximation proposed by [107].

6.2. THEORETICAL ANALYSIS

The theoretical analysis in this section is based on the model described in [22] and [59]. An AR-coated laser oscillates in a large number of longitudinal modes. Therefore, we have to replace the single rate equation (2.17) by M rate equations for the number of photons in each of the M longitudinal cavity modes. All of these M rate equations are coupled through the common rate equation for the total number of carriers, N (eq. 6.2.25/26 in [59]):

$$\dot{S}_m = v_{gr} \cdot (g_m - \alpha_L) \cdot S_m + R_{sp}(\lambda_m) \tag{6.1}$$

$$\dot{N} = \frac{I_a}{q} - \frac{N}{\tau_e} - \sum_m v_{gr} \cdot g_m \cdot S_m \tag{6.2}$$

where $S_m = S(\lambda_m)$ represents the photon population in the m^{th} longitudinal mode, $g_m = g_N(\lambda_m)$, (5.12), the gain per unit length for the m^{th} mode and λ_m is the wavelength of this mode. It is convenient to choose the mode-number m such that the separation between λ_m and the wavelength of peak gain, λ_p, (5.13), is given by

$$\lambda_m - \lambda_p = m \cdot \Delta\lambda_{in} \tag{6.3}$$

where $\Delta\lambda_{in} = (\lambda_p^2 / 2 \cdot L_{in} \cdot n_{gr})$ is the spacing between longitudinal modes. The total loss α_L per unit length is

$$\alpha_L = \alpha_s + \alpha_R \tag{6.4}$$

where α_R is the mirror loss distributed equally over the length of the active medium, (2.5), and α_s is the material loss in the active region. For the solitary laser, α_R is independent of the wavelength of the longitudinal modes. The distribution of power in the longitudinal modes is governed by the spectral dependence of the gain. The spontaneous emission $R_{sp}(\lambda_m)$ into the m^{th} mode is given by (2.24)

$$R_{sp}(\lambda_m) = n_{sp} \cdot K_R \cdot v_{gr} \cdot g_m \tag{6.5}$$

where we neglect the wavelength dependence of the inversion parameter n_{sp} [47]. The independent variable in the calculations that follow is the carrier density n, where $n = N/V$, N is the total number of carriers in the active region, and $V = w \cdot d \cdot L_{in}$ is the volume of the active region with width w and height d. The total rate of spontaneous carrier recombination, N/τ_e, is a function of the carrier-lifetime τ_e, where τ_e is dependent on the carrier density [59]

$$1/\tau_e = a + bn + cn^2. \tag{6.6}$$

The coefficients a,b and c are recombination constants describing non-radiative and radiative recombination [59],[108]. So far we have assumed τ_e to be constant. Since we are dealing in this section with the laser operation at very different levels of gain and carrier density this assumption is no longer valid.

In steady state operation, the photon and carrier populations are constant ($\dot{S}_m = 0$, $\dot{N} = 0$). We obtain from (6.1) and (6.2)

$$S_m = \frac{R_{sp}(\lambda_m)}{v_{gr}(\alpha_L - g_m)} \tag{6.7}$$

and

$$I_a = q \left(\frac{N}{\tau_e} + \sum_m v_{gr} \cdot g_m \cdot S_m \right). \tag{6.8}$$

The output powers per facet, P_{m1} and P_{m2}, at wavelength λ_m in photons per second in the case of equal facet reflectivities are given by (eq. 6.2.27 of [59])

$$P_{m1} = P_{m2} = \frac{1}{2} \cdot \alpha_R \cdot v_{gr} \cdot S_m. \tag{6.9}$$

Equations (6.1), (6.7) and (6.8) are based on the assumption that the change in photon-population per unit volume dS_m/dV is constant over the length of the cavity and the mirror-loss α_R can be distributed over the length of the active region (2.5). For lasers with low mirror-reflectivities, the dependence of the field intensity on the position z along the active region (Fig. 6.1) cannot be neglected. In the following we will therefore rederive the equations for S_m and the total

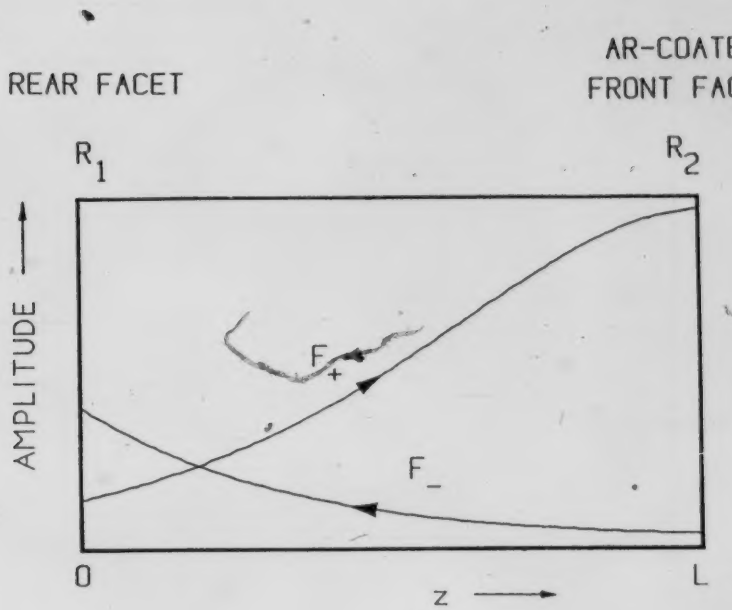

Fig. 6.1: Sketch of the forward and backward travelling waves within the active region of a one-side AR-coated laser diode.

output powers per facet, P_1 and P_2, by introducing a z-dependent light intensity $F_m(z)$ in photons per unit area per second per mode

$$F_m(z) = v_{gr} \cdot dS_m/dV. \tag{6.10}$$

Taking the derivative of (6.1) with respect to volume and using (6.4) leads to

$$\frac{d}{dt}\left(\frac{dS_m}{dV}\right) = v_{gr}\cdot(g_m - \alpha_s)\cdot\frac{dS_m}{dV} - v_{gr}\cdot\alpha_R\cdot\frac{dS_m}{dV} + \frac{R_{sp}(\lambda_m)}{V}. \tag{6.11}$$

In (6.11) the components of loss due to scattering, α_s, as the light travels through the active region are separated from the facet loss, α_R. We introduce a forward and backward travelling component F_{m+} and F_{m-} of F_m, where

$$F_m(z) = F_{m+}(z) + F_{m-}(z). \tag{6.12}$$

For the steady state case ($\partial F_{m+/-}/\partial t = 0$) we can write

$$\frac{dF_{m+/-}(z)}{dt} = \frac{dz}{dt}\,\frac{\partial F_{m+/-}(z)}{\partial z} + \frac{\partial F_{m+/-}(z)}{\partial t} = \pm v_{gr} \cdot \frac{\partial F_{m+/-}(z)}{\partial z} \qquad (6.13)$$

Inserting (6.10) and (6.13) into (6.11) leads to [22]

$$\pm \frac{\partial F_{m+/-}(z)}{\partial z} = (g_m - \alpha_s) \cdot F_{m+/-}(z) + \frac{R_{sp}{}^{0}(\lambda_m)}{2V \cdot v_{gr}} \qquad (6.14)$$

where the mirror loss is no longer considered as being distributed over the length of the active region but is accounted for in the boundary conditions for $F_{m+/-}(0)$ and $F_{m+/-}(L_{in})$. Also, the spontaneous emission rate is divided into two components that contribute equally to F_{m+} and F_{m-}, and is given by

$$R_{sp}{}^{0}(\lambda_m) = n_{sp} \cdot v_{gr} \cdot g_m . \qquad (6.15)$$

We recall from the discussion associated with (2.24), that the factor K_R in the definition of $R_{sp}(\lambda_m)$ accounts for the increase in the amount of spontaneous emission that is coupled into the lasing mode if a z-dependence of the photon density exists due to loss of photons at the output facets. K_R is therefore a correction factor for the spontaneous emission rate that reduces the error made in the rate equations (6.1) by neglecting the z-dependence of the photon density in those rate-equations. However in (6.14) and in the remainder of this chapter, the increase of the spontaneous emission due to the z-dependence of the photon-density is included in the model and we therefore have to omit K_R.

The total photon population in the m^{th} mode is

$$S_m = \frac{d\,w}{v_{gr}} \int_0^{L_{in}} F_m(z) \cdot dz . \qquad (6.16)$$

We assume the carrier density along the z-axis is constant and therefore that the gain g_m and spontaneous emission rate $R_{sp}{}^{0}(\lambda_m)$ are independent of z. A more general numerical analysis that takes spatial gain

saturation due to carrier depletion by the z-dependent photon density into account, is contained in [109] and [110]. The errors introduced in our analysis by neglecting the spatial gain saturation will be discussed later. Integration of (6.14) yields an expression for F_{m+} and F_{m-},

$$F_{m+/-}(z) = F_{m0+/-} \exp\{\pm(g_m - \alpha_s)\cdot z\} - \frac{R_{sp}^{0}(\lambda_m)}{2V\cdot(g_m - \alpha_s)\cdot v_{gr}} . \quad (6.17)$$

The constants F_{m0+} and F_{m0-} can be obtained from the boundary conditions for $F_{m+/-}(0)$ and $F_{m+/-}(L_{in})$, namely $F_{m+}(0) = F_{m-}(0)\cdot R_1$ and $F_{m-}(L_{in}) = F_{m+}(L_{in})\cdot R_2$ (Fig. 6.1). The output power P_{m1} and P_{m2} in the m^{th} mode in photons per second from face 1 and 2, respectively, is given by $P_{m1} = (1-R_1)\cdot F_{m-}(0)$ and $P_{m2} = (1-R_2)\cdot F_{m+}(L_{in})$, respectively. We obtain from (6.17) in agreement with [22]

$$P_{m_i} = \frac{(1 - R_i)(G_{ms} - 1)(1 + R_j G_{ms})}{L_{in}\cdot(g_m - \alpha_s)(1 - R_i R_j \cdot G_{ms}^{2})} \cdot \frac{R_{sp}^{0}(\lambda_m)}{2} \quad (6.18)$$

where

$$G_{ms} = \exp\{(g_m - \alpha_s)\cdot L_{in}\} \quad (6.19)$$

and $(i,j) = (1,2)$ or $(2,1)$.

$G_{ms} = G_s(\lambda_m)$ is the single pass gain at the wavelength λ_m. The total output power in mW is the summation of the power emitted in the individual modes

$$P_i = \hbar\omega \sum_m P_{m_i} , \qquad i = 1,2. \quad (6.20)$$

To calculate the current in the active region (6.8), we need to determine the number of photons stored in the cavity in the m^{th} mode. From (6.16) and (6.17) we obtain

$$S_m = \frac{R_{sp}^{0}}{v_{gr}\cdot(g_m-\alpha_s)} \cdot \{ \frac{(1 - G_{ms}^{-1})^2\cdot(2 + (R_1+R_2)\cdot G_{ms})}{4\cdot\ln(G_{ms})\cdot(R_1R_2)^{1/2}\cdot\sinh\{(\alpha_L-g_m)\cdot L_{in}\}}$$

$$- \frac{1 - G_{ms}^{-1}}{\ln(G_{ms})} + 1\}. \quad (6.21)$$

Using (6.18), (6.21) can be rewritten to yield an expression for S_m as a function of P_{m1} and P_{m2}

$$S_m = \frac{1}{v_{gr}(g_m - \alpha_s)} \cdot \{[1 - G_{ms}^{-1}] \cdot [\frac{P_{m_2}}{1 - R_2} + \frac{P_{m_1}}{1 - R_1}] - R_{sp}^{0}(\lambda_m) \; [\frac{1 - G_{ms}^{-1} - \ln (G_{ms})}{\ln (G_{ms})}]\}. \qquad (6.22)$$

(6.21) and (6.22) are alternative expressions for the number of photons in the m^{th} longitudinal mode.

Equations (6.8) and (6.21) for the current in the active region and (6.18) to (6.20) for the output power from the two facets of the laser are key equations. They provide I_a, P_1 and P_2 in implicit form as a function of the carrier density n and the gain g_m (eqs. (5.12) and (5.13) give $g_m = g_N(\lambda)$ as a function of n and λ_m). Calculating all variables for a series of n and λ_m values and summing over all modes allows us to determine theoretical estimates of the LI-characteristics

$$P_1(n) = P_1 (I_a(n)) \qquad (6.23)$$

and

$$P_2(n) = P_2 (I_a(n)). \qquad (6.24)$$

Before we continue with analyzing the LI-curves in the next section, we wish to digress briefly to compare our general equations, (6.21) and (6.22) to the more familiar expressions (6.7) and (6.9), respectively. Both (6.22) and (6.9) provide a relation between the output power and the number of photons in the active medium. For laser operation above threshold, it is assumed that gain and loss are equal, therefore $g_m - \alpha_s = \alpha_R$ and $G_{ms} = (R_1 R_2)^{-1/2}$. It is also assumed that spontaneous emission is negligible compared to stimulated emission, therefore $P_{m1}, P_{m2} >> R_{sp}^{0}$. Using those assumptions and assuming $R_1 = R_2$, (6.22) simplifies to

$$S_m = \frac{1}{v_{gr}\, \alpha_R} (P_{m1} + P_{m2}). \qquad (6.25)$$

Noting that $P_{m1} = P_{m2}$ in the case of equal facet reflectivities, (6.25) is equivalent to (6.9).

Both (6.21) and (6.7) provide an expression for S_m as a function of R_{sp}, g_m, α_s and the mirror loss. In one case the mirror loss is expressed in terms of R_1 and R_2, in the other case by α_R. Again we assume operation is above threshold and therefore replace $g_m - \alpha_s$ in (6.21) with $\alpha_R = (1/2L_{in}) \cdot \ln(1/R_1R_2)$, and G_{ms}^{-1} with $(R_1R_2)^{1/2}$. We also use the approximation $\sinh(x) = x$ for $x \ll 1$ and obtain from (6.21)

$$S_m = \frac{R_{sp}^{0}(\lambda_m)}{v_{gr}(\alpha_L - g_m)} \left[\frac{(r_1 + r_2)(1 - r_1r_2)}{2r_1r_2 \ln(r_1r_2)}\right]^2 . \qquad (6.26)$$

Noting that $R_{sp}^{0}(\lambda_m) \cdot K_R = R_{sp}(\lambda_m)$ from (6.5) and (6.15), comparing (6.7) and (6.26) provides the same expression for K_R as (2.26). In conclusion, our general result for S_m contains the correction factor K_R. It was therefore correct in (6.14) to start the derivation of the expression for S_m with a definition of the spontaneous emission rate that does not contain K_R. Also, we showed that the more familiar expressions (6.7) and (6.9) are special cases in our general expressions (6.21) and (6.22) and we have therefore provided a test for our results.

6.3. GENERAL MODELLING

We are concerned with the modelling of the power and gain vs. current characteristic of individual devices. Initially we had to determine which of the parameters needed in the calculation of this characteristic could be considered constant between devices and which change and consequently need to be separately determined for each device. We found through a parametric study of this problem that taking into account the varying leakage characteristics of lasers of the same type (yielding three parameters) and determining as a fourth parameter the effective width, w, of the active region for each type of laser led to agreement between calculated and measured results for different lasers. These four device dependent parameters are determined using a curve-fitting technique that is based on a knowledge of R_2 and a

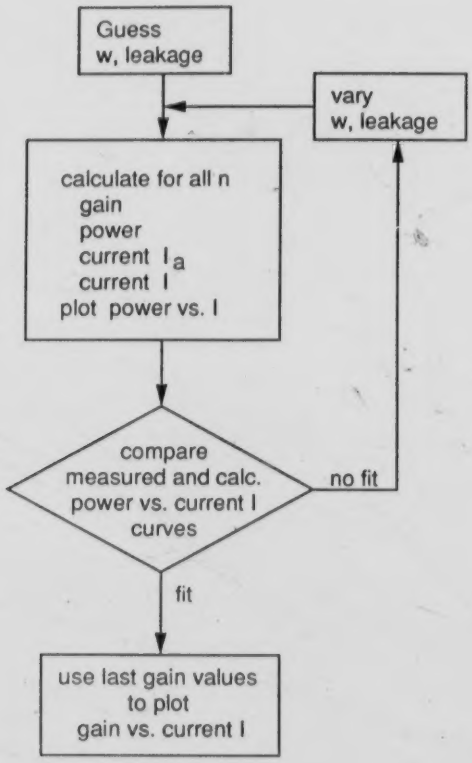

Fig. 6.2: Block diagram of the curve-fitting procedure.

comparison of calculated and measured LI-curves of the uncoated and the one-side coated laser (Fig. 6.2).

6.3.1. Computation of LI-Characteristics

To compute the LI-characteristics (and the gain vs. current characteristic) we start with a carrier density n (Fig. 6.2). In a first iteration a value for the device dependent parameter w is assumed and the gain, g_m, photon population, S_m, and output powers, P_1 and P_2, calculated using eqs. (5.12) and (5.13), (6.22) and (6.18) to (6.20), respectively. In the next step the values of n, g_m and S_m provide the active region current, I_a, using (6.8). I_a is a non-measurable quantity. The measurable quantity is the terminal current, I, which can be

calculated considering current leakage (Section 6.3.4). Repeating the above procedure for a set of carrier densities leads to the calculated power vs. current (and gain vs. current) characteristic of the laser.

The relation between carrier density and current is highly non-linear since the carrier density saturates above threshold at the value of $n = n_{th}$. To be able to determine a suitable set of carrier-density values, for which we then calculate output power, gain and current-values, we estimate a value of the threshold carrier density, n_{th}, from (5.13) by assuming $g_p = \alpha_L$

$$n_{th} = (n_{tr} + \alpha_L/\Gamma \cdot A). \tag{6.27}$$

Equations (6.4) and (2.5) determine α_L for given facet reflectivities R_1 and R_2. To obtain a well spaced set of output power vs. current values for varying facet reflectivities we found it convenient to use the following set of 100 carrier density values,

$$n_i = (n_{th} - n_{tr}) \cdot \frac{2}{\pi} \tan^{-1} \frac{(i-1)^3 \cdot \Delta x^3}{10} + n_{tr} \tag{6.28}$$

where

$$\Delta x = .06\ (5 + \log R_2), \tag{6.29}$$

and $i = 1, 2, \ldots 100.$

Relation (6.28) is purely empirical. It ensures a close spacing between adjacent values of n_i as n_i approaches n_{th}. If computation time is not an issue the set of carrier densities can be increased in size to obtain any desired resolution in the resulting set of output power vs. current values.

The numerical values used in this study for the general parameters are listed in Table 6.1. The values of n_{tr}, a and b are taken from Table 6.1 in [59] and A, c and α_s are from [105]. Our value of $n_{sp} = 1.8$ is between the values 1.7 and 2 quoted in [59] and [111], respectively. L_{in} and d values are typical for the lasers used in our experiment [59] and the value for Γ is found from the thickness of the active layer ([112] and Fig. 2.5 of [59]). The value of W is obtained

Table 6.1: Values for general semiconductor laser parameters.

R_0	reflectivity of the uncoated facet	= 35%
n_{gr}	group index	= 4
v_{gr}	group velocity	= $0.75 \cdot 10^{10}$ cm/s
L_{in}	length of the active region	= 0.025 cm
d	height of the active region	= 0.2 μm
Γ	confinement factor for d = 0.2 μm	= 0.47
n_{tr}	transparency carrier-density	= $1 \cdot 10^{18}$ cm^{-3}
a	recombination coefficient	= $1 \cdot 10^{8}$ s^{-1}
b	recombination coefficient	= $1 \cdot 10^{-10}$ cm^3/s
c	recombination coefficient	= $4 \cdot 10^{-29}$ cm^6/s
q	electron charge	= $1.6 \cdot 10^{-19}$ As
A	gain coefficient (A=dg/dn)	= $2.3 \cdot 10^{-16}$ cm^2
n_{sp}	inversion parameter	= 1.8
α_s	material loss	= 20 cm^{-1}
λ_p	wavelength of peak-gain	≈ 1.3 μm
W	measure of the width of the gain spectrum	= 0.47 $\mu m^{3/2}$
$\Delta\lambda_{in}$	longitudinal mode spacing (= 150 GHz)	= 0.84 nm

Table 6.2: Values for device dependent parameters

Serial Number	Type	measured values					parameters determined in the calculations			
		η_{ext} mW/mA @3 mW	I_{t0} mA @20°C	I_{t2} mA @20°C	R_2	Ref.	η_0	I_0 mA	$1/I_n$ 1/mA	w μm
1. TY 224	FLD 130	.177	15.0	39	.05%	a	.60	2	1/300	1.7
2. TH 557	FLD 130	.183	11.7	22	2%	a	.62	-1	1/300	1.7
3. 6M3772	HLP5400	.175	28.6	56.0	.07%	b	.56	12.2	0	2.05
4. 6M3771	HLP5400	.165	35.4	59.6	.26%	b	.53	18.0	0	2.05
5. 5F3432	HLP5400	.160	32.5			c				

[a] this work
[b] Reference [113]
[c] Reference [113], device of [106]

by curve fitting (5.12) to the data presented by T.P. Lee [100] for a 1.3 μm laser. In our calculations we consider 50 modes (m = -50, -49, ...,0, ...50) on each side of the wavelength of peak gain (λ_p-λ_0).

Fig. 6.3 shows the LI-characteristics (P_2 vs I_a for varying R_2) for w = 1.7 μm (Section 6.3.5) calculated using the above method and the parameters in Table 6.1. The slope of the LI-curve initially increases for decreasing residual reflectivity due to increased output-coupling at the coated facet. The distinct knee in the LI-characteristic disappears when R_2 is small due to the increase in spontaneous emission at high carrier densities. For very low R_2 the power reflected at the coated facet (Fig. 6.1) is low compared to the spontaneous emission coupled into the mode in the vicinity of the coated facet and the device does not break into coherent oscillation as the current is increased [109]. Therefore, particularly for low output powers, the LI-curves with R_2 < .1% approach the characteristic of a superluminescent diode (traces g and h in Fig. 6.3). However, it should be noted that it is still possible to distinguish between devices with residual reflectivities as low as R_2 = .01% and R_2 = .035% by observing the LI-characteristics at high output powers P_2 (Fig. 6.3). The LI-curve with shallowest slope in Fig. 6.3 is calculated for a device with two AR-coated facets of residual reflectivity R_1 = .1% and R_2 = .05%.

6.3.2. Gain vs. Current Characteristics

The gain and current associated with each carrier density is determined during the calculation of the LI-curves (Fig. 6.2). Although the wavelength dependence of the gain is taken into account in the calculations, we will plot in the following only the value of peak gain, which occurs at the wavelength λ_p, (5.12) and (5.13). Fig. 6.4 shows a plot of the single-pass gain at wavelength λ_p vs. current characteristic $G_{ps}(n) = G_{ps}(I_a(n))$ for the same parameters as in Fig. 6.3, where

$$G_{ps} = \exp\{(g_p - \alpha_s)\cdot L_{in}\}. \qquad (6.30)$$

The strong gain-saturation above lasing threshold can be clearly seen for the uncoated device and for one-side AR-coated devices with

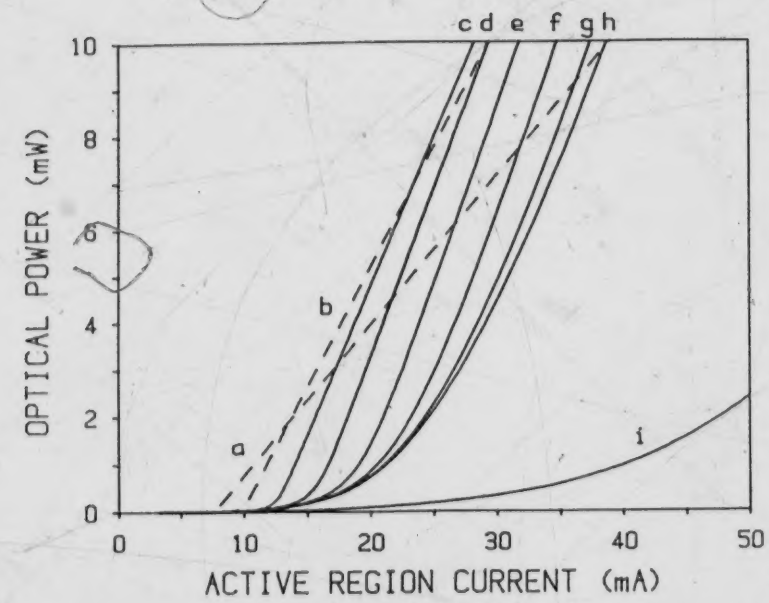

Fig. 6.3: Light versus active region current-characteristic for various facet reflectivities. Graphs a to h: one side AR-coated laser with respectively R_2 = 35%, 11%, 3.5%, 1.1%, .35%, .11%, .035%, 0.011% and R_1 = 35%. Graph i: both side AR-coated laser with R_1 = .1% and R_2 = .05%.

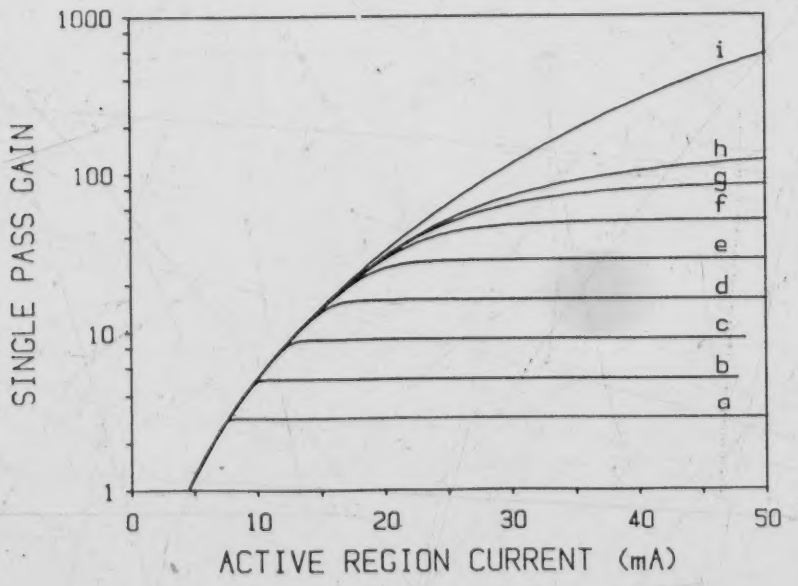

Fig. 6.4: Gain versus active region current-characteristic for various facet reflectivities. R_1 and R_2 have the same values as in Fig. 6.3.

relatively low quality AR-coatings. The gain saturates at a level where the peak-single pass gain is equal to the mirror loss

$$G_{ps,sat} = (R_1 \cdot R_2)^{-1/2}. \qquad (6.31)$$

We note from Fig. 6.4 that the gain vs current-curve of the one-side coated device extends over a large range of gain values for low values of R_2 (traces g and h) and follows closely, up to a single pass gain of approximately 40, the gain vs. current characteristic of the optical amplifier with two AR-coated facets (uppermost trace in Fig. 6.4). We conclude from this that the gain vs. current characteristic can be estimated for a particular amplifier if the LI-characteristic can be accurately modelled under conditions of low R_2.

6.3.3. Nominal Threshold Current

Although devices with one AR-coated facet of low residual reflectivity do not have a distinct knee in their LI-characteristic, we nevertheless introduce for discussion purposes a "nominal threshold current" that is based on a reference power level of P_r = 3 mW as shown in Fig. 6.5. Fig. 6.6 shows a plot of the residual reflectivity, R_2, of the coated facet vs. this nominal threshold current (solid line). We note from Fig. 6.6 that the increase in the nominal threshold current saturates with reducing R_2 for $R_2 < .1\%$.

From Figs. 6.3 and 6.5 it is apparent that the nominal threshold current is affected by the value chosen for the reference power level. If the reference power level is increased, the nominal threshold current increases when R_2 is small (the dashed line in Fig. 6.6 is calculated for P_r = 6 mW). To avoid saturation of the increase of the nominal threshold current with decrease in R_2 the reference power level should be chosen as high as possible. The LI-curves supplied to us by the laboratory which did the AR-coating of the HLP5400 devices, were for a maximum power level of 3.5 mW [113]. Therefore, we chose to use the value of P_r = 3 mW in this chapter.

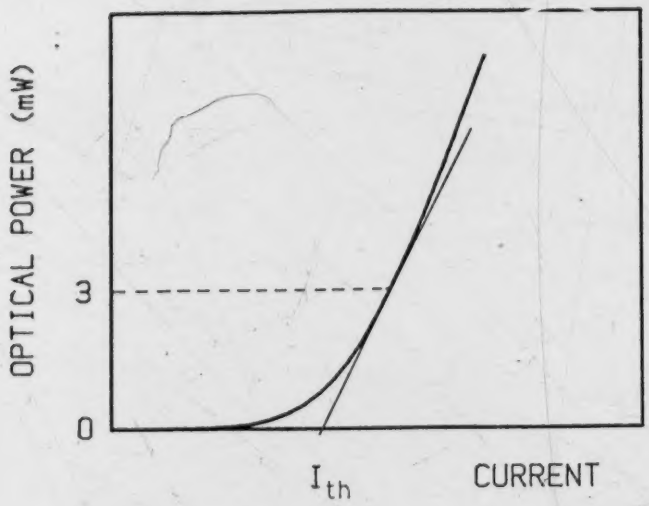

Fig. 6.5: Sketch of the tangent to the LI-curve that defines the *nominal* threshold current, I_{th}, for a laser with given facet reflectivities.

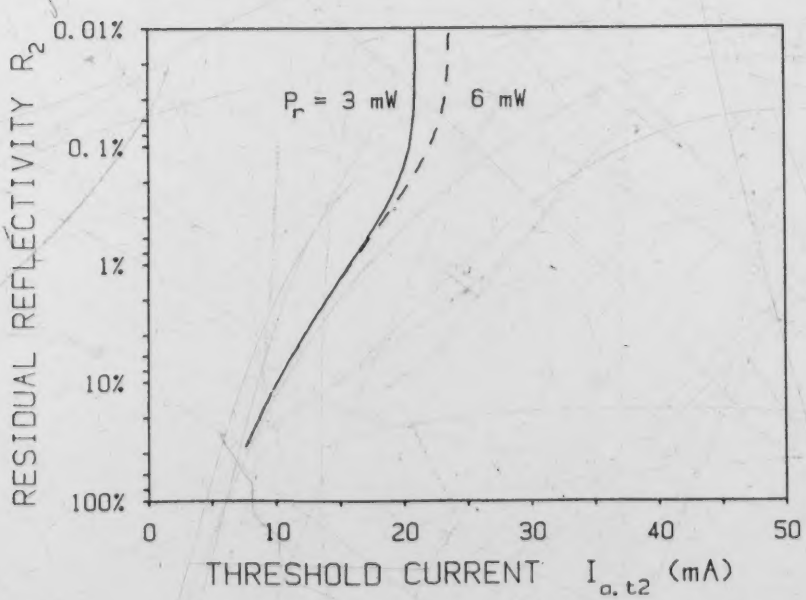

Fig. 6.6: Plot of the residual reflectivity vs. nominal threshold current for the active region of a one-side AR-coated laser.

6.3.4. Leakage Current

All output power and gain curves have so far been considered as functions of the current in the active region, I_a. These plots are altered to be functions of terminal current, I, by modelling of the leakage characteristics. Dutta et. al. [114] have considered the leakage characteristics of different types of laser. To keep the number of additional parameters to a minimum, we approximate their results with a simplified relation between terminal current and active region current:

$$I = I_a/\eta + I_0 \qquad \text{for } I_a>0 \tag{6.32}$$

where $$\eta = \eta_0 (1-I_a/I_n). \tag{6.33}$$

Here I_0 is the constant portion of the leakage current, η is the efficiency of current injection into the active region when $I > I_0$ and I_n is a curve-fitting parameter. Relations (6.32) and (6.33) are plotted in Fig. 6.7. Equation (6.33) reflects the decrease of η with increasing

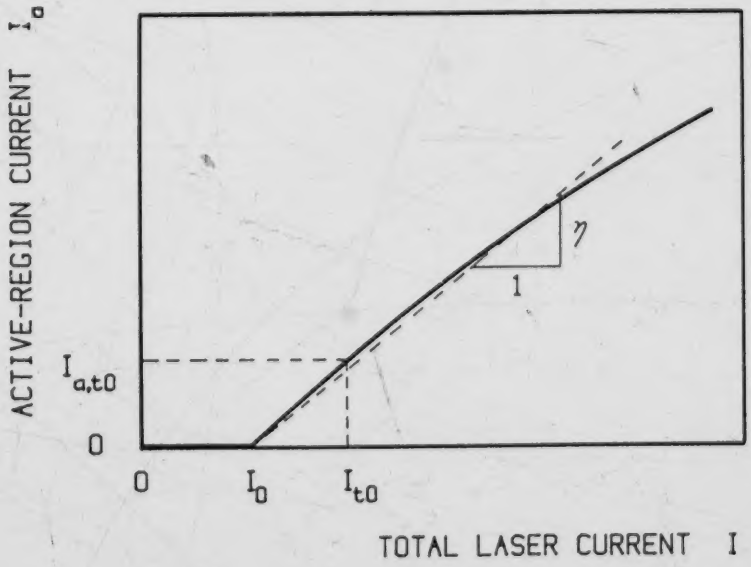

Fig. 6.7: Sketch of the relationship between active region current, I_a, and diode terminal current, I.

current, an effect that is particularly pronounced for V-groove laser-structures [114] like the FLD 130-laser diode used in our experiments.

The parameters I_0, η_0 and I_n are evaluated by comparing the measured LI-characteristics of the uncoated laser to the calculated LI-curve for the uncoated laser. We use the calculated LI_a-curve defined by (6.24), e.g. Fig. 6.3(a), and scale the current axis using (6.32) and (6.33) to obtain an LI-plot based on a first estimate of I_0, η_0 and I_n. An iterative procedure is then used in which η_0 and I_n are changed to obtain a close match between the slope of the calculated and measured LI-curves. I_0 is determined similarly by comparing the measured and calculated threshold currents.

Alternatively, if $(1/I_n) = 0$, for example for the EMBH-laser used, the parameters η_0 and I_0 can be calculated directly from the measured threshold current and the external quantum efficiency, η_{ext}, of the uncoated laser. For the *uncoated* laser strong gain-saturation is observed above the lasing threshold and low output power at threshold (Figs. 6.3 and 6.4). To calculate η_0 and I_0 we can therefore assume for the uncoated laser that (1) the peak gain at threshold is equal to the loss ($g_p \approx \alpha_{R0}+\alpha_s$, $\alpha_{R0} = -(1/L_{in})\cdot\ln(R_0)$), and (2) the stimulated emission is negligible ($S_m = 0$). Strong gain-saturation means that the carrier density, n, above threshold does not increase and is clamped at its threshold value $n_{t0} = n_{th}(R_1-R_2-R_0)$ (6.27). If n remains constant at n_{th}, the part of the active region current that supports the spontaneous recombination of carriers also remains constant at its threshold value, $I_{a,t0}$ (from (6.6) and (6.8) with $S_m=0$), where

$$I_{a,t0} = q\cdot V\cdot n_{t0}/\tau_e(n_{t0}). \tag{6.34}$$

Any additional current that is injected into the active region leads to an increase in output power. The ratio of the increase in output power to the increase in current above threshold (external quantum efficiency η_{ext}) can be used to estimate η_0

$$\eta_0 = 2\,\frac{q\lambda}{\hbar c}\cdot\frac{\alpha_{R0}+\alpha_s}{\alpha_{R0}}\cdot\eta_{ext}. \tag{6.35}$$

The factor $\alpha_{R0}/(\alpha_{R0}+\alpha_s)$ accounts for the decrease in the external quantum efficiency with respect to η_0 due to scattering and absorption of photons within the cavity [59]. The factor $\hbar c/q\lambda$ (=.95 mW/mA at 1.3 μm wavelength) represents the ratio of energy per photon to charge per carrier. The external quantum efficiency is measured per facet, hence the factor 2 in (6.35). Finally, inserting the current values at threshold into (6.32) we obtain an expression for the constant part of the leakage current

$$I_0 = I_{t0} - I_{a,t0}/\eta_0 . \tag{6.36}$$

6.3.5. Width of the active region

We will now consider the method for determining the numerical value for w. The effect of w on I_a and thus on the power and gain vs. current characteristics can be seen from equation (6.34) in which the volume $V = w \cdot d \cdot L_{in}$ is a proportionality constant between the active region current and the total rate of spontaneous recombination, n/τ_e, at a given carrier density. The carrier density itself is a linear function of the peak gain (5.13). The length of the active region determines the longitudinal mode-spacing and the thickness of the active layer the confinement factor. This leaves the width of the active region as the only independent variable contributing to the volume of the active region. In the calculations the value of w is therefore used to adjust the amount of threshold current increase that is obtained for a given change in the facet-reflectivity. The measured change in the LI-curves due to coating and a knowledge of the residual reflectivity of the AR-coated facet lead to a unique value of w during the curve-fitting procedure. The resulting value for w can be viewed as a scaling factor for the current axis in the gain vs. current curve.

Because w is obtained from curve-fitting it is not necessarily exactly equal to the geometrical width of the active region. Thus w should be considered as an effective width of the active region. However, the values we obtain are in reasonable agreement with geometrical width values that are quoted in the literature [59] for the

types of lasers used in our experiments (V-groove and EMBH-laser). Also, reassuringly, several samples of lasers of identical type yielded the same value of w.

6.4. SPECIFIC DEVICE MODELLING

6.4.1. Comparison of Calculated and Measured LI-Characteristics

In this section we compare the calculated and measured LI-characteristic of devices before and after AR-coating. The measured values of η_{ext} listed in Table 6.2 are obtained from the original LI-curves of the uncoated lasers, provided by the manufacturer of the individual devices. The values of I_{t0}, I_{t2} (nominal threshold current of the one-side coated laser) and R_2 were determined from the measured LI-curves before and after AR-coating of the first facet and from the ASE-spectrum of the one-side coated laser [96]. The LI-and ASE-measurements for the V-groove lasers FLD 130 were done as part of this work, measurements for the EMBH laser HLP 5400 were provided by [113].

The calculated results shown in Fig. 6.8(a) apply to the device TY 224. They are obtained from the calculated power vs. active-region current characteristics (Fig. 6.3) by scaling the current axis to account for the current leakage (η_0 = .6, I_0 = 2 mA and I_n = 300 mA). Fig. 6.8(a) shows (i) the power vs. current curves before coating, (ii) the power from the coated facet, after single-facet coating and (iii) the power from the uncoated facet. The measured values are indicated by crosses and the calculated characteristics by solid lines.

The solid line (ii) in Fig. 6.8(a) is calculated using the measured value of R_2 = .05% and the dashed line using R_2 = .06%. The slightly higher value for R_2 leads to a better curve-fit. The value of R_2 = .05% is calculated from the measured ASE-spectrum using the improved technique of Westbrook [97] to account for the effect of the limited resolution of the monochromator (.3 nm in our case) on the measurement and to avoid as a result underestimation of R_2. We assume that the remaining uncertainty in the experimental value of R_2 explains the better curve-fit for the higher value of R_2.

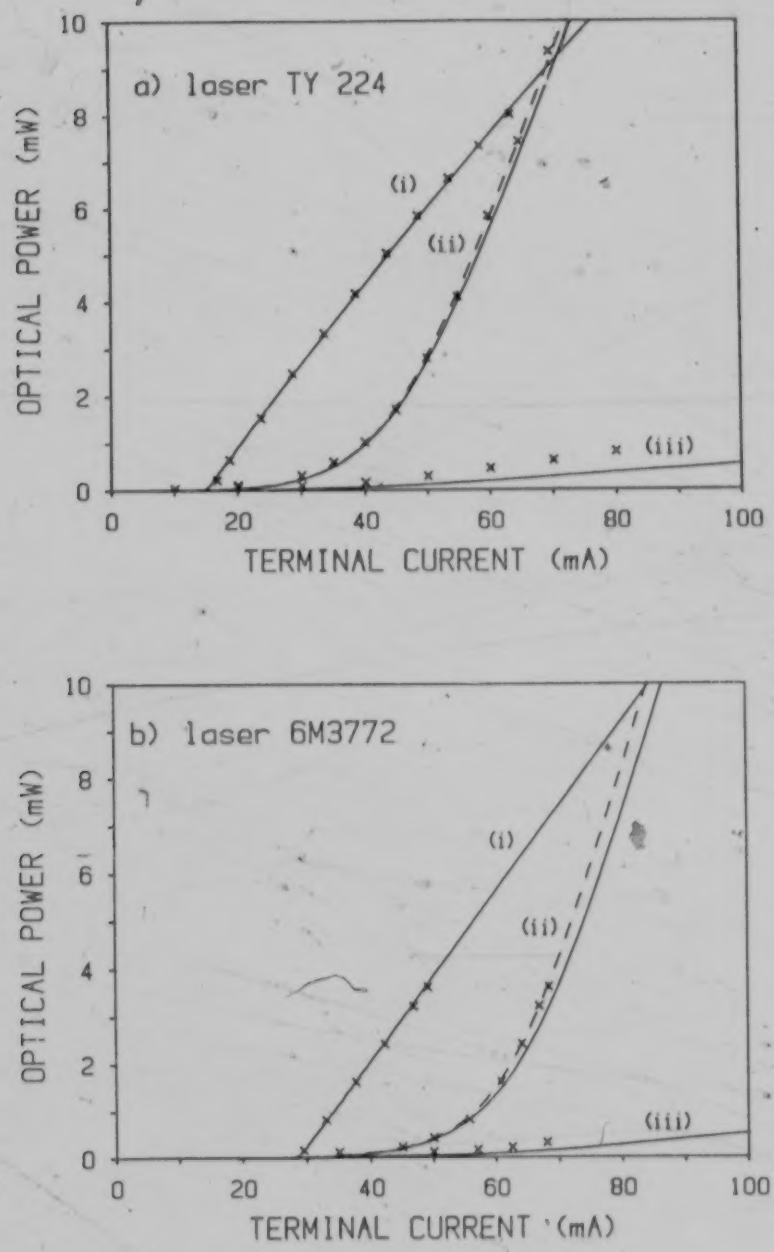

Fig. 6.8: Comparison of the calculated LI-characteristics (solid and dashed lines) with measured values (crosses) for individual lasers. The graphs show the characteristics of (i) the uncoated laser, (ii) the power emitted from the coated facet of the one-side coated device and (iii) the power from the uncoated facet.

In Fig. 6.8(b) the LI-curves before and after coating of one facet (residual reflectivity of R_2 = .07%) are plotted as solid lines for device 6M3772. The curve fit for the LI-curve of the uncoated laser was obtained using η = .56, I_0 = 12.2 mA, and $(1/I_n)$ = 0. Curve-fitting to the LI-curve of the one-side coated laser leads to w = 2.05 μm. All other parameters are the same as for laser TY 224. The dashed line represents the calculated LI-curve for the one-side coated device for the power emitted from the coated facet, when R_2 = .1%. As in the previous case, better agreement between the measured [113] and calculated LI-curve for the coated device is obtained, if a residual reflectivity is used in the calculations that is slightly higher than the measured one.

We find that the calculated and measured LI-characteristic for the power from the coated facet of the one-side coated device can be brought into agreement over the range of output powers indicated in Fig. 6.8 if about 100 longitudinal modes are considered in the calculations and the axial dependence of the photon density in the active region is taken into account.

The power P_1 emitted from the uncoated facet is underestimated in our simulations (trace (iii) in Fig. 6.8). We attribute this discrepancy to the fact that our simulation does not account for spatial gain-saturation [109],[110] due to carrier-depletion by the large light intensity travelling towards the coated facet (see Fig. 6.1). Reduced gain in the portion of the active region that is close to the coated facet leads initially to a reduction of the output power P_2. However, the reduced stimulated emission leads to an oversupply of carriers, which in turn increases the carrier density, the gain, and finally the output power. This feedback mechanism leads to an almost fixed total output power for a given current, if the amount of current necessary to support the increase in spontaneous emission due to increased carrier density is negligible compared to the current that supports the stimulated emission. However, this process does change the ratio of output powers in favour of the output from the uncoated rear facet, since the addition of an increased amount of spontaneous emission per unit length of travel to the <u>low</u> amplitude wave originating from the coated facet leads to a higher effective gain per unit length for this

wave than for the high amplitude wave originating from the uncoated laser facet.

Equation (17) which expresses the change of the average light intensity $F_m(z)$ as a sum of the contributions due to stimulated emission ($g_m \cdot F_m$), loss ($\alpha_s \cdot F_m$) and spontaneous emission (R_{sp}), shows that the relative contribution of the stimulated emission to the increase of $F_m(z)$ will be larger for a low $F_m(z)$.

As long as the output power from one facet is large compared to the output power from the other facet, the change in the ratio of the output powers due to spatial gain-saturation does not significantly affect the larger of the two output powers, in this case the power P_2 emitted from the coated facet. We consider this to be the reason for the good agreement between the calculated LI-curves and those measured at the coated facet when R_2 is low. In contrast, for facet reflectivity above approximately 1% (i.e. with significant optical output power from the uncoated facet) the slopes of the calculated LI-curves above threshold are over-estimated for the coated facet and under-estimated for the uncoated facet compared to measured LI-curves. However the threshold currents determined from the calculated LI-curves are nevertheless consistent with the measured values, since spatial gain-saturation is not present at the low output powers that prevail at current levels close to the threshold current.

A curve fit on the LI-curve of the AR-coated laser is done to estimate the parameter w. This parameter was found in Section 6.3.5 to affect the amount of threshold current increase that is obtained for a given change in facet reflectivity. According to Section 6.3.5, it would suffice to estimate w from the amount of threshold current increase that is obtained for a given change in facet reflectivity. However, because a well-defined threshold current does not exist for very low facet reflectivities, we had to model the LI-curve of the AR-coated laser for a range of output power values and obtain from the calculated LI-curve a value for the nominal threshold current, as defined in Section 6.3.3. At the same time, modelling of a complete LI-curve is a more stringent test for the model used in the calculations, and this procedure assisted us in the selection of general laser parameters. For one-side coated lasers, with a residual reflectivity of

the coated facet above approximately 1%, a well defined knee in the LI-characteristic is present. In this case, the tangent on the LI-curve above threshold provides a single value of the threshold current independent of the slope of the LI-curve. The fact that the slopes of the LI-curves of these lasers are not predicted correctly with our model does not, therefore, affect our estimate of w. In conclusion, we expect our model to be sufficiently accurate to allow us to determine the correct resonator loss versus threshold current and gain versus current characteristics.

6.4.2. Deduced Gain vs. Current Characteristic

Figures 6.9(a) and (b) show the calculated peak-gain vs. current characteristic for (i) the uncoated, (ii) the one-side coated and (iii) the both-side coated devices of Figures 6.8(a) and (b). For the both-side coated amplifier we assume in Fig. 6.9(a) and (b) residual reflectivities of R_1=.1% and R_2=.05%. The calculated gain vs. current characteristic of the 6M3772 amplifier (trace (iii) of Fig. 6.9(b)) is compared with measured values (dots in Fig. 6.9(b)) obtained by Enning et.al. [106] for a travelling wave amplifier made from the same type of laser (device 5F3432 of Table 6.2). The threshold currents of the two uncoated devices are I_{t0} = 28.6 mA and 32.5 mA [113], respectively. Both amplifiers reach a single pass gain of $G_{ps}=(1/R_0)$= 2.8 at their respective I_{t0}, i.e. with an offset of 3.9 mA. Apart from this offset, the measured data for the device of [106] and the calculated gain vs. current characteristic for the 6M3772 device agree well over a wide range of currents as is evident in Fig. 6.9(b).

6.4.3. Difference Between Individual Devices

The difference between devices of the same type is represented in our model by different leakage characteristics. We note from Table 6.2 that η_{ext} does not vary significantly between different uncoated lasers, in contrast to the threshold current I_{t0}. Thus, the constant part of the leakage current, I_0, is the only parameter that changes significantly between lasers. This parameter basically provides a current offset for the power and gain vs. current characteristics for different

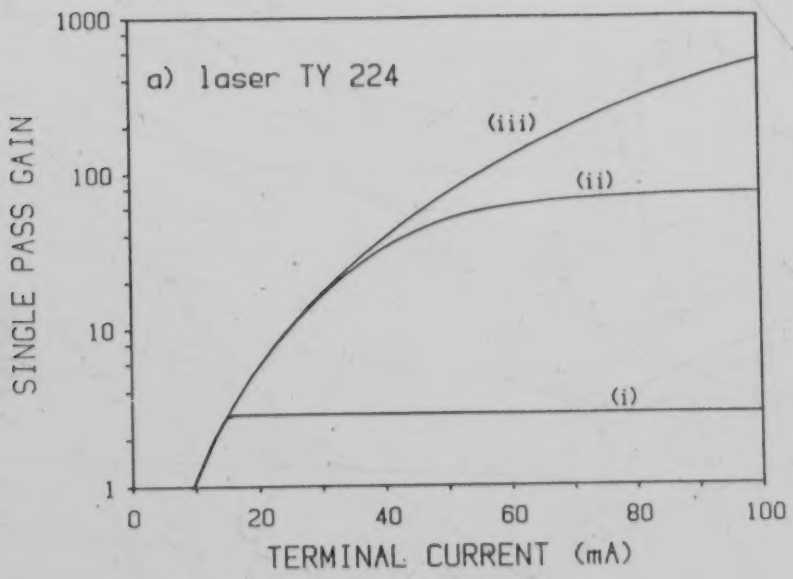

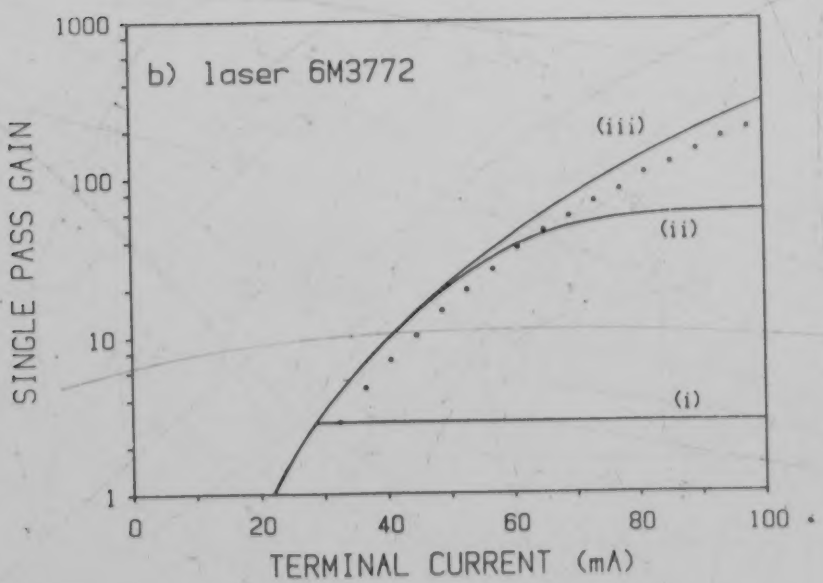

Fig. 6.9: Calculated peak single-pass gain vs. current characteristic for the two lasers of Fig. 6.8. The graphs show the characteristics of (i) the uncoated device, (ii) the one-side AR-coated device and (iii) the both side AR-coated device. Measured values [106] for a device of the same type (HLP5400) as the one used in Fig. 6.9(b) are indicated by dots.

devices of the same structure, those having constant value for w. The current offset is equal to the difference in I_{t0} of the individual devices (e.g. Fig. 6.9(b). If we eliminate the different offsets by plotting power and gain vs. $I-I_{t0}$, the characteristics of lasers of the same type are predicted in our model to be identical apart from the small difference in the slope of the characteristics that is caused by the variation of η_{ext} between different devices.

6.4.4. Change of the Nominal Threshold Current

We now return to the problem of determining the amount of optical feedback from the change of the threshold current of the laser. After the specific device parameters have been determined through curve-fitting, our model can be used to calculate the LI-characteristic of this particular device for different facet reflectivities R_x and the nominal threshold currents, I_{tx}, can then be determined (Fig. 6.5). The graph of the R_x vs. $I_{tx}-I_{t0}$ characteristic given in Fig. 6.10 is for (a) laser TY 224 with η_0, I_0. I_n and w values given in Table 6.2 and (b) laser 6M3772. The measured operating points for these two lasers, marked by the rectangles R1 and R3 respectively, have to lie on the R_x vs. $I_{tx}-I_{t0}$ curve because they were used to determine w. The fact that R3 does not lie exactly on this curve can be attributed to the limited accuracy of the curve fit and uncertainty in the measured value of the residual reflectivity of the coated facet, as discussed in Section 6.4.1 in conjunction with the solid lines (ii) in Fig. 6.8(a) and (b).

Measured operating points for a second set of devices (rectangles R2 and R4 for devices TH 557 and 6M3771 respectively) are plotted in Fig. 6.10 and are very close to the curve of residual reflectivity vs. threshold current characteristic derived from the first set of lasers (TY 224 and 6M3772). Thus, in our experiments, the characteristics of devices of the same type become comparable if they are plotted using a $(I-I_{t0})$-axis (Sect. 6.4.3). We suggest, based on the good agreement between the operating points of the second set of devices with the previously calculated R_x vs. $(I_{tx}-I_{t0})$-characteristic, that this characteristic can be used to estimate the residual reflectivity after coating of a second device, if the second device is sufficiently similar

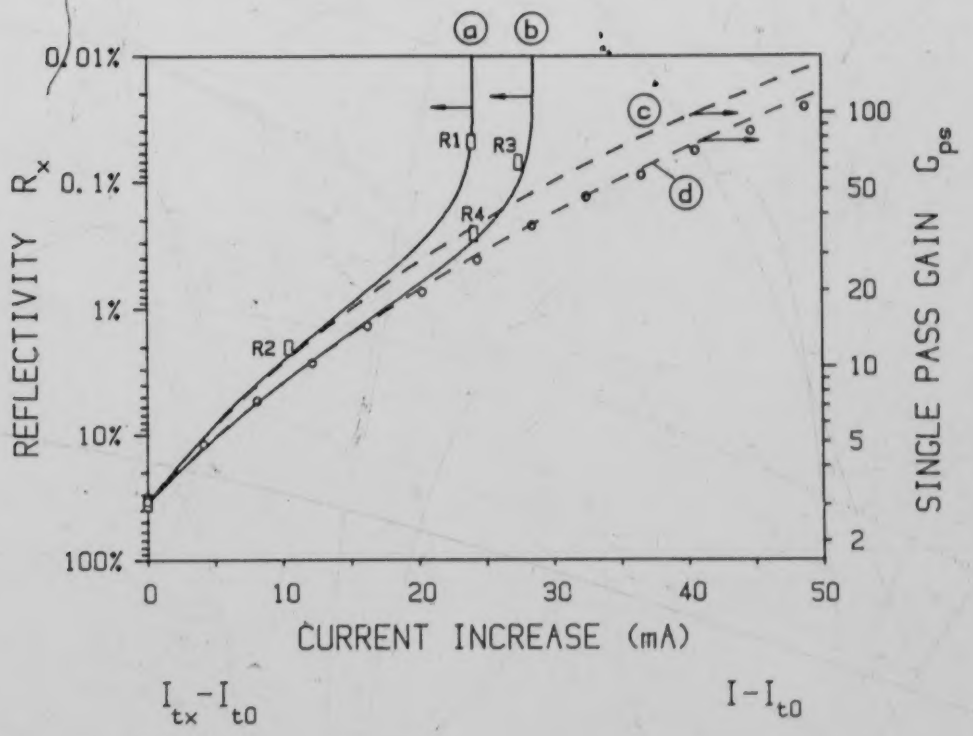

Fig. 6.10: Plot of the reflectivity R_x vs. increase in the nominal threshold current $I_{tx}-I_{t0}$ for the one-side AR-coated devices (a) TY 224 and (b) 6M3772. Also, plot of the single pass gain G_{ps} vs. current increase with respect to the threshold current of the uncoated laser, $I-I_{t0}$, for the same two devices ((c) TY 224 and (d) 6M3772)). The rectangles indicate the measured values of (R_2, I_{t2}) for the lasers of table II, the circles indicate the measured values of (G_{ps}, I) obtained in [106] for the device 5F3432.

(of the same type (w=const.)) to the device used initially to obtain the R_x vs. $(I_{tx}-I_{t0})$ curve.

We will now use the R_x vs. $(I_{tx}-I_{t0})$ characteristic to estimate, from the change in threshold current, the amount of optical feedback applied to the coated facet of a laser for example in the external grating configuration of Fig. 5.2. From the measured threshold current I_{tx} with optical feedback we determine a value for R_x using the R_x vs. $(I_{t0}-I_{t0})$ characteristic of Fig. 6.10. In the case of frequency selective optical feedback, if we ensure that in-phase feedback is

provided (Section 5.4.1) and the wavelength of the returned light coincides with the gain maximum (Section 5.4.2), which corresponds in Fig. 5.15 to oscillation at P4, the value we obtain for R_x is equal to $R_e(\omega)_{max}$ of (5.9) and the level of optical feedback is, from (5.9)

$$R_{ex} = \left(\frac{\sqrt{R_x} - \sqrt{R_2}}{1 - \sqrt{R_x R_2}} \right)^2 . \qquad (6.37)$$

The conditions in the preceding paragraph for optical feedback are easily met experimentally, by changing the wavelength of optical feedback to determine the lowest observable threshold current, I_{tx}. In the case of Fig. 5.9, I_{tx} = 16.6 mA. If we provide feedback that is not wavelength selective, $\alpha_G(\lambda)$ in Fig. 5.15 is replaced by a straight line through P2 and P4, and the laser oscillates automatically under the condition that provides the minimum threshold gain and (6.37) applies.

It has been suggested by [107] that the strength of optical feedback can be estimated from the change of threshold current, assuming proportionality between the threshold current and the resonator loss. Therefore, [107],

$$\frac{I_{tx}}{I_{t0}} = \frac{\alpha_{mat} - (1/2L_{in}) \cdot \ln(R_0 R_x)}{\alpha_{mat} - (1/2L_{in}) \cdot \ln (R_0 R_0)} . \qquad (6.38)$$

where it is assumed in [107] that α_{mat} is equal to the scattering loss, α_s, in the laser. (6.38) leads to a straight line through point R0 in Fig. 6.11. The slope depends on the values of I_{t0} and α_{mat}. If we choose α_{mat} = 30 cm^{-1} for laser TY 224 (I_{t0} = 15 mA) and α_{mat} = 15 cm^{-1} for laser TH 557 (I_{t0} = 11.7 mA), respectively, we obtain the solid line in Fig. 5.11. In the range of R_x = .3% to 35% this solid line is a good approximation for the R_x vs. I_{tx} characteristic, the dotted line in Fig. 6.11 which was calculated from our detailed model for these two V-groove lasers. This dotted line is identical to curve (a) in Fig. 6.10. Therefore, if we use α_{mat} in (6.38) as a curve-fitting constant, we can replace the complicated analysis of the last few pages with the much simpler relation (6.38). It is interesting to note that [18] obtains α_{mat} = 60 cm^{-1} from a fit of the tuning characteristic of an external

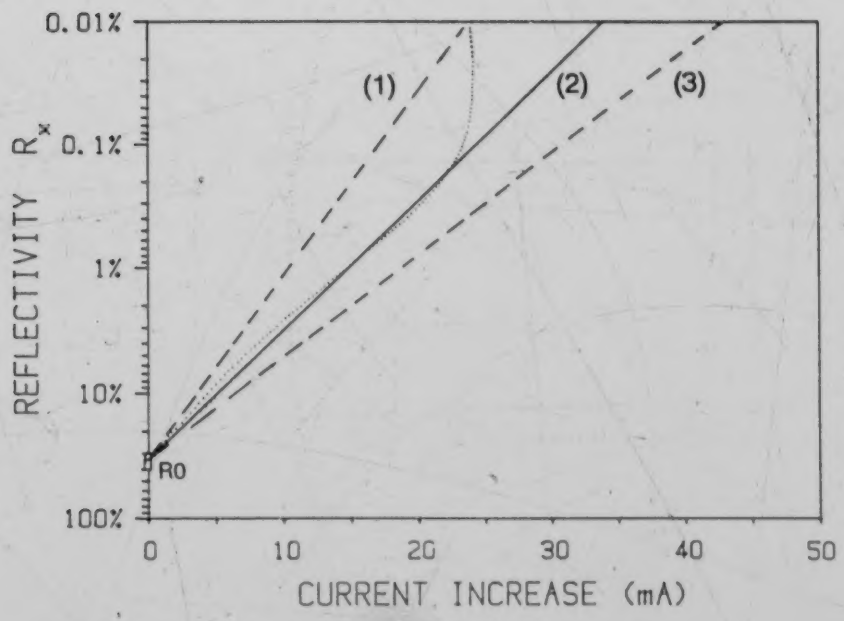

Fig. 6.11: Plot of the reflectivity R_x vs. increase in the nominal threshold current I_{tx}-I_{t0} for one-side AR-coated devices. The dotted line is identical to curve (a) in Fig. 6.10. (1) to (3) are calculated from (6.38), using I_{t0} = 15 mA and (1) α_{mat} = 60 cm^{-1}, (2) α_{mat} = 30 cm^{-1} and (3) α_{mat} = 15 cm^{-1}. Other pairs of parameter values can be found that lead to the same graphs. For instance, the values I_{t0} = 11.7 mA and α_{mat} = 15 cm^{-1} or I_{t0} = 21 mA and α_{mat} = 60 cm^{-1} produce a graph that is identical to the solid line.

grating laser to a relation similar to (6.38). α_{mat} = 60 cm^{-1} is definitely larger than the typical value for α_s of ~ 20 cm^{-1} [22]. The feedback levels and the value of R_2 in the experiments of [18] indicate that the value of I_{t0} was ~ 20 mA in those experiments. However, α_{mat} = 60 cm^{-1} and I_{t0} = 21 mA used in (6.38) lead also to the solid line in Fig. 6.11 and provides therefore a good approximation of the dependence of threshold current on resonator loss for the particular laser used in the experiments of [18]. We conclude that α_{mat}, as it appears in (6.38), should be treated as a curve-fitting constant to obtain

reasonable agreement of (6.38) with the observed dependence of the threshold current on the resonator loss. In a physical sense, α_{mat} is not strictly equal to α_s. The strong dependence of (6.38) on α_{mat} precludes a reliable estimate of the reflectivity based on the threshold current change and (6.38), unless a method is devised to determine α_{mat} for the particular laser used in the experiment. Only for threshold currents of the solitary laser in the range of I_{t0} = 11 to 15 mA, the value of α_{mat} that leads to reasonable estimates of the reflectivity, is found to be comparable to the value of α_s (Fig. 6.11, trace (2)).

A comparison of the reflectivity vs. threshold-current characteristic with the calculated gain vs. current characteristic (the dashed lines (c) and (d) in Fig. 6.10 correspond to graph (iii) in Fig. 6.9(a) and (b), respectively) indicates that the assumption of gain = loss at the nominal threshold current I_{t2}

$$G_{ps}(I_{t2}) = (R_0 \cdot R_x)^{-1/2} \tag{6.39}$$

is accurate for $R_x > 1\%$. In (6.39), $G_{ps}(I_{t2})$ is the single pass gain at λ_p when the optical amplifier is operated at the current I_{t2}. The measured single pass gain vs. current shown in Fig. 6.9(b) is indicated by circles in Fig. 6.10. The measured and calculated values for this gain versus $(I - I_{t0})$-characteristic agree well. This was anticipated in Sect. 6.4.3.

6.5. CONCLUSION

A new method to calculate the gain vs. current characteristic of an individual laser amplifier has been presented. The method applies to travelling wave amplifiers that are derived from semiconductor lasers by AR-coating both facets. It relies on a knowledge of certain general parameters, the LI-characteristics of the laser before and after the first coating has been applied and a measurement of the residual reflectivity of the first coating. These measurements are normally done during the coating process and therefore require no additional experimental effort.

The gain vs. current characteristic is different for each specific laser amplifier. Therefore one of the main objectives in this work was to determine which parameters account for this difference. We found that it was necessary to determine the leakage characteristics of each laser separately. A relatively simple relationship between terminal current and active region current, containing three independent parameters, proved to be sufficient. All three parameters can be determined from the LI-characteristic of the uncoated laser. A fourth parameter, the effective width of the active region, is derived from the observed change of the LI-characteristic due to coating and a knowledge of the residual reflectivity. We found that these four parameters, along with a set of fixed general parameters, were sufficient to provide good agreement between calculated and measured results for different lasers.

It was observed that both the power and gain vs. current characteristics of different devices of the same structure become comparable if plotted against $I-I_{t0}$, where I_{t0} is the threshold current of the uncoated device. The reflectivity R_x was plotted for a specific laser against the change in threshold-current $I_{tx}-I_{t0}$ and it is proposed that this dependency can be used to estimate the strength of optical feedback for this and any other laser of the same type. Compared to other methods that rely on estimating the optical feedback from the change of the threshold current [107], the proposed technique is expected to be more accurate since it makes use of experimental data (operating points) on the R_x vs. $(I_{tx}-I_{t0})$ characteristic of the specific laser used in the feedback arrangement. Reassuringly, the values of optical feedback determined with the proposed method lead to good agreement between the calculated and the measured tuning characteristics of an external grating laser (Chapter 5).

7. RING LASER

7.1. INTRODUCTION

The unidirectional fiber ring arrangement, used for our experiments with weak optical feedback in Chapter 4 and shown in Fig. 4.1(a), has to our knowledge not yet been reported in the literature. We found in Section 4.3 that the behavior of the laser in this arrangement for weak feedback is the same as for an arrangement with reflective feedback, essentially because the Fabry-Perot cavity of the semiconductor is the dominant cavity for weak feedback. Nevertheless, the ring feedback arrangement has certain experimentally attractive features as described in Chapter 4. When strong optical feedback is applied in a ring arrangement, the ring cavity dominates over the semiconductor cavity and the resonance condition is satisfied not only by a standing wave but also by a travelling wave.

The discussion in the literature as to whether or not the standing wave pattern in the solitary laser cavity has a significant effect on the laser behavior, has not come to a satisfactory conclusion (see for instance [115]). Of particular interest regarding the spectral behavior of the semiconductor laser is whether the standing wave pattern induces spectral holeburning due to a spatial modulation of the gain in the semiconductor cavity. Spectral holeburning in turn, would reduce the stability of single-mode oscillation of the laser. Therefore, a laser that relies on travelling waves as opposed to standing waves is likely to have improved single mode stability. The ring feedback arrangement with optical isolator described in this chapter, is an arrangement that supports only travelling waves.

Resonance in a fiber ring cavity that includes a semiconductor laser as the gain medium as shown in Fig. 7.1 requires that the gain of the semiconductor compensates the fiber to laser coupling-losses on both sides of the laser and the loss provided by coupling part of the light out of the fiber ring. At this level of gain, which is expected to be between 50 and 100, the semiconductor cavity itself has to be well below

(a)

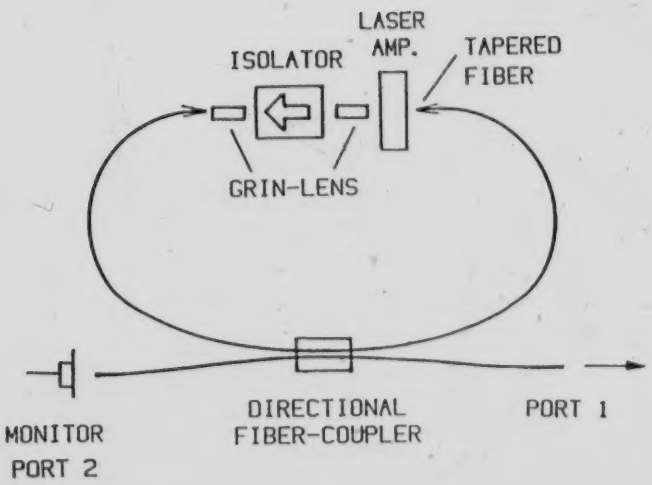

(b)

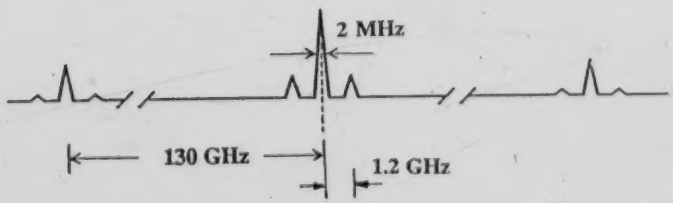

Fig. 7.1: Sketch of (a) the semiconductor-fiber ring laser and (b) its spectral characteristics.

lasing threshold. We therefore require high quality AR-coatings on both facets of the laser. These coatings convert the semiconductor laser to a semiconductor travelling wave amplifier (TWA). During the last three years, three research groups [116]-[118] have published experimental results on the behavior of a travelling wave amplifier in a bidirectional fiber ring. Fiber ring lengths of 1 to 3 meters were used by all three authors, which resulted in a close spacing of the longitudinal modes. Wang et. al. [117] observed accordingly, oscillation of their fiber ring laser in a large number of longitudinal modes. However, single-mode operation at 1.55 μm was observed by [116], employing polarization preserving fiber, and by [118] at 870 nm, employing a multiple quantum well (MQW)-laser. The requisite frequency selectivity was provided by birefringence in the polarization preserving fiber [116] and by the narrow gain profile of the MQW-laser used by [118].

A ring resonator has to be unidirectional if standing waves are to be suppressed. We achieved unidirectionality in our experiment by inserting an optical isolator in the ring. In the following we compare the properties of a semiconductor fiber ring laser that contains an optical isolator, to the properties of the same ring laser without optical isolator. Our investigations are limited to a description of experimental results, which are the LI-curves and the spectral properties of the ring laser, observed with a monochromator, Fabry-Perot interferometer and a self-heterodyne setup, Fig. A.1, to obtain various degrees of resolution.

7.2. LI-CHARACTERISTICS

The semiconductor TWA used in the following experiments was device # 6M3772 of Table 6.2, with R_2 = .07%, determined from the ASE spectrum of the one-side coated laser. Using (13) and (16) of [98], a value of $(R_1R_2)^{1/2}$ ~ .1% can be determined from the measured gain, G ~ 23 dB, and amplifier passband ripple, 3 dB, at this value of gain of the two side-coated laser. The experimental data on the device was provided by [113].

The fiber ring consisted of the 1.3 μm single-mode fiber-pigtails of a fused fiber coupler. The circumference of the fiber ring was 17 cm,

including the optical-isolator assembly shown in Fig. 7.1. The laser to fiber coupling efficiency was ~ 20% at the front and at the rear facet of the laser amplifier. 50% of the light was coupled out of the fiber ring by the fiber coupler. Since we did not use polarization preserving fibers in the fiber ring, additional loss of ~ 40% is encountered due to the polarization mismatch of the light after one roundtrip. The bending loss was measured to be ~ 20%. The above values lead to a total expected loss of light in the fiber ring by a factor of ~ 100. An increase of the laser to fiber coupling efficiency from 20% to 25% reduces this loss factor from 100 to 65.

From the threshold current of 63 mA (Fig. 7.2) of the ring laser with optical isolator, the threshold current of the uncoated laser of 28.8 mA, and Fig. 6.10, we estimate the single pass gain of the ring laser at the threshold current to be $G_{ps} \approx 52$. Since oscillation takes place at the frequencies where the resonance of the semiconductor cavity and the ring cavity are in phase, (6.37) applies and we obtain, using $R_x = 1/52$ and $R_2 = .1\%$, an equivalent external reflectivity of $R_{ex} = 1.2\%$ which leads to a loss factor in the fiber ring of ~ 83. This is a reasonable value, considering the loss budget discussed in the preceding paragraph.

Traces (1) and (2) in Fig. 7.2(a), recorded at port #1 and #2 (Fig. 7.1(a)) respectively, show clearly that the laser emits light above threshold predominantly towards the output port #1. Traces (1) and (2) were recorded simultaneously as also were traces (3) and (4). Traces (2) and (4) show little change in power in port #2 due to the presence or absence of stimulated emission of radiation towards port #1. We conclude that our attempt to build a unidirectional ring laser was successful.

The power coupled out of the fiber ring and travelling in the single-mode fiber toward port #1 is high. At 5 mA above lasing threshold we observe an output power of 400 μW from port #1 when the isolator is in the ring. This output power corresponds to an estimated optical power passing through the left facet of the TWA of ~ 4mW (3 dB coupler loss, 20% laser to fiber coupling efficiency) and to an external quantum efficiency of 0.080 mW/mA including coupling losses. This value compares favorably with the external quantum efficiency of 0.175 mW/mA

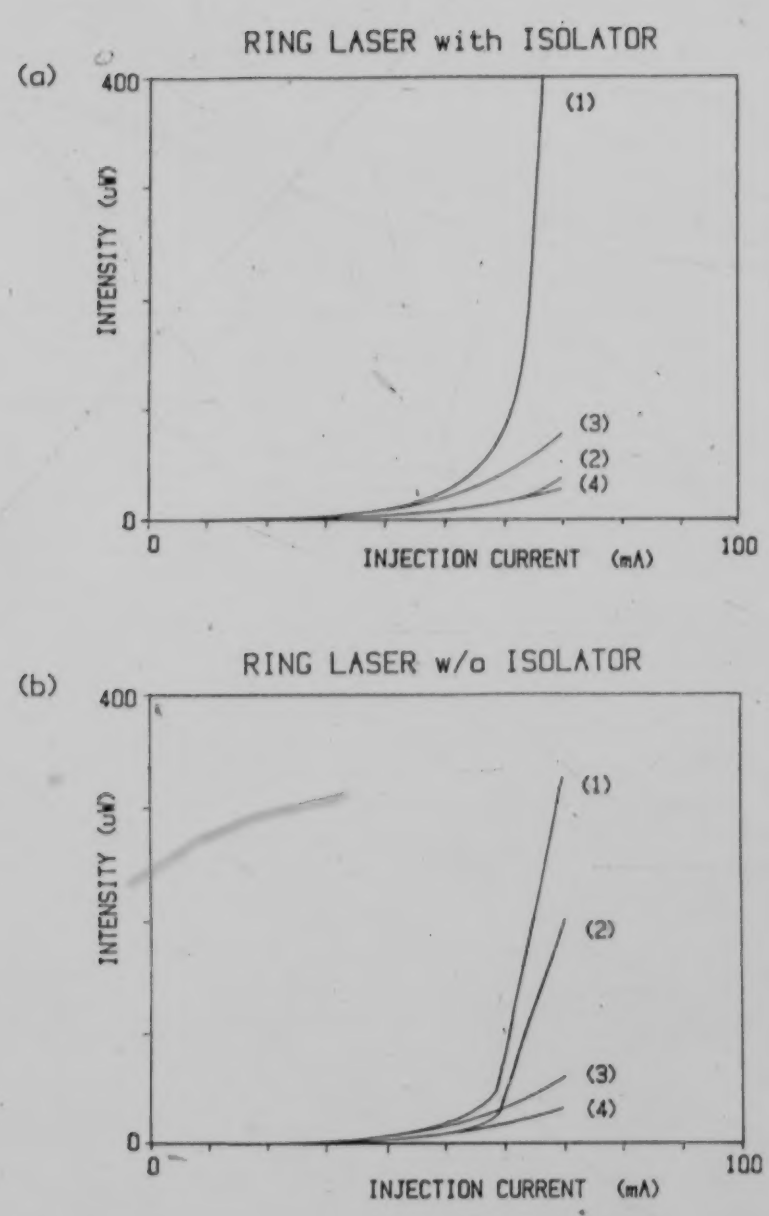

Fig. 7.2: Light versus current (LI-) curve of the ring laser with an optical amplifier (# 6M3772) in the fiber ring. (a) with an optical isolator as part of the ring and (b) without isolator. The length of the ring is 17 cm. The 4 traces in each graph are: (1): output of port 1, (2) output of port 2. The traces (3) and (4) correspond to the output of port 1 and 2, respectively, when the ring feedback is interrupted by misalignment of the right (3) or left (4) tapered fiber (see Fig. 7.1).

for the uncoated solitary laser without coupling losses. The slope of the LI-curve of the power from port #1 of the unidirectional ring laser is approximately equal to the sum of the slopes of LI-curves from port #1 and #2 of the bidirectional ring laser. The unidirectional ring laser allows us therefore to collect the power normally emitted in a Fabry-Perot laser in two directions, and to realize this power in only one direction. An increase of the output power at port #1 above the value of 400 μW is possible, but we were not certain about the laser to fiber coupling efficiency and therefore about the power travelling in the laser. The fear of destroying the laser amplifier prevented us from experimenting at higher injection currents. However, according to Thompson ([22], p.273), the absence of standing waves at the facets, which is ensured in the unidirectional ring laser, leads to a three times increased damage threshold for the laser facets. We would therefore expect that the amplifier output can be increased in our configuration until about 2 mW of optical power is detected in the fiber at output port #1, without affecting the facets of the TWA.

7.3. SPECTRAL CHARACTERISTICS

The spectral characteristics of the fiber-ring laser were examined with the experimental arrangement shown in Fig. A.1. The monochromator provided the absolute values of wavelength with a resolution of 0.3 nm. With and without the optical isolator, the ring laser oscillates in two to three longitudinal modes of the semiconductor cavity, Fig. 7.3, separated by 0.73 nm or 130 GHz. The presence of the spectral components, labelled "-1" and "+1" in the beat spectrum observed with the self-heterodyne setup, Fig. 7.4 and 7.5, indicates that the ring laser also oscillates in several ring cavity modes. The external cavity modes are separated by 1.2 GHz from the center mode in the beat spectrum (the center mode is at 80 MHz (Appendix A and B)). The value of 1.2 GHz agrees with the separation of longitudinal modes of the 17-cm long ring. The linewidth of each mode is seen from Fig. 7.6 to be ~2 MHz for the ring laser with optical isolator. This value for the linewidth is obtained noting from (B.1) that 3 dB below the maximum of the beat

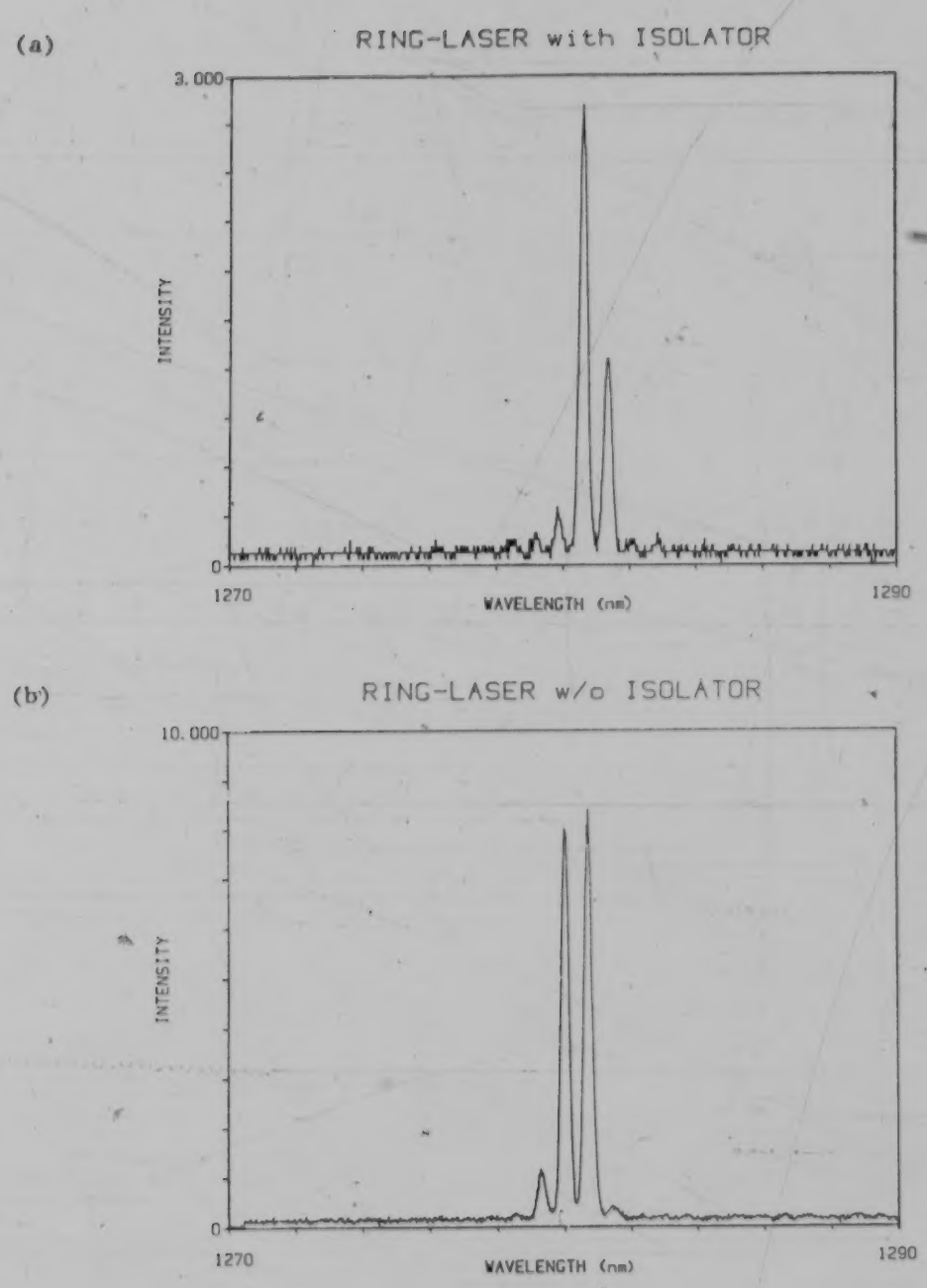

Fig. 7.3: Optical power spectrum of the fiber-ring laser, (a) with and (b) without optical isolator as part of the fiber ring, as recorded with a monochromator. The travelling wave amplifier # 6M3772 is operated at 66 mA injection current and is part of the 17 cm long ring-laser arrangement

(a)

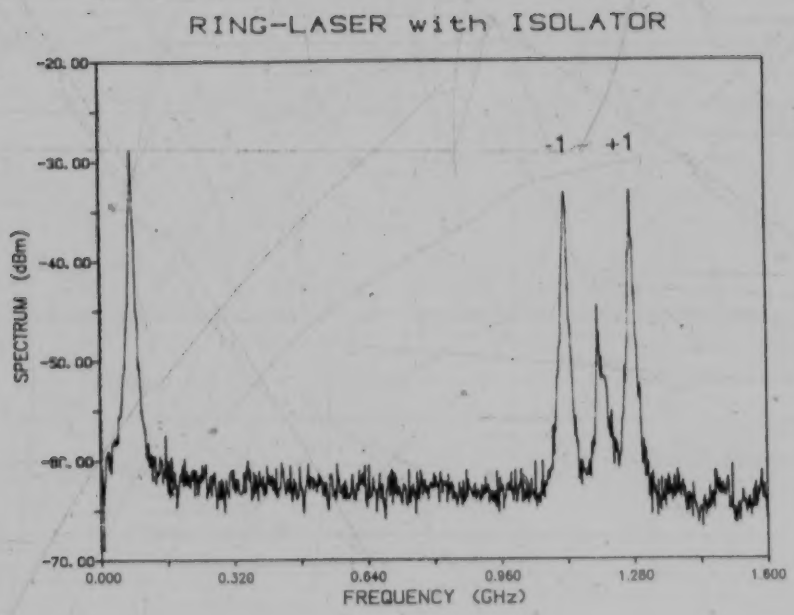

(b)

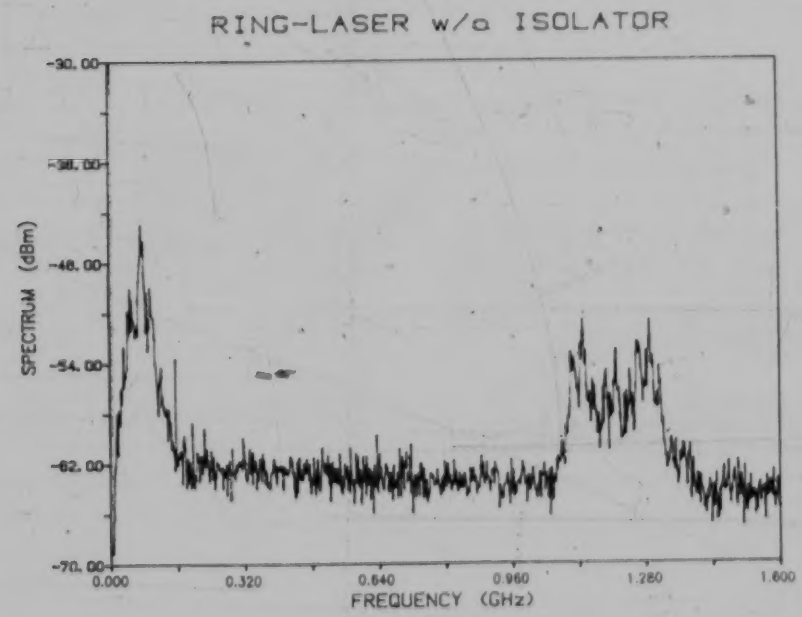

Fig. 7.4: Self-heterodyne beat spectra of the fiber-ring laser, (a) with and (b) without optical isolator as part of the fiber ring. The same operating conditions apply as in Fig. 7.3.

(a)

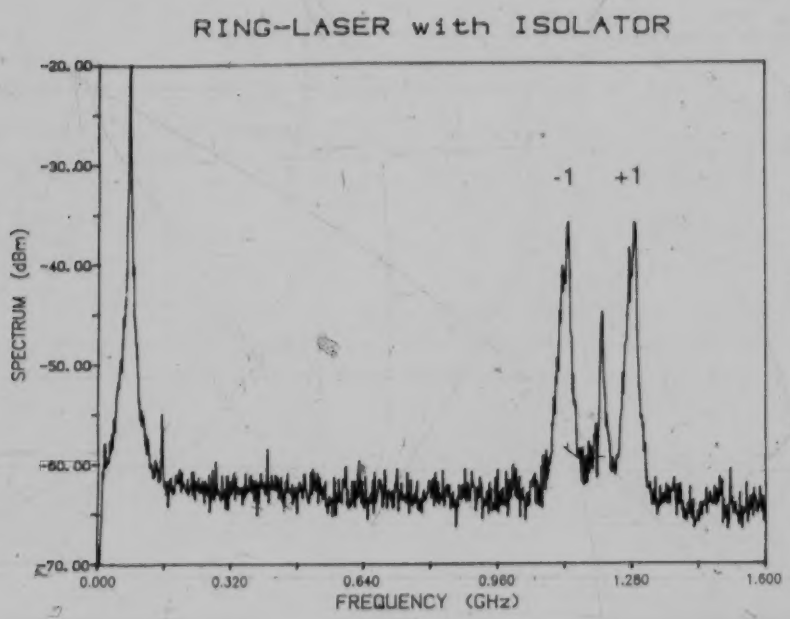

(b)

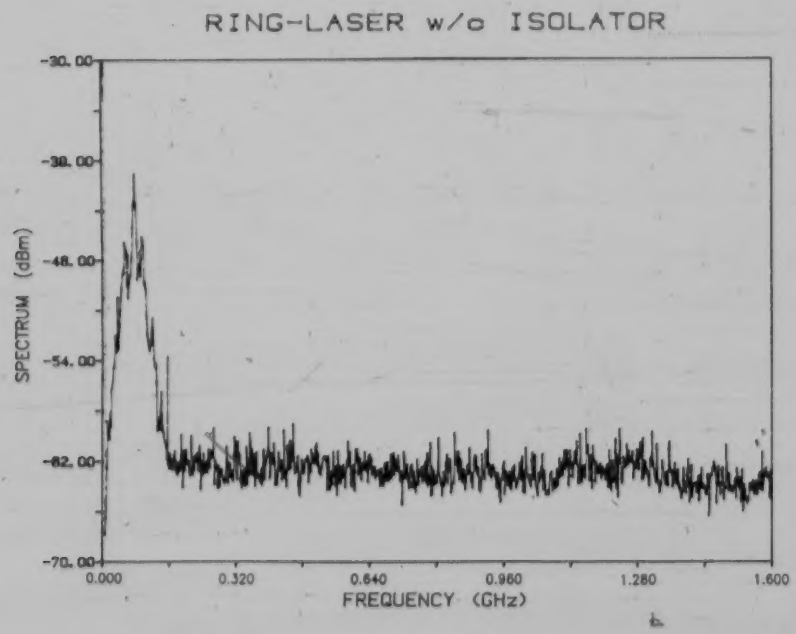

Fig. 7.5: Self-heterodyne beat spectra of the fiber-ring laser, (a) with and (b) without optical isolator as part of the fiber ring. The same operating conditions apply as in Fig. 7.3 and 7.4, except that the fiber-ring length is adjusted to yield narrowest linewidth for the mode displayed at 80 MHz and low power for the components at ±1.2 GHz separation from this mode.

spectrum the full width of this spectrum is $2 \cdot \Delta\nu_0$ or 10 dB below maximum the full width is $6 \cdot \Delta\nu_0$. Fig. 7.1(b) provides a sketch of the optical power spectrum of the ring laser. In conclusion, although the linewidth of the individual modes in the fiber-ring laser is low, the presence of several longitudinal modes in the optical spectrum is not desirable.

The self-heterodyne spectra shown in Fig. 7.5 were recorded for an alignment of the fiber-taper positions, i.e. for a fiber ring length, that leads to narrowest linewidth of the center mode and lowest power in the neighboring ring cavity modes. For the ring laser without optical isolator, it is possible to find an alignment that leads to oscillation in one ring cavity mode only (Fig. 7.5(b)). However, the stability of this operating point is poor and fluctuations away from the point of single-mode stability occurs within a few seconds. A closer look at the beat spectrum at 80 MHz for this ring laser, shown in Fig. 7.6(b), reveals the presence of external cavity modes separated from line-center by 25 MHz. We attribute those modes to reflections off the fiber cleave at the end of the 4m-long fiber section that connects the optical amplifier through the two fiber couplers "CA" and "CB" to the acousto-optic frequency shifter, Fig. A.1. These external cavity modes are clearly not present when the optical isolator was used, Fig. 7.6(a). We conclude that the intermittent oscillation in a single mode for the laser without isolator is achieved when the ring cavity resonances, the 4-m long reflective-cavity resonance and the semiconductor cavity resonance are aligned to provide a common resonance at one frequency.

The reduction in the frequency stability of the ring laser without isolator compared to the ring laser with isolator is evident from Fig. 7.7(a) and (b). For the ring laser without isolator, Fig. 7.7(b), the optical spectrum as recorded with a Fabry-Perot Interferometer is clearly broader, indicating oscillation in about 30 ring cavity modes, and less stable than for the ring laser with isolator. Fig. 7.7(a) and (b) show two traces each, recorded for different fiber-alignment with respect to the optical amplifier to show the degree of dependence of this alignment on the spectrum.

With the optical isolator as part of the assembly, the fiber ring laser is protected from optical reflections entering the laser through its main port #1. Therefore, a stable optical spectrum is to be

(a)

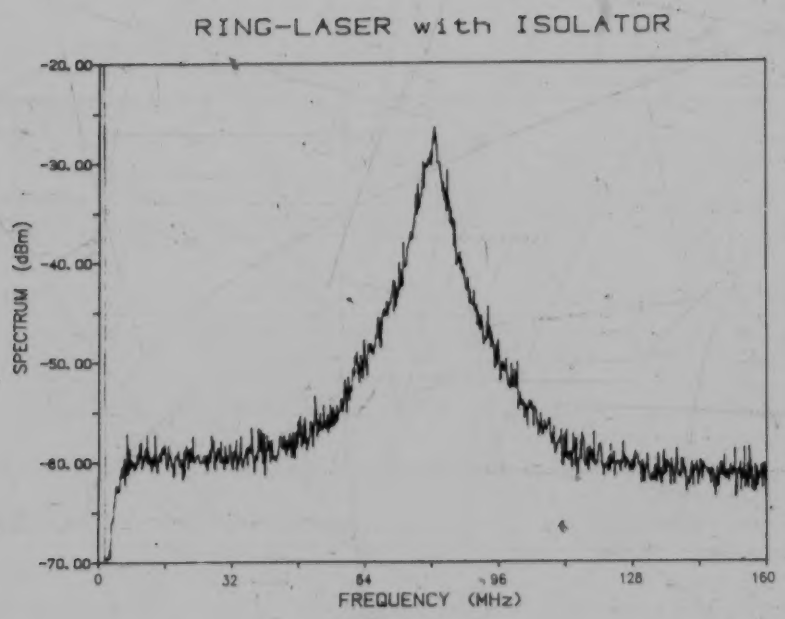

(b)

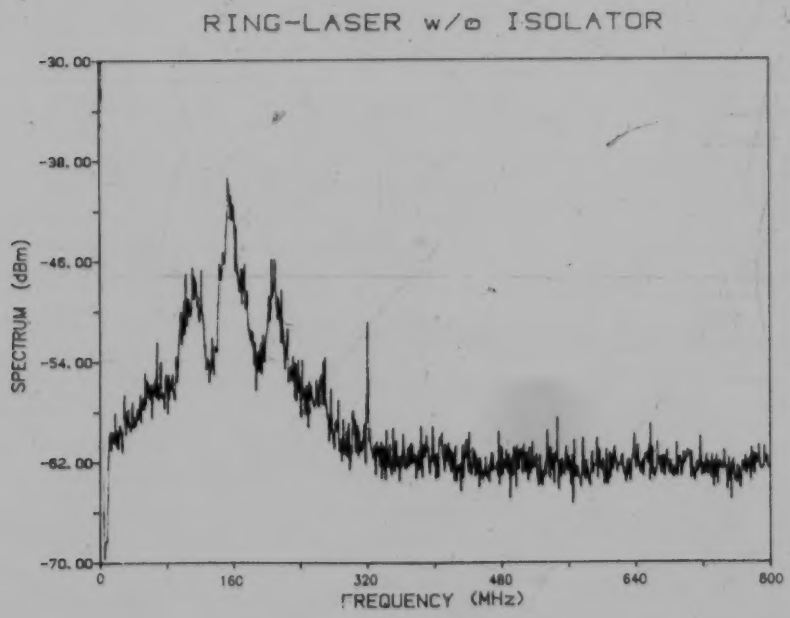

Fig. 7.6: Self-heterodyne beat spectra of the fiber-ring laser, (a) with and (b) without optical isolator as part of the fiber ring. The same operating conditions apply as in Fig. 7.3, except that the recordings cover a different frequency range than in Fig. 7.3.

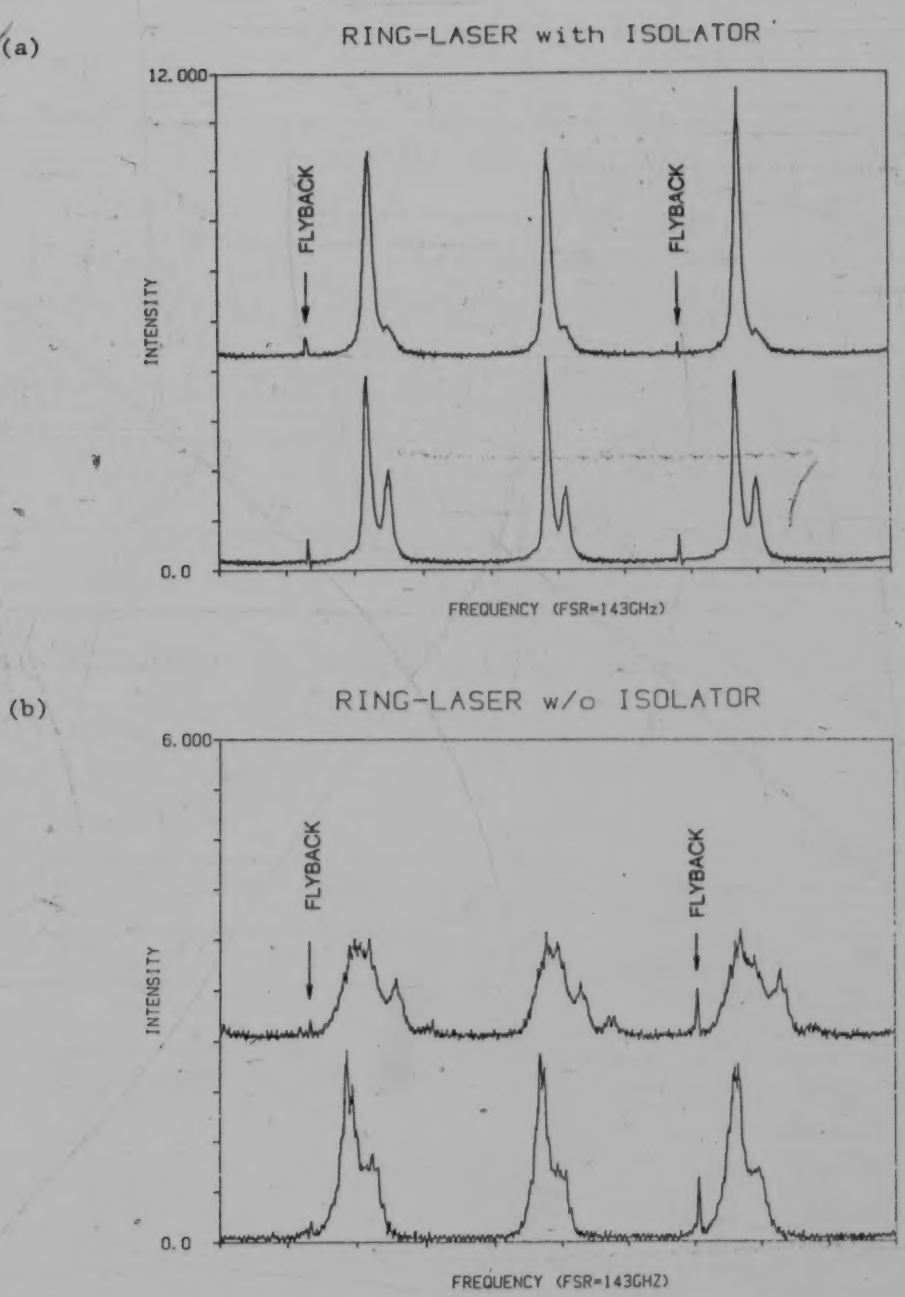

Fig. 7.7: Optical power spectra of the fiber-ring laser recorded with a Fabry-Perot interferometer, (a) with and (b) without optical isolator as part of the fiber ring. The free spectral range of the FP-interferometer is 143 GHz and the Finesse ~ 30. The lower trace of Fig. 7.7(a) shows a recording of the same optical power spectrum as Fig. 7.3, except using a different instrument and plotted versus frequency instead of wavelength.

expected. Three frequency selective mechanisms determine the oscillation frequency of the ring laser, namely the gain profile of the semiconductor medium, the resonance of the semiconductor cavity and the resonance of the ring cavity. An added degree of frequency selectivity is required to ensure single mode oscillation of the ring laser, much the same as provided by the optical grating in the case of an external grating laser (Section 5). The optical grating provides selectivity upon reflection of light and is therefore not practicable for the ring laser. A transmission filter that provides a degree of frequency selectivity similar to the grating, for instance a narrow band interference filter that can be tuned by tilting [119], can be expected to transform the ring laser into a stable narrow linewidth source emitting at a single frequency.

The considerations of Section 5 on tunability and stability of the external grating laser would apply in the same way to a ring laser with frequency selective in-line filter. The use of a wavelength dependent optical coupler in the fiber ring is proposed as another option to obtain an added degree of frequency selectivity for the fiber ring laser. The width of the passband of the overcoupled fused fiber coupler [120] is in the range of several tens of nm or larger, and therefore not sufficient to provide discrimination between ring cavity modes, separated by 1.2 GHz or .0067 nm. However, the integrated resonant optical transformer proposed by [121], which is essentially an integrated optical coupler with FWHM of the passband of ~ 10 GHz, provides even better frequency selectivity than the optical grating used for the external grating laser and would therefore be sufficient for stabilization of the ring laser.

7.4. CONCLUSION

The LI-curves and the spectral properties of a semiconductor fiber ring laser have been investigated. With an optical isolator as part of the ring, the optical field due to stimulated emission was observed to travel only in one direction in the ring. The external quantum efficiency of the unidirectional ring laser was equal to the sum of the

external quantum efficiencies per facet of the bidirectional ring laser. The ring laser was observed to oscillate in two to three longitudinal modes of the semiconductor (130 GHz separation) and for each semiconductor cavity mode in several modes of the ring cavity (1.2 GHz separation) with linewidth ~ 2 MHz.

Our experiments do not reveal a significant difference in the spectral behavior of a unidirectional and bidirectional semiconductor ring laser, apart from the increased stability for the ring laser with an optical isolator due to the prevention of optical reflections, external to the ring laser, from affecting the laser.

To achieve oscillation in a single ring cavity mode, additional frequency-selectivity has to be provided. For this purpose we propose the use of an in-line transmission-type optical bandpass filter with a few tenths of nanometer spectral width, such as an interference filter [119] or a wavelength dependent optical coupler [121]. With this additional optical filter we expect the ring laser to achieve spectral stability similar to the external grating laser. Unfortunately, the required in-line bandpass filters are not commercially available to date. An advantage of a tunable ring laser compared to the external grating laser would be the improved stability of the optical feedback path, which would be comprised of optical waveguides, and the simplied alignment, requiring only laser to fiber coupling procedures.

Apart from the spectral properties of the ring laser in steady state operation, we suggest that further study is desirable on the dynamic properties of the unidirectional ring laser. A modulation of the injection current of the travelling wave amplifier with a period that is equal to the inverse of the roundtrip-time in the ring cavity is expected to lead to mode-locked operation of the ring laser. Even with sinusoidal modulation of the injection current of a one-side coated laser, coupled to a passive external cavity of 7.5 cm length, modelocked pulses of 7.7 ps FWHM at a repetition rate of 2 GHz were observed by Eisenstein et.al. [63]. Eisenstein's assumption is that the pulse width in his arrangement is ultimately limited by the transit time of the pulse through the active cavity. In a unidirectional ring arrangement the pulse travels only once through the active region and we therefore expect even shorter pulses.

8. CONCLUSIONS

This thesis has been concerned with the effects of optical feedback on the characteristics of semiconductor lasers. The work was aimed at improving the spectral performance of the semiconductor laser by providing optical feedback. A sufficiently detailed treatment of the feedback properties is provided, so as to enable the range of parameter values best suited for the improvement of the spectral characteristics of the semiconductor laser to be determined. Experimental results are provided for devices under these optimized feedback conditions.

The delay-differential equations describing the laser with optical feedback provide an accurate description of most of the properties of the semiconductor laser with optical feedback. However, these equations need to be solved numerically, or analytically using small signal analysis, for a certain set of parameter values and do not provide an overview of the spectral properties that are to be expected under certain feedback conditions. Our discussion of the effect of the value of the feedback parameter on the spectral characteristics and stability of laser operation has been based on a different solution technique, namely a graphical representation of the resonance conditions of a laser in a gain versus frequency chart, when this laser is coupled to an external resonator. This type of plot is found to be effective because the coupling between gain and resonance frequency of the semiconductor cavity, described by the linewidth enhancement factor α and represented clearly in the gain versus frequency chart, is responsible for many of the unusual effects observable in a semiconductor laser with optical feedback, including the presence of several external cavity modes for weak feedback and bistability for strong feedback.

Without anti-reflection coating of the semiconductor laser, one is restricted to work in the domain of weak optical feedback, where the semiconductor cavity is dominant compared to the external cavity. The maximum feedback level that can be applied without inducing "coherence collapse" [13] of the optical output of the laser is ~ -40 dB. This feedback level was found to be related to the frequency span of the

external cavity modes and to the relaxation oscillation frequency of the laser. Because this feedback level is very low and dependent only on the fixed parameters of the laser, the linewidth reduction obtainable with weak feedback is small.

The presence of a large number of external cavity modes in the optical power spectrum is another problem associated with a laser exposed to weak optical feedback from an external cavity. The spectrum of a laser with weak optical feedback has been measured with sufficient resolution to show the frequency of the external cavity modes with respect to the oscillation frequency of the solitary laser and the distribution of power in these modes. From a comparison of the measured spectrum with the predicted frequency and chirp reduction of the individual external cavity modes, as derived from the oscillation condition graph, it is found that the mode with the minimum linewidth is also the mode with maximum output power. A longer duration of stay in the mode with minimum linewidth and therefore higher average power in this mode is predicted by the frequency fluctuation model proposed in this thesis. The model is found to provide also an estimate of experimentally observed mode-hopping frequencies and an explanation for the presence of a regime with stable single mode operation, Regime III of [17], which is a weak feedback regime. Agreement is found between the functional dependence of the feedback level that leads to coherence collapse and the feedback level that leads to a frequency span of external cavity modes equal to the relaxation oscillation frequency.

We found that stable narrow linewidth and single mode operation in the weak feedback domain could be obtained by choosing an external cavity length short enough to provide an external cavity mode spacing in the GHz range, and to choose a feedback level just below the level that leads to coherence collapse. Starting from a solitary laser oscillating in several longitudinal semiconductor cavity modes, we obtained single mode oscillation with a sidemode suppression > 1:20 and a linewidth reduction of ~ 50, i.e. from 100 MHz to 2 MHz, with a feedback level of ~ 43 dB from a fiber ring assembly of 17 cm length. The fiber ring assembly was found to be easy to align and, with an optical isolator in the ring, was insensitive to unwanted optical reflections entering the laser assembly through the main output port of the fiber ring.

A second stable domain of operation exists under strong optical feedback conditions. To realize strong optical feedback, it is necessary to apply an AR-coating to one facet of the laser and to apply strong optical feedback through the AR-coated facet. A large number of external cavity modes are present in this domain of operation if frequency selective optical feedback is not provided. When a frequency selective reflector is used, such as a diffraction grating, single mode operation with a side-mode suppression ratio greater than 30 dB and linewiths below 10 kHz are realized [37]. Also this arrangement allows tuning of the optical frequency to anywhere within a band of 50 nm (2000 THz).

The effect of the value of the residual reflectivity on the tuning range of the external grating laser, the tuning characteristic and the stability of single mode oscillation has been analyzed in this thesis. It has been shown that bistability in the tuning characteristic of an external grating laser can be explained using the loss versus frequency graph plotted for different carrier density levels. A periodically repeating domain of stable single mode oscillation was identified for the high reflectivity laser, which coincides with the condition of large detuning from the solitary laser mode and with the regime of high output power due to large detuning. For the low reflectivity laser, stable single mode operation was found to be independent of the detuning from the solitary laser mode provided grating and lens are carefully aligned.

A comparison between the stability of the laser with weak and strong frequency selective feedback provides us with the following findings. For strong feedback, a fraction of a wavelength change in the external cavity length alters the oscillation frequency of the device within a range of $\Delta\nu_{ex}$, where $\Delta\nu_{ex}$ is the separation of external cavity modes. However in contrast to the laser with weak optical feedback, the stability of oscillation of the extended cavity laser is not affected by this change in the external cavity length. If the external grating laser is used as a local oscillator, this means that a change of feedback phase leads to a drift in the beat-frequency between the received signal and the local oscillator signal, but never to a total loss of signal. In addition, small changes in the operating conditions

of the semiconductor laser, i.e. changes in the injection current and temperature of the semiconductor cavity, are, to first order, not affecting the oscillation frequency of the device and in particular are not affecting the stability of oscillation. This is again not true for the laser with weak optical feedback, where changes in the injection current and temperature of the laser do affect the oscillation frequency of the compound cavity and since the arrangement is sensitive to changes in the phase of the returned light, do affect the stability of oscillation.

For weak feedback it is of little consequence whether the optical feedback is provided by an external mirror having frequency independent reflectivity or by an external grating. Single mode oscillation can be obtained in both cases, however as mentioned above, with very limited stability. For strong feedback, frequency selective optical feedback is necessary to obtain single-mode oscillation. Wavelength independent, strong optical feedback provides a large number of external cavity modes under all operating conditions and is therefore undesirable. In conclusion, the laser with strong, wavelength dependent, optical feedback has not only better spectral characteristics than the laser with weak optical feedback, but is also substantially more stable and frequency tunable.

To be able to compare theoretical and experimental results, it was necessary for us to determine the strength of optical feedback applied to a laser. For this purpose a detailed study of the change of the LI-characteristic of different semiconductor lasers due to AR-coating of one of their facets has been performed. As a result of this study a method was developed to predict the gain versus current characteristic of individual semiconductor laser amplifiers and the amount of optical feedback applied to a one-side AR-coated laser.

Finally, the spectral properties of a unidirectional semiconductor optical-fiber ring laser have been investigated. The optical power spectrum indicates oscillation of the ring laser in several longitudinal modes of the semiconductor cavity and several external cavity modes. To reduce the number of longitudinal modes that are oscillating, the insertion of two types of in-line optical bandpass filters has been suggested for further studies.

A main conclusion of this thesis is that whenever the purity of the optical spectrum is crucial in a transmission scheme, the laser has to be protected from unwanted optical reflections to realize a level of unwanted feedback of less than ~ -70 dB. With intentionally applied optical feedback, the most effective way to increase the spectral purity of a given laser is by means of strong frequency selective optical feedback. This type of feedback does provide the added benefit of providing tunability of the laser frequency.

A practical implementation of frequency selective optical feedback calls for integrated solutions, which are presently sought after by a variety of research labs in the form of multisection DFB and DBR lasers [6]. Integrated solutions based on those devices exhibit substantially higher linewidths, because the cavity lengths of those devices are very short and the energy stored in a short cavity is low. Also, the tuning range obtained to date is approximately 10 times less than for an external grating laser with a low residual reflectivity of the coated facet. For further investigation we suggest the development and use of frequency selective fiber optic components that are not based on semiconductor cavities to apply strong optical feedback. Examples of these devices, already being investigated, are wavelength dependent couplers [120], and passive wave guides that provide evanescent wave coupling to gratings adjacent to the wave guide [121]. To provide tunability, those gratings could be created by surface acoustic waves.

REFERENCES

[1] R.F. Bloom, E. Mohn, C. Risch, and R. Salather, "Microwave self modulation of a diode laser coupled to an external cavity," *IEEE J. Quantum Electron.*, vol. QE-6, pp. 328-334, 1970.

[2] O. Hirota and Y. Suematsu, "Noise properties of injection lasers due to reflected waves," *IEEE J. Quantum Electron.*, vol. QE-15, pp. 142-149, 1979.

[3] N.A. Olsson, W.T. Tsang, H. Temkin, N.K. Dutta, and R.A. Logan, "Bit error rate saturation due to mode partition noise induced by optical feedback," *J. Lightwave Technol.*, vol. LT-3, pp. 215-218, Apr. 1985.

[4] K. Kobayashi and M. Seki, " Microoptic grating multiplexers and optical isolators for fiber-optic communications," *IEEE J. Quantum Electron.*, vol. QE-16, pp. 11-22, Jan. 1980.

[5] M. Fukuda, M. Nakao, K. Sato, and Y. Kondo, "1.55 μm tunable DFB laser with narrow linewidth and high power," *IEEE Phot. Techn. Lett.*, vol. 1, pp. 6-7, Jan. 1989.

[6] K. Kobayashi and I. Mito, "Single frequency and tunable laser diodes," (invited paper), *J. Lightwave Technol.*, vol. LT-6, pp. 1623-1633, Nov. 1988.

[7] R. Lang and K. Kobayashi, "External optical feedback effects on semiconductor injection laser properties," *IEEE J. Quantum Electron.*, vol. QE-16, pp. 347-355, Mar. 1980.

[8] L. Goldberg, H.F. Taylor, A. Dandridge, J.F. Weller, and R.O. Miles, "Spectral characteristics of semiconductor lasers with optical feedback," *IEEE J. of Quantum Electr.*, vol. QE-18, pp. 555-564, 1982.

[9] F. Favre and D. Le Guen, "Emission frequency stability in single-mode-fibre optical feedback controlled semiconductor lasers," *Electr. Lett.*, vol. 19, pp. 663-665, Aug. 1983.

[10] E. Patzak, H. Olesen, A. Sugimura, S. Saito, and T. Mukai, "Spectral linewidth reduction in semiconductor lasers by an external cavity with weak optical feedback," *Electron. Lett.*, vol. 19, pp. 938-940, Oct. 1983.

[11] R.A. Suris and A.A. Tager, "Coherence and spectral properties of radiation emitted by an semiconductor laser with an external reflector," *Sov.J.Quantum Electron.*, vol 14, pp. 21-26, Jan. 1984.

[12] B. Tromborg, J.H. Osmundsen, and H. Olesen, "Stability analysis for a semiconductor laser in an external cavity," *IEEE J. Quantum Electron.*, vol. 20, pp. 1023-1032, Sept. 1984.

[13] D. Lenstra, B.H. Verbeek and A.J. den Boef, "Coherence Collapse in single-mode semiconductor lasers due to optical feedback," *IEEE J. Quantum Electron.*, vol. QE-21, pp. 674-679, June 1985.

[14] J.H. Osmundson, *Semiconductor Lasers with Optical Feedback*, Ph.D-Thesis, Electromagnetics Institute, Technical University of Denmark, Lyngby, Denmark, June 1985.

[15] H. Olesen, J.H. Osmundsen and B. Tromborg, "Nonlinear dynamics and spectral behavior for an external cavity laser," *IEEE J. Quantum Electron.*, vol. QE-22, pp. 762-773, June 1986.

[16] H. Temkin, N.A. Olsson, J.H. Abeles, R.A. Logan, and M.B. Panish, "Reflection noise in index-guided InGaAsP lasers," *IEEE J. Quantum Electron.*, vol. QE-22, pp. 286-293, Feb. 1986.

[17] R.W. Tkach and A.R. Chraplyvy, "Regimes of feedback effects in 1.5-μm distributed feedback lasers," *J. Lightwave Techn.*, vol. LT-4, pp. 1655-1661, Nov. 1986.

[18] P. Zorabedian, W.R. Trutna, and L.S. Cutler, "Bistability in grating-tuned external-cavity semiconductor lasers," *IEEE J. Quantum Electron.*, vol. 23, pp. 1855-1860, Nov. 1987.

[19] J. Mørk, B. Tromborg, and P.L. Christiansen, "Bistability and low-frequency fluctuations in semiconductor lasers with optical feedback: a theoretical analysis," *IEEE J. Quantum Electron.*, vol. QE-24, pp. 123-133, Feb. 1988.

[20] G.C. Dente, P.S. Durkin, K.A. Wilson, and C.D. Moeller, "Chaos in the coherence collapse of semiconductor lasers," *IEEE J. Quantum Electron.*, vol. QE-24, pp. 2441-2447, Dec. 1988.

[21] N. Schunk and K. Petermann, "Numerical analysis of the feedback regimes for a single-mode semiconductor laser with external feedback," *IEEE J. Quantum Electron.*, vol. QE-24, pp. 1242-1247, July 1988.

[22] G.H.B. Thompson, *Physics of Semiconductor Laser Devices*, John Wiley & Sons, Chichester, GB, 1980.

[23] J.O. Binder and G.D. Cormack, "Mode selection and stability of a semiconductor laser with weak optical feedback," to be published, *IEEE J. Quantum Electron.*, Nov. 1989.

[24] J.O. Binder and G.D. Cormack, "Spectral characteristics of a semiconductor laser with optical fiber-ring feedback," *Techn. Dig., 13th-Europ. Conf. on Optical Comm., ECOC'87*, Helsinki, Finland, vol. 1, pp. 93-96, Sept. 1987.

[25] M.W. Fleming and A. Mooradian, "Spectral characteristics of external-cavity controlled semiconductor lasers," *IEEE J. Quantum Electron.*, vol. QE-17, pp. 44-59, Jan. 1981.

[26] R. Wyatt and W.J. Devlin, "10-kHz linewidth 1.5um InGaAsP external cavity laser with 55 nm tuning range," *Electr. Lett.*, vol. 19, pp. 110-112, 1983.

[27] A.H. Gnauck, R.A. Linke, B.L. Kasper, K.J. Polloch, K.C. Reichmann, R. Valenzuela, and R.C. Alferness, "Coherent lightwave transmission at 2 Gb/s over 170 km of optical fiber using phase modulation," *Postdeadline Papers, Optical Fiber Comm. Conf. OFC/IOOC '87*, Reno, Nevada, paper PD10, Jan. 1987.

[28] D.W. Smith, " Techniques for multigigabit coherent optical transmission," *J. Lightwave Technol.*, vol. LT-5, pp. 1466-1478, Oct. 1987.

[29] D. Hoffmann, H. Heidrich, G. Wenke, R. Langenhorst, and E. Dietrich, "Integrated optics eigth-port 90° hybrid on $LiNbO_3$," *J. Lightwave Technol.*, vol. LT-7, pp. 794-803, May 1989.

[30] R.J.S. Pedersen, I. Garrett, and G. Jacobsen, "Measurement of the statistics of DFB laser frequency fluctuations," *Electron. Lett.*, vol. 24, pp. 585-586, May 1988.

[31] M.G. Oberg and N.A. Olsson, "Wavelength dependence of noise figure of a travelling-wave GaInAsP/InP laser amplifier," *Electron. Lett.*, vol. 24, pp. 99-100, Jan. 1988.

[32] N.A. Olsson and J.P. van der Ziel, "Performance characteristics of 1.5-μm external cavity semiconductor lasers for coherent optical communication," *J. Lightwave Technol.*, vol. LT-5, pp. 510-515, April 1987.

[33] V. Yu, A.P. Bogatov, P.G. Eliseev, O.G. Okhotnikov, G.T. Pak, et. al., "Bistable operation and spectral tuning of injection laser with external dispersive cavity," *IEE Proc.*, vol. 129, Pt. J, pp. 77-82, 1982.

[34] A. Somani, private communications.

[35] R.J.S. Pederson, private communications.

[36] J.O. Binder, G.D. Cormack and A. Somani, "Intermode tuning characteristics of an InGaAsP laser with optical feedback from an external grating reflector," *IEEE Pacific Rim Conf. on Comm., Comp. and Sign. Proc., Proceedings*, Victoria, B.C., Canada, pp. 22-26, June 1989.

[37] A. Somani, *Linewidth Reduction and Frequency Modulation of a 1.3 micron Semiconductor Laser with Strong Frequency Selective Optical Feedback*, M.Sc. Thesis, University of Alberta, Edmonton, Canada, Spring 1988.

[38] A. Somani, P.A. Goud, and C.G. Englefield, "Real-time monitoring of laser diode facet reflectivity while being coated with SiO_x," *Appl. Optics*, vol. 27, pp. 1391-1393, Apr. 1988.

[39] J.O. Binder and G.D. Cormack, "Prediction of the gain vs. injection-current characteristic of individual semiconductor laser amplifiers," submitted for publication, Dec. 1988.

[40] A. Yariv, *Optical Electronics*, 3rd Ed., Holt, Rinehart and Winston, New Tork, 1985.

[41] J.T. Verdeyen, *Laser Electronics*, Prentice Hall Inc., Englewood Cliffs, 1981.

[42] A. Mooradian, "Spectral characteristics of semiconductor lasers," in *Physics of New Laser Sources*, ed. N.B. Abraham et al., pp. 123-148, Plenum Press, New York, 1984.

[43] P. Brosson, W.W. Ruehle, N.B. Patel, and J.E. Ripper, "Optical Coupling of two injection lasers: A new experimental approach to study the gain broadening mechanism," *IEEE J. of Quantum Electr.*, vol. QE-17, pp. 714-717, 1981.

[44] W. Elsaesser and E.O. Goebel, "Multimode Effects in the spectral linewidth of semiconductor lasers," *IEEE J Quantum Electron.*, vol QE-21, pp. 687-691, June 1985

[45] Y. Yamamoto, "AM and FM quantum noise in semiconductor lasers - Part I: theoretical analysis," *IEEE J. of Quant. Electr.*, vol. QE-19, pp. 34-46, June 1983.

[46] C.H. Henry, "Theory of the linewidth of semiconductor lasers," *IEEE J. Quantum Electron.*, vol. QE-18, pp. 259-263, Feb. 1982.

[47] C.H. Henry, "Phase noise in semiconductor lasers," (invited paper), *J. Lightwave Techn.*, vol. LT-4, pp. 298-311, Mar. 1986.

[48] M. Lax, "Fluctuations from the nonequilibrium steady state," *Rev. Mod. Phys.*, vol. 32, pp. 25-64, 1960.

[49] M. Lax, "Quantum noise X. Density-matrix treatment of field and population-difference fluctuations", *Phys. Rev.*, vol. 157, pp. 213-231, 1967.

[50] M. Lax and W.H. Louisell, "Quantum noise IX: Quantum Fokker-Planck solution for laser noise," *IEEE J. Quantum Electron.*, vol. QE-3, pp. 46-58, 1967.

[51] M. Lax, "Classical noise V: Noise in self-sustained oscillators," *Phys. Rev.*, vol 160, pp. 290-307, 1967.

[52] M. Lax, "Quantum noise IV. Quantum theory of noise sources," *Phys. Rev.*, vol. 160, pp. 290-307, 1967.

[53] M. Lax, "Quantum noise VII. The rate equation and amplitude noise in lasers," *IEEE J. Quantum Electron.*, vol. QE-3, pp. 36-46, 1967.

[54] D.E. McCumber, "Intensity fluctuations in the output of cw laser oscillators I," *Phys. Rev.*, vol. 141, pp. 306-322, 1966.

[55] M. Lax, "Classical noise IV: Langevin methods," *Rev. Mod. Phys.*, vol. 38, pp. 541-565, 1966.

[56] H. Olesen, J.H. Osmundson, and B. Tromborg, "Nonlinear dynamics and spectral behavior for an external cavity laser," *IEEE J. Quantum Elect.*, vol. QE-22, pp. 762-773, June 1986.

[57] C.H. Henry, "Theory of the phase noise and power spectrum of a single mode injection laser," *IEEE J. Quantum Electron.*, vol. QE-19, pp. 1391-1397, Sept. 83.

[58] N. Schunk and K. Petermann, "Noise analysis of injection-locked semiconductor injection lasers," *IEEE J. Quantum Electr.*, vol. QE-22, pp. 642-650, May 1986.

[59] G.P. Agrawal and N.K. Dutta, *Long-Wavelength Semiconductor Lasers*, Van Nostrand Reinhold, New York, 1986.

[60] K. Ujihara, "Phase noise in a laser with output coupling," *IEEE J. Quantum Electron.*, vol. QE-20, pp. 814-818, July 1984.

[61] C.H. Henry, "Theory of spontaneous emission noise in open resonators and its application to lasers and optical amplifiers," *J. Lightwave Techn.*, vol. LT-4, pp. 288-297, March 1986.

[62] E. Schoell, "Dynamic theory of picosecond optical pulse shaping by gain-switched semiconductor laser amplifiers," *IEEE J. Quantum Electron.*, vol. QE-24, pp. 435-442, Feb. 1988.

[63] G. Eisenstein, R.S. Tucker, U. Koren, and S.K. Korotky, "Active mode-locking characteristics of InGaAsP-single mode fiber composite cavity lasers," *IEEE J. Quantum Electr.*, vol. QE-22, pp. 142-148, Jan. 1986.

[64] J.C. Goodwin, *Diode Laser Dynamics*, Ph.D. thesis, McMaster University, Hamilton, Ontario, Canada, 1983.

[65] K. Vahala and A. Yariv, "Semiclassical theory of noise in semiconductor lasers - Part II," *IEEE J. Quantum Electron.*, vol. QE-19, pp. 1102-1109, June 1983.

[66] K. Kikuchi and T. Okoshi, " Measurement of FM noise, AM noise and field spectra of 1.3 μm InGaAsP DFB lasers and determination of the linewidth enhancement factor," *IEEE J. Quantum Electron.*, vol. QE-21, pp. 1814-1818, Nov. 1985.

[67] L.D. Landau and E.M. Lifshitz, *Statistical Physics*, 1st ed., Reading, MA, Addison Wesley, 1958.

[68] J.G. Proakis, *Digital Communications*, McGraw-Hill, New York, 1983.

[69] R.W. Tkach and A.R. Chraplyvy, "Phase noise and linewidth in an InGaAsP DFB laser," *J. Lightwave Technol.*, vol. LT-4, pp. 1711-1716, Nov. 1986.

[70] B. Moslehi, "Noise power spectra of optical two-beam interferometers induced by the laser phase noise," *J. Lightwave Technol.*, vol. LT-4, pp. 1704-1709, Nov. 1986.

[71] S. Haykin, *Communication Systems*, John Wiley, New York, 2nd ed., 1983.

[72] I. Garrett and G. Jacobsen, "Statistics of laser frequency fluctuations in coherent optical receivers," *Electron. Lett.*, vol. 22, pp. 168-170, Jan. 1986.

[73] I. Garrett, G. Jacobsen, and R.J.S. Pedersen, "Filtered laser beat-frequency fluctuations," *IEE Proc.*, vol. 135, Pt. J, Dec. 1988.

[74] G. Jacobsen and I. Garrett, "Optical ASK heterodyne receiver: comparison of a theoretical model with experiment," *Electron. Lett.*, vol. 22, pp. 170-171, Jan. 1986.

[75] P. Spano, S. Piazzola and M. Tamburrini, "Theory of noise in semiconductor lasers in the presence of optical feedback," *IEEE J. Quantum Electr.*, vol. QE-20, pp. 350-357, Apr. 1984.

[76] G.P. Agrawal, "Line narrowing in a single-mode injection laser due to external optical feedback," *IEEE J. Quantum Electron.*, vol. QE-20, pp. 468-471, May 1984.

[77] J.P. Crutchfield, J.D. Farmer, N.H. Packard, and R.S. Shaw, "Chaos," *Scientific American*, vol. 255, pp. 46-57, Dec. 1986.

[78] K.Ikeda, H. Daido, "Optical Turbulence: chaotic behavior of transmitted light in a ring cavity", *Phys. Rev. Lett.*, vol. 45, pp. 709-712, Sept. 1980.

[79] N.B. Abraham, et al., "Overview on instabilities in laser systems," *J. Opt. Soc. Am. B*, vol. 2, No. 1, pp. 7-14, Jan. 1985.

[80] J.R. Tredicce, et al., "Instabilities in lasers with an injected signal, *J. Opt. Soc. Am. B*, vol. 2, No. 1, pp. 173-183, Jan. 1985.

[81] Y. Cho and T. Umeda, "Chaos in laser oscillations with delayed feedback: numerical analysis and observation using semiconductor lasers", *J. Opt. Soc. Am. B*, vol. 1, pp. 497-498, June 1984.

[82] G.C. Dente, P.S. Durkin, K.A. Wilson, and C.E. Moeller, "Chaos in the coherence collapse of semiconductor lasers," *IEEE J. Quantum Electron.*, vol. QE-24, pp. 2441-2447, Dec. 1988.

[83] R.F. Kazarinov and C.H. Henry, "The relation of line narrowing and chirp reduction resulting from the coupling of a semiconductor laser to a passive resonator," *IEEE J. Quantum Electron.*, vol. QE-23, pp. 1401-1409, Sept. 1987.

[84] B. Tromborg, H. Olesen, X. Pan, and S. Saito, "Transmission line description of optical feedback and injection locking for Fabry-Perot and DFB lasers," *IEEE J. Quantum Electron.*, vol. QE-23, pp. 1875-1889, Nov. 1987.

[85] K. Kikuchi and T. Okoshi, "Simple formula giving spectrum-narrowing ratio of semiconductor laser output obtained by optical feedback," *Electron. Lett.*, vol. 18, pp. 10-11, 1982.

[86] C.H. Henry, R.F. Kazarinov, "Instability of semiconductor lasers due to optical feedback from distant reflectors," *IEEE J. Quantum Electr.*, vol. QE-22, pp. 294-301, Febr. 1986.

[87] J. Mørk and B. Tromborg, "Limits of stable operation of AR-coated semiconductor lasers with strong optical feedback," *Electron. Lett.*, vol. 24, pp. 1065-1066, Aug. 1988.

[88] S. Saito, O. Nilsson, and Y. Yamamoto, "Oscillation center frequency tuning, quantum FM-noise, and direct frequency modulation characteristics in external grating loaded semiconductor laser," *IEEE J. Quantum Electron.*, vol. QE-18, pp.961-970, 1982.

[89] C.J. Nielson and J.H. Osmundsen, "Linewidth stabilization of semiconductor lasers in an external cavity," *J. Opt. Comm.*, vol. 5, pp. 42,45, 1984.

[90] N. Schunk and K. Petermann, "Minimum bit rate of DPSK transmission for semiconductor lasers with a long external cavity and strong linewidth reduction," *J. Lightwave Technol.*, vol. LT-5, pp. 1309-1314, Sept. 1987.

[91] G.A. Acket, D. Lenstra, A.J. Den Boeef and B.H. Verbeek, "The influence of feedback intensity on longitudinal mode properties and optical noise in index-guided semiconductor lasers," *IEEE J. Quantum Elect.*, vol. QE-20, pp. 1163-1169, 1984.

[92] G.D. Cormack and J.O. Binder, *A fibre feedback InGaAsP laser*, Final Report submitted to the Dept. of Comm., Ottawa, Contract 06ST.36100-5-0143, March 1986.

[93] Frederick Chan, *Linewidth and FM Noise Reduction of a 1.3 Micron GRECC Semiconductor Laser using Electrical Feedback*, M.Sc. Thesis, University of Alberta, Edmonton, Canada, Spring 1988.

[94] Mischa Schwartz, *Information Transmission, Modulation, and Noise*, McGraw-Hill, New York, Ch. 6.13 and 7.1, 1970.

[95] G.-D. Khoe and H.G. Kock, "Laser-to-monomode-fiber coupling and encapsulation in a modified TO-5 package," *J. Lightwave Technol.*, vol. LT-3, pp. 1315-1319, Dec. 1985.

[96] B.W. Hakki and T.L. Paoli, "Gain spectra in GaAs double-heterostructure injection lasers," *J. Appl. Phys.*, vol. 46, pp. 1299-1306, 1975.

[97] L.D. Westbrook, "Measurement of dg/dN and dn/dN and their dependence on photon energy in $\lambda = 1.5$ μm InGaAsP laser diodes," *IEE Proc.*, vol 133, Pt. J, pp. 135-142, 1986.

[98] M.J. O'Mahony, "Semiconductor laser optical amplifiers for use in future fiber systems," *J. Lightwave Techn.*, vol. LT-6, pp. 531-544, April 1988.

[99] D. Marcuse, "Computer model of an injection laser amplifier," *IEEE J. Quantum Electron.*, vol. QE-19, pp. 63-73, Jan. 1983.

[100] T.P. Lee, "Light sources for fiber systems," in *Tutorial Sessions, Conf. on Opt. Fiber Comm. OFC'88*, New Orleans, p. 88, Jan. 1988.

[101] N.A. Olsson and C.L. Tang, "Coherent optical interference effects in external-cavity semiconductor lasers," *IEEE J. Quantum Electron.*, vol. QE-17, pp. 1320-1323, Aug. 1981.

[102] R.F. Kazarinov, C.H. Henry and R.A. Logan, "Longitudinal mode self-stabilization in semiconductor lasers," *J. Appl. Phys.*, vol. 53, pp. 4631-4644, July 1982.

[103] R. Wyatt, "Spectral linewidth of external cavity semiconductor lasers with strong, frequency-selective feedback," *Electron. Lett.*, vol. 21, pp. 658-659, 1985.

[104] U. Krueger and K. Petermann, "The power-independent part of the semiconductor laser linewidth explained by the rate equations," *Techn. Dig., 13th Europ. Conf. on Optical Comm., ECOC '87*, Helsinki, Finland, vol. 1, pp. 131-134, Sept. 1987.

[105] J. Wang, H. Olesen, and K.E. Stubkjaer, "Recombination, gain and bandwidth characteristics of 1.3-μm semiconductor laser amplifiers," *J. Lightwave Techn.*, vol. LT-5, pp. 184-189, Jan. 1987.

[106] B. Enning, G. Grosskopf, S.U. Lee, R. Ludwig and H.G. Weber, "Two channel 560 Mbit/s DPSK transmission experiments with two cascaded in-line broadband optical amplifiers," *Postdeadline Papers, Optical Fiber Comm. Conf. OFC'88*, New Orleans, 1988, paper PD20-3.

[107] N.A. Olsson and N.K. Dutta, "Effect of external optical feedback on the spectral properties of cleaved coupled-cavity semiconductor lasers," *Appl. Phys., Lett.*, vol. 44, pp. 840-842, 1984.

[108] R. Olshansky, C.B. Su, J. Manning, and W. Powazinik, "Measurement of radiative and nonradiative recombination rates in InGaAsP and AlGaAs light sources," *IEEE J. Quantum Electron.*, vol. QE-20, pp. 838-854, Aug. 1984.

[109] D. Marcuse and I.P. Kaminow, "Computer model of a superluminescent LED with lateral confinement," *IEEE J. Quantum Electron.*, vol. QE-17, pp. 1234-1244, July 1981.

[110] J. Boeck and M.-C. Amann, "AlGaAs/GaAs double-heterostructure superluminescent diodes for optical transmission systems," *Frequenz*, vol. 33, pp. 278-283, 1979.

[111] G.Wenke, R. Gross, P. Meissner and E. Patzak, "Characteristics of a compact three cavity laser configuration," *J. Lightwave Techn.*, vol. LT-5, pp. 608-615, April 1987.

[112] D. Botez, "Optimal cavity design for low-threshold-current-density operation of double-heterojunction diode lasers," *Appl. Phys. Lett.*, vol. 35, pp. 57-60, July 1979.

[113] R. Ludwig and G. Grosskopf, private communication.

[114] N.K. Dutta, D.P. Wilt, and R.J.Nelson, "Analysis of leakage currents in 1.3-μm InGaAsP real-index-guided lasers," *J. Lightwave Techn.*, vol. LT-2, pp. 201-208, June 1984.

[115] C.B. Su, "Dielectric grating induced by cavity standing wave as a new explanation of origin of nonlinear gain in semiconductor diode lasers," *Electron. Lett.*, vol. 24, pp. 370-371, Mar. 1988.

[116] R.M. Jopson, G. Eisenstein, M.S. Whalen, K.L. Hall, U. Koren, and J.R. Simon, "A 1.55-um semiconductor-optical fiber ring laser," *Appl. Phys. Lett.*, vol. 48, pp. 204-206, Jan 20, 1986.

[117] J. W. Wang, H. Olesen, B. Tromborg, and K.E. Stubkjaer, "Characterization of a fiber-optic ring laser," *Techn. Dig., 12-th Europ. Conf. on Optical Comm., ECOC '86*, Barcelona, Spain, pp. 105-108, Sept. 1986.

[118] S. Tain, K. Kojima, S. Noda, K. Kyuma, K. Hamanaka, and T. Nakayama, " Narrow spectral linewidth semiconductor optical-fiber ring laser," *Appl. Phys. Lett*, vol. 49, pp. 1328-1330, Nov. 1986.

[119] P. Zorabedian and W.R. Trutna, "Interference-filter tuning of a semiconductor laser in a misalignment-tolerant degenerate external," *Techn. Dig., Conf. on Opt. Fiber Comm. OFC'88*, New Orleans, paper WQ27, Jan. 1988.

[120] M. Eisenmann and E. Weidel, " Single-mode fused biconical couplers for wavelength division multiplexing with channel spacing between 100 μm and 300 nm," *Techn. Dig., 13th Europ. Conf. on Optical Comm., ECOC '87*, Helsinki, Finland, vol. 1, pp. 9-12, Sept. 1987.

[121] R.F. Kazarinov, C.H. Henry, and N.A. Olsson, "Narrow-band resonant optical reflectors and resonant optical transformers for laser stabilization and wavelength division multiplexing," *IEEE J. Quantum Electron.*, vol. QE-23, pp. 1419-1425, Sept. 1987.

[122] H.C. Lefevre, "Single-mode fibre fractional wave devices and polarization controllers," *Electr. Lett.*, vol. 16, pp. 778-779, 1980.

[123] R.D. Anderson, *An Investigation of the Effects of External Cavity Feedback on Semiconductor Lasers*, M.Sc. thesis, University of Alberta, Edmonton, Canada, Spring 1986.

[124] G.D. Cormack, J.O. Binder, and M.E. Shewchuk, "The EF-FFT (Extended Function Fast Fourier Transform) applied to the analysis of time domain reflectometer waveforms," *IEEE Pacific Rim Conf. on Comm., Comp. and Signal Proc., Proceedings*, pp. 444-446, Victoria, B.C. Canada, June 1987.

[125] G.D.Cormack and J.O. Binder, "The extended function fast Fourier transform (EF-FFT)," *IEEE Trans. Instrum. and Meas.*, vol. IM-38, pp. 730-735, June 1989.

[126] K. Kikuchi and T. Okoshi, "High resolution measurement of the spectrum of semiconductor laser," *Japan. Annual Review on Electronics, Comp., Telecomm., Opt. Devices and Fibres*, 1982. Published by Ohmsha Ltd., Tokyo, Japan and North Holland Publishing Co., Amsterdam, Netherlands, pp. 51-59, 1982.

[127] T. Okoshi, K. Kikuchi, and A. Nakayama, "Novel method for high resolution measurement of laser output spectrum," *Electron. Lett.*, vol. 16, pp. 630-631, 1980.

[128] J.A. Armstrong, "Theory of interferometric analysis of laser phase noise," *J. Opt. Soc. Amer.*, vol. 56, pp. 1024-1031, 1966.

[129] L.E. Richter, H.I. Mandelberg, M.S. Kruger, and P.A. McGrath, "Linewidth determination from self-heterodyne measurements with subcoherence delay times," *IEEE J. Quantum Electron.*, vol. QE-22, pp. 2070-2074, Nov. 1986.

APPENDIX A: EXPERIMENTAL SETUP

The experimental setup shown in Fig. A.1 was used to determine the spectral characteristics of the laser with optical feedback. The two ports B1 and B2 of the fiber coupler CB are the input ports to the measurement setup, providing simultaneous access to a self-heterodyne setup, a Fabry-Perot interferometer and a monochromator, each having a different spectral resolution. The Fabry-Perot interferometer is a Burleigh model RC 110 and the monochromator a McPherson model 270, .35 meter monochromator. The self-heterodyne setup consists of the two fiber couplers CB and CC, the two optical paths between these couplers one of which contains a fiber delay line of 800 m length and a polarization controller [122], and the other an acousto-optic frequency-shifter (Matsushita, shifter EFL-M080Y03, and driver SPC 080Y03), also, at the output, the APD (Antel AR-G15), electrical amplifier and spectrum analyzer. The portion of the light from the upper output port of coupler CC is divided into two parts with the fiber coupler CD. The collimated light from the output ports of coupler CD is passed to a monochromator and Fabry-Perot interferometer.

The external grating laser was coupled to port B3 of coupler CB, in addition to the laser with fiber ring feedback, which is already shown in Fig. A.1, to determine the spectral characteristic of the external grating laser and to obtain a beat spectrum between the two lasers. Depending on the laser that is turned on, the configuration with two lasers allows us to observe the self-heterodyne beat spectrum of either laser and the optical spectrum with the Fabry-perot interferometer or monochromator. To observe a beat signal between the lasers, both are turned on and the frequency of the external grating laser changed until the spectral components of the two lasers are indistinguishable with the monochromator and Fabry-Perot interferometer. In this situation, the two laser frequencies are close enough to yield a difference frequency visible on the spectrum analyzer shown in Fig. A.1. The components in the beat spectrum that are due to the two paths in the self-heterodyne setup can be eliminated be turning off the acousto-optic frequency

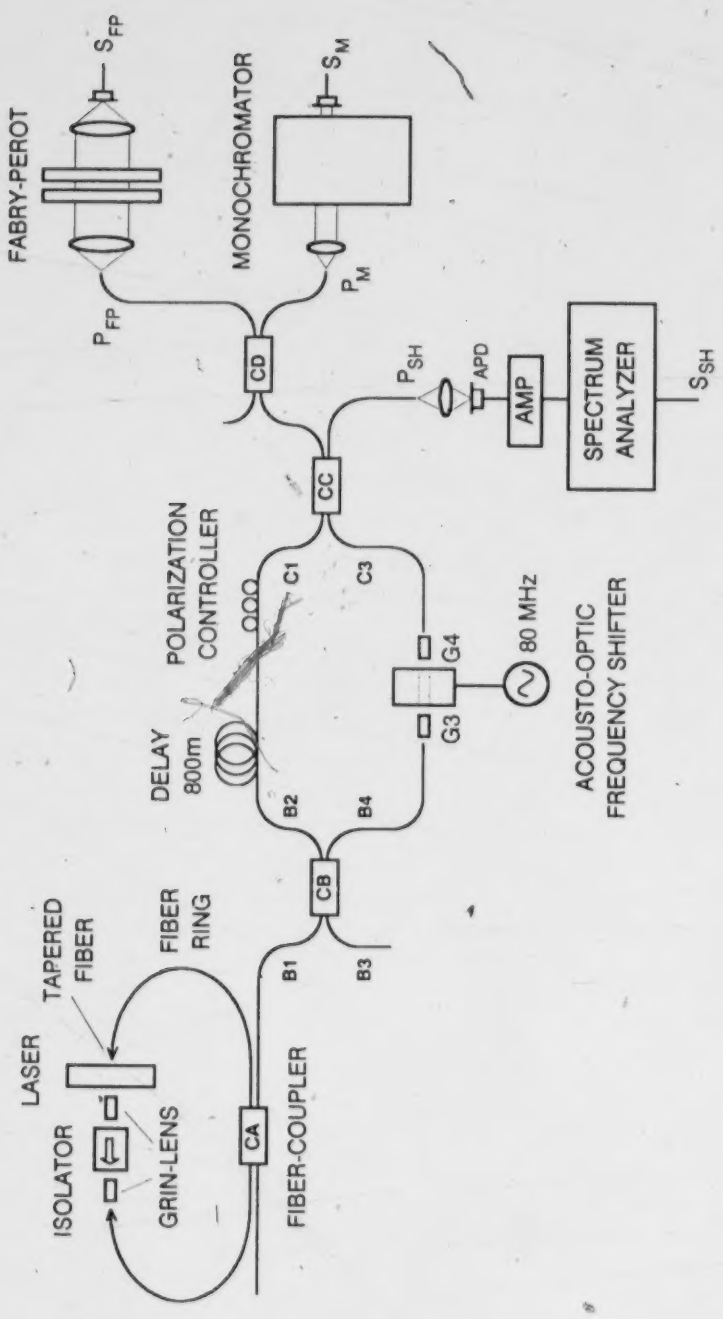

Fig. A.1: Sketch of the laser with fiber-ring feedback, coupled to the measurement setup, consisting of the self-heterodyne setup, a Fabry-Perot interferometer and a monochromator.

shifter. This interupts the lower optical path between couplers CB and CC completely.

All fiber couplers in Fig. A.1 have approximately 50% coupling ratio. Couplers CA, CB and CD have been manufactured by Gould (model 1300 BA) and coupler CC by Opto-Electronics Inc.(model FS10-1300-1). The data from the manufacturer specifies a coupling ratio (C.R.= B4/(B2+B4)) and excess power loss (E.L.= -10 log[(B2+B4)/B3]) for coupler CB, C.R. = 58% and E.L.= .27 dB, for coupler CC, C.R. = 52% and E.L.= 1.0 dB and for coupler CD, C.R.= 59% and E.L.= .03dB. For the coupler used in the short fiber ring experiment (17 cm ring length) the values were C.R.= 58% and E.L.= 1.17 dB. 93 μW of input power into port B3 resulted in a power level of 38 μW measured in B2, 52 μW in B4, 25 μW in C1, 8 μW in C3, P_{SH} ~ (3.8 + 11.9) μW, P_{FP} ~ (1 + 3.1) μW and P_M ~ (1.5 + 4.5) μW. At a bias level of 28 V the APD dark current due to the power transmitted through the fiber delay line and the acousto-optic frequency shifter was measured to be 17.5 μA. We note that the above power budget includes the coupling losses of fused fiber splices, at B2 and C1, and V-groove butt coupled fibers at B1 and C2.

A mechanical chopper wheel and lock-in amplifier, Ithaco 397EO and Stanford SR530, were used with, respectively, the Fabry-Perot interferometer and the monochromator, to increase the signal to noise ratio. The choppers were mounted to interupt the optical signal appearing at the output of the Fabry-Perot and the input to the monochromator. It was necessary to mount these mechanical choppers separately from the optical table to prevent mechanical vibrations from affecting the external cavity lasers.

The lens at the input of the Fabry-Perot interferometer was an Ealing achromat, NA = .4, f = 16 mm, AR-coated for 1.3 μm operation. The Fabry-Perot output lens was an AR-coated, 25 cm focal-length unit from Burleigh Instruments. The collimating lens at the input of the monochromator was a x40, NA = .65, uncoated microscope objective. The input and output slit widths of the monochromator were set at 50 or 80μm, depending on the desired spectral resolution. All GRIN-rod lenses were .23 pitch AR-coated, number SLW1.8-23-B2-130 from Nippon Sheet Glass Co., except for the lens closest to the laser which was a plano convex .18 pitch AR-coated GRIN-rod lens model PCH1.8-22-B/BC-130,

selected to provide a lower level of reflections back into the laser and higher laser to fiber coupling efficiency.

In the fiber-ring feedback arrangement, a Hitachi 1.3 μm BH-laser, model HLP 5400, Serial No 5B 2398, was used. The optical isolator, NEC OD 8313-B (-30 dB isolation), and the GRIN-rod lens on each side of the isolator, were mounted as one unit on a single xyz-translation stage with additional axial fine control provided by a piezo micrometer, Physik Instrumente model P-280.1, having 30 μm travel. Fractional wavelength control in the axial position of optical components relative to the laser facets allows us to identify spectral changes in the laser output caused by reflections off the surfaces of the GRIN-rod lenses and the optical isolator. The tapered fiber ends on each side of the laser were mounted on xyz translation stages with additional fine control provided by P-280.1 piezo electric block translators. The physical dimensions of the optical feedback arrangement need to be kept constant within a fraction of an optical wavelength during the time taken for the measurements. Also, the resonance frequency of the semiconductor cavity has to be kept sufficiently constant during the measurements to prevent significant changes in the resonance frequency of the semiconductor cavity compared to the external cavity mode spacing, $\Delta\nu_{ex}$. The resonance frequency of the semiconductor cavity depends on the injection current and the temperature. From typical dependencies of -3 GHz/mA and -20 GHz/°K [9] and a 1 m long ring cavity that has $\Delta\nu_{ex}$ = 200 MHz, we can conclude that current control [123] and temperature control [124] are required. The current and temperature control circuits developed and used in the present work stabilized the current to within a few mA and the temperature to within ~ .001°K.

Details on the external grating laser are provided in [37]. The collimating lens is a critical element in this setup. In addition to the AR-coated Ealing achromat (N.A.= .4, f = 16 mm) mentioned in [37], we have also obtained good results with a Melles-Griot 06 GLC 001 lens (N.A.= .615, f = 6.5 mm). The collimating lens was mounted in our experiments on an xyz-translation stage with additional fine-control provided by P-280.1 piezo-micrometers.

If the linewidth of the laser is of the order of MHz, the power in the beat signal in the self-heterodyne spectrum is distributed over a

large frequency band and the amplitude of the spectral density is therefore low. Also, we had to observe external cavity modes separated from the center frequency of oscillation of the laser by up to 1.2 GHz. A low-noise wideband amplifier was therefore required to amplify the output signal from the APD in order to obtain observable traces on the spectrum analyzer. This amplifier was built with three Avantek MSA-0370-21 amplifier chips each containing a two stage amplifier. The total gain was 37 dB over a passband defined by the -3dB frequencies of 10 MHz and 1.8 GHz. The amplifier chips were mointed on Duroid board of .01 inch thickness and 50 Ohm microstrip design procedures were used. The frequency response of the amplifier was determined by measuring its step response. Time domain data for the input and output signals were obtained with a sampling oscilloscope. A discussion of the Extended Function Fast Fourier Transform (EF-FFT) method, used to obtain the frequency response from the time domain data, and the application of this technique to the characterization of the three stage amplifier described above, is contained in [124] and [125].

APPENDIX B: SELF-HETERODYNE TECHNIQUE

The self-heterodyne method for high resolution measurement of the spectrum of semiconductor lasers was first described by Kikuchi and Okoshi [126], [127].

A frequency shifted component of the output signal of the laser is heterodyned with a time delayed output signal of the same laser (Fig. A.1). If the delay time is large compared to the coherence time of the laser output, two uncorrelated signals with equal linewidth are combined and mixed by the photo detector. In the case of a Lorentzian output spectrum of the laser with FWHM, or linewidth, of $\Delta\nu_0$, (2.62), the beat spectrum $W_{SH}(\omega)$ also has a Lorentzian shape, however with a FWHM of $2\Delta\nu_0$ [Kik],

$$W_{SH}(\omega) = \frac{4\pi\Delta\nu_0}{(2\pi\Delta\nu_0)^2 + (\omega - \omega_{SH})^2} \cdot \tag{B.1}$$

Here $\omega_{SH} = 2\pi \cdot 80$ MHz is the frequency shift imposed by the acousto-optic frequency shifter. Kikuchi et.al. [126] showed that (B.1) provides a good approximation to the observed beat spectrum (which is the power spectrum of the APD current) as long as $\Delta\nu_0 > .5\tau_d$, where τ_d is the differential time delay between the two optical paths. In our case, $\Delta\nu_0 > 130$ kHz. The assumption of a white FM noise spectrum for the laser leads to the general expression for the beat spectrum of [127]-[129]

$$W_{SH}(f+f_{SH}) = W_0 \cdot \left\{ e^{-2\pi\Delta\nu_0\tau_d\delta(f)} + \frac{\Delta\nu_0}{\pi\{f^2+(\Delta\nu_0)^2\}} \right.$$

$$\left. \cdot \{1 - e^{-2\pi\Delta\nu_0\tau_d} \cdot [\cos(2\pi\tau_d f) + \frac{\Delta\nu_0}{f} \cdot \sin(2\pi\tau_d f)]\} \right\} \tag{B.2}$$

The error in eq. (1.4.15) of [126] is corrected in (B.2). W_0 in (B.2) is a proportionality factor. Curve fitting of the measured beat

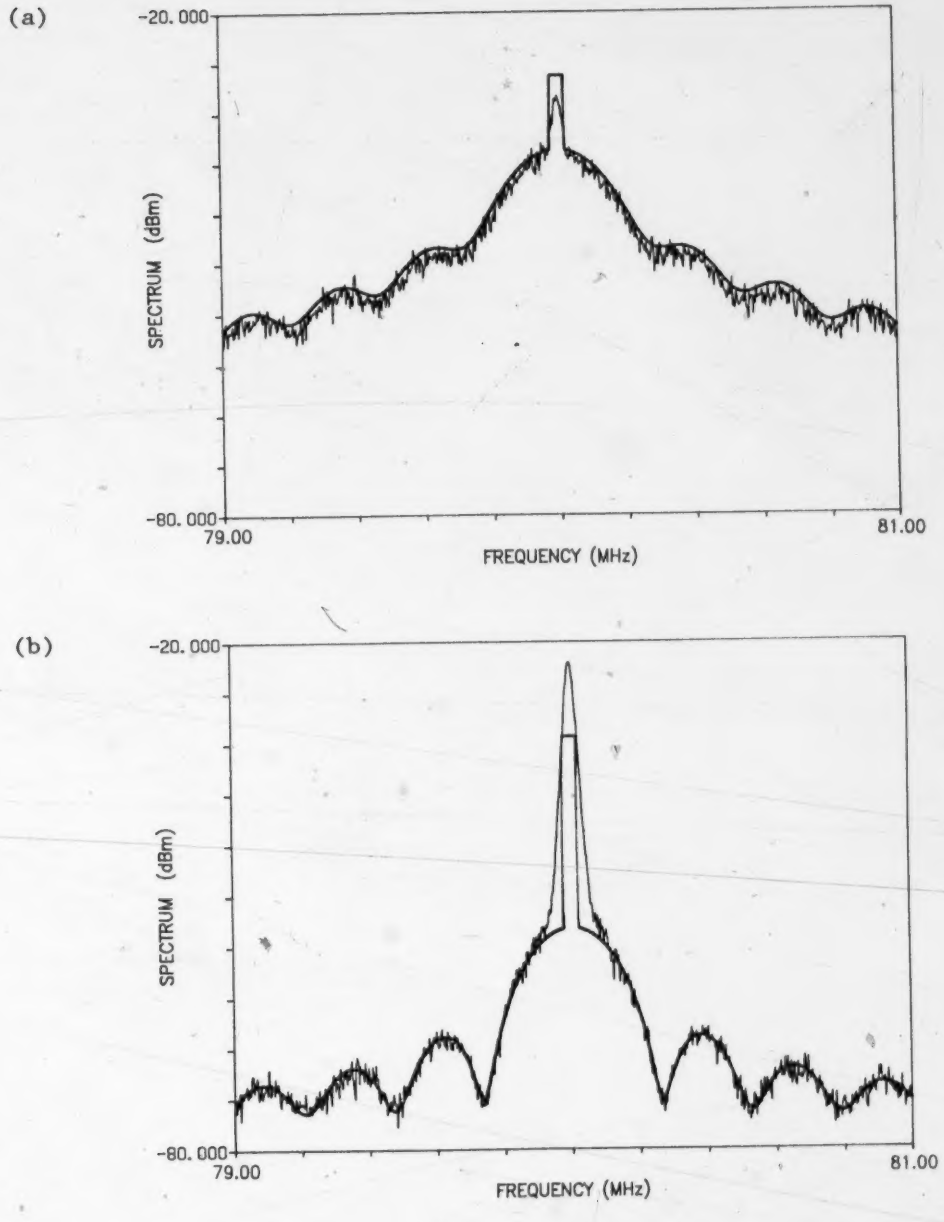

Fig. B.1: Plot of the measured delayed self-heterodyne beat spectrum of the external grating laser in (a) Regime III and (b) Regime IV of Section 5.2.1. Also, calculated functions using (B.2) for (a) $\Delta\nu$ = 52 kHz and (b) $\Delta\nu$ = 5.4 kHz.

spectrum, Fig. B.1, to the calculated spectrum from (B.2) allows us to determine linewidths below the resolution limit of the self-heterodyne setup. The shot noise and receiver noise are taken into account in the curve fitting procedure by adding a constant noise floor W_n to the calculated power spectrum.

The noise floor displayed on the spectrum analyzer, after the accousto-optic frequency shifter was turned off, provided the value of W_n = -76 dBm, which was used in the curve fit of Fig. B.1. W_0 was taken as the factor necessary to obtain equal areas under the linear plot of the calculated and measured beat spectrum. We note that this area is proportional to the optical power in the output of the laser, irrespective of the laser-linewidth. $\Delta\nu_0$ was the curve fitting parameter. (B.2) contains a delta-function at 80 MHz. The output from the spectrum analyzer provides us therefore at 80 MHz with a copy of the filter characteristic of the IF-bandpass filter of the spectrum analyzer. Since (B.2) does not include the effect of the spectrum analyzer filter on the displayed spectrum, we restricted our curve-fitting algorithm to operate on the frequency band of 79 MHz to 79.85 MHz in Fig. B.1

The self-heterodyne technique provides a version of the laser output spectrum, that has the center frequency shifted to 80 MHz. For a laser exposed to weak optical feedback, the overall width of the laser output spectrum can be large compared to 80 MHz because the laser oscillation fluctuates between external cavity modes as shown in Figs. 4.3 and 4.4.

The shift of the spectra shown in Fig. 4.3 to lower frequencies centered on 80 MHz leads to spectral components in the negative frequency domain. These components are displayed by a spectrum analyzer as components in the positive frequency domain. To give an example, Fig. B.2 shows three recordings of the self-heterodyne beat spectrum of a laser with optical feedback from a 129 cm long fiber ring (τ_{ex}^{-1} = 180 MHz) for 3 different levels of optical feedback [24]. These beat spectra can be directly compared to the beat spectra shown in Fig. 4.3, obtained for the same laser with fiber-ring feedback, however recorded using a reference laser.

We designated the spectral components in the self-heterodyne beat spectrum with positive integer numbers for external cavity modes at

(a)

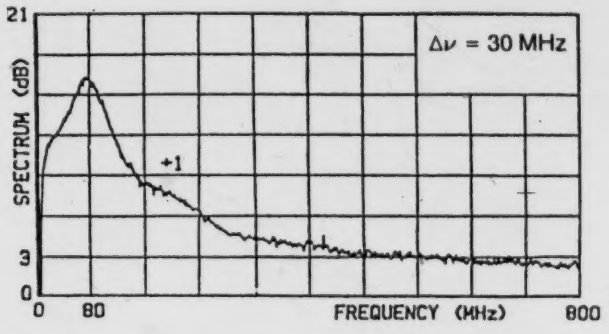

(b)

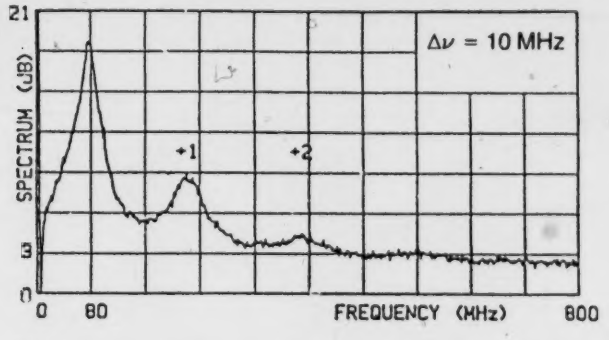

(c)

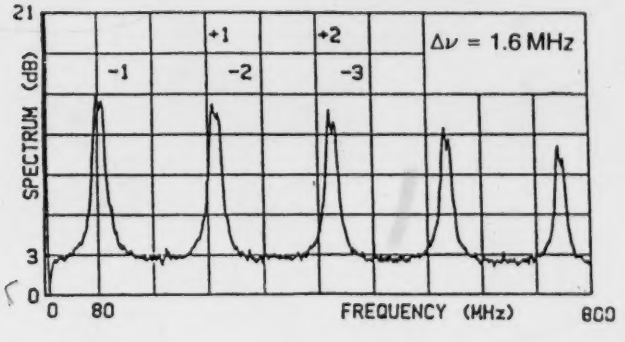

Fig. B.2: Delayed self-heterodyne beat spectra for a laser with fiber ring feedback (L_{ex} = 129 cm) for three different levels of optical feedback (a) R_{ex} ~ -65 dB, (b) -55 dB and (c) -40 dB.

frequencies above the center mode and with negative integer numbers for external cavity modes at frequencies below the center mode. The external cavity mode separation in Fig. B.2(c) is ~ 165 MHz. The frequency of the component labelled "-1" is therefore -85 MHz, but is displayed by the spectrum analyzer at +85 MHz. Finally, we note that all beat spectra of lasers considered in this thesis show the envelope of the noise power spectrum displayed by the spectrum analyzer. Positive and negative frequency components can be considered uncorrelated noise components and can be added in the power spectrum to obtain the one-sided power spectrum.

Fig. 4.7 shows the heterodyne beat spectrum between the optical signal from a laser with fiber ring feedback and a reference laser. The original trace displayed by the spectrum analyzer is reproduced in Fig. B.3. External cavity modes are spaced apart with frequency intervals $\Delta\nu_{ex}$. The constant spacing allows us to identify negative frequency components labelled "N" in Fig. B.3 in the spectrum analyzer trace, and redraw the beat spectrum, as shown in Fig. 4.7, with positive frequency and negative frequency components of the external cavity modes separated.

Let us now consider the case of the acousto-optic frequency shifter being omitted from the setup. Whenever the output of a laser is split into two paths of different paths, a shifted version of the laser spectrum is displayed. Without one path being frequency shifted, the two-sided beat spectrum is centered on DC. Accurate detection of the DC-component in RF-spectrum analyzers is generally not possible. The linewidth of the laser, the ratio between the center mode amplitude and the external cavity mode amplitudes in the laser spectrum can therefore not be determined accurately using the latter method. However, the spacing of external cavity modes can be observed and the origin of undesired reflection determined.

In conclusion, the self-heterodyne beat spectrum is the result of a convolution of the laser output spectrum with itself and not a precise representation of the laser spectrum shifted from optical frequencies to electrical frequencies. Nevertheless, the self-heterodyne technique is a useful tool to observe the linewidth and the external cavity mode spacing in the output spectrum of a laser.

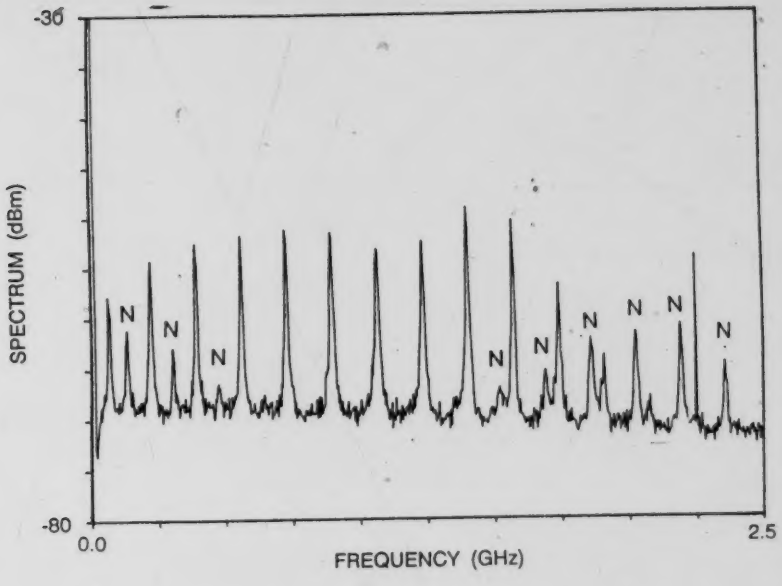

Fig. B.3: Original recording of the heterodyne beat spectrum shown in Fig. 4.7.

APPENDIX C: LI-CHARACTERISTICS OF THE EXTERNAL GRATING LASER

LI-curves are shown in Fig. C.1(a) and (b) for laser TY 224 at ~15° (1) before AR-coating, (2) after coating and (3) after coating and with optical feedback from the grating applied at different wavelengths. Fig. C.1(a) and (b) are copies of the original recordings that were used to obtain Figs. 5.8(a) and (b). The LI-curves in Fig. C.1(a) and (b) where obtained using an xy-plotter, with a voltage proportional to the laser drive current being applied to the horizontal drive of the plotter and a voltage proportional to the optical output power of the laser applied to the vertical.

In Chapter 5 we found that the compound cavity loss of the external grating laser depends on the position of the frequency of maximum feedback, ω_G, relative to the resonance frequency of the semiconductor cavity, ω_m. The resonance frequency of the laser changes as the current is increased due to (1) a change in the temperature of the semiconductor and (2) a change in the carrier density. In order to obtain the LI-curve of the laser for the case of both in-phase optical feedback and out-of-phase feedback, the grating was rotated by small amounts several times during the recording of one LI-curve to yield a maximum of optical output power (in-phase feedback) and a minimum of optical output power (out-of-phase optical feedback). Each LI-curve was recorded several times on the same graph. This procedure leads to the "rough" appearances of the LI-curves shown in Fig. C.1(a) and (b). Figs. 5.8(a) and (b) are obtained from recordings like Fig. C.1 by plotting only the envelope of highest and lowest output power for a given LI-curve.

Unfortunately, Figs. C.1(a) and (b) also contain a trace of an invalid LI-curve, interrupted at ~ 50 mA, and several vertical lines attached to the LI-curve, that were caused by accidental interruption of the optical feedback path.

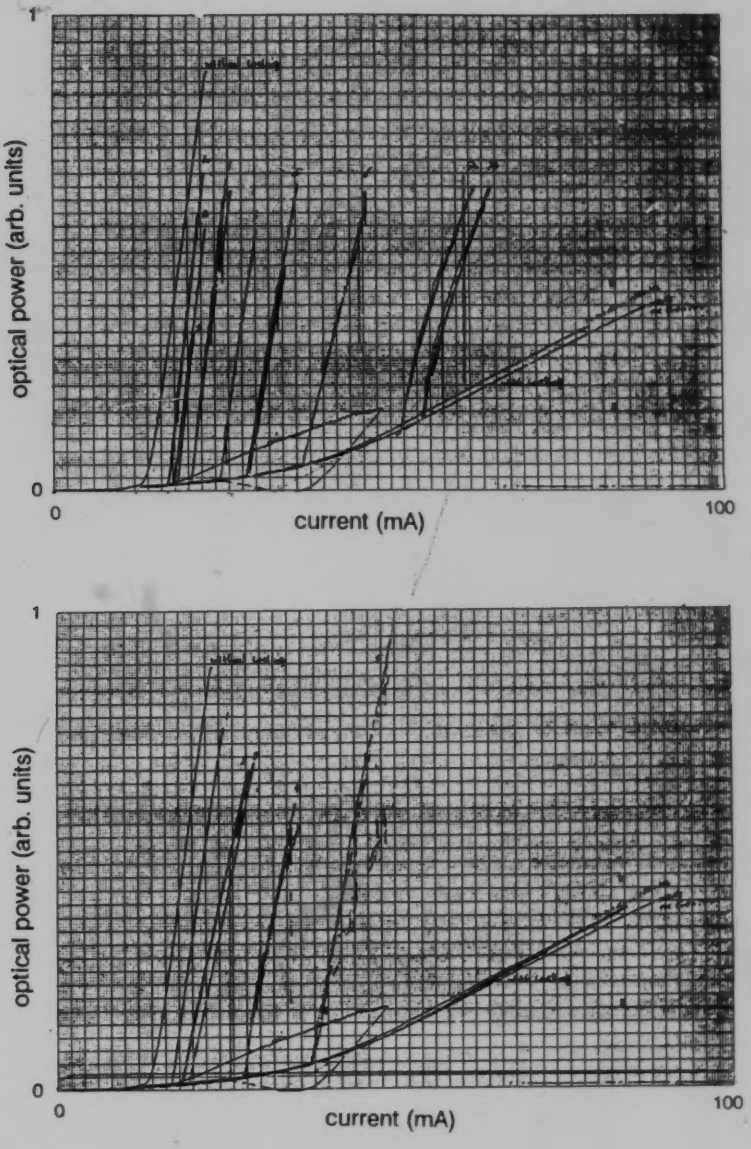

Fig. C.1: Original recordings of the LI-characteristics of the laser with frequency selective feedback provided by the diffraction grating at different wavelengths. The labels for the traces shown are provided in Fig. 5.8(a) and (b).